



**IChF**

Institute of Physical Chemistry PAS

Ph.D. Dissertation

**Analysis of Secondary Organic Aerosol  
from Isoprene and Butadiene with  
Hyphenated Mass Spectrometry**

---

Klara Nestorowicz



Institute of Physical Chemistry of the Polish Academy  
of Sciences, Kasprzaka 44/52, 01-224 Warsaw

# Analysis of Secondary Organic Aerosol from Isoprene and Butadiene with Hyphenated Mass Spectrometry

Klara Nestorowicz

Ph.D. Thesis

This dissertation was prepared within the International Ph.D. Studies of the Institute  
of Physical Chemistry of the Polish Academy of Sciences in Warsaw

Supervisor: Rafał Szmigielski, Prof.

Biblioteka Instytutu Chemii Fizycznej PAN

F-B.573/24



10000000116111

Auxiliary Supervisor: Krzysztof Rudziński, Ph.D. Eng.

Warsaw, June 2023

A-21-7

H 66

k-k-219

k-g-186



B. 573/24

## Acknowledgements

I would like to thank my research advisors:

Rafał Szmigielski, Prof. for the opportunity to learn the secrets of atmospheric chemistry.

Krzysztof Rudziński, Ph.D. Eng. for great support, friendship, and endless patience.

I would further like to acknowledge:

Mohammed Jaoui, Ph.D. from the U.S. Environmental Protection Agency for research collaboration and an opportunity to work on ISO and 13BD SOA projects.

Witold Danikiewicz, Prof. from the Institute of Organic Chemistry, Polish Academy of Sciences for important insights and comments on mass spec structural identification and elucidation.

Grzegorz Spólnik, M.Sc. for research collaboration and introduction into UPLC-MS analyses.

Ewa Bulska, Prof. and Julio Torres, Ph.D. from the University of Warsaw for a successful collaboration on 13BD SOA and HOMs research.

Krzysztof Skotak, M.Sc. and Anna Degórska, Ph.D. from the Institute of Environmental Protection – National Research Institute for the opportunity to participate in many interesting field campaigns.

Krzysztof Klejnowski, Ph.D. Eng. and Barbara Mathews Ph.D. Eng. from the Institute of Environmental Engineering, Polish Academy of Sciences for performing thermo-optical measurements.

All colleagues from the Environmental Chemistry Group of the Institute of Physical Chemistry, Polish Academy of Sciences, especially Monika Asztemborska, Ph.D. Eng. for useful advice on chromatographic analyses, and Agata Błaziak, Ph.D. Eng. for valuable help in organic synthesis.



## Abstract

Atmospheric aerosol (AA) originates from direct emissions or transformation of various volatile organic compounds (VOCs) emitted by biogenic and anthropogenic sources, and resides in the lowest layer of the atmosphere – the troposphere. Chemical reactions of volatile organic compounds with oxidizing reagents present in the atmosphere, like hydroxyl radicals ( $\bullet\text{OH}$ ), ozone ( $\text{O}_3$ ), and nitrate radicals ( $\text{NO}_3\bullet$ ), are driven by solar radiation and play a significant role in the chemistry of the troposphere. Therefore, the troposphere can be perceived as a chemical reactor where thousands of gas-phase, heterogeneous and aqueous-phase reactions produce a complex mixture of products. Fine aerosol particles ( $\text{PM}_{2.5}$ ) of primary and secondary origin are a significant constituent of AA as they influence weather and climate directly by scattering incoming solar radiation and indirectly by acting as cloud condensation nuclei (CCN) in clouds formation and ice nuclei (IN) in ice crystals formation. They affect human health and cause respiratory, cardiovascular, infectious, and allergic diseases, as they are efficiently transported into the thoracic and tracheobronchial regions of the respiratory system. Secondary organic aerosol (SOA) is a substantial part of  $\text{PM}_{2.5}$  particles, however only 10–15% of the organic species in SOA have been successfully and reliably identified so far (Prather et al., 2008; Noziere et al., 2015; Glasius and Goldstein, 2016).

In my Ph.D. thesis, I focused on the identification of unrecognized SOA components in the  $\text{PM}_{2.5}$  fraction formed from two different aerosol precursors – isoprene (2-methylbuta-1,3-diene, ISO) and buta-1,3-diene (13BD) – using UPLC–MS techniques. The studies conducted can be divided into five stages: (1) investigation of the chemical composition of aerosol formed in the smog-chamber experiments from two precursors – isoprene and 1,3-butadiene; (2) determination of the influence of relative humidity and acidity on the formation of identified ISO and 13BD SOA components; (3) comparison of smog-chamber results with ambient aerosol samples collected in rural (Diabla Góra, Zielonka) and polluted sites in Poland (Godów, Kaskada); (4) proposal of molecular structures for identified novel SOA components based on product ion mass spectra and high-resolution MS measurements (when authentic standards were unavailable), and confirmation of other compounds (organic hydroxy acids) with commercially available or synthesized standards; (5) quantification of significant and novel components of isoprene and butadiene SOA in field samples with reference to

smog-chamber results on the influence of RH and acidity on SOA formation in the atmosphere.

The two investigated compounds – ISO and 13BD – are homologs, however, they are emitted into the atmosphere from totally different sources. Isoprene is the most abundant and widely studied biogenic VOC, while 1,3-butadiene is a VOC of anthropogenic origin. The formation of SOA from ISO and 13BD was examined in collaboration with the U.S. Environmental Protection Agency (EPA) in a series of experiments conducted in an in-door smog chamber. The effect of relative humidity and acidity of seed aerosol on the formation of ISO and 13BD components was investigated. Contrary to other studies, the concentrations of the majority of ISO and 13BD compounds detected and the total yields of secondary organic carbon (SOC) decreased with increasing RH level, more sharply in experiments with acidic seed than non-acidic. Thus, the increase of the liquid water content of an aerosol system did not promote the formation of ISO and 13BD organosulfates (OSs), nitrooxy- (NOSs) and nitrosooxy- organosulfates (NSOSs). Under acidic conditions and low RH levels, the formation of isoprene and butadiene products containing sulfate moieties was enhanced comparing to non-acidic conditions at the same RH level.

The observed ISO- and 13BD-derived products were thoroughly characterized using UPLC–ESI–HRMS technique followed by the interpretation of obtained analytical data, including product ion mass spectra with accurate mass measurements. All mass spectrometric analyses were performed in the negative ion mode, as the investigated compounds had reasonable ionization efficiencies to deprotonated ions ( $[M-H]^-$ ). The molecular structures of newly identified compounds were elucidated. Several novel SOA components were discovered i.a.: 3-methylthreonic acid organosulfate (MW 230), 2-methylthreonic acid nitrooxy-organosulfate (MW 275), and 2-methyltartaric acid organosulfate (MW 244) in ISO SOA; and glyceric acid organosulfate (MW 186), malic acid organosulfate (MW 214), threonic acid organosulfate (MW 216), and 1,2,3,4-butanetetrol nitrooxy-organosulfate (MW 247) in 13BD SOA. Those compounds were also found in ambient aerosol from trace to substantial amounts. The chemical structures proposed for highly oxygenated acids formed from ISO and 13BD were based on the product ion mass spectra and confirmed against appropriate synthesized or purchased standard compounds. The syntheses of novel ISO hydroxy organic acids – 2-methyltartaric acid (2-MTA) and 2- and 3-methylthreonic acids (2-, 3-MTrA) were performed. The compounds were proposed as highly oxygenated molecular (HOM)

tracers of aged isoprene aerosol as they were also found in ambient aerosol samples in amounts ranging from 0.8 to 2.8 ng m<sup>-3</sup> on average.

In order to prove the link between smog-chamber experiments and ambient atmospheric processes, the UPLC–ESI–HRMS analyses of fine ambient aerosol (PM<sub>2.5</sub>) samples collected at four various sites in Poland were conducted. High concentrations and diversity of isoprene SOA components detected in Zielonka (Bory Tucholskie) and Diabla Góra (Puszcza Borecka) sampling sites revealed a large share of terrestrial vegetation in local emissions. The total amount of detected ISO-derived organosulfates and nitrooxy-organosulfate at those sampling sites were 474.9 ± 149.3 ng m<sup>-3</sup> and 324.0 ± 76.0 ng m<sup>-3</sup>, which accounted for approx. 7.9% and 7.1% of the total OC mass, respectively. The most abundant compounds were 2-methyltetrol NOS (MW 261) and 2-methyltetrol OS (MW 216), which contributed significantly to the mass of ISO SOA. Moreover, Zielonka ambient aerosol was the richest one in 13BD SOA components containing sulfate moieties, although not as chemically diverse as in ISO SOA. The total amount of detected compounds was 14.0 ± 5.3 ng m<sup>-3</sup>, which accounted for 0.24% of the OC mass. Besides, malic acid organosulfate (MW 214) was the most abundant OS detected (13.3 ± 5.0 ng m<sup>-3</sup>). Moreover, malic acid, a known secondary organic aerosol tracer was a highly abundant 13BD-derived component at all investigated sites. The greatest amounts of those compound was detected in Zielonka at the level of 93.7 ± 31.7 ng m<sup>-3</sup>. The sources of two mentioned compounds in the atmosphere could be direct 1,3-butadiene emission and biomass burning in nearby households. 1,2,3,4-butanetetrol OS (MW 202) was not detected in ambient aerosol, while its analogue 2-methyltetrol OS (MW 216) formed from isoprene was a highly abundant key tracer of ISO SOA.

This Ph.D. thesis presents results of the comprehensive studies on the chemical composition of isoprene and 1,3-butadiene SOA, which forms in the troposphere, the lower part of the Earth's atmosphere. Advanced research tools, including smog chambers and hyphenated mass spectrometry techniques were used for that purpose. The influence of relative humidity and acidity on the formation of individual 13BD and ISO SOA components was examined. Revealing ISO and 13BD SOA composition under laboratory conditions enabled the firm identification of the complex composition of ambient aerosol. The results presented may fill the gaps in understanding of chemical transformations of isoprene and butadiene in the atmosphere and the formation of secondary organic aerosol from those precursors. Several significant and novel



<sup>13</sup>BD- and ISO-derived components were identified and their concentrations were determined both in smog-chamber experiments and ambient fine aerosol. Moreover, organosulfates and other SOA components detected in this study are expected to enhance the capacity of ambient aerosol as cloud condensation nuclei (CCN) impacting the air quality. The data obtained in this study will pave the way for better description of the complex and time-varying chemical composition of SOA and may improve the performance of air quality models.

## Streszczenie

Aerozol atmosferyczny (AA) powstaje w najniższej warstwie atmosfery – troposferze – w wyniku bezpośredniej emisji lub przemian wielu różnych lotnych związków organicznych (LZO) emitowanych ze źródeł biogenicznych i antropogenicznych. Reakcje chemiczne lotnych związków organicznych z reagentami utleniającymi obecnymi w atmosferze, takimi jak rodniki hydroksylowe ( $\bullet\text{OH}$ ), ozon ( $\text{O}_3$ ) i rodniki azotanowe ( $\text{NO}_3\bullet$ ), są inicjowane przez promieniowanie słoneczne i odgrywają znaczącą rolę w chemii atmosfery. Stąd też troposferę można postrzegać jako reaktor chemiczny, w którym tysiące reakcji zachodzących w fazach gazowej, heterogenicznej i wodnej wytwarzają niezwykle złożoną mieszaninę produktów. Drobne cząsteczki aerozolu (frakcja  $\text{PM}_{2.5}$ ) pochodzenia pierwotnego i wtórnego wpływają na pogodę i klimat bezpośrednio poprzez rozpraszanie docierającego promieniowania słonecznego, jak i pośrednio, działając jako zarodki kondensacji chmur (CCN) i zarodki lodu (IN). Wpływają one także znacząco na zdrowie człowieka, powodując choroby układu oddechowego i sercowo-naczyniowego oraz choroby zakaźne i alergiczne, ponieważ skutecznie docierają w głąb układu oddechowego. Wtórny aerozol organiczny (SOA) stanowi znaczną część frakcji  $\text{PM}_{2.5}$ , jednak dotychczas tylko 10–15% związków organicznych zawartych w SOA zostało wiarygodnie zidentyfikowanych (Prather i in., 2008; Noziere i in., 2015; Glasius i Goldstein, 2016).

W mojej pracy doktorskiej skupiłam się na identyfikacji nierozpoznanych składników wtórnego aerozolu organicznego (SOA) frakcji  $\text{PM}_{2.5}$ . Zbadałam skład chemiczny wtórnego aerozolu organicznego wytworzonego z dwóch różnych prekursorów – izoprenu (2-metylobuta-1,3-dien, ISO) i buta-1,3-dien (13BD) – przy użyciu techniki wysokosprawnej chromatografii cieczowej sprzężonej ze spektrometrią mas (UPLC-MS). Prowadzone przeze mnie badania mogę podzielić na pięć etapów: (1) badanie składu chemicznego aerozolu wytwarzanego w eksperymentach w komorze aerozolowej z dwóch prekursorów – izoprenu i 1,3-butadienu; (2) określenie wpływu wilgotności względnej i kwasowości na powstawanie wykrytych składników izoprenowego i butadienowego SOA; (3) porównanie wyników otrzymanych w eksperymentach w komorze aerozolowej z próbkami aerozolu atmosferycznego pobranymi w Polsce na terenach wiejskich (Diabla Góra, Zielonka) oraz zanieczyszczonych (Godów, Kaskada); (4) propozycja struktur chemicznych wykrytych nowych składników wtórnego aerozolu organicznego w oparciu

o fragmentacyjne widma masowe i wysokorozdzielcze pomiary MS (gdy wzorce były niedostępne), oraz potwierdzenie struktur innych związków (hydroksykwasów) za pomocą dostępnych na rynku lub zsyntetyzowanych wzorców; (5) oznaczenie ilościowe składników izoprenowego i butadienowego SOA w próbkach aerozolu atmosferycznego, w odniesieniu do eksperymentów w komorze aerozolowej, z próbą określenia wpływu wilgotności względnej i kwasowości na powstawanie wtórnego aerozolu organicznego w atmosferze. Dwa badane związki – ISO i 13BD – są homologami, jednak trafiają do atmosfery z całkowicie różnych źródeł. Izopren jest najobficiej występującym i najszerzej badanym biogenicznym LZO, podczas gdy 1,3-butadien jest LZO pochodzenia antropogenicznego. Powstawanie wtórnego aerozolu organicznego z obydwu prekursorów zbadano we współpracy z amerykańską Agencją Ochrony Środowiska (U.S. EPA) w serii eksperymentów przeprowadzonych w komorze aerozolowej. Zbadano wpływ wilgotności względnej i kwasowości aerozolu na powstawanie składników ISO i 13BD. W przeciwieństwie do innych badań, stężenia większości wykrytych związków oraz całkowita wydajność tworzenia wtórnego węgla organicznego (SOC) malały wraz ze wzrostem wilgotności względnej – bardziej istotnie w doświadczeniach przeprowadzonych w warunkach kwaśnych, z dodatkiem kwasu siarkowego ( $H_2SO_4$ ). Co więcej, wzrost zawartości wody w układzie aerozolowym nie sprzyjał tworzeniu organosiarczanów (OS), nitrooksy- (NOS) i nitrozooksyorganosiarczanów (NSOS). W warunkach kwaśnych i przy niskich poziomach wilgotności względnej, powstawanie produktów izoprenowych i butadienowych zawierających ugrupowania siarczanowe było wydajniejsze w porównaniu z warunkami bezkwasowymi przy tym samym poziomie wilgotności względnej.

Zaobserwowane produkty utleniania izoprenu i butadienu scharakteryzowano dokładnie przy użyciu wysokorozdzielczej techniki UPLC–MS wyposażonej w źródło typu elektrosprej (ESI), a następnie dokonano dokładnej interpretacji uzyskanych danych analitycznych, w tym fragmentacyjnych widm masowych z dokładnymi pomiarami masy. Wszystkie analizy spektrometryczne przeprowadzone zostały w trybie jonów ujemnych ze względu na dobrą wydajność jonizacji i tworzenia jonów deprotonowanych ( $[M-H]^-$ ) badanych związków. Na podstawie przeprowadzonych analiz zaproponowano i wyjaśniono struktury molekularne nowo zidentyfikowanych związków. Odkryto kilka nowych składników wtórnego aerozolu organicznego, w tym m.in.: organosiarczan kwasu 3-metylotreonowego (MW 230), nitrooksy-organosiarczan kwasu 2-metylotreonowego (MW 275) i organosiarczan kwasu 2-metylowinowego (MW 244)

w izoprenowym SOA; oraz organosiarczan kwasu glicerynowego (MW 186), organosiarczan kwasu jabłkowego (MW 214), organosiarczan kwasu treonowego (MW 216) i nitrooksy-organosiarczan 1,2,3,4-butanotetrolu (MW 247) w butadienowym SOA. Wykryte związki zidentyfikowano także w aerozolu atmosferycznym w ilościach od śladowych do znacznych. Struktury chemiczne zaproponowane dla wysoko utlenionych kwasów utworzonych z ISO i 13BD oparto na zarejestrowanych fragmentacyjnych widmach masowych oraz potwierdzono w odniesieniu do zsyntetyzowanych lub kupionych związków wzorcowych. W ramach badań przeprowadzono syntezy nowych izoprenowych hydroksykwasów – kwasu 2-metylowinowego (2-MTA) oraz kwasów 2- i 3-metylotreonowych (2-, 3-MTrA) – które zaproponowano jako wysoce utlenione związki (HOMs) o charakterze wskaźników starzenia się aerozolu izoprenowego. Związki te zidentyfikowano w próbkach aerozolu w ilościach od 0.8 do 2.8 ng m<sup>-3</sup>.

Aby udowodnić związek pomiędzy eksperymentami w komorze aerozolowej a procesami atmosferycznymi, przeprowadzono analizy UPLC-MS próbek drobnej frakcji aerozolu atmosferycznego (PM<sub>2.5</sub>) pobranej w czterech różnych miejscach w Polsce. Wysokie stężenia i różnorodność składników izoprenowego SOA wykryte w Zielonce (Bory Tucholskie) i w Diablej Górze (Puszcza Borecka), miały związek z dużym udziałem roślinności leśnej w lokalnych emisjach. Łączna ilość wykrytych organosiarczanów i nitrooksy-organosiarczanów powstałych z izoprenu wyniosła odpowiednio 474.9 ± 149.3 ng m<sup>-3</sup> i 324.0 ± 76.0 ng m<sup>-3</sup>, co stanowiło ok. 7.9% i 7.1% całkowitej masy węgla organicznego (OC). Najliczniej występującymi związkami były nitrooksy-organosiarczan 2-metylotetrolu (MW 261) i organosiarczan 2-metylotetrolu (MW 216), które znacząco wpływały na skład chemiczny ISO SOA. Ponadto próbki zebranego aerozolu na terenie Zielonki były najbogatsze w składniki 13BD SOA, choć nie był on tak zróżnicowany chemicznie jak wtórny aerozol organiczny powstały z izoprenu. Łączna zawartość wykrytych związków z ugrupowaniami siarczanowymi wyniosła 14.0 ± 5.3 ng m<sup>-3</sup>, co stanowiło 0.24% masy OC. Największy udział miał organosiarczan kwasu jabłkowego (MW 214), który oznaczono na poziomie 13.3 ± 5.0 ng m<sup>-3</sup>. Kwas jabłkowy, znany wtórny związek organiczny będący składnikiem aerozolu butadienowego, również został wykryty w Zielonce w znaczącej ilości 93.7 ± 31.7 ng m<sup>-3</sup>. Źródłem obu wspomnianych związków w atmosferze może być bezpośrednia emisja 1,3-butadienu, ale również spalanie biomasy w pobliskich gospodarstwach domowych. Organosiarczan 1,2,3,4-butanotetrolu (MW 202) nie został

wykryty w zbadanych próbkach aerozolu atmosferycznego, podczas gdy jego analog – organosiarczan 2-metylotetrolu (MW 216) jest kluczowym składnikiem izoprenowego wtórnego aerozolu organicznego.

W niniejszej pracy doktorskiej przedstawione zostały wyniki kompleksowych badań składu chemicznego wtórnego aerozolu organicznego powstałego z izoprenu i 1,3-butadienu, który tworzy się w troposferze, dolnej części atmosfery ziemskiej. Wykorzystano w tym celu zaawansowane narzędzia badawcze, w tym komory aerozolowe oraz techniki sprzężonej spektrometrii mas. Zbadano wpływ wilgotności względnej i kwasowości na powstawanie poszczególnych składników 13BD i ISO SOA. Określenie składu ISO i 13BD SOA w warunkach laboratoryjnych umożliwiło jednoznaczną identyfikację złożonego składu próbek aerozolu. Niemniej jednak, ze względu na mnogość zmiennych, które ostatecznie wpływają na skład chemiczny SOA w atmosferze, trudno jest jednoznacznie skorelować dane meteorologiczne, trajektorie wsteczne mas powietrza i inne parametry fizykochemiczne z określonymi związkami ISO i 13BD SOA oraz wydajnością ich tworzenia. Określenie takich zależności wymagałyby pełnego modelowania chemii atmosfery, co wykraczało poza zakres tej pracy. Przedstawione wyniki mogą natomiast wypełnić luki w zrozumieniu przemian chemicznych izoprenu i butadienu w atmosferze oraz powstawania wtórnego aerozolu organicznego z tych prekursorów. Co więcej, zidentyfikowano nowe składniki pochodzące z 13BD i ISO, a ich stężenia ustalono zarówno w eksperymentach w komorze aerozolowej, jak i w drobnym aerozolu atmosferycznym. Dane uzyskane w tej pracy mogą posłużyć do lepszego opisu zmiennego w czasie składu chemicznego wtórnego aerozolu organicznego, przez co poprawią wydajność modeli jakości powietrza.

The undertaken research was partially supported by the National Science Centre

Project no. NCN UMO-2014/15/B/ST10/04276



NATIONAL SCIENCE CENTRE  
POLAND



## List of Abbreviations

Abbreviation	Meaning
13BD	1,3-Butadiene
13BDOOH	1,3-Butadiene Hydroxy Hydroperoxide
AA	Atmospheric Aerosol
AAE	Acrylic Acid Epoxide
ACN	Acetonitrile
ACR	Acrolein
APAN	Acryloyl Peroxynitrate
APCI	Atmospheric Pressure Chemical Ionization
AVOCs	Anthropogenic Volatile Organic Compounds
BC	Black Carbon
BEPOX	1,3-Butadiene Epoxydiol
BVOCs	Biogenic Volatile Organic Compounds
CAAA	Clean Air Act Amendments
CCN	Cloud Condensation Nuclei
CN	Condensation Nuclei
CE	Collision Energy
CI-MS	Chemical Ionization Mass Spectrometry
CID	Collision-Induced Dissociation experiments
CO	Carbon oxide
CO <sub>2</sub>	Carbon dioxide
EC	Elemental Carbon
ECHA	European Chemicals Agency
EEA	European Environmental Agency
EIC	Extracted Ion Chromatogram
EPA	Environmental Protection Agency
ESI	Electrospray Ionization
ESI (-)	Electrospray Ionization in the negative mode
EUSAAR	European Supersites for Atmospheric Aerosol Research
FID	Flame Ionization Detection
GA	Glyceric acid
GC-FID	Gas Chromatography coupled with Flame Ionization Detection
GC-MS	Gas Chromatography coupled with Mass Spectrometry
H <sub>2</sub> SO <sub>4</sub>	Sulfuric Acid
HESI	Heated Electrospray Ionization
HC	Hydrocarbon
HCD	High-energy Collision Induced Dissociation
HILIC	Hydrophilic Interaction Liquid Chromatography
HOMs	Highly Oxygenated Molecules
HRMS	High Resolution Mass Spectrometry
HVS	High-Volume Sampler
IC	Inorganic Carbon
IARC	International Agency for Research on Cancer
IEPOX	Isoprene Epoxydiol
IN	Ice Nuclei
IPCC	Intergovernmental Panel on Climate Change
IPCS	International Programme on Chemical Safety
ISO	Isoprene
ISOPOOH	Isoprene Hydroxy Hydroperoxide
ISOP(OOH) <sub>2</sub>	Isoprene Dihydroxy Dihydroperoxide
JRC	Joint Research Centre
LC	Liquid Chromatography
LC-MS	Liquid Chromatography coupled with Mass Spectrometry
LOD	Limit of Detection
LOQ	Limit of Quantification
LVS	Low-Volume Sampler
<i>m/z</i>	Mass to Charge Ratio



MA	Malic Acid
MACR	Methacrolein
MBO	2-Methyl-3-Buten-2-ol
MAE	Methacrylic Acid Epoxide
MeOH	Methanol
MErA	Methylerythronic acid
MGA	Methylglyceric acid
MPAN	Methacryloyl Peroxynitrate
MS	Mass Spectrometry / First order Mass Spectrum
MS/MS	Second order Mass Spectrum / Product Ion Mass Spectrum
MTA	Methyltartaric Acid
MTrA	Methylthreonic Acid
MT	Methyltetrols
MW	Molecular Weight
MVK	Methyl Vinyl Ketone
ND	Not Detected
NO	Nitrogen Oxide
NO <sub>3</sub>	Nitrate Radicals
NO <sub>x</sub>	Nitrogen Oxides
NOS	Nitrooxy-Organosulfate
NMR	Nuclear Magnetic Resonance
NSOS	Nitrosooxy-Organosulfate
O <sub>3</sub>	Ozone
OA	Organic Aerosol
OC	Organic Carbon
OH	Hydroxyl Radical
OM	Organic Matter
OS	Organosulfate
Q-TOF-HRMS	Quadruple Time-of-Flight High-Resolution Mass Spectrometry
PM	Particulate Matter
PM <sub>1.0</sub>	Ultra-fine particles of aerodynamic diameter ≤1.0 μm
PM <sub>2.5</sub>	Fine particles of aerodynamic diameter ≤2.5 μm
PM <sub>10</sub>	Coarse particles of aerodynamic diameter ≤10 μm
PN-EN	Polish norm – English version
POA	Primary Organic Aerosol
PTR-MS	Proton Transfer Ionization Mass Spectrometry
RH	Relative Humidity
RPLC	Reversed-Phase Liquid Chromatography
RT	Retention Time
SD	Standard Deviation
SIA	Secondary Inorganic Aerosol
SOA	Secondary Organic Aerosol
SOC	Secondary Organic Carbon
TA	Tartaric Acid
TC	Total Carbon
TIC	Total Ion Current Chromatogram
TOT	Thermo-optical Transmittance
TrA	Threonic Acid
TrtA	Tartronic Acid
UPLC-MS	Ultrahigh Performance Liquid Chromatography coupled with Mass Spectrometry
UV	Ultraviolet Spectrophotometry
VOCs	Volatile Organic Compounds
WHO	World Health Organization
WINSOC	Water-Insoluble Organic Compounds
WSOC	Waters-Soluble Organic Compounds

## Table of contents

Acknowledgements .....	iii
Abstract .....	v
Streszczenie .....	ix
List of Abbreviations .....	xv
1. Literature review .....	1
1.1 Atmospheric aerosol .....	1
1.1.1 Classification, sources, and implications .....	2
1.1.2 Secondary organic aerosol (SOA).....	11
1.1.2.1 Isoprene SOA .....	15
1.1.2.2 Butadiene SOA.....	24
1.2 Analytical techniques for determining the chemical composition of atmospheric aerosol	32
1.2.1 Off-line techniques .....	33
1.2.1.1 Sample preparation.....	34
1.2.1.2 Liquid chromatography coupled with mass spectrometry (LC-MS).....	37
1.3 Objectives of thesis .....	39
2. Experimental .....	42
2.1. Methodology and materials.....	42
2.1.1 Smog chamber experiments .....	42
2.1.1.1 Isoprene SOA .....	44
2.1.1.2 Butadiene SOA.....	46
2.1.2 Ambient aerosol samples .....	47
2.1.3 Thermo-optical method for OC/EC determination .....	54
2.1.4 Analysis of air mass back trajectories .....	57
2.1.5 Sample preparation.....	57
2.1.6 Preparation of standard solutions and calibration curves for LC-MS analyses.....	59
2.1.7 Qualitative UPLC-MS analyses .....	61
2.1.8 Quantitative UPLC-MS analyses .....	62
2.2 Synthesis of authentic standards .....	63
2.2.1 Isoprene SOA .....	64
2.2.2 Butadiene SOA.....	66
3. Results.....	67
3.1 Smog chamber samples.....	67
3.1.1 Identification of isoprene and butadiene SOA components.....	67
3.2 Influence of relative humidity and acidity on isoprene and butadiene SOA formation .....	72
3.2.1 Isoprene SOA .....	72
3.2.2 Butadiene SOA.....	77

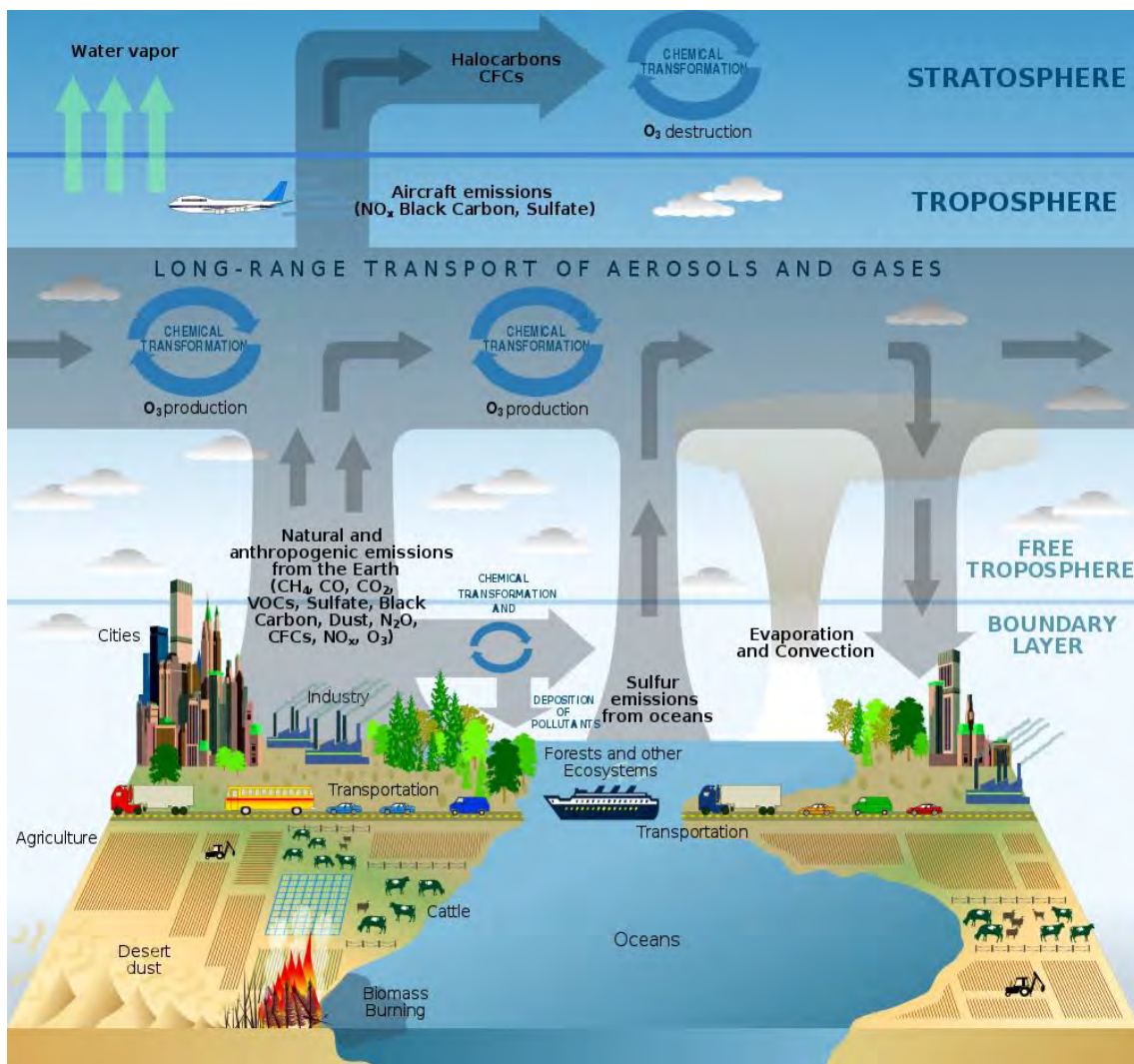
3.3 Investigation of isoprene and butadiene SOA compounds in fine aerosol.....	81
3.3.1 Organosulfates formation from isoprene.....	81
3.3.2 Organosulfates formation from butadiene.....	89
3.3.3 Organic acids formation from isoprene.....	100
3.3.4 Organic acids formation from butadiene.....	104
3.4 Ambient fine aerosol.....	109
3.4.1 OC and EC concentrations.....	110
3.4.2 Back trajectories of air masses.....	114
3.4.3 Quantitative characterization of ambient aerosol.....	119
3.4.3.1 Isoprene SOA.....	120
3.4.3.2 Butadiene SOA.....	129
4. Summary and conclusions.....	140
5. References.....	143
6. Appendix.....	162
List of publications and patent applications.....	177
Oral presentations at national and international conferences.....	178
Poster presentations at national and international conferences.....	178

# 1. Literature review

## 1.1 Atmospheric aerosol

The Earth's atmosphere is a mixture of various gases, in which the main components are nitrogen ( $\text{N}_2$ ; 78.1%), oxygen ( $\text{O}_2$ ; 20.9%), and argon ( $\text{Ar}$ ; 0.9%). Numerous trace constituents, like helium ( $\text{He}$ ), neon ( $\text{Ne}$ ), methane ( $\text{CH}_4$ ), hydrogen ( $\text{H}_2$ ), carbon dioxide ( $\text{CO}_2$ ), water vapor, ozone ( $\text{O}_3$ ), sulfur-, nitrogen-, and halogen-containing compounds, ammonia ( $\text{NH}_3$ ), and atmospheric aerosols (AA), build up the remaining 0.1% (Holloway and Wayne, 2015; Seinfeld and Pandis, 2016). The latter originate from direct emissions or transformation of various volatile organic compounds (VOCs) emitted by biogenic and anthropogenic sources and reside in the lowest layer of the atmosphere – the troposphere, which extends up to 15 km above the Earth's surface and accounts for about 90% of the total atmospheric mass (Holloway and Wayne, 2015; Seinfeld and Pandis, 2016). The troposphere strongly interacts with the Earth's ecosystems, that significantly affect its chemical composition. Changes in atmosphere composition result in air pollution, climate changes, and depletion of the ozone layer. Sources and sinks, chemical transformation, and transport of residual gases and particulate matter (PM) determine the atmosphere's composition, as shown in **Figure 1**.

Chemical reactions of volatile organic compounds with oxidizing reagents present in the atmosphere, like hydroxyl radicals ( $\bullet\text{OH}$ ), ozone ( $\text{O}_3$ ), and nitrate radicals ( $\text{NO}_3\bullet$ ), are driven by solar radiation and play a significant role in the chemistry of the troposphere. Therefore, the troposphere can be perceived as a chemical reactor where thousands gas-phase, heterogeneous and aqueous-phase reactions produce a complex mixture of products, including PM. The emission of primary trace compounds and the production of secondary trace compounds, e.g., secondary inorganic aerosol (SIA) and secondary organic aerosol (SOA), change the composition of ambient air and affect the environment, human health, and life quality. Therefore, it is necessary to get insights into the transformations of atmospheric trace compounds and the chemical composition of atmospheric aerosols formed. This knowledge will provide data essential for exposure, risk, and air quality assessment and management.



**Figure 1.** The cycles of various components in the Earth's atmosphere (Rozaini, 2012)

### 1.1.1 Classification, sources, and implications

Atmospheric aerosol is a suspension of solid particles or liquid droplets in ambient air with physical and chemical characteristics depending on the morphology, fraction, surface, shape, and chemical composition of the particles, all varying with location (Hinds, 1998; Jacobson, 2002; Colbeck and Lazaridis, 2010; Gieré and Querol, 2010; Juda-Rezler and Toczko, 2016; Seinfeld and Pandis, 2016). It can have a form of mist, fog, and haze composed of liquid particles or ash, dust, smoke, fume, and smog composed of solid particles. Aerosol particles consist of inorganic and organic components. Organic aerosol (OA), also known as organic matter (OM), originates from natural and anthropogenic sources. It is distinguished either as primary organic aerosol (POA) or secondary organic aerosol (SOA; Chapter 1.1.2 contains a broader description). Natural sources of POA include volcanic eruptions, dust storms, forest and grassland fires, living vegetation, sea spray, and uplifted mineral dust, whereas anthropogenic

sources include various types of industries, agriculture, transportation, construction, and biomass burning (Poschl, 2005; Letcher, 2015; Juda-Rezler and Toczko, 2016).

Aerosol particles can be divided into fractions according to their aerodynamic diameters ( $\varphi$ ), that is a diameter of a sphere with a density of  $1 \text{ g cm}^{-3}$ , having the falling speed in the air the same as the given particle. Depending on the size, particles are classified as ultrafine or  $\text{PM}_1$  ( $\varphi < 1 \text{ }\mu\text{m}$ ), fine or  $\text{PM}_{2.5}$  ( $\varphi < 2.5 \text{ }\mu\text{m}$ ), and coarse or  $\text{PM}_{10}$  ( $\varphi < 10 \text{ }\mu\text{m}$ ), where PM stands for particulate matter (Hinds, 1998; Juda-Rezler and Toczko, 2016). Aerosol particles undergo various formation, transformation, and removal processes in the atmosphere. Those processes, including nucleation, gas-to-particle partitioning, coagulation, accumulation, and condensation, change the particle size, phase, structure, and chemical composition (Poschl, 2005).

Aerosol particles generally can form in the atmosphere in two modes (Hussein et al., 2018):

- 1) accumulation mode, which includes particles with a diameter between  $0.1\text{--}2.5 \text{ }\mu\text{m}$ ,
- 2) coarse mode, which includes particles with diameters between  $2.5\text{--}10 \text{ }\mu\text{m}$ .

The characterization of selected PM fractions, including their composition, physicochemical properties, and formation and removal processes, is presented in **Table 1**.

**Table 1:** Characterization of fine- and coarse-mode particles (adapted from U.S. EPA report, 2004; WHO guideline, 2006; Juda-Rezler and Toczko, 2016; Seinfeld and Pandis, 2016)

	Fine particles		Coarse particles
	< 0.1 $\mu\text{m}$	0.1 – 2.5 $\mu\text{m}$	2.5 – 10 $\mu\text{m}$
<b>Formation processes</b>	Combustion processes, fresh high-temperature emissions, and atmospheric reactions		Break-up of large solids/droplets
<b>Formation</b>	Nucleation	Condensation	Mechanical disruption (crushing, grinding, abrasion of surfaces)
	Condensation	Coagulation	Evaporation of sprays
	Gas-to-particle conversion	Accumulation	Suspension of dust
	Coagulation	Reactions of gases in or on particles	Reactions of gases in or on particle
		Evaporation of fog and cloud droplets in which gases have dissolved and reacted	
<b>Composition</b>	Sulfate	Sulfate, nitrate, ammonium, hydrogen ions	Suspended soil or street dust
	Elemental carbon	Elemental carbon	Fly ash from uncontrolled combustion of coal, oil, and wood
	Metal compounds	A variety of organic compounds	Nitrates/chlorides from nitric acid/hydrochloric acid
	Organic compounds with a very low saturation vapor pressure at ambient temperature	Metals: compounds of lead, cadmium, vanadium, nickel, copper, zinc, manganese, iron, etc.	Oxides of crustal elements (silicon, aluminum, titanium, iron)
		Particle-bound water	Calcium carbonate, sodium chloride, sea salt
		Secondary inorganic aerosol (SIA), secondary organic aerosol (SOA)	Pollen, molds, fungal spores
			Plant and animal debris
			Tyre, brake pad, and road wear debris
			Volcanic eruptions
<b>Solubility</b>	Probably less soluble than accumulation mode	Often soluble, hygroscopic, and deliquescent	Largely insoluble and nonhygroscopic
<b>Sources</b>	Combustion	Combustion of coal, oil, gasoline, diesel fuel, wood	Resuspension of industrial dust and soil tracked onto roads and streets
	Atmospheric transformation of sulfur dioxide and organic compounds	Atmospheric transformation products of nitrogen oxides, sulfur dioxide, and	
	High-temperature processes		

		organic carbon, including biogenic organic species	Suspension from disturbed soil (e.g., farming, mining, unpaved roads)
		High-temperature processes, smelters, steel mills, etc.	Construction and demolition
			Uncontrolled coal and oil combustion
			Ocean spray
			Biological sources
<b>Atmospheric half-life</b>	Minutes to hours	Days to weeks	Minutes to days
<b>Removal processes</b>	Grows into accumulation mode	Forms cloud droplets and deposits in rain	Dry deposition by fallout
	Diffuses to raindrops	Dry deposition	Scavenging by falling raindrops
			Sedimentation
<b>Travelled distance</b>	Meters to tens of kilometers	Hundreds to thousands of kilometers	Meters to hundreds of kilometers
<b>Respiratory system absorption</b>	Lung interstitium	Alveoli	Trachea
			Bronchi
			Nasopharynx

The estimated global annual PM emission exceeds 12000 Tg. Up to 98% of particles originate from natural sources, with the largest share of sea salt, mineral dust, volcanic particles, and organic aerosol formed from volatile organic compounds. Only 2% of particulate matter has anthropogenic origins (Andreae and Rosenfeld, 2008; Seinfeld and Pandis, 2016).

The estimated global emissions of PM from biogenic and anthropogenic sources are presented in **Table 2**.

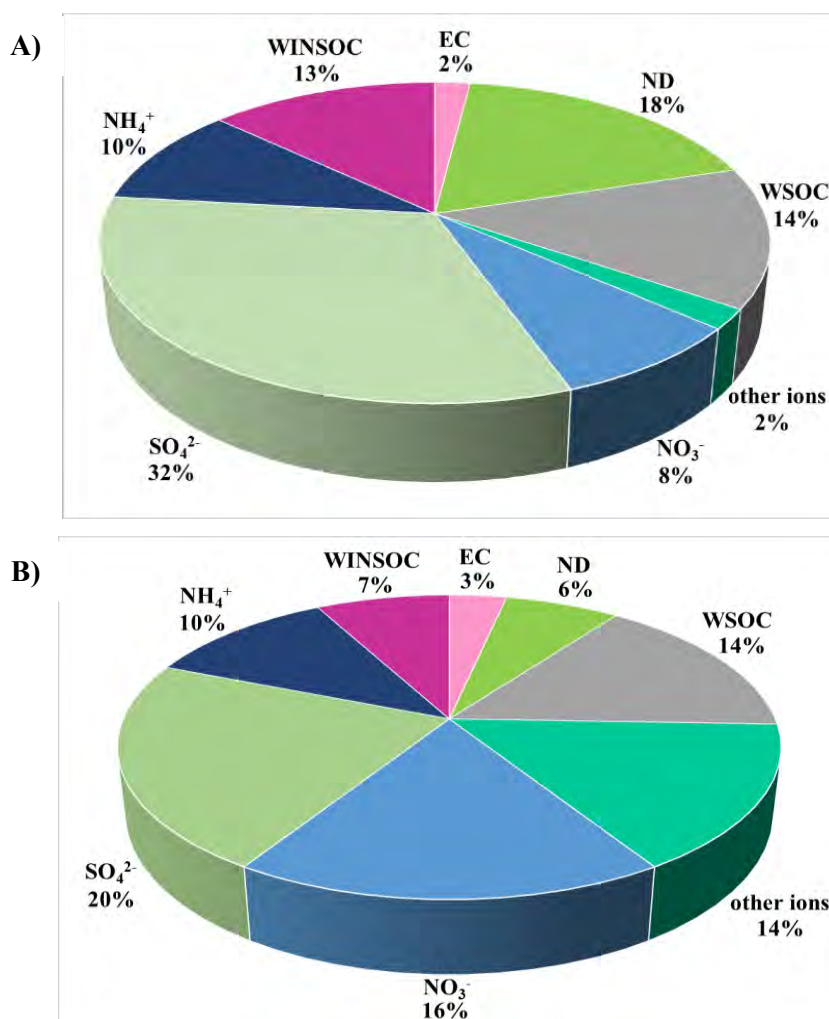


**Table 2:** Global estimations of PM emissions from biogenic and anthropogenic sources (adapted from Seinfeld and Pandis, 2016; Tomasi et al., 2017; McNeill, 2017)

Source	Type of PM	Estimated flux (Tg yr <sup>-1</sup> )	References		
<b>Biogenic</b>	<b>Primary</b>	Mineral dust	1000 – 2150 Andreae and Rosenfeld, 2008; Huneus et al., 2011		
		Sea salt	3000 – 30000 Bond et al., 2004; Andreae and Rosenfeld, 2008		
		Volcanic dust	4 – 90 Jaenicke, 1988		
		Biological debris	15 – 70 Andreae and Rosenfeld, 2008		
	<b>Secondary</b>	Sulfates	107 – 374 Andreae and Rosenfeld, 2008		
		Nitrates	12 – 27 Andreae and Rosenfeld, 2008		
		Organic aerosol from VOCs	835 – 1000 Jaenicke, 2005; Tsigaridis et al., 2006		
		<b>Anthropogenic</b>	<b>Primary</b>	Industrial dust	40 – 130 Andreae and Rosenfeld, 2008
				Black carbon	2 – 29 Bond et al., 2013
				Organic aerosol	15 – 90 Liousse et al., 1996
<b>Secondary</b>	Sulfates		50 – 122 Liao et al., 2003, 2004		
	Nitrates		40 – 118 Liao et al., 2004; IPCC, 2001		

Particulate matter emissions are also monitored at regional and local scales. According to the World Health Organization (WHO report; 2013), PM<sub>2.5</sub> constitutes around 50–70% of the PM<sub>10</sub> fraction at most European locations. In general, PM<sub>2.5</sub> mass concentrations were up to 50 µg m<sup>-3</sup> in rural areas and up to 200 µg m<sup>-3</sup> in highly polluted urban areas (Finlayson-Pitts and Pitts, 2000). The chemical composition of individual PM fractions differs. Putaud et al. (2010) showed that the chemical composition of PM<sub>2.5</sub>, PM<sub>2.5-10</sub>, and PM<sub>10</sub> fractions measured at 60 monitoring stations across Europe varied significantly. The main components of PM<sub>10</sub> and PM<sub>2.5</sub> measured were organic compounds, sulfates, and nitrates. Moreover, the mean contribution of SO<sub>4</sub><sup>2-</sup> and NH<sub>4</sub><sup>+</sup> ions was comparable for all European regions and did not exceed 20% and 12%, respectively. Zappoli et al. (1999) investigated the chemical composition of aerosol

particles with  $\phi < 1.5 \mu\text{m}$  ( $\text{PM}_{1.5}$ ) collected at polluted (San Pietro Capofiume, Italy) and rural (K-Puszt, Hungary) sites in Europe. They estimated the average percentage composition of fine aerosol and distinguished the following components: organic matter (OM) divided into water-soluble organic compounds (WSOC) and water-insoluble organic compounds (WINSOC), elemental carbon (EC) and sulfate, nitrate, and ammonium ions (e.g.,  $\text{SO}_4^{2-}$ ,  $\text{NO}_3^-$ ,  $\text{NH}_4^+$ ). In that study, OM constituted 27% and 21% of the total aerosol mass at rural and polluted sites. Elemental carbon (EC) at both sites was detected at a similar level – 2% and 3%, respectively. The main inorganic component detected was  $\text{SO}_4^{2-}$  ion at an average level of 32% and 20%, respectively. The chemical composition of the analyzed aerosol differed and was not fully identified – unrecognized part (ND) constituted 18% and 6%, respectively. **Figure 2** shows the AA chemical composition determined by Zappoli et al. (1999).

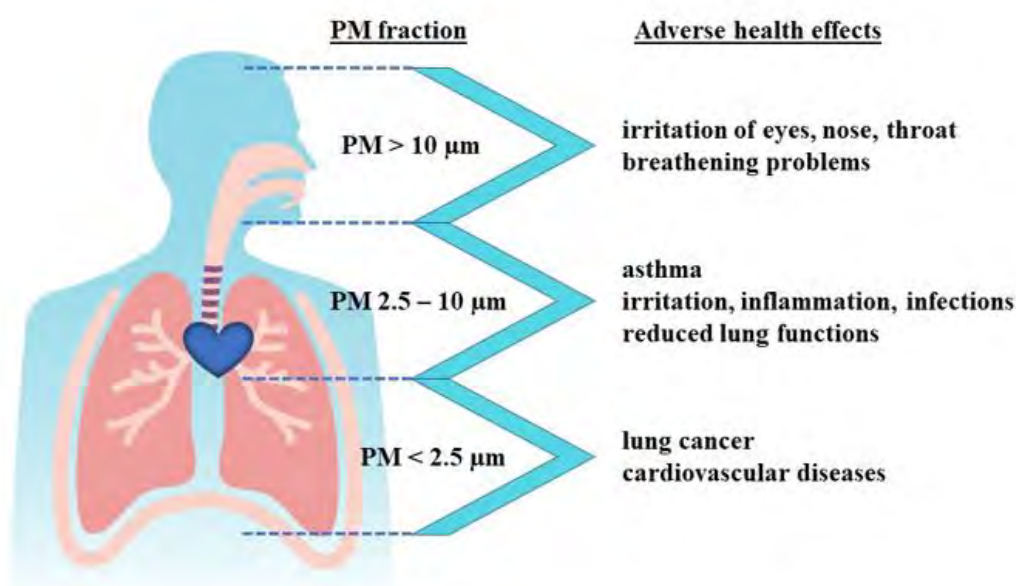


**Figure 2.** Average chemical composition of aerosol mass at rural (A) and polluted (B) sampling sites in Europe (adapted from Zappoli et al., 1999)

According to **Figure 2**, a great part of the aerosol mass was sulfate, nitrate, and ammonium salts. The sum of those three components at rural and polluted sites accounted for 50% and 46% of the average total mass, respectively. However, for the rural background sites, sulfates contribution was substantial, and for polluted areas, nitrates also became a significant component (Putaud et al., 2004). Both salts form in the atmosphere mainly through chemical processes from precursor gases ( $\text{SO}_2$ ,  $\text{NO}_x$ , and  $\text{NH}_3$ ).  $\text{SO}_2$  and  $\text{NO}_x$  react in the gas and liquid phase to form sulfuric acid and nitric acids, respectively, which undergo neutralization by ammonia to produce secondary particles, referred to as secondary inorganic aerosol (SIA). SIA formation strongly depends on chemical and meteorological factors, such as the level of gaseous precursors, the concentration of atmospheric oxidants, the characteristics of preexisting aerosol particles, the air temperature and humidity (Baek et al., 2004; Baek and Aneja, 2004; Pathak et al., 2009; Squizzato et al., 2013). Furthermore, ammonium sulfate and ammonium nitrate are considered relevant sources of aerosol seeds and condensation nuclei (CN) in the atmosphere. They may interact with volatile organic compounds (VOCs) and promote the growth of aerosol particles (Stockwell et al., 2003; Borrego and Miranda, 2007; Squizzato et al., 2013; Juda-Rezler and Toczko, 2016; Aksoyoglu et al., 2017). The second major component of fine aerosol was organic matter (OM), revealed and collected at rural background sites and polluted areas by Zappoli et al. (1999). The share of this fraction in aerosol mass can vary significantly depending on sources, season, and geographical location. Many studies indicated that organic aerosol (OA) might account for 20–60% of PM mass at continental mid-latitudes (Saxena and Hildemann, 1996; Kanakidou et al., 2005) and even 90% in tropical forests (Andreae and Crutzen, 1997; Roberts et al., 2001; Zhang et al., 2007; Docherty et al., 2008).

The chemical composition of aerosol particles is rather complex and diverse. It strongly depends on the emission sources, lifetimes of single components in the atmosphere (from hours to weeks), geographical location, and terrain and meteorological conditions. Thus, the same amount of  $\text{PM}_{2.5}$  in two various places of the world will affect human health and the Earth's climate differently due to distinct chemical composition – the relative abundance of multiple components can vary by order of magnitude or even more (Seinfeld and Pandis, 1998; Raes et al., 2000; Poschl, 2005; Juda-Rezler and Toczko, 2016).

In the 1980s, the first data on the impact of atmospheric aerosols on human health and life was reported (Raizenne et al., 1989). Nowadays, in many countries, including Poland, the awareness of the harmful effects of aerosols is growing year by year (Heal et al., 2012; EEA report, 2014; Khan, 2021). In 2012, the International Agency for Research on Cancer (IARC) characterized total air pollution and particulate matter as carcinogenic to humans (group I), including components such as 1,3-butadiene, wood dust, tobacco smoke, polychlorinated biphenyls, products of residential coal combustion and components of diesel engine exhausts (IARC monographs, 2012; Loomis et al., 2013). PM<sub>10</sub> fraction tends to collect in the upper respiratory tract, while PM<sub>2.5</sub> particles can penetrate the lower part of the respiratory system. Aerosol particles are efficiently transported into the thoracic and tracheobronchial regions of the respiratory system, where they induce various well-documented adverse cardiovascular and respiratory responses (Kim et al., 2014). They can damage alveoli and lung tissue and move further into the bloodstream and the body. **Figure 3** presents a scheme of inhalation exposure to particulate matter with possible adverse health effects that may affect certain parts of the respiratory system.



**Figure 3.** Inhalation exposure to aerosol particles with possible adverse health effects on the respiratory system (elaborated based on Kim et al., 2014; EEA website: "How air pollution affects our health"; WHO guideline, 2021)

The substantial health impact of aerosol particles attracts great research interest (Kim et al., 2014; Cohen et al., 2017; Thompson et al., 2018; Khan, 2021). Long-term clinical trials indicated that exposure to elevated PM<sub>2.5</sub> levels had been associated with an increased risk of cardiopulmonary and lung cancer mortality (Pope et al., 2002;

Beelen et al., 2008; Krewski et al., 2009). The PM<sub>2.5</sub> fraction accounted for over 400 thousand premature deaths in 28 European countries, including nearly 80% of respiratory diseases and lung cancer (EEA report, 2014). Nowadays, there is no evidence for any exposure level below which no adverse health effects occur. However, many studies confirm that decreased PM levels significantly reduce the death rates in adults and children (Bayer-Oglesby et al., 2005; Downs et al., 2007; Schindler et al., 2009; WHO report, 2013). Besides, PM spreads biological organisms, reproductive materials, and pathogens (bacteria, pollen, spores, viruses), affecting human health and causing respiratory, cardiovascular, infectious, and allergic diseases (Pope and Dockery, 2006).

Fine particles of primary and secondary origin influence weather and climate directly by scattering incoming solar radiation and indirectly by acting as cloud condensation nuclei (CCN) in clouds formation and ice nuclei (IN) in ice crystals formation (Poschl, 2005; Sun and Ariya, 2006). Consequently, atmospheric aerosol modifies Earth's radiation budget and has a direct effect on the warming or cooling of Earth's climate. Positive radiative forcing (causing global warming) is mainly influenced by the presence of greenhouse gases and black carbon (BC) emissions from anthropogenic sources, which reduce the reflectance of ice and snow surfaces (Flanner et al., 2007; Letcher, 2015). Contrary, aerosol particles emitted from forested areas affect atmospheric circulation and the abundance of greenhouse and reactive trace gases, and they induce the cooling effect (Kulmala et al., 2004; Kanakidou et al., 2005; Carlton et al., 2009; Hallquist et al., 2009; Letcher et al., 2015). The studies conducted so far poorly quantified the possible role of AA in affecting the Earth's climate. Therefore, the influence of aerosol particles on radiation and cloud formation is a key source of uncertainty in future climate modeling (Letcher, 2015). That shortcoming also applies to SOA formation bearing many knowledge gaps in the transformation, physicochemical mechanisms, chemical composition, and properties of SOA (Poschl, 2005).

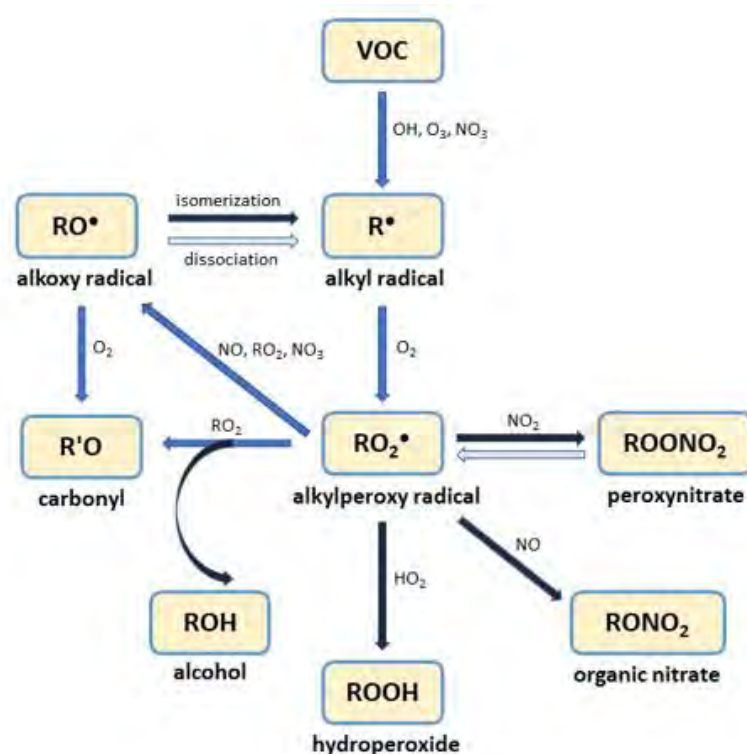
Aerosol particles may induce environmentally harmful processes – after dry deposition onto ground and vegetation surfaces, they may affect photosynthesis and though chemistry and biology of the whole ecosystems (Bell and Treshow, 2004; Juda-Rezler and Toczko, 2016). AA particles deposited on the leaf surface affect the physiological traits of plants. PM can be dissolved by rain or fog and further removed from the leaf surface, or it may penetrate the leaves through the cuticular layer and stomata, resulting in reduced photosynthesis and transpiration (Lindberg et al., 1982; Markert, 1995; Rossini Oliva and Raitio, 2003; Burkhardt, 2010). Nonetheless,

deposition onto the vegetation surfaces can serve as a sink for atmospheric aerosols in urban areas, absorbing pollution like organic matter, chemicals, and heavy metals that adhere to the particles (Tallis et al., 2011). Therefore, the sizeable total green area within cities can effectively capture PM, thereby improving urban air quality (Beckett et al., 2000; McDonald et al., 2007; Mitchell et al., 2010).

Secondary organic aerosol constitutes a significant part of the PM<sub>2.5</sub> fraction. Despite the research, only a small part of the atmospheric aerosol composition has been reliably identified (Noziere et al., 2015; Glasius and Goldstein, 2016). The organic fraction accounts for up to 50% of the PM<sub>2.5</sub> fraction, although only 10–15% of the organic species have been successfully identified (Prather et al., 2008). As the chemical composition of fine particles remains largely unrevealed, while that fraction has many environmental and health implications, I focused in my thesis on the identification of unrecognized SOA components in the PM<sub>2.5</sub> fraction.

### 1.1.2 Secondary organic aerosol (SOA)

Secondary organic aerosol (SOA) is formed in the atmosphere through complex photochemical, chemical, and physical processes involving biogenic and anthropogenic volatile organic compounds (VOCs), atmospheric oxidants, like hydroxyl radicals ( $\bullet\text{OH}$ ), nitrogen oxide ( $\text{NO}_3$ ) or ozone ( $\text{O}_3$ ), and gaseous pollutants like sulfur dioxide ( $\text{SO}_2$ ), nitrogen oxides ( $\text{NO}_x$ ) and carbon oxide ( $\text{CO}$ ). Most of the first-generation products are formed in the gas phase (Seinfeld and Pandis, 1998). These compounds, such as aldehydes, ketones, alcohols, organonitrates, carboxylic acids, organic peroxides, keto-alcohols, hydroxyorganic acids, etc., are more polar and have lower volatility than their precursors. They can partition into particulate phase and undergo heterogeneous reactions on dry solid surfaces, or liquid water and react further by multiphase chemistry on aerosol surfaces (Calogirou et al., 1999; Atkinson and Arey, 2003; Seinfeld and Pankow, 2003; Kroll and Seinfeld, 2008; Hallquist et al., 2009; Juda-Rezler and Toczko, 2016). The simplified mechanism of the oxidation and degradation of VOCs in the atmosphere is presented in **Scheme 1**. Dark blue arrows indicate the formation of compounds of lower volatility, which potentially contribute to SOA formation. On the other hand, light blue arrows signify the increase in the compound's volatility.



**Scheme 1.** Simplified mechanism for the atmospheric oxidation and degradation of biogenic VOCs (adapted from Kroll and Seinfeld, 2008; Hallquist et al., 2009)

Less volatile compounds can partition between atmospheric phases according to the gas-to-particle partitioning theory developed by Pankow (1994). The compounds divide between the gas phase (air) and the condensed phase (particulate matter) according to the temperature-dependent equilibrium partitioning coefficient  $K_P$ , which is given by Equation 1 (Pankow, 1994; Juda-Rezler and Toczko, 2016):

$$K_P = \frac{C_{PM}}{C_G \times M} \quad (\text{m}^3 \mu\text{g}^{-1}) \quad (1)$$

where:  $C_{PM}$  is the mass concentration of a component in the particulate-associated phase ( $\mu\text{g m}^{-3}$ ),  $C_G$  is the mass concentration of a component in the gas phase ( $\mu\text{g m}^{-3}$ ), and  $M$  is the mass concentration of the total suspended particulate material ( $\mu\text{g m}^{-3}$ ) – it can be OA or aqueous phase (Juda-Rezler and Toczko, 2016).

Some studies have shown that chemical and photochemical transformation of VOCs could run in the atmospheric aqueous phase (Jang et al., 2002; Tolocka et al., 2004; Rudzinski, 2004, 2006; Rudzinski et al., 2009, 2016; Loeffler et al., 2006; Silva Santos et al., 2006; Noziere et al., 2009, 2010, 2011). VOCs can react *via* photochemistry, acid catalysis, and interactions with inorganic constituents in the aqueous phase forming organic acids, oligomers, and organosulfates (Carlton et al., 2006; Surratt et al., 2007a; Rudzinski et al., 2009; Szmigielski, 2016). However, after water

evaporation, some products may partition into the gas phase, while others may remain in the particle phase (Loeffler et al., 2006). Consequently, manifolds of reactions, called aging, can define OA formation and affect the growth of particles and their atmospheric fate (Griffin et al., 2005; Juda-Rezler and Toczko, 2016).

The dependence between the organic aerosol mass formed ( $M$ ) and the particular aerosol precursor (e.g., hydrocarbon; HC) is expressed by Equation 2, and it can be extended to the SOA formation (Odum et al., 1996):

$$Y_{SOA} = \frac{\Delta M}{\Delta HC} \quad (2)$$

where:  $Y_{SOA}$  is the yield of secondary organic aerosol formed,  $\Delta M$  is the mass concentration of the resulting organic matter ( $\mu\text{g m}^{-3}$ ),  $\Delta HC$  is the mass concentration of the reacted hydrocarbon (aerosol precursor) ( $\mu\text{g m}^{-3}$ ).

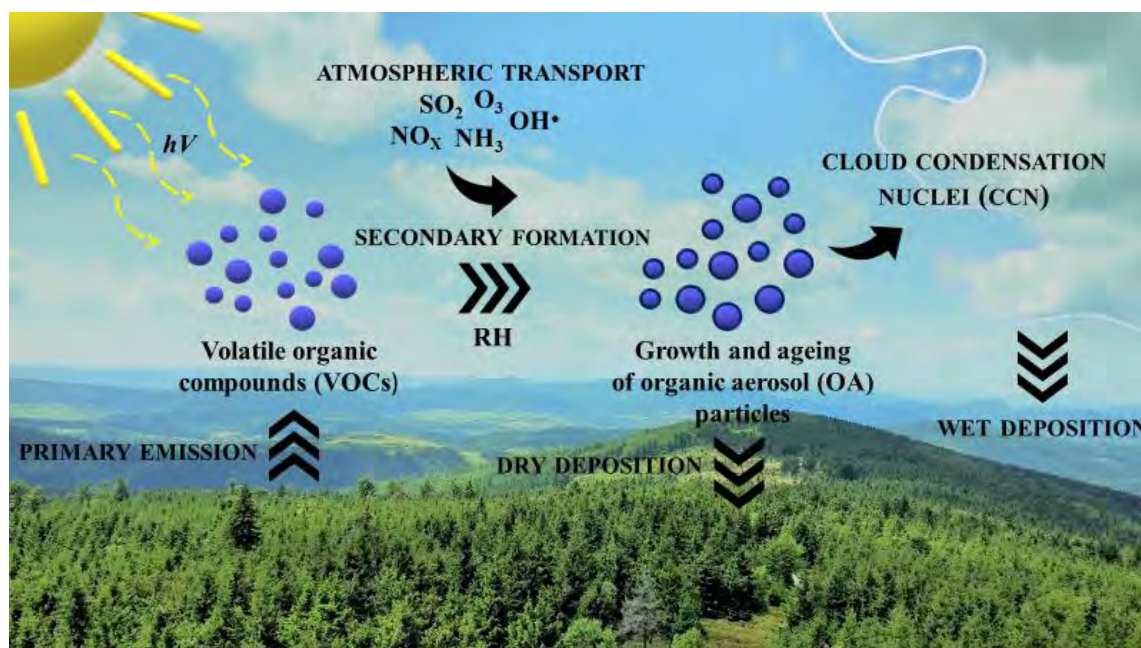
In addition, the formula given by Odum et al. (1996) is the basis for representing laboratory SOA yield data in smog chamber studies (Hallquist et al., 2009).

SOA contribution to OM is substantial and accounts for 20–80% of total organic mass, depending on seasons and geographical location (Dechapanya et al., 2004; de Gouw et al., 2005; Lanz et al., 2007, 2008; Carlton et al., 2009). Previous research demonstrated that even 90% of SOA is formed from biogenic VOCs (BVOCs), the main source of which is terrestrial vegetation. The annual flux of BVOCs in the atmosphere was estimated at 75–1000 Tg (Guenther et al., 2012; Safieddine et al., 2017). These compounds showed higher reactivity towards atmospheric oxidants than anthropogenic VOCs (AVOCs; Atkinson and Arey, 2003; Kanakidou et al., 2005; Volkamer et al., 2006). **Figure 4** presents possible atmospheric processes leading to the aerosol formation from biogenic VOCs in the atmosphere.

The estimated share of AVOCs was 10–25% of total VOCs emission, with the global flux at 100–160 Tg  $\text{y}^{-1}$ . Therefore, SOA formation from these compounds has been underestimated (Tsigaridis and Kanakidou, 2003; Montero-Montoya et al., 2018). However, AVOCs emission is hazardous, toxic, and carcinogenic (Nazaroff and Weschler, 2004; Cohen et al., 2005; Weschler and Nazaroff, 2008; Montero-Montoya et al., 2018; Li et al., 2021). Thus, it is of great concern in SOA research as it may elevate morbidity and mortality rates (Khare and Gentner, 2018). To date, U.S. EPA classified approx. 190 air pollutants, of which 97 are VOCs (David and Niculescu, 2021). These compounds emitted in urban areas from, i.a., biomass burning, vehicle exhaust, and fuel combustion, were characterized as an essential



source of anthropogenic SOA (Robinson et al., 2007; Gentner et al., 2012; Khare and Gentner, 2018).



**Figure 4.** Scheme of atmospheric processes and aerosol formation from BVOCs (own elaboration)

To date, biogenic and anthropogenic biomass burning has been considered the second-largest source of VOCs in the atmosphere. Its emission was estimated at 60–400 Tg y<sup>-1</sup> (Andreae and Merlet, 2001; Giglio et al., 2013; Chen et al., 2019). Compounds emitted during burning react further and form many aging products and increase SOA yields (Andreae and Merlet, 2001; Tkacik et al., 2017; Lim et al., 2019). According to Bond et al. (2013), biomass burning accounts for 85% of POA emissions worldwide and is a source of many compounds and possible SOA precursors, like 1,3-butadiene (details in Chapter 1.1.2.2). The chemical composition of biomass burning SOA has been investigated and varies widely (Reid et al., 1998; Robinson et al., 2007; de Gouw and Jimenez, 2009; Grieshop et al., 2009 a,b; Yokelson et al., 2009; DeCarlo et al., 2010; Cubison et al., 2011; Hennigan et al., 2011; Andreae, 2019).

Developing VOC mechanisms of secondary aerosol formation in the atmosphere is still under investigation. To reveal the missing reactions, properties, and chemical composition of SOA, extensive research is carried out. Particular attention has been paid to smog-chamber experiments, which play a crucial role in resolving SOA formation and transformation mechanisms. The formation and growth of aerosol particles are investigated under precisely controlled simulated conditions, as similar to

the atmospheric ones as possible. Moreover, the chemical transformation pathways of single aerosol precursors can be investigated. Details of smog-chamber experiments as the basis of aerosol chemistry research are given in Chapter 2.1.1. In addition, measurements of ambient air carried out at various rural background and urban monitoring sites enable the identification of SOA trace compounds – potential markers and the key compounds used for SOA source apportionment. However, incorporating data on biogenic and anthropogenic SOA formation into the atmospheric models is difficult (Goldstein and Galbally, 2007; Volkamer et al., 2009; Carlton et al., 2009; Hallquist et al., 2009), mainly due to:

- 1) significant uncertainty of aerosol precursor emissions,
- 2) unrecognized SOA precursors,
- 3) missing data on physical and chemical processes that contribute to SOA formation (i.a., cloud processing),
- 4) translation of laboratory data to the atmospheric processes,
- 5) uncertainties of ambient SOA composition measurements.

Moreover, the components of SOA particles react continuously in the atmosphere through multiple reactions and thus change the composition and the amount of organic aerosol. Several attempts have been made in the past years, and some corrections were introduced in SOA yields of selected precursors. Also, a new-designed model was used to handle the complexity of SOA formation and its volatility (Andersson-Skold and Simpson, 2001; Schell et al., 2001; Johnson et al., 2004, 2005; Srivastava et al., 2022). But still, heterogeneous reactions of SOA were not well defined, so current atmospheric models can easily underestimate SOA contribution (Kroll and Seinfeld, 2008; Hallquist et al., 2009; Srivastava et al., 2022). Therefore, SOA contribution is usually not included in the air quality assessment models (Tsigaridis et al., 2014; Juda-Rezler and Toczko, 2016; Shrivastava et al., 2017; Bates and Jacob, 2019) that remain a challenge facing researchers.

#### **1.1.2.1 Isoprene SOA**

Isoprene (2-methylbuta-1,3-diene, C<sub>5</sub>H<sub>8</sub>, ISO) is the most abundant non-methane unsaturated hydrocarbon emitted by plants to the atmosphere. Its global emission is estimated to be between 400–800 Tg yr<sup>-1</sup>. It accounts for more than half of the budget of all biogenic VOC emissions and roughly equals the global methane emission (Guenther et al., 2006, 2012; Sindelarova et al., 2014; Claeys and Maenhaut, 2021).

The primary source of isoprene is terrestrial vegetation. ISO is synthesized *in vitro* in plastids (chloroplasts) from pyruvate and glyceraldehydes-3-phosphate (Kesselmeier and Staudt, 1999). It is emitted by various trees species (Haapanala et al., 2006; Hellen et al., 2006; Ekberg et al., 2009; Pacifico et al., 2009):

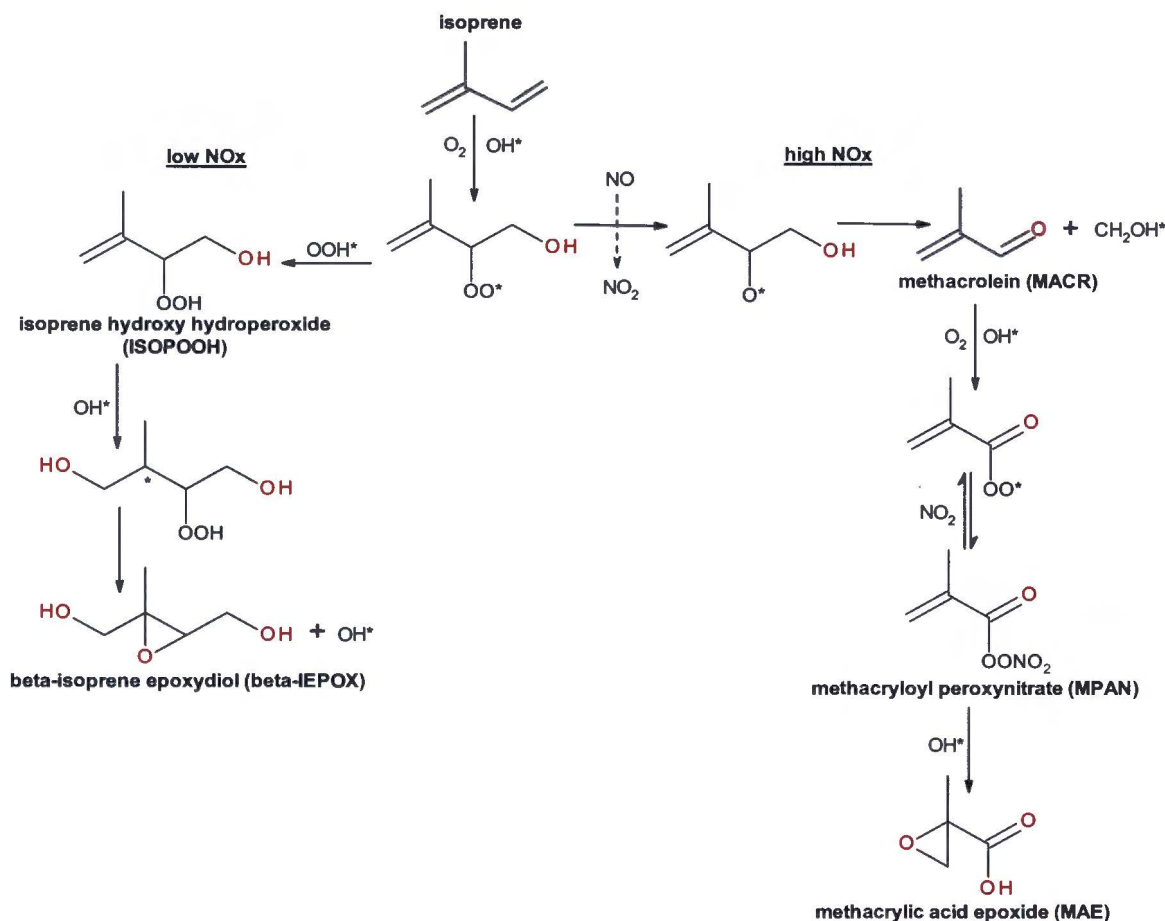
- 1) broad-leaved, e.g., the aspen, the sedge, the oak, the eucalypt, and the willow;
- 2) needle-leaved, e.g., the spruce, the fir, palms, shrubs, vines, and mosses.

ISO emission can occur as a result of plant self-defense against various pollutants. Furthermore, biotic stress (induced by pests and diseases), and abiotic stress (induced by intense solar radiation, low or high temperatures, drought, and strong winds), can trigger its emission (Logan et al., 2000; Sharkey et al., 2008; Penuelas and Staudt, 2010). ISO concentrations measured in forested areas commonly vary between 3–30  $\mu\text{g m}^{-3}$  (Kesselmeier et al., 2002; Sharkey et al., 2008; Guenther et al., 2012). Isoprene is also emitted by marine phytoplankton and seaweeds and detected in ambient air over the oceans (Baker et al., 2000; Matsunaga et al., 2002; Shaw et al., 2003), with its global emission estimated at 1–10 Tg per year (Carlton et al., 2009). Other natural sources of ISO include molds and bacteria (Kuzma et al., 1995; Fall and Copley, 2000), animals, and humans, where the latter can exhale even 4 Tg of isoprene per year (Fenske and Paulson, 1999; Diskin et al., 2003).

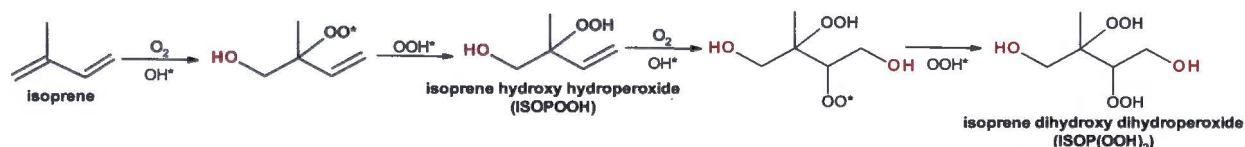
The anthropogenic sources of isoprene include combustion processes and evaporation of fuels in the rural and urban atmosphere (Derwent et al., 1995; McLaren et al., 1996; Borbon et al., 2003). Reimann et al. (2000) proposed that vehicle exhaust can contribute to a significant portion of the anthropogenic emissions of ISO. Previous studies also indicate that the possible anthropogenic sources of isoprene are tobacco smoke, biomass burning, garden wastes, and chemical technology (Wilkins and Larsen, 1996; Leber, 2001; Pouli et al., 2003; Baek and Jenkins, 2004; Gaeggeler et al., 2008).

Isoprene reacts readily with hydroxyl radicals ( $\bullet\text{OH}$ ), nitrate radicals ( $\text{NO}_3\bullet$ ), and ozone ( $\text{O}_3$ ), with typical reaction lifetimes varying from hours to days (1.7 h, 0.8 h, and 1.3 days, respectively; Seinfeld and Pandis, 1998). Previous research provided versatile data on ISO transformations with a wide range of possible gas-phase products reported, e.g., isoprene hydroxy hydroperoxides (ISOPOOH), diols, hydroxycarbonyls, formaldehyde, hydroxyacetone, methyl vinyl ketone (MVK), methacrolein (MACR), 3-methyl furan, various nitrates and dinitrates, glyoxal, methylglyoxal, glycolaldehyde, methacryloyl peroxyxynitrate (MPAN), carbon oxide (CO) and carbon dioxide ( $\text{CO}_2$ )

(Rudzinski, 2004; Carlton et al., 2009; Paulot et al., 2009; Glasius and Goldstein, 2016; Wennberg et al., 2018). **Scheme 2** briefly summarizes ISO oxidation pathways through two intermediate species – methacrylic acid epoxide (MAE) at high-NO<sub>x</sub> conditions and isoprene epoxydiols (IEPOX) at low-NO<sub>x</sub> conditions, while **Scheme 3** presents a recently studied non-IEPOX formation pathway at low-NO<sub>x</sub> conditions through dihydroxy dihydroperoxide ISOP(OOH)<sub>2</sub>.

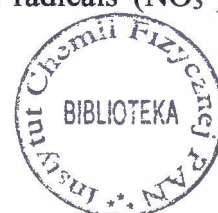


**Scheme 2.** Proposed mechanism for isoprene epoxydiol (IEPOX) and methacrylic acid epoxide (MAE) formation in the gas-phase oxidation of isoprene (adapted from Surrat et al., 2010; Lin et al., 2013; Claeys and Maenhaut, 2021)

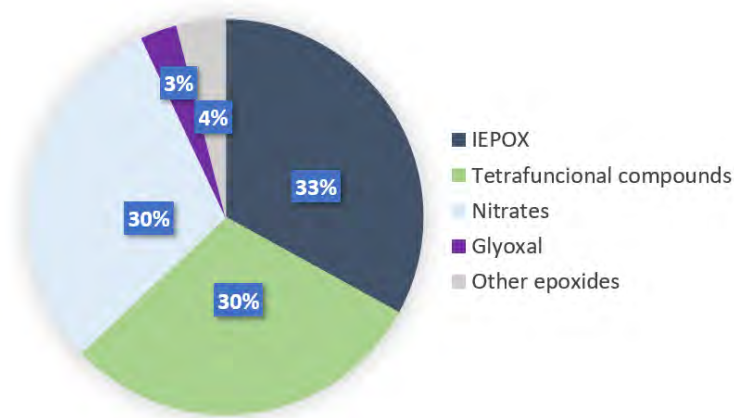


**Scheme 3.** Proposed mechanism for isoprene dihydroxy dihydroperoxide (ISOP(OOH)<sub>2</sub>) formation in the gas-phase oxidation of isoprene (adapted from Riva et al., 2017; D'Ambro et al., 2017)

A comprehensive review of the gas phase oxidation mechanisms of isoprene and its major products, initiated by hydroxyl radicals ( $\cdot\text{OH}$ ), nitrate radicals ( $\text{NO}_3\cdot$ ),



ozone (O<sub>3</sub>), and chlorine atoms (Cl), was developed by Wennberg et al. (2018). The authors present recent laboratory and theoretical studies and provide a nearly complete understanding of ISO chemistry and formation. Moreover, newly proposed ISO oxidation mechanisms have been verified by Bates and Jacob (2019). The authors showed that the computational simulations based on them have atmospherically relevant implications. They pointed out three main ISO reaction pathways in the atmosphere: *via* isoprene epoxydiols (IEPOX), organonitrates, and tetrafunctional C<sub>5</sub>-compounds, e.g. ISOP(OOH)<sub>2</sub> (Liu et al., 2016; D'Ambro et al., 2017; Riva et al., 2017; Bates and Jacob, 2019). Each pathway contributed to approx. 30% of global annual means of ISO SOA (Figure 5).

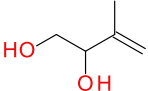
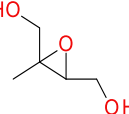
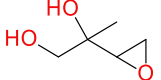


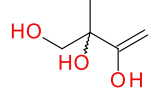
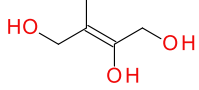
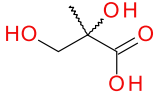


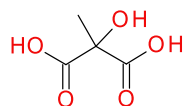
**Figure 5.** Computationally simulated shares of ISO reaction pathways in the atmosphere that form secondary organic aerosol (adapted from Bates and Jacob, 2019)

Since ISO is hardly soluble in water, it hasn't been initially considered a direct precursor of SOA. ISO was thought to participate only in photooxidation processes and not to contribute to atmospheric aerosol (Pandis et al., 1991), despite the study of Went (1960), who first recognized the "blue haze" phenomenon over forested areas and attributed its formation to biogenic VOCs emissions. However, at the beginning of the 2000s, this view had changed with the findings of Pedersen and Sehested (2001), Claeys et al. (2004a,b), and Rudzinski (2004). Pedersen and Sehested (2001) investigated the aqueous-phase reactions of ISO, methyl vinyl ketone (MVK), and methacrolein (MACR) with ozone. Rudzinski (2004) performed ISO aqueous-phase reactions with sulfate radicals. Claeys et al. (2004a,b) identified two isomers of 2-methyltetrols (2-MT; 2-methylthreitol and 2-methylerythritol), 2-methylglyceric acid (2-MGA), and three isomeric C<sub>5</sub>-alkene triols in the field samples collected over the Amazon rainforest in Brazil and a continental K-puszta forest in Hungary. The authors provided

the first field evidence showing that the oxidation products of isoprene contribute to ambient organic aerosol. The studies mentioned above laid the foundations for subsequent isoprene research. Since then, heterogeneous and aqueous-phase reactions have been considered sources of ISO SOA components. Further field and laboratory studies confirmed the presence of various compounds of isoprene SOA (Wang et al., 2004, 2005; Edney et al., 2005; Kourtchev et al., 2005; Kroll et al., 2006; Plewka et al., 2006; Surratt et al., 2006, 2007a, 2008, 2010; Kleindienst et al., 2007; Lewandowski et al., 2008; Szmigielski et al., 2007; Gomez-Gonzalez et al., 2008; Jaoui et al., 2008; Ng et al., 2008; Lukacs et al., 2009; Paulot et al., 2009; Zhang et al., 2012; Shalamzari et al., 2013; Tao et al., 2014; Hettiyadura et al., 2015; Szmigielski, 2016; Nestorowicz et al., 2018; Spolnik et al., 2018; Jaoui et al., 2019; Wach et al., 2020, etc.). This extensive research revealed other SOA components, including various ISO-related organosulfates and nitrooxy-organosulfates, which have been detected in the smog chamber and ambient aerosol samples collected at many sampling sites around the world, including U.S. and Europe. Moreover, diesters formed *via* esterification of two 2-methylglyceric acid residues were characterized in the smog-chamber experiments under high NO<sub>x</sub> conditions and ambient aerosol. Furthermore, aged-SOA markers were identified, i.a. methylthreonic acid (MTrA), methylerythronic acid (MErA), and methyltartaric acid (MTA) with corresponding OSs and NOSs. Plewka et al. (2006), Kleindienst et al. (2007), Lewandowski et al. (2008), Surratt et al. (2008) and Lukacs et al. (2009) indicated that isoprene SOA products reach substantial concentrations in ambient air during the day and summer when the terrestrial emission is enhanced. Those findings emphasize that isoprene is one of the leading precursors of various marker compounds and SOA formation in the atmosphere. ISO oxidation products efficiently partition into the condensed phase and impact the growth of OA in the atmosphere. Therefore, today ISO is considered one of the most important VOCs from the point of view of atmospheric chemistry (Carlton et al., 2009). **Table 3** summarizes the main compounds of isoprene SOA.

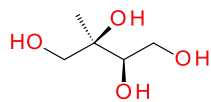
**Table 3:** Summary of the main secondary organic aerosol compounds formed from isoprene

Molecular structures, chemical names and molecular weights (g mol <sup>-1</sup> )	References
 <p>3-methyl-3-butene-1,2-diol MW 102 Da</p>	Wang et al., 2005; Surratt et al., 2006
 <p>2-methyl-2,3-epoxy-but-1,4-diol (beta-IEPOX) MW 118 Da</p>	Paulot et al., 2009; Surratt et al., 2010; Zhang et al., 2012
 <p>2-methyl-3,4-epoxy-but-1,2-diol (delta-IEPOX) MW 118 Da</p>	
 <p>3-methyltetrahydrofuran-3,4-diol MW 118 Da</p>	Zhang et al., 2012
 <p>2-methyl-1,3,4-trihydroxybut-1-ene (C<sub>5</sub>-alkene triols) MW 118 Da</p>	
 <p>3-methyl-2,3,4-trihydroxybut-1-ene (C<sub>5</sub>-alkene triol) MW 118 Da</p>	Claeys et al., 2004b; Wang et al., 2005; Ion et al., 2005; Kourtchev et al., 2005; Surratt et al., 2006, 2010; Cui et al., 2018
 <p>3-methyl-2,3,4-trihydroxybut-1-ene (C<sub>5</sub>-alkene triol) MW 118 Da</p>	
 <p>2-methylglyceric acid (2-MG) MW 120 Da</p>	Claeys et al., 2004b; Edney et al., 2005; Ion et al., 2005; Surratt et al., 2006; Kourtchev et al., 2008; Lin et al., 2013; Nestorowicz et al., 2018



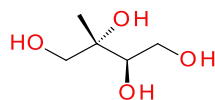
2-methyltartronic acid  
(2-MTrA)  
**MW 134 Da**

Jaoui et al., 2019

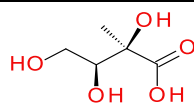


2-methylthreitol  
**MW 136 Da**

Claeys et al., 2004a; Wang et al., 2004;  
Edney et al., 2005; Surratt et al., 2006, 2010;  
Noziere et al., 2011; Nestorowicz et al., 2018

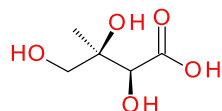


2-methylerythritol  
**MW 136 Da**

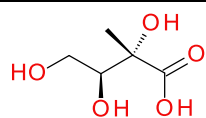


2-methylthreonic acid  
(2-MTrA)  
**MW 150 Da**

Jaoui et al., 2019

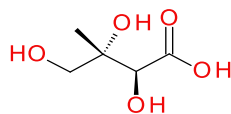


3-methylthreonic acid  
(3-MTrA)  
**MW 150 Da**

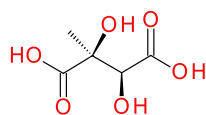


2-methylerythronic acid  
(2-MErA)  
**MW 150 Da**

Jaoui et al., 2019



3-methylerythronic acid  
(3-MErA)  
**MW 150 Da**

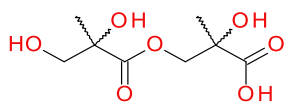


2-methyltartaric acid  
(2-MTA)  
**MW 164 Da**

Jaoui et al., 2019

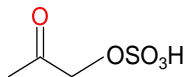
---





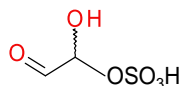
2-methylglyceric acid dimer  
MW 222 Da

Surratt et al., 2006



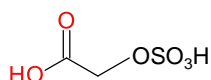
hydroxyacetone organosulfate  
MW 154 Da

Schindelka et al., 2013



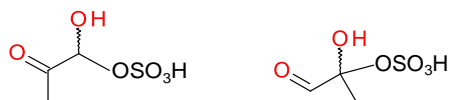
glyoxal organosulfate  
MW 156 Da

Liggio et al., 2005; Surratt et al., 2007a, 2008;  
Gomez-Gonzalez et al., 2008;  
Shalamzari et al., 2013; Nguyen et al., 2014



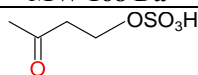
glycolic acid organosulfate  
MW 156 Da

Gomez-Gonzalez et al., 2008;  
Olson et al., 2011; Shalamzari et al., 2013;  
Chen et al., 2020



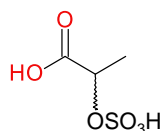
methylglyoxal organosulfate  
MW 168 Da

Liggio et al., 2005; Surratt et al., 2007a, 2008;  
Gomez-Gonzalez et al., 2008



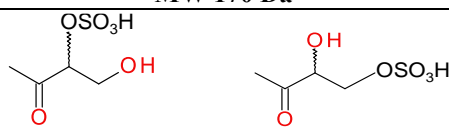
1-hydroxybutane-3-one organosulfate  
MW 168 Da

Schindelka et al., 2013; Shalamzari et al., 2013



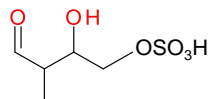
lactic acid organosulfate  
MW 170 Da

Olson et al., 2011; Shalamzari et al., 2013



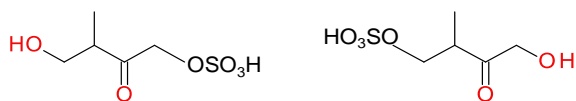
3,4-dihydroxybutan-2-one organosulfate  
MW 184 Da

Schindelka et al., 2013; Shalamzari et al., 2013;  
Hettiyadura et al., 2015; Riva et al., 2016b



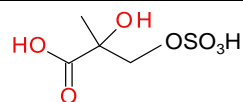
IEPOX-derived organosulfate  
MW 198 Da

Tao et al., 2014



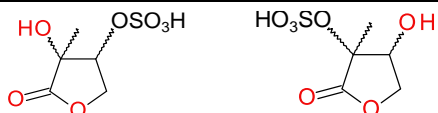
C<sub>5</sub>-alkene triols organosulfate  
MW 198 Da

Riva et al., 2016b



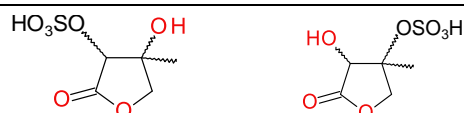
2-methylglyceric acid organosulfate  
(2-MG OS)\*  
MW 200 Da

Surratt et al., 2007a; Gomez-Gonzalez et al., 2008; Lin et al., 2013; Schindelka et al., 2013; Shalamzari et al., 2013; Hettiyadura et al., 2015; Nestorowicz et al., 2018; Chen et al., 2020

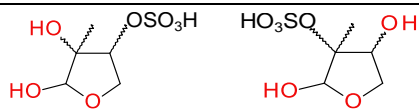


2(3H)-furanone, dihydro-3,4-dihydroxy-3-methyl organosulfate  
MW 212 Da

Hettiyadura et al., 2015;  
Nestorowicz et al., 2018; Spolnik et al., 2018,  
Chen et al., 2020; Wach et al., 2020

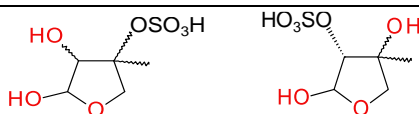


2(3H)-furanone, dihydro-3,4-dihydroxy-4-methyl organosulfate  
MW 212 Da



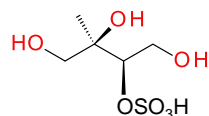
2,3,4-furantriol, tetrahydro-3-methyl organosulfate  
MW 214 Da

Hettiyadura et al., 2015;  
Nestorowicz et al., 2018; Spolnik et al., 2018;  
Chen et al., 2020



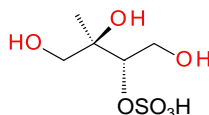
2,3,4-furantriol, tetrahydro-4-methyl organosulfate  
MW 214 Da

Hettiyadura et al., 2015;  
Nestorowicz et al., 2018; Spolnik et al., 2018;  
Chen et al., 2020

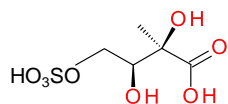


2-methylthreitol organosulfate  
(2-MT OS)\*  
MW 216 Da

Surratt et al., 2007a, 2008, 2010;  
Gomez-Gonzalez et al., 2008;  
Riva et al., 2016b; Nestorowicz et al., 2018;  
Spolnik et al., 2018

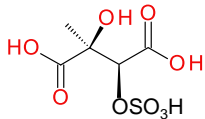
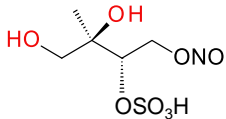
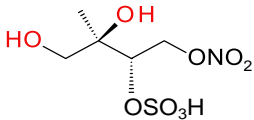
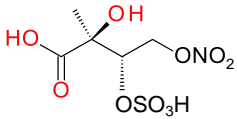
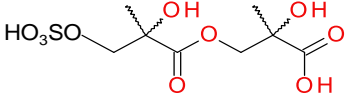


2-methylerythritol organosulfate  
(2-MT OS)\*  
MW 216 Da



2-methylthreonic acid organosulfate  
(2-MTrA OS)\*  
MW 230 Da

Nestorowicz et al., 2018

 <p>2-methyltartaric acid organosulfate (2-MTA OS)* <b>MW 244 Da</b></p>	Nestorowicz et al., 2018
 <p>2-methyltetrol nitrosooxy-organosulfate (2-MT NSOS)* <b>MW 245 Da</b></p>	Nestorowicz et al., 2018
 <p>2-methyltetrol nitrooxy-organosulfate (2-MT NOS)* <b>MW 261 Da</b></p>	Surratt et al., 2007a, 2008; Gomez-Gonzalez et al., 2008; Nestorowicz et al., 2018
 <p>2-methylthreonic acid nitrooxy-organosulfate (2-MTrA NOS)* <b>MW 275 Da</b></p>	Nestorowicz et al., 2018
 <p>2-methylglyceric acid dimer organosulfate <b>MW 306 Da</b></p>	Surratt et al., 2008

\* one representative isomer was shown

This thesis explores the findings on ISO SOA formation and its chemical composition under various relative humidity (RH) conditions in smog-chamber experiments. It provides novel insights into the formation of ISO-related organosulfates (OSs), nitrooxy-organosulfates (NOSs), nitrosooxy-organosulfates (NSOSs), and highly oxygenated organic acids, which were not reported previously. Moreover, the smog-chamber findings were compared with ambient aerosol.

### 1.1.2.2 Butadiene SOA

Anthropogenic precursors emitted in urban and industrial areas significantly influence the formation of atmospheric aerosol. 1,3-Butadiene (buta-1,3-diene, C<sub>4</sub>H<sub>6</sub>, 13BD) is an important anthropogenic organic compound released to the atmosphere through industrial processing of petroleum for synthetic rubber, resins and plastics production, automobile exhausts and gasoline emissions, tobacco smoke, and biomass combustion (Eatough et al., 1990; Penn and Snyder, 1996; Sorsa et al., 1996;

Thornton-Manning et al., 1997; Ye et al., 1998; Dollard et al., 2001; Pankow et al., 2004; Anttinen-Klemetti et al., 2006; Berndt and Boge, 2007, Hurst, 2007). Except the areas near petrochemical plants, vehicle exhausts is the dominant source of 1,3-butadiene emissions (HEI report, 2007). 13BD can also have biogenic origin as it is occasionally released during forest fires (Curren et al., 2006).

13BD is hazardous according to the Clean Air Act Amendments (CAAA; U.S. EPA report, 1996), carcinogenic, toxic, mutagenic, and genotoxic in humans and other mammals (Acquavella, 1996; Hughes and IPCS, 2001; U.S. EPA report, 2002; IARC monographs, 2012). Moreover, U.S. EPA demonstrated that 1,3-butadiene emitted with vehicle exhausts significantly induces the risk of lung cancer (Amodio et al., 2013). The global annual emission of 13BD to the atmosphere reaches 6 million tons (Berndt and Boge, 2007) and contributes to atmospheric SOA, especially in urban areas. Therefore, its concentration in urban air should be monitored. There are little literature data on 13BD levels in the urban atmosphere of Europe. However, the reported concentrations ranged between 2 and 20  $\mu\text{g m}^{-3}$  (WHO guideline, 2005). Moreover, a mean 1,3-butadiene concentration of 0.1–6.9  $\mu\text{g m}^{-3}$  was reported for ambient air samples collected in U.S. cities in the late 80' (U.S. EPA report, 1989). In Canada, 13BD concentrations in ambient air were up to 14.1  $\mu\text{g m}^{-3}$  (Bell et al., 1991). Nonetheless, Curren et al. (2006) observed that 13BD levels in selected cities of Canada decreased substantially between the years 1995 – 2003. The annual mean concentrations ranged from 0.05 to 0.92  $\mu\text{g m}^{-3}$ , with the highest level of 2.58  $\mu\text{g m}^{-3}$ . Dollard et al. (2007) showed that 1,3-butadiene concentrations measured in Great Britain's rural areas, urban non-industrialized, industrialized urban areas, and regions of high-traffic highways between the years 1993 and 2004 were significantly reduced in all assessed places.

According to the European Chemicals Agency (ECHA) registration, the production volume of 13BD ranges from 1 million to even 10 million tons per year. In Poland, 13BD is produced by the following companies: Henkel Polska Sp. z o.o. (Warsaw), Polski Koncern Naftowy ORLEN SA (Płock), Synthos Dwory 7 Sp. z o.o., sp. j. (Oświęcim), and Tire Company Dębica SA (Dębica) (Kilanowicz et al., 2018). Therefore, air quality monitoring should include concentrations of this compound in ambient air. Unfortunately, 13BD is not commonly monitored in Poland's rural and urban atmosphere. Only the regional background monitoring station in Zielonka (Bory Tucholskie) measured 1,3-butadiene concentrations in ambient air (Kozakiewicz, 2021). The mean concentrations of 13BD determined in 2020 were

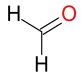
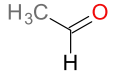
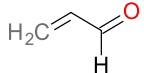
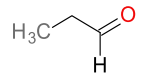
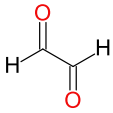
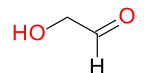
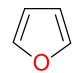
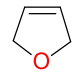
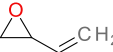
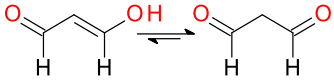
between 0.04 and 5.89  $\mu\text{g m}^{-3}$ . The maximum level of 13BD was observed during the summer period and explained by the local anthropogenic emissions or the influx of polluted air masses from remote areas (Kozakiewicz, 2021).

13BD has high reactivity and a short lifetime. It reacts in the atmosphere with hydroxyl radicals ( $\bullet\text{OH}$ ), nitrate radicals ( $\text{NO}_3\bullet$ ), ozone ( $\text{O}_3$ ), and chlorine atoms ( $\text{Cl}$ ) and transforms into many potentially toxic compounds, like acrolein and formaldehyde, according to the CAAA (Notario et al., 1997; Liu et al., 1999; Kramp and Paulson, 2000; Doyle et al., 2004; Angove et al., 2006; Sakurai et al., 2013). The dominant atmospheric reactions of 13BD during daytime and nighttime are reactions with hydroxyl and nitrate radicals, respectively (Stutz et al., 2010). Some products of those reactions have been identified in ambient air (Feltham et al., 2000; Doyle et al., 2004; Baker et al., 2005; Fu et al., 2008a). The most abundant and significant gas-phase products observed during 13BD photooxidation in smog chambers or flow reactors were formaldehyde and acrolein, and these compounds were identified in the studies of Liu et al. (1999), Kramp and Paulson (2000), Berndt and Boge (2007) and Jaoui et al. (2014). Liu et al. (1999) investigated the gas-phase products of 13BD oxidation with hydroxyl radicals ( $\bullet\text{OH}$ ) and ozone ( $\text{O}_3$ ). Beside the main components – formaldehyde and acrolein, the authors reported also glycolaldehyde, glyceraldehyde, 3-hydroxy-propanaldehyde, hydroxyacetone, and malonaldehyde. Berndt and Boge (2007) among products of hydroxyl radicals reactions with 13BD detected 4-hydroxy-2-butanal, nitrates, and furan. Moreover, well-known 1,3-BD degradation products are: 1,2-epoxy-3-butene (1,3-butadiene monoxide), 1,2,3,4-diepoxybutane (1,3-butadiene diepoxide), propanal, 2,5-dihydrofuran, CO, and CO<sub>2</sub> (Jenkin et al., 1998; Liu et al., 1999; Baker et al., 2005; Vallecillos et al., 2019). Previous research significantly advanced characterization of 13BD oxidation products and their role in SOA formation (Liu et al., 1999; Kramp and Paulson, 2000; Angove et al., 2006; Berndt and Boge, 2007; Sato, 2008; Sato et al., 2011; Jaoui et al., 2014). Nevertheless, 13BD SOA composition has not been fully characterized. To date, only a few smog chamber studies focused on 13BD SOA formation (Angove et al., 2006; Sato, 2008; Sato et al., 2011; Jaoui et al., 2014), while the effects of aerosol acidity and relative humidity were investigated solely by Lewandowski et al. (2015) and Ren et al. (2016). Angove et al. (2006) identified 18 components of 1,3-butadiene SOA, including formic acid, glyceric acid, glycolic acid, glyoxal, glyoxalic acid, threose, erythrose, erythritol, threitol, which represented 75–80% of total SOA mass. Sato (2008) photooxidized a 13BD/NO/CH<sub>3</sub>ONO/air mixture

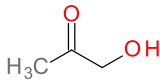
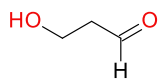
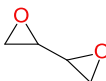
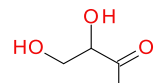
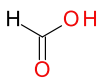
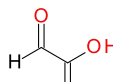
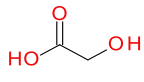
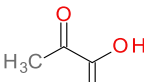
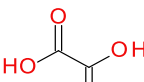
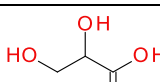
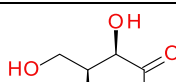
and detected nitric acid, glyoxylic acid, pyruvic acid, oxalic acid, tetrols, nitrooxy-butanetriols and dinitrooxy-butanediols in SOA formed. Sato et al. (2011) studied SOA formation from 13BD/NO<sub>x</sub> and 13BD/NO<sub>x</sub>/H<sub>2</sub>O<sub>2</sub> and tentatively identified some oligomeric compounds like glyceric acid oligomers. Jaoui et al. (2014) investigated gas- and particle-phase organic products from 13BD photooxidation experiments in the presence and absence of NO<sub>x</sub>. The main purpose was the identification of possible markers of ambient aerosol originating from 13BD. Those authors used GC-MS derivatization and non-derivatization techniques to reveal around 60 oxygenated organic compounds in gas and particle phases and tentatively identified 31 of them. Oxygenated compounds such as threitol, erythritol, glyceric acid, malic acid, tartaric acid, and threonic acid were detected in both smog-chamber experiments and ambient aerosol samples. The authors estimated the contribution of 13BD to organic aerosol in ambient PM<sub>2.5</sub> fraction by using the GC-MS method reported by Kleindienst et al. (2007). They also proposed a possible mechanism of 13BD SOA formation in the gas phase involving two intermediate species – acrylic acid epoxide (AAE) at high-NO<sub>x</sub> conditions and 2,3-epoxy-1,4-butanediol (BEPOX) at low-NO<sub>x</sub> conditions (**Scheme 4**). Both compounds, e.g., BEPOX and AAE, can react in the particle phase and form SOA components. Moreover, polyols with C<sub>4</sub>-skeleton have high water solubility and can act as endogenous aerosol seeds and contribute to cloud formation (Angove et al., 2006; Ekstrom et al., 2009). Notably, the mechanism of 13BD reactions in the gas phase corresponds to that proposed previously for isoprene (see Chapter 1.1.3, Scheme 2). The mechanisms are similar because ISO and 13BD are homologs and conjugated dienes.

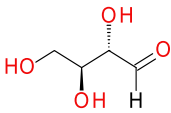
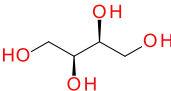
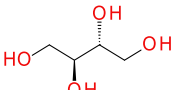
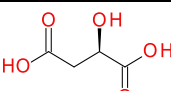
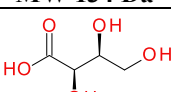
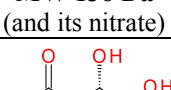
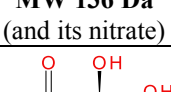
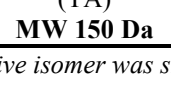


**Table 5:** Summary of the main gas- and particle-phase components formed from 1,3-butadiene

Molecular structures, chemical names, and molecular weights (g mol <sup>-1</sup> )	References
 Formaldehyde <b>MW 30 Da</b>	Grosjean et al., 1994; Liu et al., 1999; Kramp and Paulson, 2000; Angove et al., 2006; Berndt and Boge, 2007; Jaoui et al., 2014
 Acetaldehyde <b>MW 44 Da</b>	Grosjean et al., 1994; Jaoui et al., 2014; Vallecillos et al., 2019
 Acrolein <b>MW 56 Da</b>	Grosjean et al., 1994; Liu et al., 1999; Kramp and Paulson, 2000; ; Baker et al., 2005; Berndt and Boge, 2007; Jaoui et al., 2014; Vallecillos et al., 2019
 Propanal <b>MW 58 Da</b>	Grosjean et al., 1994; Vallecillos et al., 2019
 Glyoxal <b>MW 58 Da</b>	Grosjean et al., 1994; Liu et al., 1999; Angove et al., 2006; Jaoui et al., 2014
 Glycolaldehyde <b>MW 60 Da</b>	Liu et al., 1999; ; Baker et al., 2005; Angove et al., 2006; Jaoui et al., 2014
 Furan <b>MW 68 Da</b>	Berndt and Boge, 2007; Vallecillos et al., 2019
 2,5-Dihydrofuran <b>MW 70 Da</b>	Kramp and Paulson, 2000; Vallecillos et al., 2019
 13BD monoxide <b>MW 70 Da</b>	Jenkin et al., 1998; Kramp and Paulson, 2000; Vallecillos et al., 2019
 Malondialdehyde <b>MW 72 Da</b>	Liu et al., 1999; Angove et al., 2006; Jaoui et al., 2014



 Hydroxyacetone <b>MW 74 Da</b>	Liu et al., 1999
 3-hydroxy-propanaldehyde <b>MW 74 Da</b>	Liu et al., 1999; Jaoui et al., 2014
 13BD diepoxide <b>MW 86 Da</b>	Jenkin et al., 1998; Kramp and Paulson, 2000; Vallecillos et al., 2019
 Glyceraldehyde <b>MW 90 Da</b>	Liu et al., 1999; Angove et al., 2006; Jaoui et al., 2014
 Formic acid <b>MW 46 Da</b>	Angove et al., 2006
 Glyoxalic acid <b>MW 74 Da</b>	Angove et al., 2006; Sato, 2008; Jaoui et al., 2014
 Glycolic acid <b>MW 76 Da</b>	Angove et al., 2006; Jaoui et al., 2014
 Pyruvic acid <b>MW 88 Da</b>	Sato, 2008
 Oxalic acid <b>MW 90 Da</b>	Sato, 2008; Jaoui et al., 2014
 Glyceric acid (GA) <b>MW 106 Da</b>	Angove et al., 2006; Sato, 2008; Jaoui et al., 2014;
 	Angove et al., 2006; Jaoui et al., 2014; Jaoui, Nestorowicz et al., 2023, submitted

<p>Threose* MW 120 Da</p> 	<p>Angove et al., 2006; Jaoui et al., 2014; Jaoui, Nestorowicz et al., 2023, submitted</p>
<p>Erythrose* MW 120 Da</p> 	<p>Angove et al., 2006; Sato, 2008; Jaoui et al., 2014; Jaoui, Nestorowicz et al., 2023, submitted</p>
<p>Threitol* MW 122 Da (and its nitrate and dinitrate)</p> 	<p>Angove et al., 2006; Sato, 2008; Jaoui et al., 2014; Jaoui, Nestorowicz et al., 2023, submitted</p>
<p>Erythritol* MW 122 Da (and its nitrate and dinitrate)</p> 	<p>Angove et al., 2006; Sato, 2008; Jaoui et al., 2014; Jaoui, Nestorowicz et al., 2023, submitted</p>
<p>Malic acid* (MA) MW 134 Da</p> 	<p>Jaoui et al., 2014; Jaoui, Nestorowicz et al., 2023, submitted</p>
<p>Threonic acid* (TrA) MW 136 Da (and its nitrate)</p> 	<p>Angove et al., 2006; Jaoui et al., 2014; Jaoui, Nestorowicz et al., 2023, submitted</p>
<p>Erythronic acid* MW 136 Da (and its nitrate)</p> 	<p>Angove et al., 2006; Jaoui et al., 2014; Jaoui, Nestorowicz et al., 2023, submitted</p>
<p>Tartaric acid* (TA) MW 150 Da</p> 	<p>Jaoui et al., 2014; Jaoui, Nestorowicz et al., 2023, submitted</p>

\* one representative isomer was shown

13BD SOA formation should be thoroughly investigated since its components may affect human health. Degradation products, such as acrolein, formaldehyde, acetaldehyde, and furan, can cause severe adverse effects in humans (Doyle et al., 2004; Woodruff et al., 2007; Golden and Holm, 2017). Moreover, 1,2-epoxy-3-butene (1,3-butadiene monoxide) and 1,2,3,4-diepoxybutane (1,3-butadiene diepoxide) are

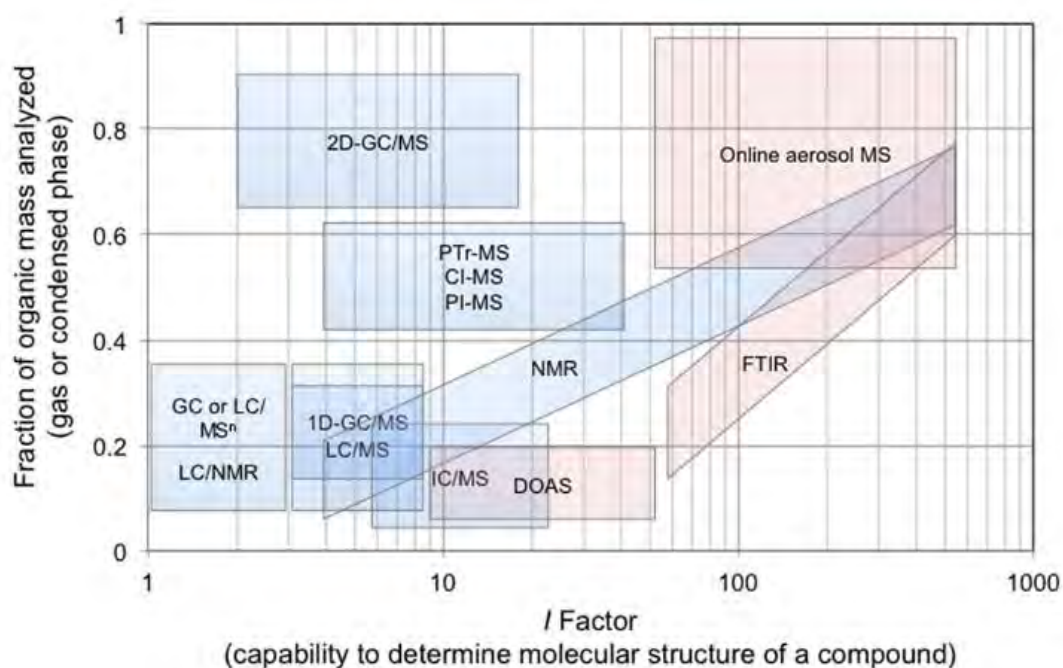
found to be even more carcinogenic than 13BD itself (Kramp and Paulson, 2000). For this reason, determining 13BD SOA composition with the detailed chemistry of 13BD is necessary for air quality modeling at local, regional, and even global scales.

This thesis explores the findings on 13BD SOA formation and its chemical composition under various RH conditions. It provides novel insights into the formation of 13BD-related organosulfates (OSs), nitrooxy-organosulfates (NOSs), and nitrosooxy-organosulfates (NSOSs), which were not previously reported. Moreover, the smog chamber findings were compared with ambient aerosol.

## **1.2 Analytical techniques for determining the chemical composition of atmospheric aerosol**

The chemical analysis of the atmospheric aerosol composition has been a challenge facing researchers. In general, *off-line* and *on-line* techniques are distinguished. *Off-line* techniques based on advanced instrumentation include gas chromatography coupled with mass spectrometry (GC-MS; Wang et al., 2005; Surratt et al., 2006; Jaoui et al., 2014), liquid chromatography coupled with mass spectrometry (LC-MS; Surratt et al., 2006, 2007a; Shalamzari et al., 2013; Riva et al., 2016b; Nestorowicz et al., 2018; Spolnik et al., 2018; Jaoui et al., 2019), Fourier transform infrared spectroscopy (FTIR; Dangler et al., 1987; Gaffney et al., 2015; Reggente et al., 2019) or nuclear magnetic resonance (NMR; Finessi et al., 2012; Zanca et al., 2017). They characterize individual organic compounds and their functional groups. However, those techniques require tedious and often time-consuming sample preparation. *On-line* techniques, including chemical ionization mass spectrometry (CI-MS; Hearn et al., 2004; Zuth et al., 2018; D'Ambro et al., 2019; Chen et al., 2020), proton transfer ionization mass spectrometry (PTR-MS; Hanse et al., 1999; Schilling et al., 2013; Yuan et al., 2012, 2013), and aerosol mass spectrometry (AMS; Surratt et al., 2006; Nash et al., 2006; Schilling et al., 2013; Chen et al., 2020; Fang et al., 2021), provide less detailed information on the aerosol composition. However, they register the composition changes in real-time by tracking diagnostic fragment ions and provide data on particle chemistry, short timescales (Jimenez et al., 2009; Pratt and Prather, 2012b; Canonaco et al., 2013; Johnston and Kerecman, 2019). Therefore, *on-line* techniques are widely used in smog chamber systems. Furthermore, simple GC-FID and GC-MS techniques can be used as *on-line* under smog-chamber experiments (Yuan et al., 2012, 2013).

Noziere et al. (2015) compared the *on-line* and *off-line* analytical techniques used to characterize atmospheric organic compounds. The techniques were described with an *I* factor, denoting their ability to elucidate the compound's molecular structure (x-axis; the *I* factor decreases with the increasing power of structure identification). **Figure 6** shows that coupling mass spectrometry with chromatographic tools significantly decreases the *I* factor.



**Figure 6.** Comparison of analytical techniques used for determining the atmospheric organic compounds based on their *I* factor (Noziere et al., 2015)

In my research, the chemical composition of ISO and 13BD SOA was analyzed with an *off-line* technique – ultrahigh-performance liquid chromatography coupled with high-resolution mass spectrometry (UPLC–HRMS). Therefore, Chapter 1.2.1 briefly describes *off-line* techniques used in SOA analyses, emphasizing LC-MS.

### 1.2.1 Off-line techniques

Nowadays, the environmental chemistry community widely uses hyphenated *off-line* techniques. The determination of AA composition is based mostly on two principal hyphenated techniques – gas chromatography and liquid chromatography coupled with mass spectrometry. They have been widely used to identify and determine the components of gas-phase samples and various aerosol matrices, including water, hail, snow, and particles (Surrat et al., 2008; Pratt and Prather, 2012a; Jaoui et al., 2014; Lewandowski et al., 2015; Riva et al., 2016b; Nestorowicz et al., 2018; Spolnik et al.,

2020; Wach et al., 2020; Jaoui, Nestorowicz et al., 2023, submitted). The choice of a particular analytical technique depends on the type of matrix and the chemical structure of the compounds investigated. The appropriate sampling, extraction technique, sample preparation, and operating conditions of the apparatus significantly impact the results obtained. Therefore, the effectiveness of analyses must be carefully controlled at each stage, from sampling to concluding. The most common example of the possible impact is the solvent-analyte reactions, which should be considered when interpreting mass spectra. Detailed information is presented in Chapter 1.2.1.1.

Currently, GC–MS and LC–MS techniques for determining AA components are complementary, as they enable recognizing different groups of atmospheric aerosol components. GC–MS technique is preferred for oxygenated, volatile compounds as it provides high sensitivity, significant separation efficiency, and proper signal-to-noise ratio (S/N). LC–MS technique is essential for characterizing polar, non-volatile, and/or thermally labile molecules that do not elute or appear in GC–MS even after derivatization. Initial reports on the LC–ESI–MS technique with reverse-phase columns and a single quadrupole analyzer revealed a complex distribution of atmospheric aerosol composition with many nominal masses, indicating the presence of isomeric and/or isobaric compounds (Gao et al., 2006; Surratt et al., 2006; Pratt and Prather, 2012a; Johnston and Kerecman, 2019). Subsequent high-resolution mass measurements allowed to distinguish isobaric compounds and confirm their molecular structures, enabling quantitative analyses based on surrogate or authentic standards. Incorporating Time-of-Flight high-resolution mass spectrometry (TOF–HRMS) empowered identifying more of unknown organic species (Hallquist et al., 2009; Pratt and Prather, 2012a; Johnston and Kerecman, 2019). This improvement of the LC-MS technique over the years resulted in better SOA identification and elucidation of possible formation pathways (Pratt and Prather, 2012a). Most significantly, ESI(-) HRMS measurements with MS<sup>n</sup> experiments provided better speciation of SOA samples, including detailed structural information on components.

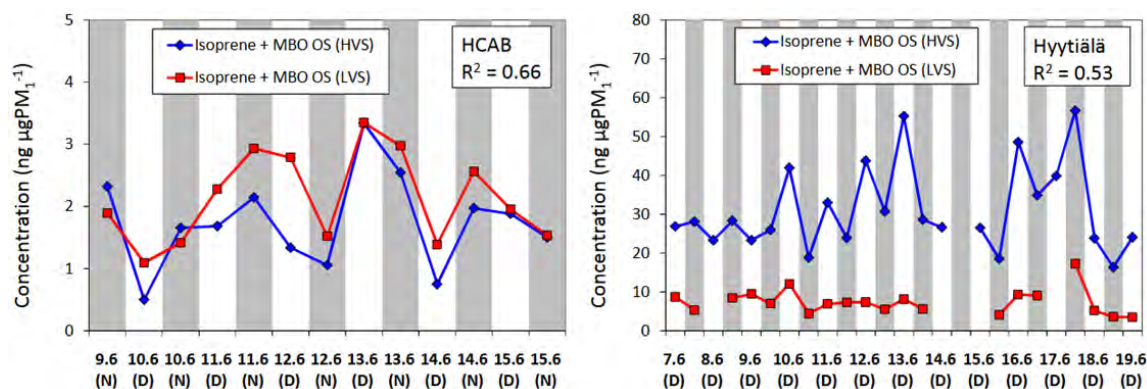
### **1.2.1.1 Sample preparation**

Sample preparation is a critical step in the atmospheric aerosol *off-line* analysis. The appropriate preparation and extraction procedures largely affect the results of chemical analyses.

Field studies and laboratory experiments commonly use filters (like quartz-fiber filters and Teflon filters) to collect aerosol particles for subsequent analyses. Inappropriate aerosol collection may lead to serious artifacts. There are two major types of artifacts (JRC report, 2009; Brüggemann et al., 2020):

1) a “positive” artifact when the filters adsorb VOCs; hence, it was shown that sulfur dioxide (SO<sub>2</sub>) and semivolatile organics might adsorb onto the filter surface and increase organosulfates formation through heterogeneous reactions,

2) a “negative” artifact when collected semivolatile components evaporate from filters. Therefore, samplers that collect AA must efficiently separate gas-phase and particle-phase species (Mutzel et al., 2015; Kristensen et al., 2016). Kristensen et al. (2016) compared the concentrations of ISO- and MBO-derived (2-methyl-3-buten-2-ol) organosulfates in organic aerosol collected with two types of samplers – LVS (low-volume filter/denuder sampler) and HVS (high-volume sampler). Field samples were collected onto quartz-fiber filters in two European countries – Denmark and Finland. The results obtained are presented in **Figure 7**.



**Figure 7.** Temporal variations of OSs identified in the day- and nighttime (grey highlight) filter samples collected by HVS (♦) and LVS denuder/filter system (■) at HCAB (H.C. Andersen's 168 Boulevard) Copenhagen, Denmark, and Hyytiälä, Finland (Kristensen et al., 2016)

Estimated concentrations of OSs differed significantly depending on the sampling site. However, the results were ambiguous and depended on the sampler type – in HCAB, the concentrations obtained with two samplers varied much less than in Hyytiälä, where the HVS results were even five times larger than LVS. The authors suggested that the differences resulted from the adsorption of gaseous organosulfate precursors (alcohols and epoxides) followed by their sulfation on the filter surface (Kristensen et al., 2016).

Various SOA compounds require specific analytical methods. The extraction solvent or a mixture of solvents should correspond to the SOA components investigated

and provide the highest extraction efficiency. SOA collected onto the filters is usually extracted with methanol, acetonitrile, Milli-Q water, or dichloromethane. Solvents can be used individually or in mixtures of various ratios. One of the most common solvents is methanol. However, methanol can react with aldehyde and ketone groups of the sample components, resulting in the formation of hemiacetals (Smith et al., 2009). It can respond with carboxylic moieties of aerosol components and form methyl esters, which may lead to the loss of the quantified species (e.g., carboxylic acids) and increase the uncertainty of the analysis (Bateman et al., 2008; Kristensen and Glasius, 2011). Moreover, Olson et al. (2011) have also shown that methanol can convert carboxy-organosulfates to methyl esters and should be avoided in quantitative analysis of those species. Despite the shortcomings, methanol is still successfully used as an extraction solvent in SOA qualitative and quantitative measurements (Zhang et al., 2012; Riva et al., 2016b; Gallimore et al., 2017; Zhou et al., 2018; Kristensen et al., 2020; Kolodziejczyk, 2020; Wach et al., 2020; Khan, 2021; Shao et al., 2022).

To date, there is no single recommended procedure for SOA sample preparation. Researchers develop their methods based on knowledge, experience, and practice. For instance, previous studies have reported that ultrasonication of filter samples can degrade AA organic constituents due to the OH radical formation, which is the atmosphere's primary oxidant. Ultrasonication can catalyze or induce various chemical reactions and change the composition of material collected for analysis (Riesz et al., 1985; Briggs, 1990; Jacobson et al., 2000; Mutzel et al., 2013; Miljevic et al., 2014). Some researchers still use ultrasonication as an extraction technique for sensitive SOA components (Hettiyadura et al., 2015; Kristensen et al., 2016; Kristensen et al., 2020). However, using organic-rich extraction solvents can minimize the risk of possible degradation processes and the formation of artifacts (Hettiyadura et al., 2015). Another extraction technique often used is Soxhlet extraction. It can be efficiently applied to persistent compounds like PAHs (Rudzinski et al., 2022). However, it involves heating and refluxing the solvent, so it may cause degradation of thermolabile analytes and should be avoided in analyses of sensitive SOA compounds. Recently orbital shaking has been recommended as a gentle extraction technique for AA samples (Jacobson et al., 2000; Bruggemann et al., 2020).

After the extraction, filter extracts usually require evaporation to dryness in a rotary evaporator or under a gentle stream of inert gas, like nitrogen. Fleming et al. (2019) demonstrated that evaporation of highly acidic filter extracts to dryness might

produce organosulfates as artifacts. They suggested monitoring the pH value of prepared filter extracts and avoiding evaporating them to dryness when pH is below 3.

Summarizing, SOA sample preparation is a demanding and important step responsible for obtaining reliable and repeatable results.

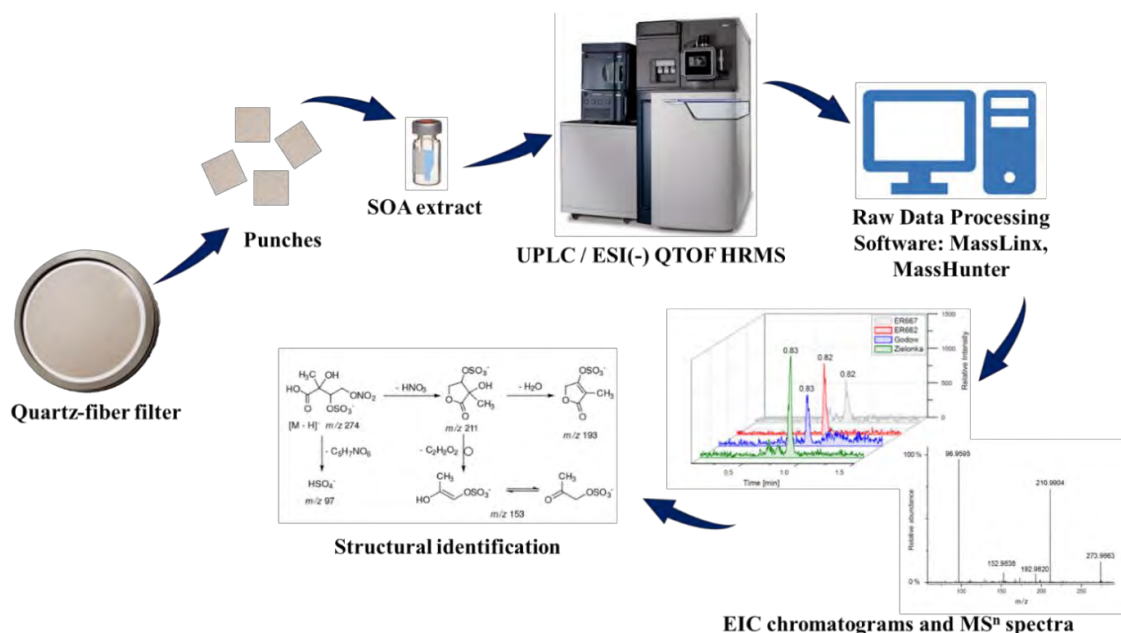
#### **1.2.1.2 Liquid chromatography coupled with mass spectrometry (LC-MS)**

Liquid chromatography (LC) is an analytical technique used to separate and detect organic compounds. Mass spectrometry (MS) is an instrumental method in which the mass of charged species produced is measured (Niessen, 2007). The advantage of coupling LC with MS is combining the separation and high-resolution identification. The sample is introduced onto a chromatographic column using a dosing system, where it is transferred by a mobile phase delivered by a high-pressure pump system (Alloway and Ayres, 1999; Niessen, 2007). A mobile phase is a mixture of water and organic solvents, like methanol, acetonitrile, and organic buffers. The components of the mixture analyzed interact with the mobile phase and the stationary phase of the chromatographic column and undergo separation due to different degrees of affinity. The retention time of individual components of the mixture depends on the conditions under which the analysis is carried out, including the mobile phase flow rate, gradient elution program, and temperature (Namiesnik and Jamrogiewicz, 1998). The outlet of the chromatographic column is introduced directly into the ion source of the mass spectrometer, which acts as a detector. There, the organic analytes are ionized. Depending on the ionization method and mechanism, only specific types of ions may arise (Płaziak, 1997; De Hoffman and Stroobant, 2007; Silverstein et al., 2008). The ion sources coupled to the LC system operate at atmospheric pressure and include atmospheric pressure chemical ionization (APCI) sources and, more often, electrospray ionization (ESI) sources. In the ESI source, the solution from the column is nebulized to charged ultrafine droplets by the high voltage applied between the capillary and the counter electrode. The solvent evaporates from the droplets with the ionized compound, while the charge accumulation leads to Coulomb explosions and finally to the formation of single ions. In the positive polarization mode, protonated ions ( $[M+H]^+$ ) and adduct ions, like sodium ions ( $[M+Na]^+$ ) or potassium ions ( $[M+K]^+$ ) are formed, while in the negative polarization mode, deprotonated ions ( $[M-H]^-$ ) occur (Namiesnik and Jamrogiewicz, 1998; Johnstone and Rose, 2001; Rohner et al., 2004; Polettoni, 2006; De Hoffmann and Stroobant, 2007; Silverstein et al., 2008). These ions



are focused into a beam by a gap system, accelerated in an electric field, and introduced into the mass analyzer, which separates them based on the mass to charge ( $m/z$ ) ratio. The most common mass analyzers in the LC–MS systems are Time-of-Flight analyzers (TOFs), triple-quadrupoles, and ion traps. The mass analyzer scans all ions across the specified range of the  $m/z$  ratios or isolates ions with selected  $m/z$  values (Niessen, 2007; Silverstein et al., 2008). It records a chromatogram, i.e., a plot of the total ion current (TIC) as a function of time, and mass spectra at preset time intervals, i.e., plots of the intensity of individual ions as a function of  $m/z$  at running time (Namiesnik and Jamrogiewicz, 1998; Niessen, 2007). The raw data recorded can be processed so that the extracted ion current (EIC) chromatograms for selected  $m/z$  values can be accessed and investigated. Moreover, collision-induced dissociation experiments (fragmentation of individual ions) can be carried out to obtain product ion mass spectra ( $MS^2$ ), which significantly improve the identification of investigated compounds. Based on the fragmentation patterns, the molecular structures of analytes can be resolved.

One of my research goals was to identify new compounds formed from ISO and 13BD in smog-chamber experiments and detected in ambient aerosol samples, including the components containing sulfate moieties, like organosulfates (OSs). OSs account for 5–30% of the organic mass fraction in  $PM_{10}$  (Surratt et al., 2008; Tolocka and Turpin, 2012; Shakya and Peltier, 2015). Most commonly, reversed-phase liquid chromatography (RPLC) has been used for the separation, identification, and quantification of organosulfates (Surratt et al., 2007a; Gomez-Gonzalez et al., 2008; Riva et al., 2016b; Nestorowicz et al., 2018; Spolnik et al., 2018; Bruggemann et al., 2019; Bruggemann et al., 2020; Spolnik et al., 2020; Wach et al., 2020). However, in the past few years, successful efforts have been made to use the hydrophilic interaction liquid chromatography (HILIC) instead of RPLC, which appeared effective in separating polar OSs (Hettiyadura et al., 2015, 2017, 2019; Cui et al., 2019; Bruggemann et al., 2020). **Figure 8** shows the simplified LC–MS *off-line* analytical procedure used, for instance, for organosulfates detection (detailed description in Chapter 2.1.4 – 2.1.7).



**Figure 8.** Scheme of a simplified off-line LC-MS analytical procedure

In this thesis, SOA components were detected in smog chamber samples and in ambient aerosol samples using UPLC / ESI(-) HRMS technique to show the consistency between laboratory and field SOA composition.

### 1.3 Objectives of thesis

As reviewed in the preceding sections, the formation of secondary organic aerosol (SOA) in the atmosphere may adversely impact air quality and, thus, contribute to climate changes and deterioration of human health. The understanding of highly complex chemical processes is a key research objective in atmospheric aerosol chemistry. In my thesis, I investigated the chemical composition of SOA formed from two different aerosol precursors – isoprene (2-methylbuta-1,3-diene, ISO) and buta-1,3-diene (13BD) – using UPLC–MS techniques. The analyses were carried out to characterize novel components in SOA samples – precursor tracers and aging products – and to assess the influence of relative humidity (RH) and particle acidity on their formation. The thesis addresses four major goals:

- 1) detailed identification of ISO SOA products in the smog-chamber experiments and ambient aerosol focused on new polar aged SOA tracers like organosulfates, nitroxy-organosulfates, nitrosooxy-organosulfates, and hydroxycarboxylic acids**

The aim was to identify new SOA components formed from isoprene. I compared samples from ISO smog-chamber experiments to ambient aerosol samples collected in

various regions of Poland with strong biogenic (Diabla Góra, Zielonka) and mixed biogenic-anthropogenic (Godów, Kaskada) emissions. Particular attention was paid to the identification of novel ISO tracers – highly oxygenated molecules (HOMs), which give molecular evidence for SOA aging in the atmosphere. ISO-derived hydroxycarboxylic acids, and their organosulfates (OSs) and nitroxy-organosulfates (NOSs) were identified through the analysis of smog chamber and field samples. The novel findings on ISO SOA chemical composition were published in Nestorowicz et al. (2018) and Jaoui et al. (2019) papers.

## **2) detailed identification of 13BD SOA products in samples from smog-chamber experiments and ambient aerosol samples, focused on new polar aged SOA tracers like organosulfates, nitrooxy-organosulfates, nitrosooxy-organosulfates, and hydroxycarboxylic acids**

This thesis provides novel insights into the chemical composition of 1,3-butadiene SOA. 13BD SOA components can significantly contribute to continental aerosol masses. Some components, e.g., tartronic acid, threonic acid, tartaric acid, and a few OSs, were detected in ambient aerosol samples collected at various sites in Poland with strong biogenic (Diabla Góra, Zielonka) and mixed biogenic-anthropogenic (Godów, Kaskada) emissions. While the SOA-bound hydroxycarboxylic acids formed from 13BD were reported in the literature (Jaoui et al., 2014), several organosulfates, nitrooxy-organosulfates, nitrosooxy-organosulfates from 13BD were detected for the first time. Their tentative structural elucidation was based on high-resolution product ion mass spectra. Those novel results are included in Jaoui, Nestorowicz et al. (2023, submitted).

## **3) the investigation of ISO and 13BD SOA formation in the smog-chamber experiments under various RH and acidity conditions by quantitative UPLC-MS technique**

This thesis refers to Lewandowski et al. (2015) and expands the explanation of the impact of relative humidity and aerosol acidity on 13BD and ISO SOA formation. Those authors conducted ISO and 13BD smog-chamber photochemical experiments across ranges of relative humidity and aerosol acidity. They demonstrated that increasing relative humidity caused a substantial reduction in secondary organic carbon (SOC) yields from ISO and 13BD. Both compounds produced higher SOA yields under acidic conditions. Based on Lewandowski et al. (2015), I carefully assumed that the homologous 13BD and ISO undergo similar physicochemical processes in the atmosphere. This thesis aimed to investigate the role of relative humidity (RH) on the formation of individual

components of SOA under acidic and non-acidic conditions in high-  $\text{NO}_x$  smog-chamber experiments, where a high level of  $\text{NO}_x$  in the system mimicked highly polluted atmosphere. The RH influence on ISO and 13BD SOA formation was presented in Nestorowicz et al. (2018) and Jaoui, Nestorowicz et al. (2023, submitted).

#### **4) the chemical characterization of several field samples targeted to ISO and 13BD SOA tracers by quantitative high-resolution UPLC-MS technique**

The last assignment in this thesis was to determine the concentrations of detected ISO and 13BD SOA components in field samples. The results were presented against the meteorological data for the sampling periods and compared with the results obtained for smog-chamber samples and available literature data.

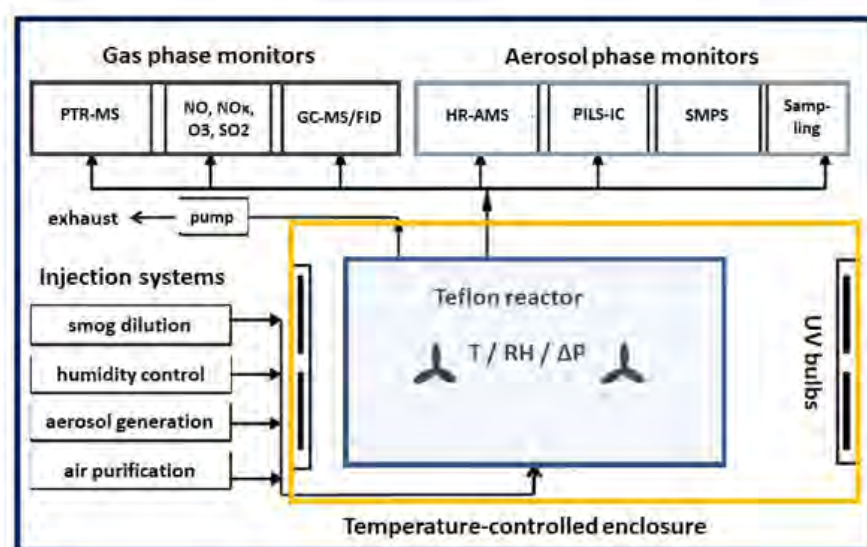
This thesis provides novel insights into SOA formation from two different aerosol precursors – isoprene and 1,3-butadiene. I have identified new products and determined the influence of RH and particle acidity on the formation of individual components. These studies may contribute to the further development of acidity-dependent SOA chemistry in air quality models.

## 2. Experimental

### 2.1. Methodology and materials

#### 2.1.1 Smog-chamber experiments

The main aim of smog-chamber experiments is to get insights into the formation and transformation mechanisms of the ambient aerosol under simplified conditions for better interpretation of experimental results. Smog-chamber experiments in precisely controlled environments explain the chemistry and transformation of SOA formed from single aerosol precursors, like isoprene,  $\alpha$ -pinene, or 1,3-butadiene (Dommen et al., 2006; Surratt et al., 2007a; Claeys et al., 2004, 2007; Szmigielski et al., 2007, 2010; Nguyen et al., 2011; Zhang et al., 2011; Lewandowski et al., 2015; Riva et al., 2016a, 2017; Nestorowicz et al., 2018; Jaoui et al., 2014, 2019). They reveal the chemical composition of secondary particles formed and allow the identification of new products connected with specific precursors and chemical mechanism. Ambient SOA is a complex mixture formed *via* complicated chemical pathways influenced by many factors such as weather, meteorology, air mass flows, and geographical location. Specific products identified in ambient samples point to SOA precursors and chemical pathways involved in its formation in the atmosphere. The results presented in this thesis are based on smog-chamber experiments carried out in collaboration with the U.S. Environmental Protection Agency (U.S. EPA). **Figure 9** shows a simplified scheme of a smog chamber, and **Figure 10** shows the photo of the U.S. EPA indoor smog-chamber system used for the experiments.



**Figure 9.** Scheme of a typical smog chamber system with on-line monitors for gas- and particle- phase measurements (adapted from Wang et al., 2014)

The U.S. EPA smog chamber is a 14.5 m<sup>3</sup> fixed-volume stainless-steel chamber. The interior walls were fused with a 40 µm PTFE Teflon coating. A combination of UV-fluorescent bulbs (300 to 400 nm) was used in the chamber as a source of radiation similar to solar radiation (Black et al., 1998; Kleindienst et al., 2006). The chamber was operated as a flow reactor with a 4 h residence time under steady-state conditions with constant aerosol distribution at pre-defined relative humidity levels and seed aerosol acidities. Two sets of isoprene/NO and butadiene/NO experiments were performed, each for two different acidities of the seed aerosol (neutral and acidic). Each set involved several stages between which the humidity level was systematically varied (**Tables 6A, 6B, and 7A, 7B**). The temperature in all experiments was kept constant between 22–28 °C. Isoprene and butadiene were obtained from Sigma-Aldrich Chemical Co. (Milwaukee, WI, USA) at the highest purity and used without further purification.



**Figure 10.** U.S. EPA indoor smog-chamber system, Research Triangle Park, North Carolina

Isoprene, butadiene, and nitrogen oxide (NO) were drawn from high-pressure cylinders and diluted with N<sub>2</sub>. The reactants were added through flow controllers into the inlet manifold, where they were diluted and mixed prior to the introduction into the chamber. For the non-acidic seed experiments with isoprene (ER667) and butadiene (ER666), the seed aerosol was prepared from ammonium sulfate solutions. For the acidic-seed experiments with isoprene (ER662) and butadiene (ER444), the seed aerosol was prepared from solutions containing equal masses of ammonium sulfate and sulfuric acid (H<sub>2</sub>SO<sub>4</sub>). Dilute aqueous solutions of ammonium sulfate, and sulfuric acid were nebulized

(TSI nebulizer, model 9302, Shoreville, MN) into the chamber as inorganic seed aerosol, with total sulfate concentration held constant to maintain stable concentrations of inorganics in the smog chamber (Lewandowski et al., 2015). The seed aerosol stream passed through a  $^{85}\text{Kr}$  neutralizer (TSI, Model 3077, Shoreville, MN) and was equilibrated at the relative humidity chosen for a particular experiment and controlled by a computer-operated system. NO, and total NO<sub>x</sub> were measured with a Thermo Electron NO<sub>x</sub> analyzer (Model 8840, Thermo Environmental, Inc., Franklin, MA, USA). Ozone formed during the irradiation was measured with a Bendix ozone monitor (Model 8002, Lewisburg, WV, USA). Temperature and relative humidity were measured with an Omega Digital Thermo-Hygrometer (Model RH411, Omega Engineering, Inc., Stamford, CT, USA). Isoprene and butadiene concentrations were measured *on-line* by gas chromatography coupled with flame ionization detection (GC-FID; Hewlett-Packard, Model 5890 GC). Chamber aerosol samples were collected on 47 mm diameter glass-fiber filters with an active surface of 17.341 cm<sup>2</sup> (Pall Gelman Laboratory, Ann Arbor, MI, USA) for 24 h at the flow rates of 16.7 L min<sup>-1</sup> or 15 L min<sup>-1</sup> in ISO and 13BD experiments, respectively. In all cases, aerosol was collected after the steady-state condition was achieved.

The concentration of secondary organic carbon (SOC) was the corrected organic carbon yield (Carbon yield), and  $\Delta\text{HC}$  was the reacted hydrocarbon mass concentration (see equation 2 in Chapter 1.1.2).

#### 2.1.1.1 Isoprene SOA

The non-acidic experiment (ER667, **Table 6A**) was conducted in the presence of ISO, NO<sub>x</sub>, and ammonium sulfate as seed aerosol (1  $\mu\text{g m}^{-3}$ ) at five different humidity levels (9%, 19%, 30%, 39%, and 49%). It served as a base for exploring the changes and nature of SOA products in the absence of significant aerosol acidity. The acidic experiment (ER662, **Table 6B**) was similar but performed in the presence of acidic seed aerosol at four relative humidity levels (8%, 18%, 28%, and 44%). The acidic experiments were conducted with inorganic seeds generated from a nebulized solution for which half of the sulfate mass was derived from sulfuric acid and the other half from ammonium sulfate ( $\frac{1}{2}$  sulfuric acid, and  $\frac{1}{2}$  ammonium sulfate; Lewandowski et al., 2015).

**Table 6A.** Initial conditions and steady-state reactant concentrations in smog-chamber experiments on isoprene photooxidation in the presence of non-acidic seed aerosol (Nestorowicz et al., 2018)

Experiment ER667: Non-acidic seed aerosol (ammonium sulfate)					
	Stage 1	Stage 2	Stage 3	Stage 4	Stage 5
RH (%)	9	19	30	39	49
Temperature (°C)	28.2	28.5	27.9	27.8	27.6
Initial ISO (ppmC)	8.11	8.29	8.25	8.25	8.19
Initial NO (ppm)	0.347	0.347	0.347	0.347	0.347
Steady-state concentrations and yields					
O <sub>3</sub> (ppm)	0.331	0.305	0.329	0.393	0.281
NO <sub>x</sub> (ppm)	0.260	0.247	0.241	0.229	0.226
ΔHC (μg m <sup>-3</sup> )	3518	3556	3558	3515	3484
Carbon Yield	0.004	0.002	0.001	0.001	0.001
SOC (μgC m <sup>-3</sup> )	13.3	7.7	4.6	3.2	3.5

**Table 6B.** Initial conditions and steady-state reactant concentrations in smog-chamber experiments on isoprene photooxidation in the presence of acidic seed aerosol (ER662) and observed carbon yields (Nestorowicz et al., 2018)

Experiment ER662: Acidic seed aerosol (½ ammonium sulfate, ½ sulfuric acid)				
	Stage 1	Stage 2	Stage 3	Stage 4
RH (%)	8	28	44	18
Temperature (°C)	27.0	27.3	26.9	27.5
Initial Isoprene (ppmC)	6.82	6.92	7.01	7.03
Initial NO (ppm)	0.296	0.296	0.296	0.296
Steady-state concentrations and yields				
O <sub>3</sub> (ppm)	0.303	0.292	0.245	0.339
NO <sub>x</sub> (ppm)	0.220	0.213	0.205	0.234
ΔHC (μg m <sup>-3</sup> )	3266	3318	3357	3472
Carbon Yield	0.011	0.003	0.001	0.005
SOC (μgC m <sup>-3</sup> )	32.3	7.9	3.8	15.7



### 2.1.1.2 Butadiene SOA

The non-acidic experiment (ER666; **Table 7A**) was conducted in the presence of butadiene, NO<sub>x</sub>, and ammonium sulfate as seed aerosol (1 μg m<sup>-3</sup>) at six different humidity levels (11%, 20%, 29%, 39%, 49%, and 62%). The acidic experiment (ER444; **Table 7B**) was similar but performed in the presence of acidic seed aerosol at four different relative humidity levels (10%, 31%, 50%, and 62%). The acidic experiments were conducted with inorganic seed generated from a nebulized solution for which two-thirds of the sulfate mass was derived from sulfuric acid and the other one-third from ammonium sulfate (1/3 sulfuric acid, and 2/3 ammonium sulfate; Lewandowski et al., 2015).

**Table 7A.** Initial conditions and steady-state reactant concentrations in smog-chamber experiments on butadiene photooxidation in the presence of non-acidic seed aerosol (ER666) and observed carbon yields (Jaoui, Nestorowicz et al., 2023, submitted)

Experiment ER666: Non-acidic seed aerosol (ammonium sulfate)						
	Stage 1	Stage 2	Stage 3	Stage 4	Stage 5	Stage 6
RH (%)	11	20	29	39	49	60
Temperature (°C)	25.3	25.3	25.1	24.7	25.0	24.7
Initial Isoprene (ppmC)	7.00	7.00	7.09	7.14	7.11	7.13
Initial NO (ppm)	-	-	0.408	-	-	-
Steady-state concentrations and yields						
O <sub>3</sub> (ppm)	0.327	0.314	0.307	0.290	0.273	0.254
NO <sub>x</sub> (ppm)	0.242	0.252	0.239	0.231	0.227	0.226
ΔHC (μg m <sup>-3</sup> )	3099	3077	3085	3030	2968	2917
Carbon Yield	0.016	0.015	0.013	0.010	0.010	0.010
SOC (μgC m <sup>-3</sup> )	45.1	40.9	34.7	27.0	26.4	24.7

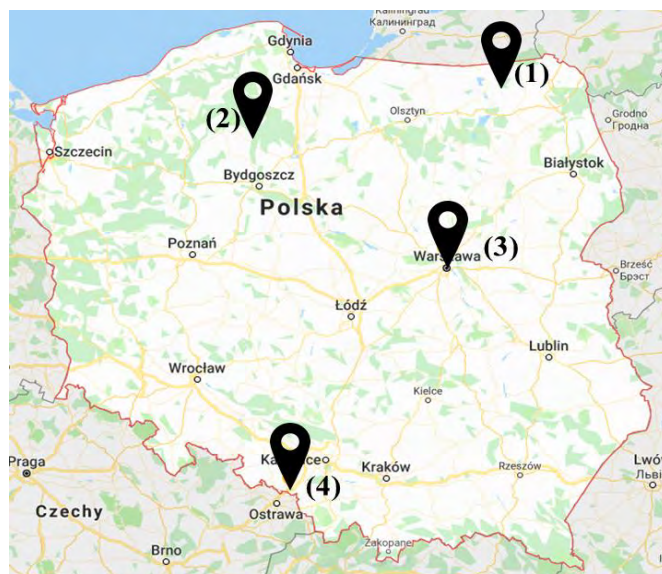
**Table 7B.** Initial conditions and steady-state reactant concentrations in smog-chamber experiments on butadiene photooxidation in the presence of acidic seed aerosol (ER444) and observed carbon yields (Jaoui, Nestorowicz et al., 2023, submitted)

Experiment ER444: Acidic seed aerosol ( $\frac{1}{3}$ ammonium sulfate, $\frac{2}{3}$ sulfuric acid)				
	Stage 1	Stage 2	Stage 3	Stage 4
RH (%)	10	31	50	62
Temperature (°C)	22.4	22.6	22.2	22.2
Initial Isoprene (ppmC)	6.88	7.02	6.81	6.92
Initial NO (ppm)	0.313	-	0.73	-
Steady-state concentrations and yields				
O <sub>3</sub> (ppm)	0.313	0.259	0.256	0.242
NO <sub>x</sub> (ppm)	0.168	0.150	0.129	0.117
$\Delta$ HC ( $\mu\text{g m}^{-3}$ )	2842	2848	2640	2611
Carbon Yield	0.024	0.016	0.014	0.013
SOC ( $\mu\text{gC m}^{-3}$ )	60.3	41.6	33.7	31.1

### 2.1.2 Ambient aerosol samples

Twenty ambient PM<sub>2.5</sub> samples were collected onto prebaked quartz-fiber filters using high-volume aerosol samplers (DHA-80, Digitel) at four sampling sites (5 filters from each) that have strong biogenic or anthropogenic emissions (**Figure 11**):

- 1) a regional suburban monitoring station in Godów, located in the Silesian Province in southern Poland (49°55'18''N 18°28'16''E) in the summer 2014 campaign,
- 2) a regional background monitoring station in Diabla Góra, in the Warmia-Masurian Province in northern Poland (54°07'33''N, 22°02'39''E), during the summer 2016 campaign,
- 3) a regional background monitoring station in Zielonka, in the Kuyavian-Pomeranian Province in northern Poland (53°39'44''N, 17°56'05''E), during the summer 2016 campaign,
- 4) the Kaskada city park, Warsaw, Poland, located in the Mazovia Province (52°16'25''N, 20°58'20''E) in the summer 2018 campaign.



**Figure 11.** Map of Poland with locations of the monitoring sites where aerosol samples were collected: (1) Diabla Góra, (2) Zielonka, (3) Kaskada, (4) Godów (<https://www.google.pl/maps/@52.1169345,18.2001338,7z/data=!4m2!1m1!3e4>)

Diabla Góra monitoring station belongs to the Institute of Environmental Protection – National Research Institute in Warsaw, Poland. The station is located in Puszcza Borecka, a large forest complex with deciduous stands and a significant admixture of spruce. Forests and agriculture surround the station: around 53% are forests, 20% arable land, 13% are meadows and pastures, and 6% wasteland. In the vicinity of the station there are a single-family residential complex heated by wood-burning oven.

Zielonka sampling station belongs to the Chief Inspectorate of Environmental Protection, Poland, and is surrounded by the Bory Tucholskie complex, which is a fresh mixed coniferous forest. The main tree species are pines, with a slight admixture of birch and spruce. The undergrowth is primarily black cherry, oak, spruce, linden, hazel, and juniper. Near the station, there is a single-family residential complex heated by wood-burning oven.

Kaskada sampling station is located within Warsaw city, close to the small city park and a frequently used freeway. Therefore, aerosol samples collected in Kaskada are strongly influenced by anthropogenic sources, especially vehicle exhausts.

Godów sampling site belongs to the Chief Inspectorate of Environmental Protection, Poland. It is situated near a coal-fired power station in Detmarovice (Czech Republic) and about 60 km South-West of the major industrial cities of the Silesian region in Poland, which hosts many coal mines and steelworks. Thus, the aerosol samples collected in Godów are strongly influenced by anthropogenic sources.

Ambient air quality measurements at the sampling sites in Poland are regulated by the Regulation of the Minister of Environment *on the evaluation of levels of substances in ambient air* from 2018 (Regulation, 2018). According to this regulation, the permissible annual PM<sub>2.5</sub> fraction level has been specified at 25 µg m<sup>-3</sup>. However, according to the updated WHO guideline (WHO guideline, 2021), the annual average concentrations of PM<sub>2.5</sub> should be narrowed to 5 µg m<sup>-3</sup>. **Table 8** presents the mean concentration of fine fraction during the years the samples were collected for this work.

**Table 8:** *The annual mean concentration of PM<sub>2.5</sub> at the selected sampling sites (data source – Państwowy Monitoring Środowiska; <https://powietrze.gios.gov.pl/>)*

Sampling site (year)	The annual mean concentration of PM <sub>2.5</sub>	
	µg m <sup>-3</sup>	Percent of the WHO recommendation
Diabla Góra (2016)	11.5	230%
Zielonka (2016)	12.2	244%
Warszawa (2018)	24.8	496%
Godów (2014)	40.0	800%

Meteorological data (temperature, relative humidity, atmospheric pressure, and solar radiation) and several chemical and physical parameters (e.g., SO<sub>2</sub>, NO<sub>x</sub>, NO<sub>2</sub>, and O<sub>3</sub> concentrations) measured at the sampling sites are presented in **Tables 9** and **10**. Generally, during the sampling periods of interest, the relative humidity levels ranged between 44.5 – 100%. The highest RH level occurred in Zielonka; however, the highest mean RH value during investigated period has been noted in Godów at 82.5%. The average temperature during sampling was around 22°C, except for Godów, where temperatures were below 15°C. All locations were influenced by nitrogen oxides (NO<sub>x</sub>) – weakly in Zielonka and Diabla Góra, where the mean levels observed were 2.1 µg m<sup>-3</sup> and 2.7 µg m<sup>-3</sup>, respectively, whereas highly at Kaskada and Godów, where the mean levels were 39.9 µg m<sup>-3</sup> and 22.0 µg m<sup>-3</sup>, respectively. The mean SO<sub>2</sub> levels ranged from 0.3 µg m<sup>-3</sup> at Diabla Góra to 3.5 µg m<sup>-3</sup> at Godów. The mean NO<sub>2</sub> levels were small in Zielonka and Diabla Góra – 1.6 µg m<sup>-3</sup> and 2.4 µg m<sup>-3</sup>, respectively, and considerable in Kaskada and Godów – 22.5 µg m<sup>-3</sup> and 16.6 µg m<sup>-3</sup>, respectively.

**Table 9: Meteorological data at the sampling sites**

Sampling site	Sample name	Mean temperature (°C)	Mean relative humidity (%)	Mean atmospheric pressure (hPa)	Mean solar radiation (W/m <sup>2</sup> )
Godów*	Godów_1	11.8	76.0		59.1
	Godów_2	11.3	94.5		24.7
	Godów_3	11.2	94.5	no data	43.2
	Godów_4	12.9	76.2		50.7
	Godów_5	14.2	71.4		57.2
Diabla Góra	B017	23.4	60.4	996.0	505.7
	B018	17.9	85.0	995.5	31.0
	B019	24.7	59.0	993.8	548.4
	B020	19.7	72.3	994.0	23.9
	B021	24.5	58.8	994.0	466.9
Zielonka	L022	24.6	65.0	1000.2	414.8
	L023	21.5	78.3	999.7	21.2
	L024	25.1	64.5	999.8	355.0
	L025	19.3	100.0	1001.3	18.0
	L026	23.5	70.9	1000.4	388.8
Kaskada**	K8043	24.3	66.3	997.9	
	K8044	19.3	86.8	998.9	
	K8045	24.8	51.3	999.0	no data
	K8046	18.4	80.9	998.2	
	K8047	26.4	44.9	997.9	

\* data provided by the nearest monitoring station at Żywiec, Poland (<http://powietrze.katowice.wios.gov.pl/archiwalne-dane-pomiarowe>)

\*\* data provided by the nearest monitoring station at Kondratowicza Street, Warsaw, Poland (adapted from <http://powietrze.gios.gov.pl>)

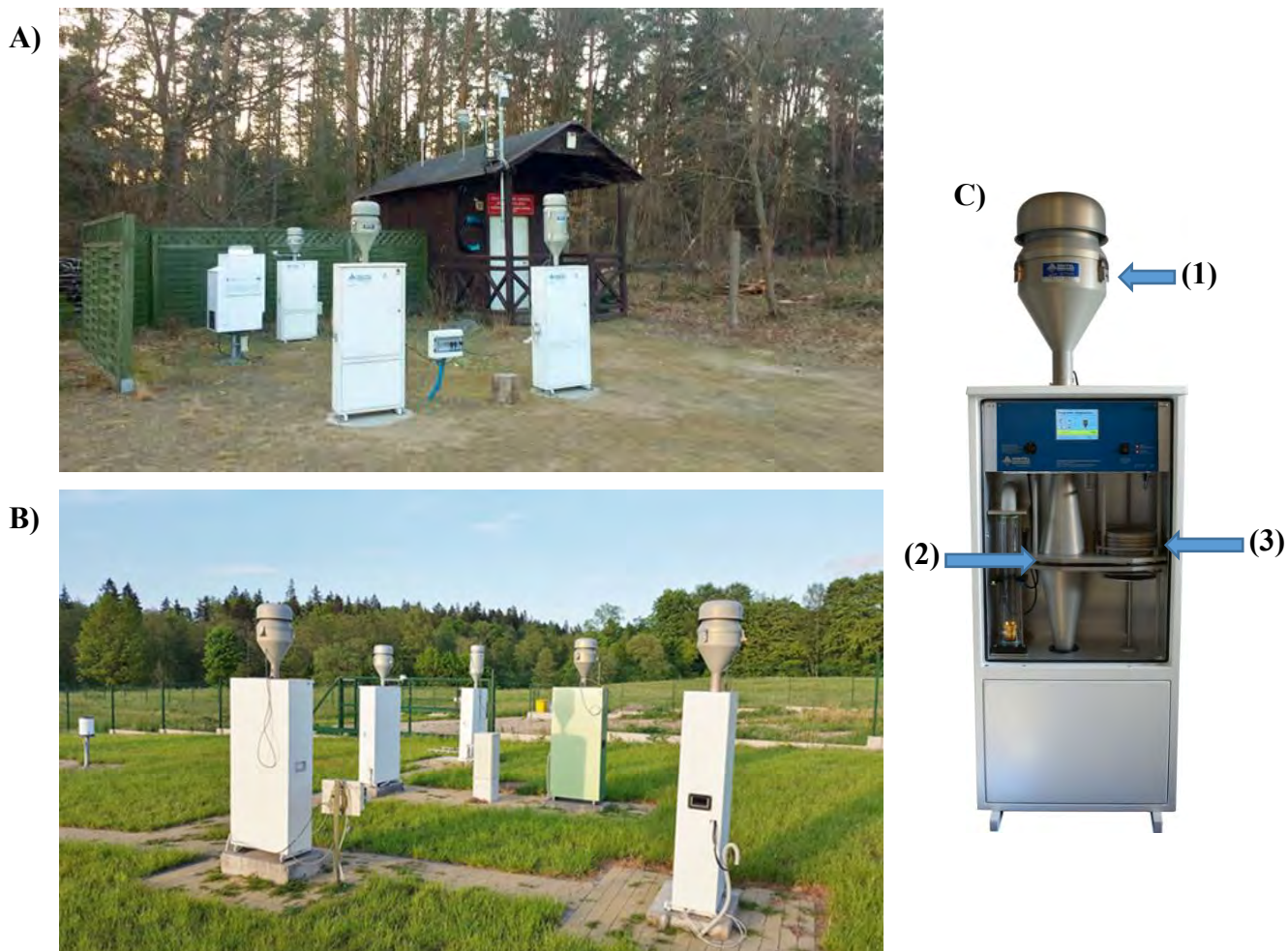
**Table 10:** Concentrations of air pollutants at the sampling sites

Sampling site	Sample name	SO <sub>2</sub> (µg m <sup>-3</sup> )	NO <sub>x</sub> (µg m <sup>-3</sup> )	NO <sub>2</sub> (µg m <sup>-3</sup> )	O <sub>3</sub> (µg m <sup>-3</sup> )
Godów*	Godów_1	5.0	17	15	50
	Godów_2	3.0	25	22	36
	Godów_3	3.0	19	12	41
	Godów_4	4.0	32	20	38
	Godów_5	5.0	17	14	65
Diabla Góra	B017	0.4	2.5	2.2	83.1
	B018	0.4	2.2	2.0	49.1
	B019	0.3	2.4	2.0	85.2
	B020	0.2	3.1	3.0	76.5
	B021	0.3	3.0	2.6	83.5
Zielonka	L022	1.1	1.5	1.1	65.2
	L023	1.4	3.0	2.3	49.7
	L024	1.0	2.0	1.3	70.8
	L025	0.6	2.5	1.9	26.3
	L026	0.8	1.7	1.3	66.2
Kaskada**	K8043	1.1	17.1	13.1	63.4
	K8044	0.6	34.4	29.8	28.8
	K8045	2.5	11.3	9.6	86.1
	K8046	1.7	124.1	49.9	15.1
	K8047	1.5	12.6	10.3	101.8

\* data provided by the nearest monitoring station at Wodzisław Śląski, Poland (adapted from <http://powietrze.gios.gov.pl>)

\*\* data provided by the nearest monitoring station at Kondratowicza Street, Warsaw, Poland (adapted from <http://powietrze.gios.gov.pl>)

**Figure 12** shows the regional background monitoring stations in Zielonka (A) and Diabla Góra (B), and a DHA-80 Digitel sampler used for aerosol collection (C). Depending on the separating head used, the DHA-80 sampler enabled precise sampling of particulate matter fractions – PM<sub>10</sub>, PM<sub>2.5</sub>, or PM<sub>1</sub>. I collected the PM<sub>2.5</sub> fraction. The air is drawn through the head (1), where the undesired aerosol fraction is cut off. The air flows into the chamber (2) and through a 15 cm quartz-fiber filter (3) on which the particles are deposited. After a sample collection, a filter containing the PM<sub>2.5</sub> fraction was wrapped in prebaked aluminum foil, packed in polyethylene (PE) bags, and stored in a deep freezer at –22°C before further analyses.



**Figure 12.** A) Zielonka monitoring station, B) Diabla Góra monitoring station, C) High-volume aerosol sampler DHA-80, Digitel (<http://www.digital-ag.com/de/en/products/high-volume-sampler-en/dha-80/>)

Quartz-fiber filters with an active surface area specified at 153.938 cm<sup>2</sup> (Whatman® QM-A quartz filters, WHA1851150, Sigma-Aldrich) were used for aerosol collection at all sites. The sampling time was 12 h, except 24 h in Godów. The sampling characteristics are summarized in **Table 11**.

**Table 11:** Sampling characteristics of the ambient aerosol collection

Sampling site	Sample name	Date	Sampling time (h)	Total airflow (m <sup>3</sup> )
Godów*	Godów_1	25.08.2014	24 h	935.1
	Godów_2	26.08.2014	24 h	
	Godów_3	27.08.2014	24 h	
	Godów_4	28.08.2014	24 h	
	Godów_5	29.08.2014	24 h	
Diabla Góra	B017	29.05.2016 day	12 h	371.5
	B018	29.05.2016 night	12 h	367.1
	B019	30.05.2016 day	12 h	372.4
	B020	30.05.2016 night	12 h	368.8
	B021	31.05.2016 day	12 h	372.4
	L022	25.07.2016 day	12 h	353.8
Zielonka	L023	25.07.2016 night	12 h	350.7
	L024	26.07.2016 day	12 h	280.7
	L025	26.07.2016 night	12 h	350.4
	L026	27.07.2016 day	12 h	353.8
Kaskada	K8043	20.07.2018 day	12 h	366.8
	K8044	20.07.2018 night	12 h	363.1
	K8045	21.07.2018 day	12 h	366.7
	K8046	21.07.2018 night	12 h	362.6
	K8047	22.07.2018 day	12 h	368.4

\* average airflow based on data available on <https://powietrze.gios.gov.pl/>

Data contained in **Table 11** were used for the quantitative analyses of SOA samples. The concentrations of aerosol components (ng m<sup>-3</sup>) detected in the field or smog-chamber samples were estimated based on equation 3:

$$C_X = \frac{\frac{(A_X \pm b)}{a} \times \frac{V_S S_F}{R_S S_P}}{F_A} \quad (\text{ng m}^{-3}) \quad (3)$$



where  $C_X$  is the amount of an analyzed SOA component in 1 m<sup>3</sup> of air (ng m<sup>-3</sup>),  $A_X$  is the chromatogram peak area of that SOA component,  $a$ ,  $b$  are the parameters of the calibration curves with linear fit:  $y = ax \pm b$ ,  $V_S$  is the solvent volume used for reconstitution of dried SOA extracts,  $R_S$  is the recovery of a selected standard compound (%),  $S_F$  is an active surface of the whole aerosol filter (cm<sup>2</sup>),  $S_P$  is the surface of a filter punch (cm<sup>2</sup>), and  $F_A$  is the total volume of air that flew through the filter (m<sup>3</sup>).

### 2.1.3 Thermo-optical method for OC/EC determination

The total mass of PM-bound carbonaceous material, i.e., total carbon (TC), can be divided into three fractions (Watson et al., 2005; JRC report, 2009):

- 1) inorganic carbon (IC; in the PM<sub>2.5</sub> fraction detected at negligible levels),
- 2) organic carbon (OC),
- 3) elemental carbon (EC) or black carbon (BC) (terms used interchangeably, depending on the analytical method by which the fraction was analyzed).

In this work, organic and elemental carbon contents were determined by a thermo-optical method (Birch and Cary, 1996). The values obtained for ambient aerosol samples in μg m<sup>-3</sup> are presented in Chapter 3.4.1 (**Table 20**).

For determination of organic carbon (OC) and elemental carbon (EC) in the PM<sub>2.5</sub> fraction, a thermo-optical analyzer with FID detection, namely 4L Main Oven Assembly Model, manufactured by Sunset Laboratory Inc. was used. The analysis was carried out using the EUSAAR\_2 protocol (**Table 12**), which was developed as the standard method for European monitoring stations under the EUSAAR project (*European Supersites for Atmospheric Aerosol Research*; Klejnowski et al., 2017). Ambient aerosol samples were collected onto quartz-fiber filters, from which a 1.5 cm<sup>2</sup> punch was cut and subjected to a two-stage analysis. Firstly, the sample was gradually heated from 200 to 650 °C in a helium stream to release the OC fraction. Then, the filter punch was heated to 850 °C in an oxidizing mixture of helium and oxygen to release EC. The compounds were separated during the heating stages under oxidative conditions and converted stoichiometrically to CO<sub>2</sub> in the presence of magnesium oxide. CO<sub>2</sub> was reduced to methane in the presence of hydrogen and a nickel catalyst and measured with a flame ionization detector (FID). OC and EC contents were corrected during the analysis based on the optical measurement of light transmittance (red laser beam). The last stage of the measurement procedure included injecting an external reference standard (glucose solution) through a fixed-volume loop to ensure stable measurement conditions and repeatability of the entire

analytical method. The high-purity gases from Air Liquide, Poland, were used in the analyses.

**Table 12:** OC/EC analysis parameters according to the EUSAAR\_2 protocol

Stage / gas flow	Temperature (°C)	Time (s)
He	200	120
He	300	150
He	450	180
He	650	180
He/O <sub>2</sub>	500	120
He/O <sub>2</sub>	550	120
He/O <sub>2</sub>	700	80
He/O <sub>2</sub>	850	70

According to the European Commission JRC report (2009), the thermo-optical method based on the EUSAAR\_2 protocol fulfills the requirements for OC and EC monitoring in the PM<sub>2.5</sub> fraction in Europe. The validation parameters determined for this measurement are presented in **Table 13**. OC/EC data obtained with the described thermo-optical method for collected field samples are presented in **Table 14**.

**Table 13:** Validation parameters determined by Eusaar 2 protocol for OC/EC measurements

Elemental carbon (EC)			Organic carbon (OC)		
LOD (µg cm <sup>-2</sup> )	LOQ (µg cm <sup>-2</sup> )	Uncertainty	LOD (µg cm <sup>-2</sup> )	LOQ (µg cm <sup>-2</sup> )	Uncertainty
0.1	0.1	5%	0.32	0.64	5%

**Table 14:** Organic carbon (OC) and elemental carbon (EC) concentrations ( $\mu\text{g cm}^{-2}$ ) obtained for the collected ambient aerosol samples

Sample name	OC ( $\mu\text{g cm}^{-2}$ )	EC ( $\mu\text{g cm}^{-2}$ )	$\frac{OC}{(OC + EC)}$
Godów_1	24.6 ± 1.4	4.0 ± 0.4	0.86
Godów_2	32.2 ± 1.8	6.8 ± 0.5	0.82
Godów_3	38.7 ± 2.1	4.8 ± 0.4	0.89
Godów_4	38.7 ± 2.1	5.7 ± 0.5	0.87
Godów_5	33.1 ± 1.9	4.9 ± 0.4	0.87
B017	12.4 ± 0.8	0.5 ± 0.2	0.96
B018	12.0 ± 0.8	0.4 ± 0.2	0.96
B019	12.2 ± 0.8	0.5 ± 0.2	0.96
B020	9.8 ± 0.7	0.5 ± 0.2	0.95
B021	10.5 ± 0.7	0.4 ± 0.2	0.96
L022	14.5 ± 0.9	0.8 ± 0.2	0.94
L023	15.5 ± 1.0	0.9 ± 0.2	0.95
L024	16.5 ± 1.0	0.3 ± 0.2	0.98
L025	10.2 ± 0.7	0.6 ± 0.2	0.94
L026	8.7 ± 0.6	0.6 ± 0.2	0.93
K8043	14.6 ± 0.9	1.7 ± 0.2	0.89
K8044	12.3 ± 0.8	2.1 ± 0.3	0.85
K8045	9.2 ± 0.7	0.9 ± 0.2	0.91
K8046	20.0 ± 1.2	12.1 ± 0.8	0.62
K8047	12.4 ± 0.8	1.4 ± 0.3	0.90

#### 2.1.4 Analysis of air mass back trajectories

For all sampling events, the back-trajectories of air masses at the sampling sites were estimated with the HYSPLIT model (Stein et al., 2015, Ralph et al., 2017), available *on-line* at the NOAA Air Resources Laboratory, USA website. The back trajectories were calculated for 24 h period preceding each sampling event. The calculations started in the first hour of the aerosol collection on the filter (7:00 AM). The flow of air masses was modeled at 50 m and 200 m heights above the ground level, respectively. The results are presented in Chapter 3.4.2 (**Figs. 46 – 49**).

#### 2.1.5 Sample preparation

For the initial analyses, two 1 cm<sup>2</sup> punches were taken from each filter and extracted twice for 30 min with 15 mL aliquots of methanol using a Multi-Orbital Shaker (PSU-20i, BioSan). High-purity methanol (LC-MS Chromasolv grade, Sigma-Aldrich, PL) was used for the extraction, reconstitution of aerosol extracts, and preparation of the LC mobile phase. The two extracts were combined and preconcentrated to 1 mL using a rotary evaporator operated at 28°C and 150 mbar (Rotavapor® R215, Büchi). The preconcentrated extract was filtered with a 0.2 µm PTFE syringe filter and evaporated to dryness under a gentle stream of nitrogen. High-purity water (resistivity 18.2 MΩ cm) from a Milli-Q Advantage water purification system (Merck, Poland) was used for the reconstitution of aerosol extracts and preparation of the LC mobile phases. The residues were reconstituted with 180 µL of 1:1 (v/v) high-purity methanol/water mixture and agitated for 1 minute. The sample preparation was optimized during the work:

- a) the number of punches selected for the extraction were taken according to the amount of OC/EC measured (more punches for lower OC values),
- b) the extraction with Multi-Orbital Shaker was optimized to 60 min with 15 mL aliquots of methanol, which increased the extraction efficiency of detected SOA components (qualitative data presented in the Appendix, **Table A1**),
- c) reconstitution technique of dried SOA extracts was optimized according to Spolnik et al. (2018) by using Milli-Q water only.

Moreover, sample injection repeatability in UPLC-MS analyses was investigated. **Table 15** shows the qualitative results of injection repeatability obtained for selected main isoprene SOA components found in Godów aerosol extract. **Table A2** in the Appendix shows the qualitative results of injection repeatability obtained for selected surrogate and authentic standard compounds. Based on data obtained it is worth to note,

that duplicated injections of the same sample volume onto the chromatographic column can generate an error within the range up to 12%.

**Table 15:** Qualitative comparison of main isoprene SOA components from Godów ambient aerosol sample (injection repeatability)

Organosulfate (MW)	Peak Area						Average Peak Area
	Inj. 1	Inj. 2	Inj. 3	Inj. 4	Inj. 5	Inj. 6	
200	213	231	226	223	235	274	234 ± 21
212	1149	1201	1110	1188	1143	1156	1158 ± 33
214	135	145	140	139	144	139	140 ± 4
216	479	504	473	547	476	474	492 ± 29

During the work the homogeneity test of the ambient aerosol filter was also conducted. The qualitative results obtained for selected tracers of isoprene SOA detected in ambient aerosol extracts from various parts of quartz-fiber filter are presented in **Table 16**.

**Table 16:** Qualitative comparison of average peak area of isoprene SOA components from four various parts of Zielonka filter surface (top, center, right side, left side; homogeneity test)

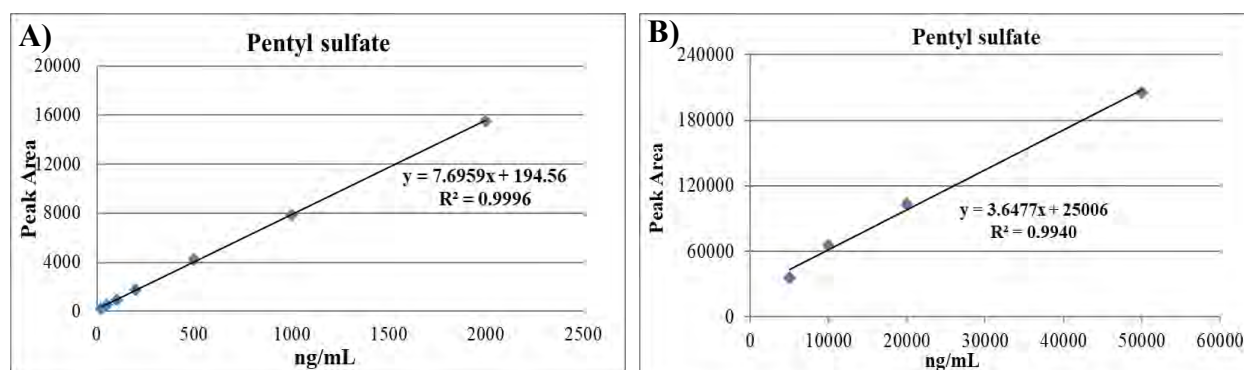
Organosulfate (MW)	Average Peak Area (parts of the filter)				Average Peak Area (the whole filter)
	Top	Center	Right	Left	
200	88	107	94	95	96 ± 8
212	117	148	111	128	126 ± 16
214	142	157	136	171	152 ± 16
216	435	479	418	408	435 ± 31

Based on the homogeneity test, I could carefully assumed that the mass and composition distribution across the filters were homogeneous so that the rectangular punches taken for further UPLC-MS analyses were representative for the whole filter. The scheme of punches taken from different parts of the filter for the homogeneity test was presented in the Appendix (**Scheme A1**). Moreover, Prządka et al. (2012) conducted gravimetric analyses of the mass deposited on a filter surface. The results revealed that the deposition is homogenous. The authors showed that the uniformity coefficient values for rectangular punches (1.5 cm<sup>2</sup>) depended slightly on their location relative to the filter center. The smallest values of the uniformity coefficient for rectangular punches were

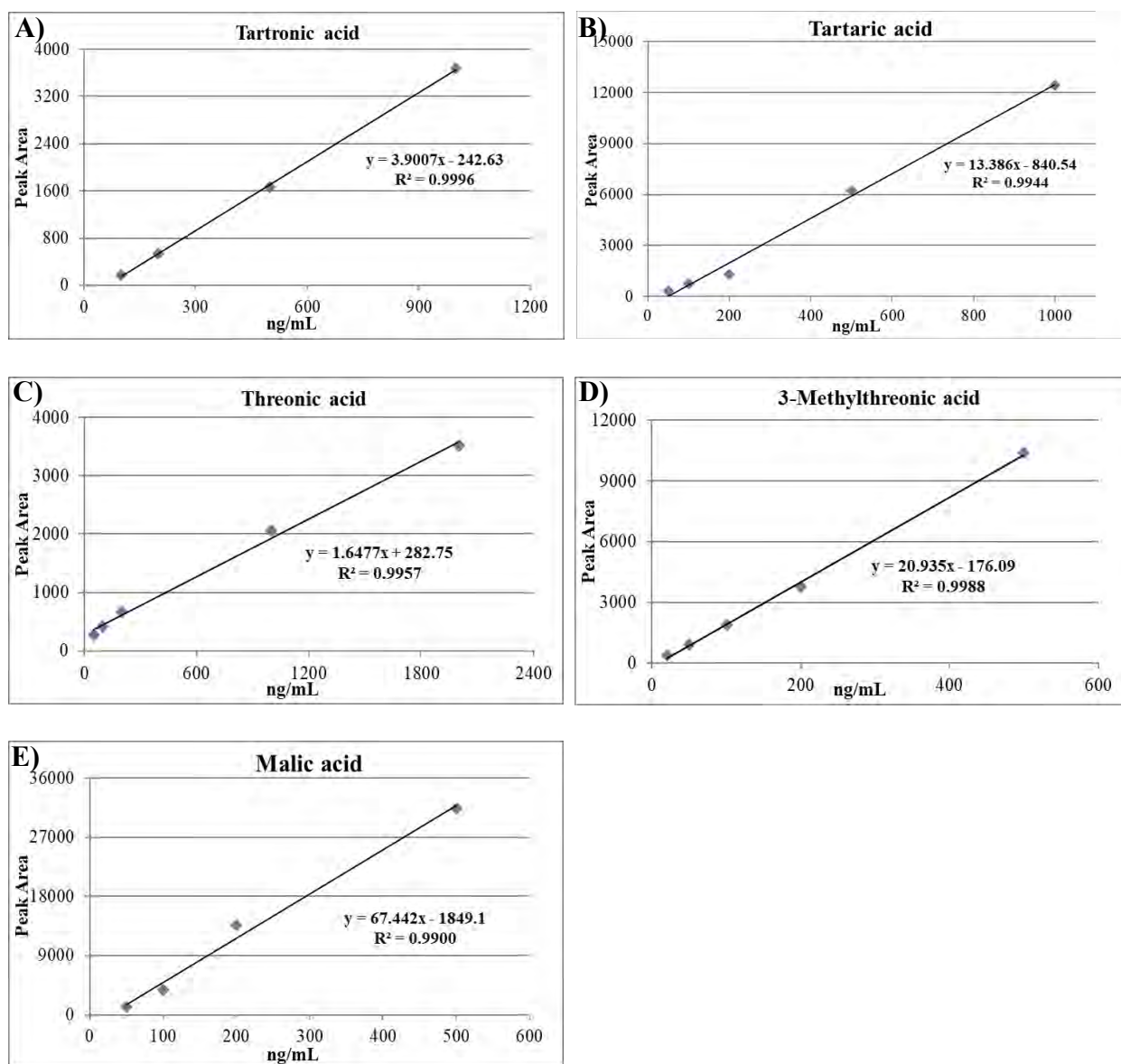
obtained for fraction PM<sub>2.5</sub> (about 0.4%). The coefficient value increased slightly as the distance from the filter center increased, but this dependence was not unambiguous. Moreover, Widziewicz et al. (2015) determined metals distribution on the quartz-fiber filters surface coated with PM. The authors assumed that the distribution is uniform when the concentration from a single punch is within  $\pm 15\%$  of the average concentration over the whole filter. The authors did not observe statistically significant differences in metals concentrations between particular punches taken from different parts of the filter. Performed for this thesis qualitative UPLC–ESI–HRMS analyses of rectangular punches with PM<sub>2.5</sub> ambient aerosol taken from different parts of the filter confirmed the findings of Prządka et al. (2012) and Widziewicz et al. (2015) on the homogenous deposition of aerosol particles on the filter surface.

### 2.1.6 Preparation of standard solutions and calibration curves for LC-MS analyses

Standard compounds for UPLC-MS analyses were purchased from Sigma Aldrich, PL at highest available purity: DL-tartaric acid (99%), D-threono-lactone ( $\geq 95\%$ ), tartronic acid ( $> 97\%$ ), DL-malic acid ( $\geq 99\%$ ) and sodium 1-pentyl sulfate (99%). 0.1 mg mL<sup>-1</sup> stock solutions of standard compounds were prepared for the quantitative analyses. The calibration curves were made over wide ranges of concentrations for the surrogate standard (sodium 1-pentyl sulfate) and authentic standards (tartronic acid, D-threonic acid, DL-tartaric acid, 3-methyl threonic acid, malic acid; **Figures 13** and **14**). The obtained data points (for at least four points) were within the linear range with a linear fit. Moreover, the SOA compounds detected were also within the range of a given calibration curve. The injection volumes of analyzed SOA extracts and standard solutions were the same.



**Figure 13.** Calibration curves of the surrogate standard – pentyl sulfate – with linear correlation equations and  $R^2$  factors over two concentration ranges



**Figure 14.** Calibration curves of authentic standard compounds – A) tartronic acid, B) tartaric acid, C) threonic acid, and D) 3-methyl threonic acid, E) malic acid, with linear correlation equations and  $R^2$  factors

As mentioned previously, organosulfates, nitroxy-organosulfates and nitrosooxy-organosulfates were quantified based on a surrogate standard – sodium 1-pentyl sulfate, for which the recovery was determined. For the quantification of hydroxy acids of ISO and 13BD SOA, the recovery of authentic standards – tartronic acid, DL-tartaric acid, D-threonic acid, malic acid, and 3-methyl threonic acid was determined. Mean values are presented in **Table 17**. Moreover, LOD (Limit of Detection) and LOQ (Limit of Quantitation) levels were determined based on equations 4 and 5 presented below:

$$LOD = \frac{3.3xSD}{a} \quad (\text{ng mL}^{-1}) \quad (4)$$

$$LOQ = \frac{10xSD}{a} \quad (\text{ng mL}^{-1}) \quad (5)$$

where SD is a Standard Deviation of the standard compound at the lowest concentration obtained, and  $a$  is the slope of the calibration curve with linear fit:  $y = ax \pm b$ .

**Table 17.** Retention times, recoveries and LOD, LOQ levels determined for the selected surrogate and authentic standards

Compound	Retention time (min)	Mean recovery (%)	LOD (ng mL <sup>-1</sup> )	LOQ (ng mL <sup>-1</sup> )
pentyl sulfate	5.94	82.1 ± 3.4	14.7	44.7
3-methyl threonic acid	0.81	84.7 ± 4.2	6.7	20.2
DL-tartaric acid	0.81	85.4 ± 9.1	25.4	77.0
D-threonic acid	0.87	60.1 ± 8.1	40.0	121.3
tartronic acid	0.82	89.0 ± 9.7	46.4	140.7
malic acid	0.82	85.8 ± 7.8	15.3	46.3

### 2.1.7 Qualitative UPLC-MS analyses

Qualitative analyses of SOA extracts were performed using two different UPLC-MS systems.

First, the extracts were analyzed by UPLC–ESI–QTOF–HRMS (ultrahigh-performance liquid chromatography-electrospray ionization (ESI)-quadruple time-of-flight high-resolution mass spectrometry) set consisting of a Waters Acquity UPLC I-Class chromatograph coupled to a Waters Synapt G2-S high-resolution mass spectrometer. The chromatographic separations were done using an Acquity HSS T3 column (2.1 mm i.d. x 100 mm, 1.8 μm particle size) at room temperature. The mobile phases consisted of 10 mM ammonium acetate (eluent A) and methanol (eluent B). To obtain appropriate chromatographic separations and responses, a 13 minutes gradient elution program was used. The chromatographic run commenced with 100% eluent A for the first 3 min. Eluent B increased from 0% to 100% from 3 to 8 min, held constant at 100% from 8 to 10 min, and then decreased from 100% to 0% from 10 to 13 min. The initial and final flow was 0.35 mL min<sup>-1</sup>, while the flow from 3 to 10 min was 0.25 mL min<sup>-1</sup>. The injection volume was 0.5–1 μL or 1–5 μL for the survey scans or MS/MS fragmentation, respectively. The Synapt G2-S spectrometer equipped with



an ESI source operated in the negative-ion mode. Optimal ESI source conditions were 3 kV capillary voltage with a 20 V sampling cone and full-width-at-half-maximum mass-resolving power of 20,000. High-resolution mass spectra were recorded from  $m/z$  50 to 600 in the MS or MS/MS modes. All data were recorded and analyzed with the Waters MassLynx V4.1 software package. During the analyses, the mass spectrometer was continuously calibrated by injecting the reference compound, leucine encephalin, directly into the ESI source.

In addition, UPLC–ESI–MS qualitative analyses were done with a Dionex UltiMate 3000 RSLC system (Thermo Fisher Scientific) coupled to an Orbitrap Fusion Tribrid mass spectrometer (Thermo Fisher Scientific) equipped with a heated electrospray ionization source (HESI). Compounds were separated with the same Acquity UPLC HSS T3 column at 40°C. Water with 10 mM ammonium formate and methanol with 10 mM ammonium formate were used as solvents A and B, respectively. Samples were loaded directly onto the analytical column at the flow rate of 0.3 mL min<sup>-1</sup> of 100% solvent A. The injection volume was 1 µL or 20 µL for the survey scans or scans with MS/MS fragmentation, respectively. The compounds were eluted from the column at the flow rate of 0.3 mL min<sup>-1</sup> with the following linear gradient: 0 min – 100% A, 3 min – 100% A, 6 min – 100% B, 9 min – 100% B, and 12 min – 100%. The eluted compounds were ionized in the HESI source, in the negative ion mode with a capillary voltage of 2.5 kV. The ion source working parameters optimized on the total ion current (TIC) values were: sheath gas flow – 35 L min<sup>-1</sup>, auxiliary gas flow – 10 L min<sup>-1</sup>, ion transfer tube temperature – 325°C, and vaporizer temperature – 275°C. Nitrogen was used as sheath and auxiliary gas. Survey scans were recorded with the Orbitrap mass analyzer at a resolving power of 60,000 in the  $m/z$  range of 50 – 300. From each survey scan, the most abundant singly charged ions were fragmented by higher energy collision-induced dissociation (HCD). The cycle time was 3 s. The product ions were analyzed with the Orbitrap analyzer at a resolving power of 15,000. After fragmentation, the masses were excluded for 30 seconds from further fragmentation. Collision energy values were optimized to obtain appropriate fragmentations of studied compounds. Survey scans and MS/MS spectra were evaluated manually using Xcalibur 3.0 (Thermo Fisher Scientific).

### **2.1.8 Quantitative UPLC-MS analyses**

The UPLC-ESI-MS/MS quantitative analyses were performed with a 1200 Infinity system coupled with 6540 UHD Accurate-Mass Q-TOF spectrometer

(Agilent Technologies) equipped with an electrospray ionization source (ESI). Compounds were separated with the Acquity UPLC HSS T3 column at 40°C. The mobile phases used for qualitative analyses were: water with 10 mM ammonium formate (solvent A) and methanol with 10 mM ammonium formate (solvent B). The samples were loaded directly onto the analytical column at the flow rate of 0.3 mL min<sup>-1</sup> of 100% solvent A. The injection volume was 2 µL or 8 µL for the survey scans or scans with MS/MS fragmentation, respectively. The compounds were eluted from the column at the flow rate of 0.3 mL min<sup>-1</sup> with the same linear gradient as for qualitative analyses conducted with the Dionex system (see Chapter 2.1.6). The eluted compounds were ionized in the negative ion mode with a capillary voltage of 2.5 kV in the ESI source. The ion source working parameters optimized for the total ion current (TIC) values were: drying gas flow – 5 L min<sup>-1</sup>, gas temperature – 150°C, and sheath gas temperature – 150°C. Nitrogen was used as sheath and drying gas. Survey scans were recorded with the Q-TOF mass analyzer at a resolving power of 20,000 in the *m/z* range of 50 – 500. MS/MS spectra were recorded in cycle time 3 s. Collision energy values were optimized to obtain good fragmentation of the studied compounds. Survey scans and MS/MS spectra were evaluated manually using MassHunter software (Agilent Technologies). All calculations were performed for deprotonated ions.

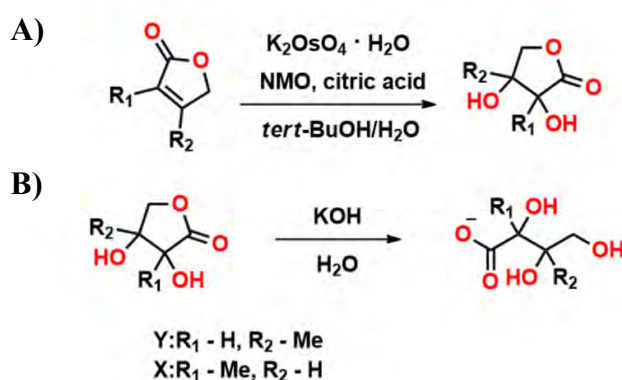
## 2.2 Synthesis of authentic standards

This work is concerned with the formation of highly oxygenated acids, which are considered tracers of aged isoprene and 1,3-butadiene SOA. The syntheses of those compounds were carried out to confirm the structures and determine the concentrations of tentatively identified components of ambient aerosol samples.

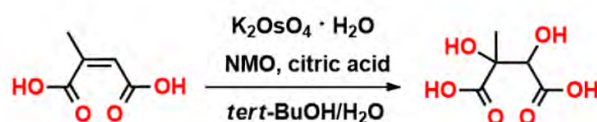
To confirm chemical structures of synthesized compounds, <sup>1</sup>H and <sup>13</sup>C NMR spectra were acquired with a Bruker 400 MHz instrument equipped with a broadband probe. The chemical shifts were given in ppm, relative to tetramethylsilane (TMS). The spectra were calibrated for the shift of deuterium oxide (D<sub>2</sub>O) used as the solvent, where the proton shift was 4.80 ppm. The coupling constants (J) were provided in Hz using the following abbreviations to denote multiplicity: s = singlet, d = doublet, dd = doublet doublet. Moreover, the structures of synthesized compounds were confirmed with the low-resolution ESI(-) mass spectra obtained with API 3000 triple-quadrupole mass spectrometer.

### 2.2.1 Isoprene SOA

The syntheses of potassium 2,3,4-trihydroxy-2-methylbutanoate and potassium 2,3,4-trihydroxy-3-methylbutanoate shown in **Scheme 5** were carried out in a two-stage process. The first step involved *cis*-dihydroxylation of 4-methyl-2(5H)-furanone or 3-methyl-2(5H)-furanone (TCI Chemicals, >97% purity), respectively, leading to the corresponding lactone *cis*-diols (**Scheme 5A**), whereas a second step was the hydrolysis of resultant lactone *cis*-diols under alkaline conditions (**Scheme 5B**; Pederson et al. (2009)). The synthesis of 2,3-dihydroxy-2-methylsuccinic acid was a one-step reaction involving 2-methylmaleic acid (Sigma Aldrich, 98% purity) followed by *cis*-dihydroxylation of the C=C bond (**Scheme 6**).



**Scheme 5.** The reaction protocol developed for synthesizing potassium 2,3,4-trihydroxy-2-methylbutanoate (2-methylthreonic acid) and potassium 2,3,4-trihydroxy-3-methylbutanoate (3-methylthreonic acid)



**Scheme 6.** The reaction protocol used for synthesizing 2,3-dihydroxy-2-methylsuccinic acid (2-methyltartaric acid).

*Cis*-dihydroxylation reaction was performed according to the method of Fattorusso et al. (2011) with minor modifications. Potassium osmate dihydrate was added to a solution of the corresponding alkene (5.1 mmol), NMO (1.1 g, 10.5 mmol), and citric acid (2.0 g, 10.5 mmol) in *tert*-BuOH:H<sub>2</sub>O mixture (20 mL) and stirred overnight at room temperature. Then the reaction solution was diluted with saturated aqueous Na<sub>2</sub>SO<sub>3</sub> (15 mL) and stirred vigorously for 1 hour. The *tert*-BuOH was evaporated, and aqueous layers were extracted with diethyl ether (5 x 15 ml), dried over anhydrous magnesium sulfate, and evaporated in vacuo. The residue was purified by flash column chromatography on silica gel 60 (approx. 17 g). The chromatographic conditions

and analytical data for the structural characterization of all synthesized products are provided below.

Dihydro-3,4-dihydroxy-4-methylfuran-2-one was isolated after dihydroxylation of 4-methyl-2(5H)-furanone as a yellowish oil (0.53 g, 3.6 mmol, 60%) after chromatography on silica gel (DCM/MeOH, 95:5 → 9:1).

$^1\text{H}$  NMR (400 MHz,  $\text{D}_2\text{O}$ )  $\delta$  4.42 (s, 1H), 4.26 (s, 2H), 1.38 (s, 3H);  $^{13}\text{C}$  NMR (101 MHz,  $\text{D}_2\text{O}$ )  $\delta$  178.71, 76.15, 75.19, 73.50, 19.74.

Dihydro-3,4-dihydroxy-3-methylfuran-2-one was isolated after dihydroxylation of 3-methyl-2(5H)-furanone as a colorless dense oil (0.56 g, 3.8 mmol, 75%) after chromatography on silica gel (DCM/MeOH, 95:5 → 9:1).

$^1\text{H}$  NMR (400 MHz,  $\text{D}_2\text{O}$ )  $\delta$  4.54 (dd,  $J = 10.9, 3.7$  Hz, 1H), 4.28 (d,  $J = 0.6$  Hz, 1H), 4.19 (s, 1H), 1.41 (s, 3H);  $^{13}\text{C}$  NMR (101 MHz,  $\text{D}_2\text{O}$ )  $\delta$  180.79, 74.15, 73.17, 73.07, 20.40.

$^1\text{H}$  NMR spectra of synthesized dihydro-3,4-dihydroxy-4-methyl-2(3H)-furanone and dihydro-3,4-dihydroxy-3-methyl-2(3H)-furanone are presented in the Appendix (**Figs. A1–A2**), and the low-resolution ESI(-) product ion mass spectra are shown in **Figs. A4–A5**.

The isolated dihydroxylactones (**Scheme 5B**) (10 mg, 0.075 mmol) were dissolved separately in  $\text{H}_2\text{O}$  (1 mL), after which KOH (4.2 mg, 0.075 mmol) was added, and the suspension was stirred for 10 min at ambient temperature (Pedersen et al., 2009).

HRMS for potassium 2,3,4-trihydroxy-2-methylbutanoate,  $m/z$  calculated for  $\text{C}_5\text{H}_9\text{O}_5^-$ ,  $[\text{M}-\text{H}]^-$ : 149.0450 Da. Found 149.0454 Da. HRMS for potassium 2,3,4-trihydroxy-3-methylbutanoate,  $m/z$  calculated for  $\text{C}_5\text{H}_9\text{O}_5^-$ ,  $[\text{M}-\text{H}]^-$ : 149.0450 Da. Found 149.0454 Da.

The synthesis of 2,3-dihydroxy-2-methyl-succinic acid was performed according to the dihydroxylation protocol described above. The final compound was isolated as a colorless oil (0.42 g, 2.8 mmol, 55%) after chromatography on silica gel (RP-18, MeOH/ $\text{H}_2\text{O}$ , 5:95).

$^1\text{H}$  NMR (400 MHz,  $\text{D}_2\text{O}$ )  $\delta$  4.50 (s, 1H), 3.00 – 2.79 (dd, 2H), 1.47 (s, 3H), HRMS for 2,3-dihydroxy-2-methyl-succinic acid,  $m/z$  calculated for  $\text{C}_5\text{H}_7\text{O}_6^-$ ,  $[\text{M}-\text{H}]^-$ : 163.0243 Da. Found 163.0246 Da.

$^1\text{H}$  NMR spectrum of 2,3-dihydroxy-2-methyl-succinic acid is presented in the Appendix (**Fig. A3**).

### 2.2.2 Butadiene SOA

D-threono-lactone (Sigma Aldrich, purity >95%) was subjected to alkaline hydrolysis described in Chapter 2.2.1 (**Scheme 5B**). The compound was dissolved in H<sub>2</sub>O (1 mL), whereupon KOH (4.2 mg, 0.075 mmol) was added, and the suspension was stirred for 10 min at ambient temperature to obtain potassium 2,3,4-trihydroxybutanoic acid (threonic acid). HRMS for potassium 2,3,4-trihydroxybutanoic acid, *m/z* calculated for C<sub>4</sub>H<sub>7</sub>O<sub>5</sub><sup>-</sup>, [M-H]<sup>-</sup>: 135.0293 Da. Found 135.0294 Da.

## 3. Results

The studies carried out and presented in my Ph.D. dissertation can be divided into five stages:

- 1) investigation of the chemical composition of aerosol produced in the smog-chamber experiments from two precursors – isoprene and 1,3-butadiene – carried out in the laboratories of the Environmental Protection Agency (EPA) in the U.S. (**Chapter 3.1**);
- 2) determination of the influence of relative humidity and acidity on the formation of detected ISO and 13BD SOA components (**Chapter 3.2**);
- 3) comparison of smog-chamber results with ambient aerosol samples collected in rural and polluted sites in Poland (**Chapter 3.3**);
- 4) proposal of molecular structures for detected novel SOA components based on product ion mass spectra and high-resolution MS measurements (when authentic standards were unavailable), and confirmation of other compounds (hydroxy acids) with commercially available or synthesized standards (**Chapter 3.3**);
- 5) quantification of significant and novel components of isoprene and butadiene SOA in field samples with reference to smog-chamber results on the influence of RH and acidity on SOA formation in the atmosphere (**Chapter 3.4**).

Revealing ISO and 13BD SOA composition under laboratory conditions enabled the firm identification of the complex composition of ambient aerosol. Moreover, the results presented may fill the gaps in understanding of chemical transformations of isoprene and butadiene in the atmosphere and the formation of secondary organic aerosol from those precursors.

### 3.1 Smog-chamber samples

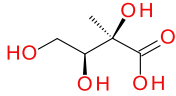
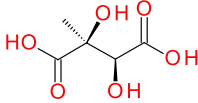
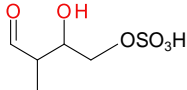
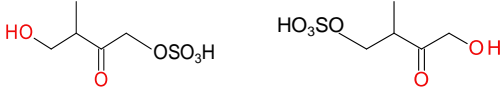
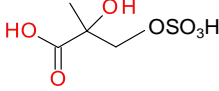
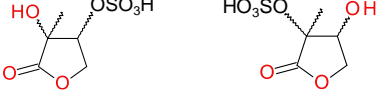

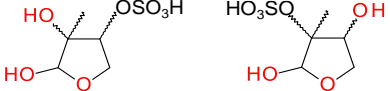
#### 3.1.1 Identification of isoprene and butadiene SOA components

In this chapter I described ISO and 13BD SOA-bound components selected for further consideration. All structures proposed for detected OSs, NOSs and NSOSs from isoprene and 1,3-butadiene are tentative (**Tables 18** and **19**). Some isoprene SOA components were previously reported in the references listed. The proposed structures of newly identified organosulfates, nitrooxy- and nitrosooxy-organosulfates were based on a detailed interpretation of product ion mass spectra, which were obtained from high-resolution UPLC-MS measurements. These compounds had reasonable ionization efficiencies for deprotonated pseudomolecular ions ( $[M-H]^-$ ). In the recorded product

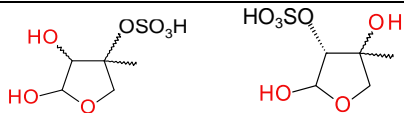
ion mass spectra, the diagnostic ions, such as bisulfate anions ( $\text{HSO}_4^-$ ,  $m/z$  97), bisulfite anions ( $\text{HSO}_3^-$ ,  $m/z$  81), and sulfate radical anions ( $\text{SO}_3^{\bullet-}$ ,  $m/z$  80 and  $\text{SO}_4^{\bullet-}$ ,  $m/z$  96) have been observed. The structural elucidation of newly identified compounds was performed based on accurate mass measurements and the following assumptions:

- a) most of the studied compounds retain the same carbon backbone of isoprene or butane;
- b) the presence of the abundant bisulfate ion with  $m/z$  97 ( $\text{HSO}_4^-$ ) indicates the presence of a hydrogen atom at the carbon atom next to the one bearing HO-SO<sub>2</sub>-O- group (Attygalle et al., 2001). However, there are some exceptions to that rule (see the detailed descriptions of fragmentation pathways proposed);
- c) when assumption (b) is not fulfilled, the elimination of sulfur trioxide ( $\text{SO}_3$ ) molecule from the precursor ion  $[\text{M}-\text{H}]^-$  is likely to occur (Szmigielski, 2013);
- d) elimination of the  $\text{HNO}_2$  and  $\text{HNO}_3$  molecules from the precursor ion indicates the presence of the nitrous (-ONO) and nitric (-ONO<sub>2</sub>) esters, respectively. A  $\beta$ -hydrogen must be present to enable  $\beta$ -elimination;
- e) bisulfate ions ( $\text{HSO}_4^-$ ,  $m/z$  97) and sulfate radical ions ( $\text{SO}_3^{\bullet-}$ ,  $m/z$  80;  $\text{SO}_4^{\bullet-}$ ,  $m/z$  96) were detected for studied compounds.

**Table 18:** *Organosulfates and other components detected in ISO SOA smog-chamber experiments*

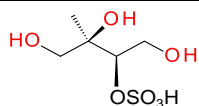
Molecular structure, chemical name, acronym, and molecular weight (g mol <sup>-1</sup> )	References
 <p>2-methylthreonic acid (2-MTrA)* <b>MW 150 Da</b></p>	Nestorowicz et al., 2018; Jaoui et al., 2019
 <p>2-methyltartaric acid (2-MTA) <b>MW 164 Da</b></p>	Nestorowicz et al., 2018; Jaoui et al., 2019
 <p>IEPOX-derived organosulfate <b>MW 198 Da</b></p>	Tao et al., 2014
 <p>C<sub>5</sub>-alkene triols organosulfate <b>MW 198 Da</b></p>	Riva et al., 2016b
 <p>2-methylglyceric acid organosulfate (2-MG OS)* <b>MW 200 Da</b></p>	Surratt et al., 2007a; Gomez-Gonzalez et al., 2008; Lin et al., 2013; Schindelka et al., 2013; Shalamzari et al., 2013; Hettiyadura et al., 2015; Nestorowicz et al., 2018; Chen et al., 2020
 <p>2(3H)-furanone, dihydro-3,4-dihydroxy-3-methyl organosulfate <b>MW 212 Da</b></p>	Hettiyadura et al., 2015; Nestorowicz et al., 2018; Spolnik et al., 2018; Chen et al., 2020; Wach et al., 2020
 <p>2(3H)-furanone, dihydro-3,4-dihydroxy-4-methyl organosulfate <b>MW 212 Da</b></p>	Hettiyadura et al., 2015; Nestorowicz et al., 2018; Spolnik et al., 2018; Chen et al., 2020
 <p>2,3,4-furantriol, tetrahydro-3-methyl organosulfate <b>MW 214 Da</b></p>	Hettiyadura et al., 2015; Nestorowicz et al., 2018; Spolnik et al., 2018; Chen et al., 2020





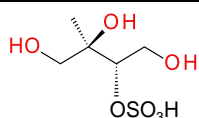
2,3,4-furantriol, tetrahydro-4-methyl organosulfate  
**MW 214 Da**

Hettiyadura et al., 2015;  
 Nestorowicz et al., 2018; Spolnik et al., 2018;  
 Chen et al., 2020

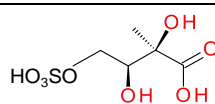


2-methylthreitol organosulfate  
 (2-MT OS)\*  
**MW 216 Da**

Surratt et al., 2007a, 2008, 2010;  
 Gomez-Gonzalez et al., 2008;  
 Riva et al., 2016b; Nestorowicz et al., 2018;  
 Spolnik et al., 2018

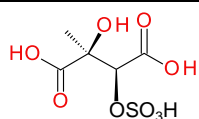


2-methylerythritol organosulfate  
 (2-MT OS)\*  
**MW 216 Da**



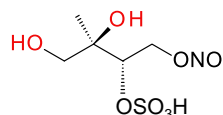
2-methylthreonic acid organosulfate  
 (2-MTrA OS)\*  
**MW 230 Da**

Nestorowicz et al., 2018



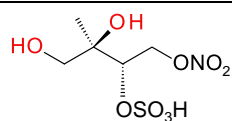
2-methyltartaric acid organosulfate  
 (2-MTA OS)\*  
**MW 244 Da**

Nestorowicz et al., 2018



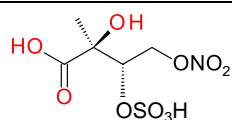
2-methyltetrol nitrosooxy-organosulfate  
 (2-MT NSOS)\*  
**MW 245 Da**

Nestorowicz et al., 2018



2-methyltetrol nitrooxy-organosulfate  
 (2-MT NOS)\*  
**MW 261 Da**

Surratt et al., 2007a, 2008;  
 Gomez-Gonzalez et al., 2008;  
 Nestorowicz et al., 2018

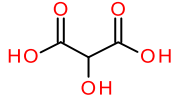
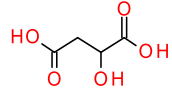
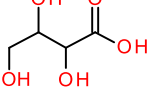
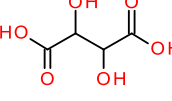
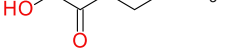
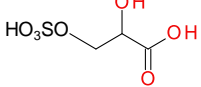
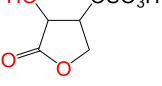
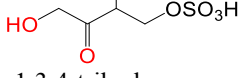
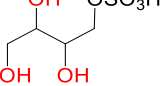


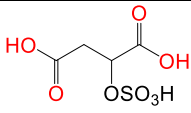
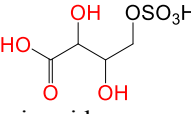
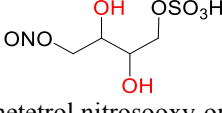
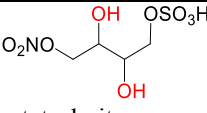
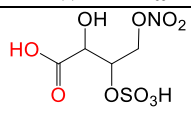
2-methylthreonic acid nitrooxy-organosulfate  
 (2-MTrA NOS)\*  
**MW 275 Da**

Nestorowicz et al., 2018

\* one representative isomer was shown

**Table 19:** Organosulfates and other components detected in 13BD SOA smog-chamber experiments

Molecular structures, chemical names, and molecular weights (g mol <sup>-1</sup> )	References
 <p>tartaric acid (TrtA) <b>MW 120 Da</b></p>	Jaoui, Nestorowicz et al., 2023, submitted
 <p>malic acid (MA) <b>MW 134 Da</b></p>	Jaoui et al., 2014; Jaoui, Nestorowicz et al., 2023, submitted
 <p>threonic acid (TrA) <b>MW 136 Da</b></p>	Angove et al., 2006; Jaoui et al., 2014; Jaoui, Nestorowicz et al., 2023, submitted
 <p>tartaric acid (TA) <b>MW 150 Da</b></p>	Jaoui et al., 2014; Jaoui, Nestorowicz et al., 2023, submitted
 <p>2-butanone, 1,4-dihydroxy- organosulfate <b>MW 184 Da</b></p>	Jaoui, Nestorowicz et al., 2023, submitted
 <p>glyceric acid organosulfate <b>MW 186 Da</b></p>	Jaoui, Nestorowicz et al., 2023, submitted
 <p>2(3<i>H</i>)-furanone, dihydro-3,4-dihydroxy- organosulfate* <b>MW 198 Da</b></p>	Jaoui, Nestorowicz et al., 2023, submitted
 <p>2-butanone, 1,3,4-trihydroxy- organosulfate* <b>MW 200 Da</b></p>	Jaoui, Nestorowicz et al., 2023, submitted
 <p>1,2,3,4-butanetetrol organosulfate* <b>MW 202 Da</b></p>	Jaoui, Nestorowicz et al., 2023, submitted

 <p>malic acid organosulfate (MA OS) <b>MW 214 Da</b></p>	Jaoui, Nestorowicz et al., 2023, submitted
 <p>threonic acid organosulfate (TrA OS)* <b>MW 216 Da</b></p>	Jaoui, Nestorowicz et al., 2023, submitted
 <p>1,2,3,4-butanetetrol nitrosooxy-organosulfate* <b>MW 231 Da</b></p>	Jaoui, Nestorowicz et al., 2023, submitted
 <p>1,2,3,4-butanetetrol nitrooxy-organosulfate* <b>MW 247 Da</b></p>	Jaoui, Nestorowicz et al., 2023, submitted
 <p>threonic acid nitrooxy-organosulfate (TrA NOS)* <b>MW 261 Da</b></p>	Jaoui, Nestorowicz et al., 2023, submitted

\* one representative isomer was shown

The chemical structures proposed for highly oxygenated acids in ISO and 13BD SOA were based on a detailed interpretation of product ion mass spectra and confirmed against appropriate synthesized and/or purchased standard compounds.

Components of ISO and 13BD SOA shown in **Tables 18** and **19** were selected for further consideration. The compounds with the butadiene or isoprene skeleton were identified and characterized in the smog-chamber experiments at various relative humidity conditions. **Chapter 3.2** contains the detailed analysis of the influence of RH and acidity on the formation of selected ISO and 13BD SOA components.

## 3.2 Influence of relative humidity and acidity on isoprene and butadiene SOA formation

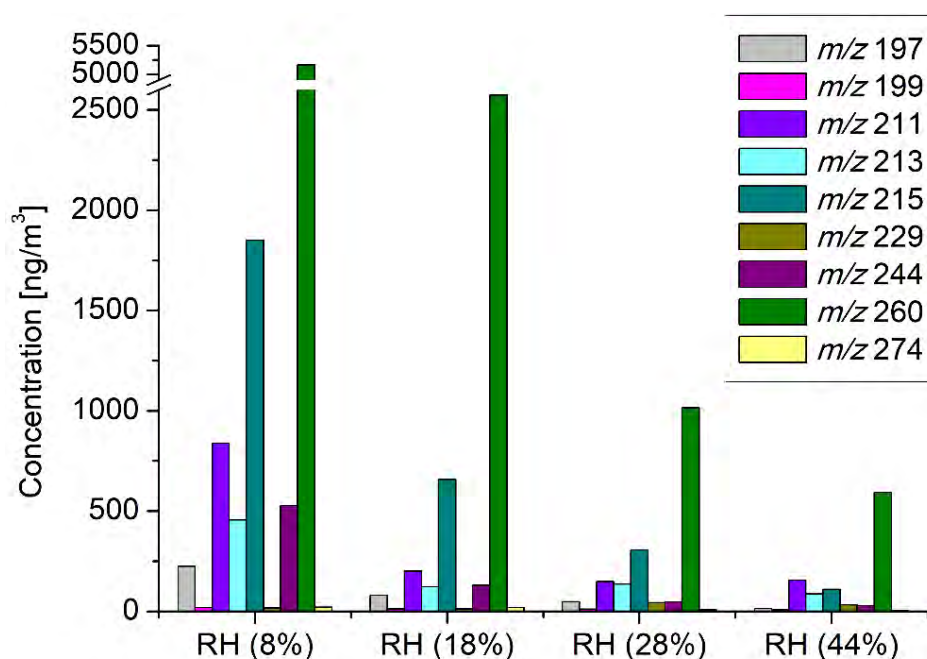
### 3.2.1 Isoprene SOA

Atmospheric organosulfates formed from various precursors are important fine aerosol-bound components (Surratt et al., 2008; Froyd et al. 2010; Stone et al., 2012; Tolocka and Turpin, 2012). The most common OSs originated from the oxidation of ISO and were identified both in smog chamber and field samples. For many of those polar

oxygenated compounds, chemical structures, fragmentation pathways and formation mechanisms have been tentatively proposed. The commonly detected of ISO SOA components had the MWs of: 154, 156, 184, 198, 200, 212, 214, 216, 260, 334, and were linked to the transformations of ISO oxidation products, such as IEPOX, methacrolein (MACR) and methyl vinyl ketone (MVK), (Surratt et al., 2007b, 2008, 2010; Gomez-Gonzalez et al., 2008; Kristensen et al., 2011; Zhang et al., 2011; Shalamzari et al., 2013; Schindelka et al., 2013; Nguyen et al., 2014; Hettiyadura et al., 2015; Riva et al., 2016a). The mechanisms of 2-methyltetrol OSs formation in the presence of acidic or non-acidic aerosol seeds were proposed by Kleindienst et al. (2006) and Riva et al. (2016a,b), respectively. Whereas Kleindienst et al. (2006) suggested the formation of highly oxygenated products through OH radical oxidation in the presence of NO<sub>x</sub> and SO<sub>2</sub>, Riva et al. (2016a,b) proposed a route *via* acid-catalyzed oxidation by organic peroxides. Isoprene-derived OSs were also formed in the aqueous-phase through the photooxidation or dark reactions of ISO in aqueous solutions containing sulfate and sulfite moieties (Rudzinski et al., 2004, 2009; Noziere et al., 2010). A detailed mechanism of this transformation has been tentatively proposed based on chain reactions propagated by sulfate and sulfite radical anions (Rudzinski et al., 2009) and confirmed by further mass spectrometric studies (Szmigielski, 2016). The acid-catalyzed formation of ISO SOA components was also suggested in aqueous phase oxidation of isoprene with H<sub>2</sub>O<sub>2</sub> (Claeys et al., 2004b).

**Figures 15** and **16** compare ISO SOA components from acidic and non-acidic smog-chamber experiments under various RH conditions determined using semi-quantitative UPLC-MS measurements. The quantitative responses were based on a comparison with selected surrogate standard with the chemical structure (sodium 1-pentyl sulfate) closest to the compound identified. Due to high NO<sub>x</sub> concentration in smog-chamber experiments, the main compound detected was 2-methyltetrol nitrooxy-organosulfate (MW 261). However, 2-methylthreitol and 2-methylerythritol organosulfates (MW 216) and nitrosooxy-organosulfates (MW 245), together with 2(3H)-furanone, dihydro-3,4-dihydroxy-methyl OSs (MW 212), were also the major components. Those compounds can derive from acid-catalyzed multiphase chemistry of IEPOX. Their maximal estimated concentrations in acidic seed experiment under low-RH conditions at 8% exceeded 5000, 1800, 800 and 500 ng m<sup>-3</sup>, respectively (**Fig. 15**). Less abundant products were: methylglyceric acid OS (MW 200), which forms *via* MAE/HMML (methacrylic acid epoxide/hydroxymethyl-methyl- $\alpha$ -lactone;

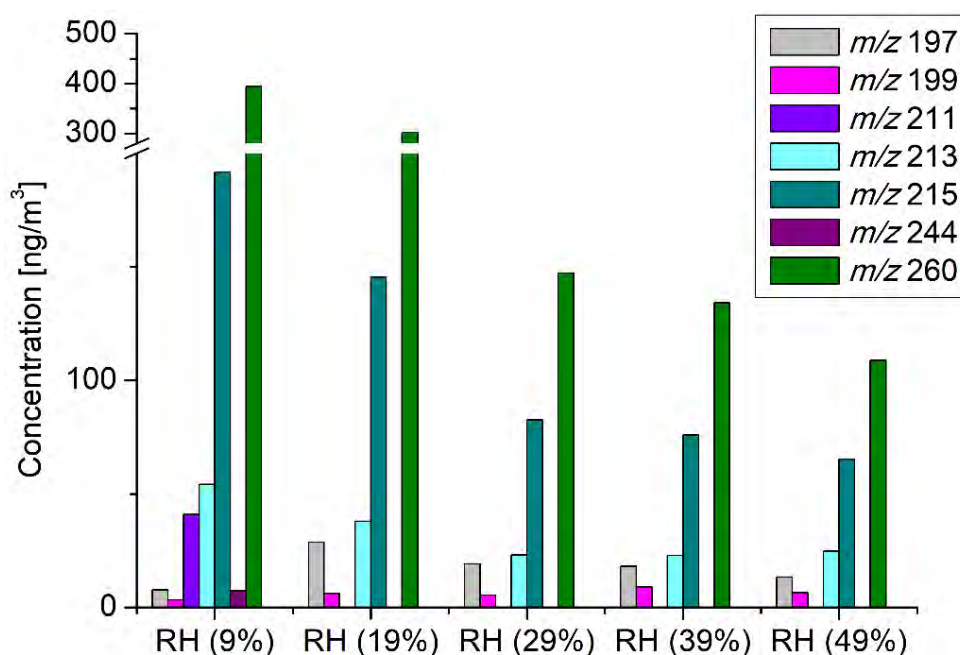
Surratt et al., 2010; Lin et al., 2012, 2013; Nguyen et al., 2015), and novel methylthreonic acid OS (MW 230) and NOS (MW 275). In acidic seed experiments, the increased RH resulted in decreased yields of ISO SOA products. Few compounds were less RH-dependent, e.g. methylthreonic acid OS and NOS (MW 230; MW 275) and 2-methylglyceric acid OS (MW 200). Consequently, total secondary organic carbon (SOC) decreased with increasing RH level (**Table 6A**). The formation of ISO-derived organosulfates was enhanced under acidic conditions (Surratt et al., 2007 a,b, 2010; Gomez-Gonzalez et al., 2008; Jaoui et al., 2010; Zhang et al., 2011).



**Figure 15.** Concentrations of OS and NOS products from the ISO acidic seed experiments determined using UPLC-MS (ER662; the numerical values are listed in **table A3** in the Appendix).

Among compounds detected in non-acidic seed experiments (**Fig. 16**), the main product was 2-methyltetrol nitrooxy-organosulfate (MW 261). However, 2-methylthreitol and 2-methylerythritol organosulfates (MW 216), together with 2,3,4-furantriol, tetrahydro-methyl organosulfate (MW 214) were also the major components. The maximal estimated product concentrations in non-acidic seed experiments under low-RH conditions at 8% exceeded 390, 190, and 50  $\text{ng m}^{-3}$ , respectively (**Fig. 16**). The concentrations of those compounds were approximately 10-fold lower, than in acidic experiments. A less abundant product was methylglyceric acid organosulfate (MW 200). Moreover, 2(3H)-furanone, dihydro-3,4-dihydroxy-methyl OSs (MW 212) and 2-methyltetrol nitrosooxy-organosulfates (MW 245) were found solely at the lowest

RH of 9%. Methylthreonic acid OS (MW 230) was detected in both sets of experiments, however only in trace amounts in non-acidic seeds experiments. 2-Methyltartaric acid OS (MW 244) was detected in both sets of experiments in trace amounts below or at the LOD, hence it was not shown in **Figs. 15** and **16**. In most cases, increasing the relative humidity resulted in decreased yields of the ISO products detected, although some compounds were observed at a similar concentrations (i.e., MGA OS and IEPOX-derived OS). Organosulfates have been formed in non-acidic experiments, probably through radical-initiated reactions in wet aerosol particles containing sulfate moieties (Noziere et al., 2010; Perri et al., 2010), hence OSs, NOSs and NSOSs detected could have been formed *via* such mechanism. The influence of RH on the product yields was mild, but noticeable. Therefore, the results obtained are not consistent with earlier studies of Dommen et al. (2006) and Nguyen et al. (2011), who revealed no effect of RH level on SOA formation in photooxidation of isoprene in the absence of sulfate aerosol seeds.

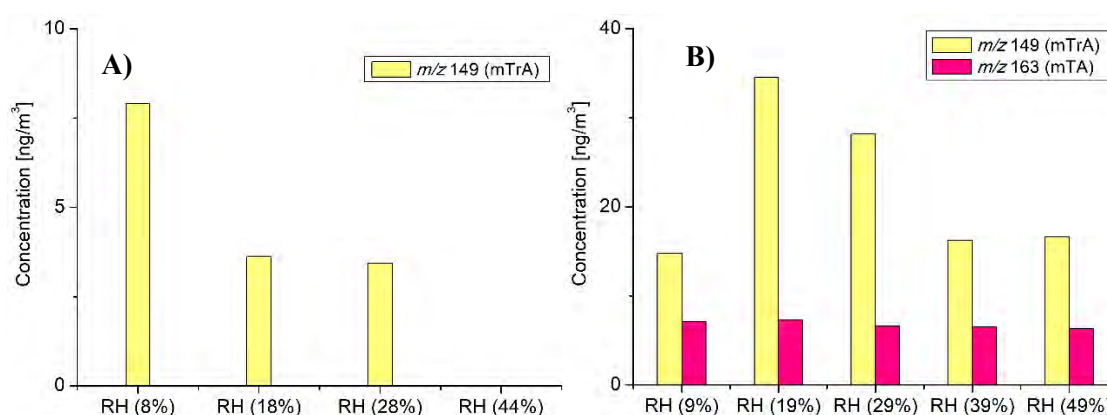


**Figure 16.** Concentrations of OS and NOS products from the ISO non-acidic seed experiments determined using UPLC-MS (ER667; the numerical values are listed in **table A4** in the Appendix)

The effect of RH on the formation of many isoprene SOA components cannot be easily predicted, although, the concentrations of the majority of compounds containing sulfate moieties decrease with increasing RH level under both, acidic and non-acidic conditions. Early smog chamber studies on ISO ozonolysis (Jang et al., 2002; Czoschke et al., 2003) showed enhanced SOA yields in the presence of acidic aerosol

seeds. Recent smog chamber results revealed that the acidity of aerosol seeds is crucial in the reactive uptake of isoprene oxidation products by particle phases (Paulot et al., 2009; Surratt et al., 2010; Lin et al., 2012; Gaston et al., 2014 a,b; Riedel et al., 2015). In the smog-chamber experiments, secondary organic carbon (SOC) produced under acidic conditions was higher, compared to non-acidic conditions under corresponding RH levels. That difference decreased to a negligible value at the highest RH level (Tables 6 A-B; 7 A-B). The formation of the individual organic compounds detected usually followed the same pattern. The amounts of most OSs, NOSs and NSOSs produced in acidic experiments were the highest at the lowest RH level and decreased with increasing RH. The effect of relative humidity on ISO SOA formation was pronounced for acidic seed aerosol, and mild for non-acidic seed aerosol. It is likely that H<sub>2</sub>SO<sub>4</sub> favors ISO SOA formation.

Figure 17 shows the concentrations of methylthreonic acids (MTrA; MW 150) and methyltartaric acid (MTA; MW 164) obtained in smog-chamber experiments. The greatest amounts of MTrA and MTA were found under non-acidic conditions at RH 19%: 35 and 8 ng m<sup>-3</sup>, respectively. The presence of methyltartaric acid was not confirmed in acidic-seed experiments, and methylthreonic acids were not detected in acidic-seed experiment at the highest RH. Therefore, high RH and high acidity conditions together with high NO<sub>x</sub> may hinder the formation of those compounds. The increase of relative humidity in non-acidic seed experiments did not affect the formation of MTA, which remained at the same concentration level, whereas the effect on MTrA formation was modest.



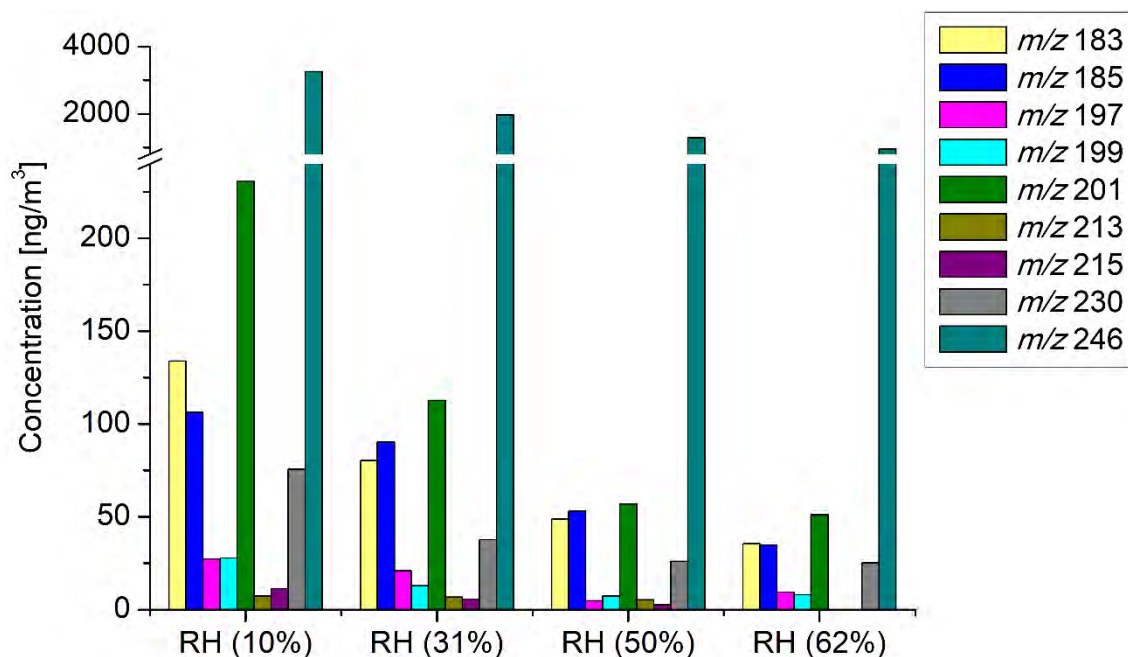
**Figure 17.** Concentrations of organic acids (HOM tracers) from the ISO acidic (A; ER662) and non-acidic seed experiments (B; ER667), determined using UPLC-MS (the numerical values are listed in tables A5 – A6 in the Appendix)

### 3.2.2 Butadiene SOA

Previous research advanced significantly the identification of 13BD oxidation products and revealed their role in 13BD SOA formation (Angove et al., 2006; Berndt and Boge, 2007; Kramp and Paulson, 2000; Liu et al. 1999; Sato, 2008; Sato et al., 2011, Jaoui et al., 2014). Still, 13BD SOA has not been fully characterized and large share remained unrevealed. Few smog-chamber studies focused on 13BD SOA formation (Angove et al., 2006; Sato, 2008; Sato et al., 2011; Jaoui et al., 2014), and only a limited number investigated the effects of acidity and relative humidity (Lewandowski et al. 2015). Jaoui et al. (2014) reported a detailed chemical characterization of gas- and particle-phase products formed through the oxidation of 13BD in the presence and absence of NO<sub>x</sub> under dry (RH 3%) and relatively humid (RH 30%) conditions. Here, the investigation of 13BD SOA formation was based on smog-chamber experiments conducted at different RH levels under acidic and non-acidic conditions. 13BD can have a significant input into aerosol masses, as some of its derivatives, e.g., malic acid (MA), threonic acid (TrA), tartaric acid (TA) and a few OSs were detected in field samples collected at various sampling sites in Poland (Chapter 3.3.2).

**Figures 18 and 19** compares the concentrations of 13BD SOA components from acidic and non-acidic smog-chamber experiments under various RH conditions, determined using semi-quantitative UPLC-MS measurements. The quantitative responses were based on the comparison with selected surrogate standard having the closest chemical structure (sodium 1-pentyl-sulfate) to the compounds identified in 13BD SOA. The major components detected in acidic seed experiments were 1,2,3,4-butanetetrol NOS (MW 247), 1,2,3,4-butanetetrol OS (MW 202), glyceric acid OS (MW 186) and 2-butanone, 1,4-dihydroxy- OS (MW 184). The maximal concentrations of those compounds were found under low-humidity conditions (RH 10%) and exceeded 3000, 230, 100 and 130 ng m<sup>-3</sup>, respectively (**Fig. 18**).

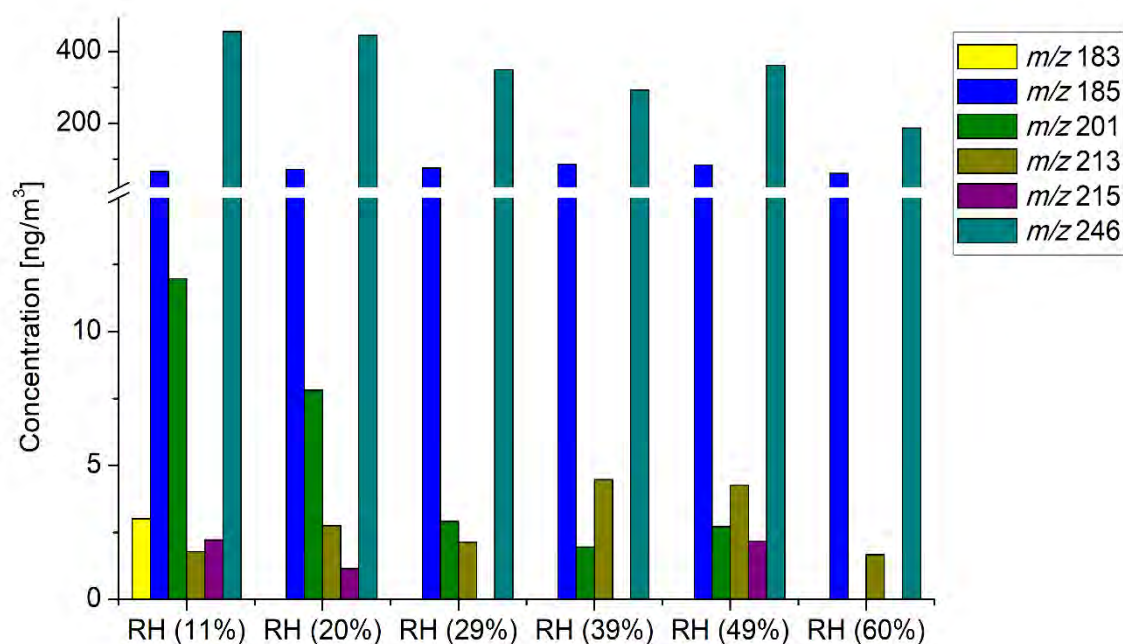




**Figure 18.** Concentrations of OS and NOS products from the 13BD acidic seed experiments determined using UPLC-MS (ER444; the numerical values are listed in **table A7** in the Appendix)

The compounds detected in experiments with acidic seed aerosol included: organosulfates derived from acid-catalyzed multiphase chemistry of BEPOX (1,2,3,4-butaneterol OS, MW 202; and 1,2,3,4-butaneterol NOS, MW 247) and acrylic acid epoxide (AAE; glyceric acid OS, MW 186) (Jaoui et al., 2014). Other compounds, like 2-butanone, 1,4-dihydroxy- organosulfate (MW 184), 1,2,3,4-butaneterol nitrosooxy-organosulfate (MW 231), 2(3H)-furanone, dihydro-3,4-dihydroxy- OS (MW 198) and 2-butanone, 1,3,4-trihydroxy- OS (MW 200) were less abundant, and their concentrations decreased with increasing RH level (**Fig. 18**). Like for the ISO SOA, total SOC decreased with increasing relative humidity (**Table 7A** and **7B**). Moreover, the increase of RH resulted in decreased concentrations of most 13BD SOA compounds detected in acidic seed experiments. However, some compounds did not follow this pattern fully, e.g. 2(3H)-furanone, dihydro-3,4-dihydroxy- OS (MW 198) and 2-butanone, 1,3,4-trihydroxy- OS (MW 200), where measured concentrations were higher for 62% RH than 50%. Moreover, those compounds along with 2-butanone, 1,4-dihydroxy- OS (MW 184), and 1,2,3,4-butaneterol NSOS (MW 231) were produced solely at acidic conditions. Glyceric acid OS (MW 186) was produced both under acidic and non-acidic conditions. At acidic conditions, the formation decreased with increasing RH, while at non-acidic conditions, the concentrations of glyceric acid OS showed a weak maximum at RH 39%. That observation is consistent with RH influence

on methylglyceric acid OS formation in ISO SOA (Nestorowicz et al., 2018). 1,2,3,4-butanetetrol OS (MW 202) was detected under both types of conditions, but it was more abundant in the acidic seed experiments with approx. 10-fold higher concentration at the lowest RH. Malic acid OS (MW 214) and threonic acid OS (MW 216) were detected in minor amounts in both smog-chamber experiments, however MA OS was not RH dependent.

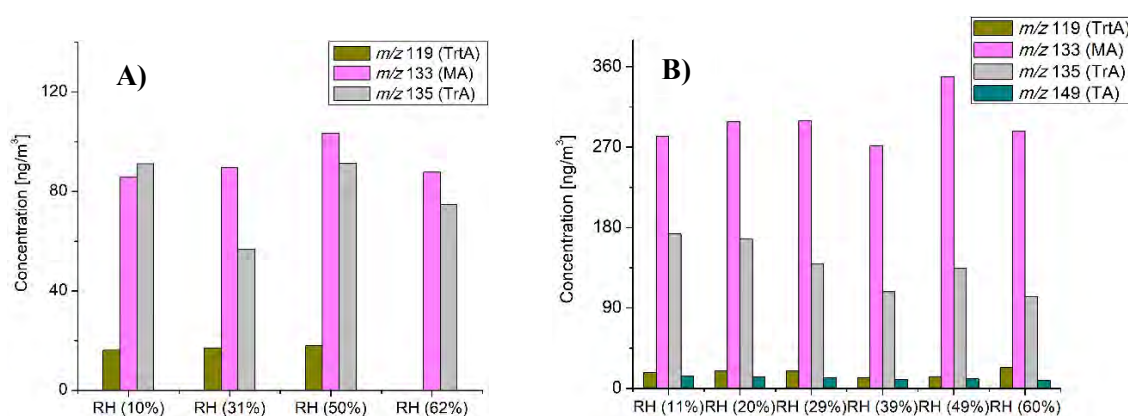


**Figure 19.** Concentrations of OS and NOS products from the 13BD non-acidic seed experiments determined using UPLC-MS (ER666; the numerical values are listed in **table A8** in the Appendix)

Threonic acid NOS (MW 261) was detected in both kinds of experiments in trace amounts below the LOD, hence it was not shown in **Figs. 18 – 19**. The most abundant compound produced in acidic and non-acidic smog-chamber experiments was 1,2,3,4-butanetetrol NOS (MW 247). The concentrations of that product were even 10-fold higher than other 13BD SOA components: for the lowest RH it reached  $3200 \text{ ng m}^{-3}$  and  $450 \text{ ng m}^{-3}$  in acidic and non-acidic seed experiments, respectively. The concentrations of detected 13BD SOA components are presented in **Tables A7–A10** in the Appendix. The formation of 13BD SOA products such as threitol, erythritol, glyceric acid, threonic acid and tartaric acid has been reported in field samples and chamber studies under low- and high-NO<sub>x</sub> conditions by Jaoui et al. (2014). The formation mechanism under low-NO<sub>x</sub> conditions has been explained by the reactive uptake of 2,3-epoxy-1,4-butanediol (BEPOX) onto acidic aerosol seeds, and under

high-NO<sub>x</sub> conditions by further oxidation of acryloyl peroxyxynitrate (APAN) to acrylic acid epoxide (AAE).

In the smog-chamber experiments, secondary organic carbon (SOC) produced under acidic conditions was higher compared to non-acidic conditions at corresponding RH levels. The formation of the individual organic compounds detected usually followed the same pattern. The highest amounts of most OSs, NOSs and NSOSs were produced at the lowest RH level in the acidic seed experiments and decreased with increasing RH. The effect of relative humidity on 13BD SOA formation was pronounced for acidic seed aerosol, and mild for non-acidic seed aerosol. Those findings may indicate that the acidic conditions enhance the formation of most 13BD SOA components.



**Figure 20.** Concentrations of organic acids (HOM tracers) from the 13BD acidic (A; ER444) and non-acidic seed experiments (B; ER666), determined using UPLC-MS (values are listed in **tables A9 - A10** in the Appendix)

In addition, **Figure 20** shows that tartronic acid (TrtA; MW 120), malic acid (MA; MW 134), threonic acid (TrA; MW 136), and tartaric acid (TA; MW 150) concentrations were greater in non-acidic seed experiments at the lowest RH level: 20, 300, 180 and 15 ng m<sup>-3</sup>, respectively. Tartaric acid was not detected in acidic seed experiments, and tartronic acid was not detected in acidic seed experiments at the highest RH level. Apparently, high relative humidity and acidic conditions may hinder the formation of those compounds. The increase of relative humidity in both kinds of smog-chamber experiments did not significantly affect the yields of TrA and MA, although the maximal concentration of MA was found at RH level of 50% (acidic seeds) and 49% (non-acidic seeds), respectively. Moreover, for non-acidic seed aerosol slight RH dependence has been observed for threonic acid (MW 136).

In following sections, I compared the components of smog-chamber aerosol samples with reference compounds in order to confirm the structures of compounds

presented in Fig. 20 and tentatively proposed by Jaoui et al. (2014) – tartronic acid (MW 120), threonic acid (MW 136), malic acid (MW 134) and tartaric acid (MW 150). Notwithstanding, the high-resolution UPLC-MS analyses focused mainly on the formation of the variety of organosulfates and nitroxy- and nitrosoxy-organosulfates. To my best knowledge, OSs and NOSs detected were characterized for the first time as 13BD SOA products present in smog-chamber experiments and ambient aerosol. Several 13BD SOA components identified in field samples prove that 13BD oxidation contributes to ambient aerosol formation.

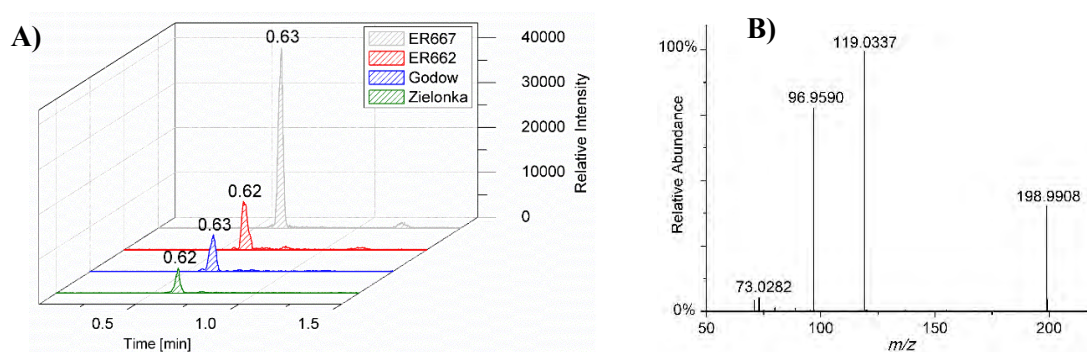
### 3.3 Investigation of isoprene and butadiene SOA compounds in fine aerosol

In my Ph.D. thesis, I focused on the detection of selected ISO and 13BD SOA components in ambient aerosol samples. Thus, I investigated the chemical composition of aerosol samples collected in various region of Poland. The Extracted Ion Chromatograms (EIC) presented in this Chapter compare the SOA components detected in smog-chamber experiments at the highest RH level with components of ambient aerosol samples. The experimental and ambient conditions were as similar as possible. The EIC results for ambient aerosol were presented only when the particular compound was present in the amounts sufficient for reliable chromatographic responses. The Chapter contains also data on structural elucidation of novel and previously reported SOA components based on product ion mass spectra recorded. Moreover, the role of strictly controlled smog-chamber experiments in revealing the chemistry and composition of atmospheric aerosol was demonstrated.

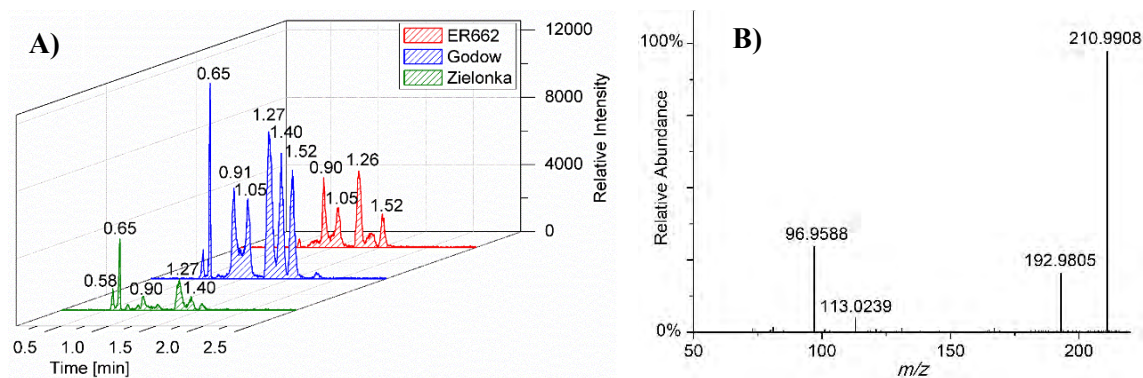
#### 3.3.1 Organosulfates formation from isoprene

The smog chamber results were compared to the composition of PM<sub>2.5</sub> samples collected at two rural sites – Zielonka (influenced mainly by biogenic precursors) and Godów (influenced both by biogenic and anthropogenic precursors). To keep the experimental and ambient conditions as similar as possible, the experiments carried under the highest relative humidities were selected: ER662 at RH 44% (acidic seeds) and ER667 at RH 49% (non-acidic seeds). **Figures 21–24** show the extracted ion chromatograms of four ISO SOA components, which were identified previously (Surratt et al., 2007a, 2008, 2010; Gomez-Gonzalez et al., 2008; Lin et al., 2013; Schindelka et al., 2013; Shalamzari et al., 2013; Hettiyadura et al., 2015; Riva et al., 2016b; Spolnik et al., 2018; Wach et al., 2020). They occurred abundantly in ambient aerosol and smog chamber samples: 2-methylglyceric acid organosulfate (MW 200),

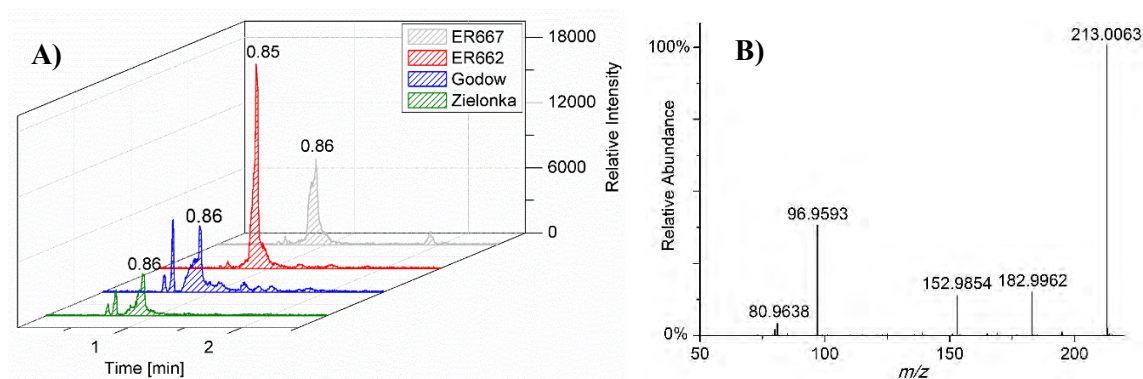
2(3H)-furanone, dihydro-3,4-dihydroxy-3-methyl- organosulfate (MW 212), 2,3,4-furantriol, tetrahydro-4-methyl organosulfate (MW 214) and 2-methyltetrol organosulfate (MW 216). The corresponding Extracted Ion Chromatograms with recorded product ion mass spectra were presented, without fragmentation schemes, since the compounds were reported previously. The present findings were consistent with earlier studies (Surratt et al., 2007a; Gomez-Gonzalez et al., 2008; Lin et al., 2013; Schindelka et al., 2013; Shalamzari et al., 2013; Hettiyadura et al., 2015; Riva et al., 2016b; Spolnik et al., 2018, Chen et al., 2020; Wach et al., 2020). For novel compounds detected, the possible chemical structures with fragmentation pathways were proposed (**Figs. 25 – 28**): 2-methylthreonic acid organosulfate (MW 230), 2-methylthreonic acid nitrooxy-organosulfate (MW 275), 2-methyltartaric acid organosulfate (MW 244). However, 2-methyltetrol nitrosooxy-organosulfate (MW 245) was detected solely in the smog chamber SOA (**Fig. 29**). The comparison of EICs shows that ISO SOA formed in the presence of acidic seed aerosol and NO<sub>x</sub> in smog-chamber experiments provide a reasonable approximation of the ambient aerosol at both sites, even though only Godów was strongly influenced by anthropogenic pollutants (NO<sub>x</sub>) from a nearby coal-fired power station. It appears that even minor amounts of NO<sub>x</sub> in the ambient atmosphere are sufficient to produce those compounds.



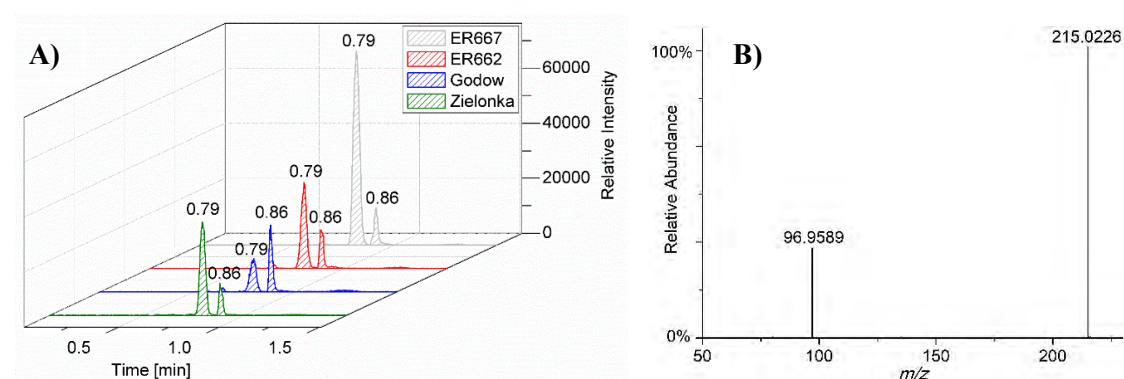
**Figure 21.** Extracted Ion Chromatograms (EIC) of 2-methylglyceric acid organosulfate with MW 200 from field studies and smog-chamber experiments (A) and ESI(-) product ion mass spectrum at RT = 0.63 min registered for SOA from the ER667 non-acidic seed aerosol experiment (B)



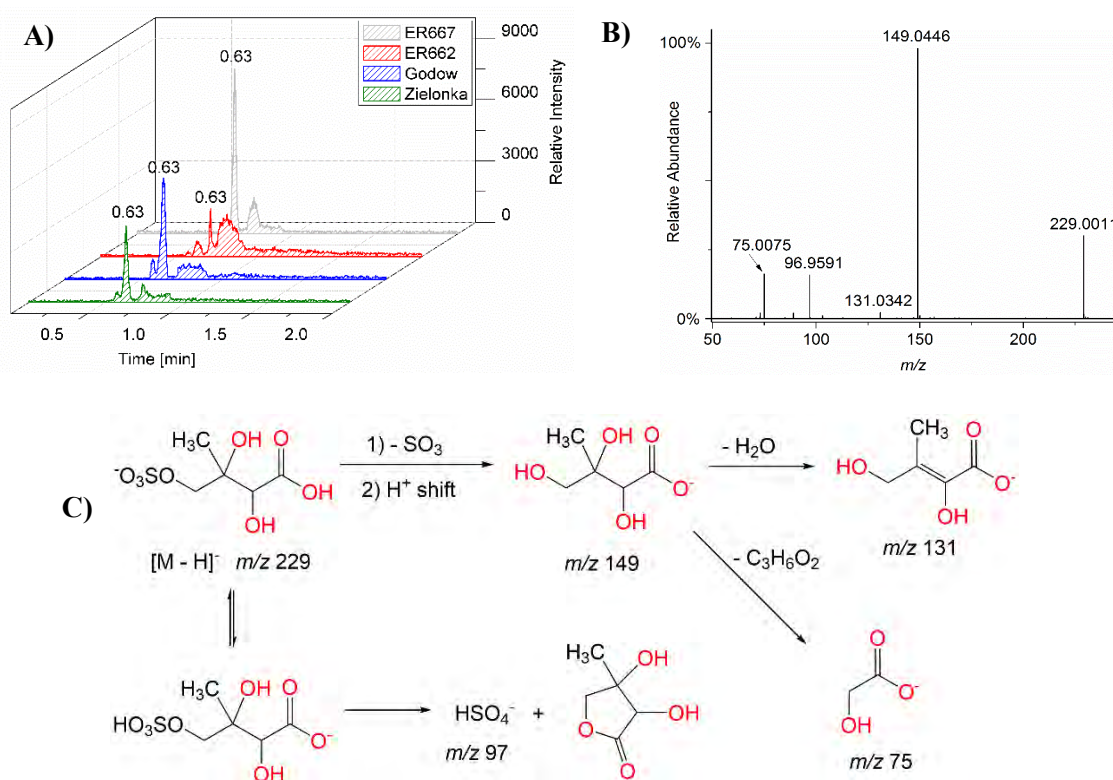
**Figure 22.** Extracted Ion Chromatograms (EIC) of 2(3H)-furanone, dihydro-3,4-dihydroxy-3-methyl-organosulfate with MW 212 from field studies and smog-chamber experiments (A) and ESI(-) product ion mass spectrum at RT = 0.90 min registered for SOA from the ER662 acidic seed aerosol experiment (B)



**Figure 23.** Extracted Ion Chromatograms (EIC) of 2,3,4-furantriol, tetrahydro-3-methylorganosulfate with MW 214 from field studies and smog-chamber experiments (A) and ESI(-) product ion mass spectrum at RT = 0.85 min registered for SOA from the ER662 acidic seed aerosol experiment (B)



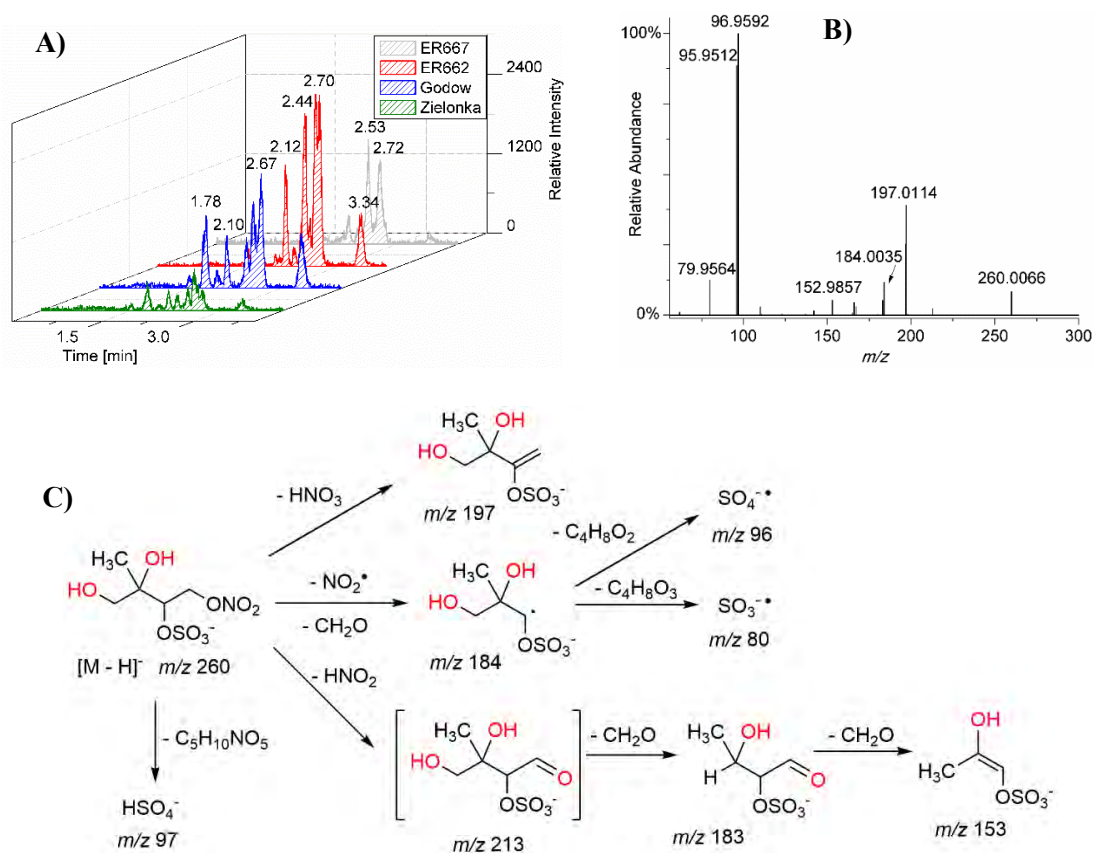
**Figure 24.** Extracted Ion Chromatograms (EIC) of 2-methyltetrol organosulfate with MW 216 from field studies and smog-chamber experiments (A) and ESI(-) product ion mass spectrum at RT = 0.79 min registered for SOA from the ER667 non-acidic seed aerosol experiment (B)



**Figure 25.** Extracted Ion Chromatograms (EIC) of 3-methylthreonic acid organosulfate with MW 230 from field studies and smog-chamber experiments (A); ESI(-) product ion mass spectrum at RT = 0.63 min registered for SOA from the ER667 non-acidic seed aerosol experiment (B) and proposed fragmentation pathway (C)

Abundant SOA component with  $m/z$  229 was determined in the smog chamber and fine aerosol samples (**Figure 25**). This OS has not been reported previously. The accurate molecular mass of that compound ( $C_5H_9O_8S$ : 229.0011 Da; error +0.7 mDa) was recorded for the Godów sample at RT = 0.63 min. It clearly indicated that the organosulfate formed *via* a much longer oxidation pathway than 2-methyltetrols OS. Two partially resolved peaks of the mass spectrometric signature of that organosulfate, indicate two chiral centers in the molecule (**Fig. 25 A**). The first eluting diastereoisomer corresponds to the peak with high abundance, while the second peak is less intensive, indicating the formation of less hindered compounds both in the chamber experiments and fine aerosol. A detailed interpretation of the product ion mass spectrum allowed to recognize the MW 230 compound as 3-methylthreonic acid organosulfate (**Fig. 25 B**, only the mass spectrum of the dominating diastereoisomer is shown). The spectrum reveals abundant fragment ion at  $m/z$  149, which may be explained through the  $SO_3$  elimination from the precursor ion  $[M-H]^-$ . Further fragmentation of  $m/z$  149 ion, i.e., a neutral loss of  $H_2O$ , reveals the simultaneous presence of  $-O-SO_3H$  and  $-CO_2H$  residues in the molecule. However, bisulfate ion ( $m/z$  97) in the product ion mass

spectrum does not unambiguously reveal the sulfation at a primary hydroxyl group in the molecule. The proposed fragmentation pathways for the MW 230 organosulfate is presented in **Fig. 25** (panel C).

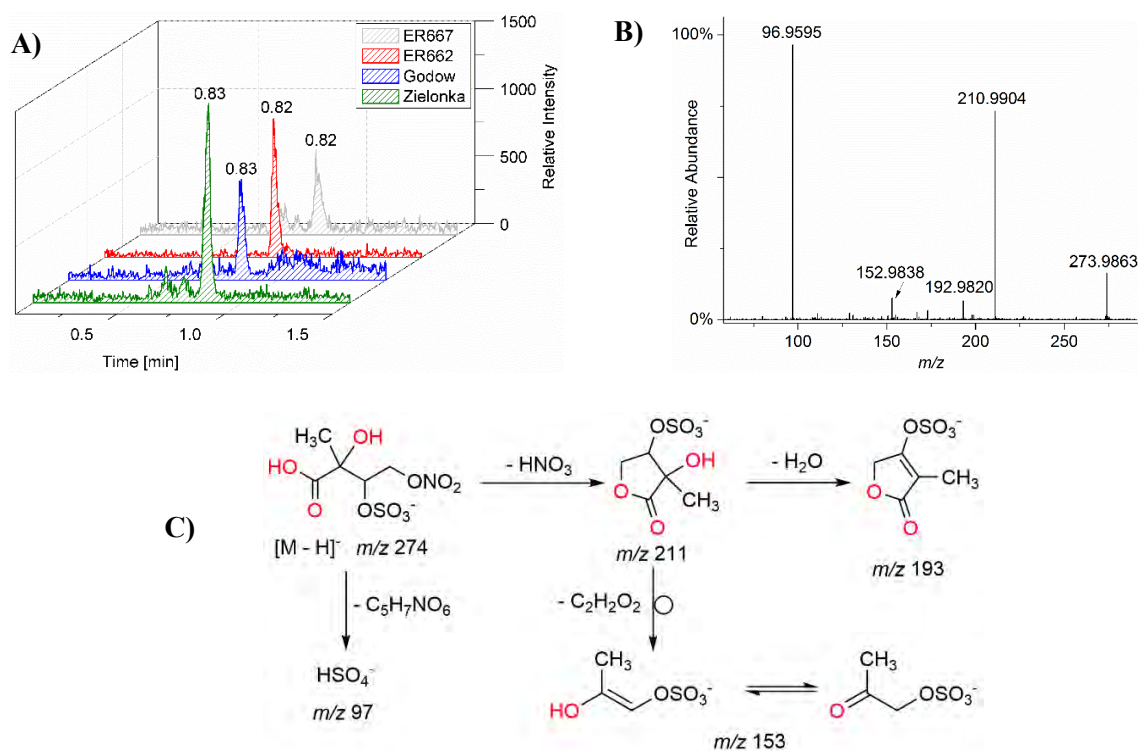


**Figure 26.** Extracted Ion Chromatograms (EIC) of 2-methyltetrol nitrooxy-organosulfate with MW 261 from field studies and smog-chamber experiments (A); ESI(-) product ion mass spectrum at RT = 2.44 min registered for SOA from the ER662 acidic seed aerosol experiment (B) and a proposed fragmentation pathway (C)

The most abundant component of ISO SOA was 2-methyltetrol nitrooxy-organosulfate  $m/z$  260 – the major early eluting compound for the smog chamber and ambient fine aerosol (**Figure 26 A**). The minor shifts in RT were mostly caused by matrix effects (Spolnik et al., 2018). The compound was reported previously (Gomez-Gonzalez et al., 2008; Surratt et al., 2007a). A detailed interpretation of ESI(-) mass spectra let propose the structure of 2-methyltetrol nitrooxy-organosulfates bearing a nitrooxy moiety at the primary hydroxyl group of 2-methyltetrol skeleton and a sulfate group at the secondary hydroxyl group (**Fig. 26 C**). The main fragmentation pathways include a neutral loss of HNO<sub>3</sub> moiety, resulting in a  $m/z$  197 base peak, and bisulfate ion (HSO<sub>4</sub>,  $m/z$  97) detachment. Another diagnostic ion with  $m/z$  184 can be assigned to a combined loss of NO<sub>2</sub> and CH<sub>2</sub>O fragments, suggesting the presence of



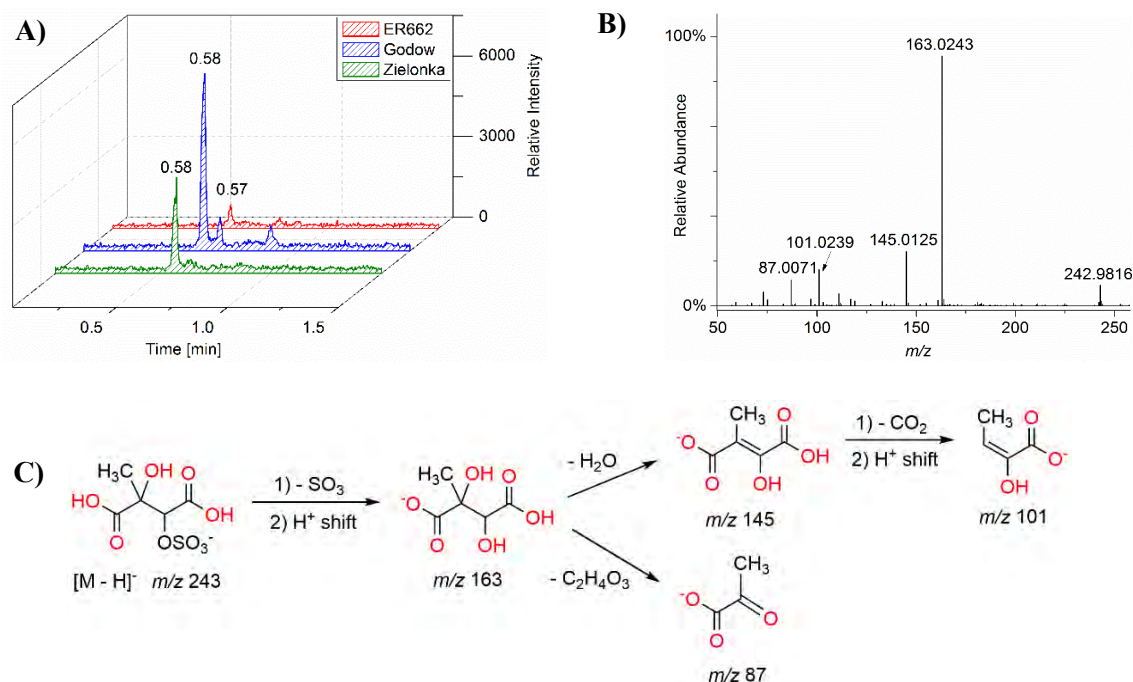
a hydroxymethyl group in the molecule. That interpretation is consistent with the presence of  $m/z$  213 and  $m/z$  183 ions. A revised structure for one isomer of 2-methylthreol NOS with the MW 261 along with the proposed fragmentation pathway was shown in **Fig. 26 B** and **C**. The accurate mass data of the deprotonated isomer ( $C_5H_{10}O_9SN$ : 260.0066 Da; error -1.0 mDa) was recorded at  $RT = 2.44$  min in SOA from the ER662 acidic seed experiment.



**Figure 27.** Extracted Ion Chromatograms (EIC) of 2-methylthreonic acid nitrooxy-organosulfate with MW 275 from field studies and smog-chamber experiments (A); ESI(-) product ion mass spectrum at  $RT = 0.82$  min registered for SOA from Zielonka fine aerosol (B) and the proposed fragmentation pathway (C)

An ISO-related organosulfate with the MW 275 was detected in noticeable quantities in the smog chamber and fine ambient aerosol samples (**Fig. 27 A**). That compound has not been reported previously, to my best knowledge. The compound fragmentation has the main transitions of  $m/z$  274  $\rightarrow$   $m/z$  211 (a loss of  $HNO_3$ ) and  $m/z$  274  $\rightarrow$   $m/z$  97 (a loss of  $C_5H_7NO_6$ ) which are shown in the product ion mass spectrum of Zielonka fine aerosol (**Fig. 27 C**). A detailed explanation of other diagnostic ions indicated the structure of 2-methylthreonic acid nitrooxy-organosulfate. Further confirmation of the MW 275 NOS structure comes from the high-resolution mass of its deprotonated form recorded at  $RT = 0.83$  min ( $C_5H_7NO_{10}S$ : 273.9873 Da, error +0.4 mDa). Due to its high oxidation state, the MW 275 nitrooxy-organosulfate could

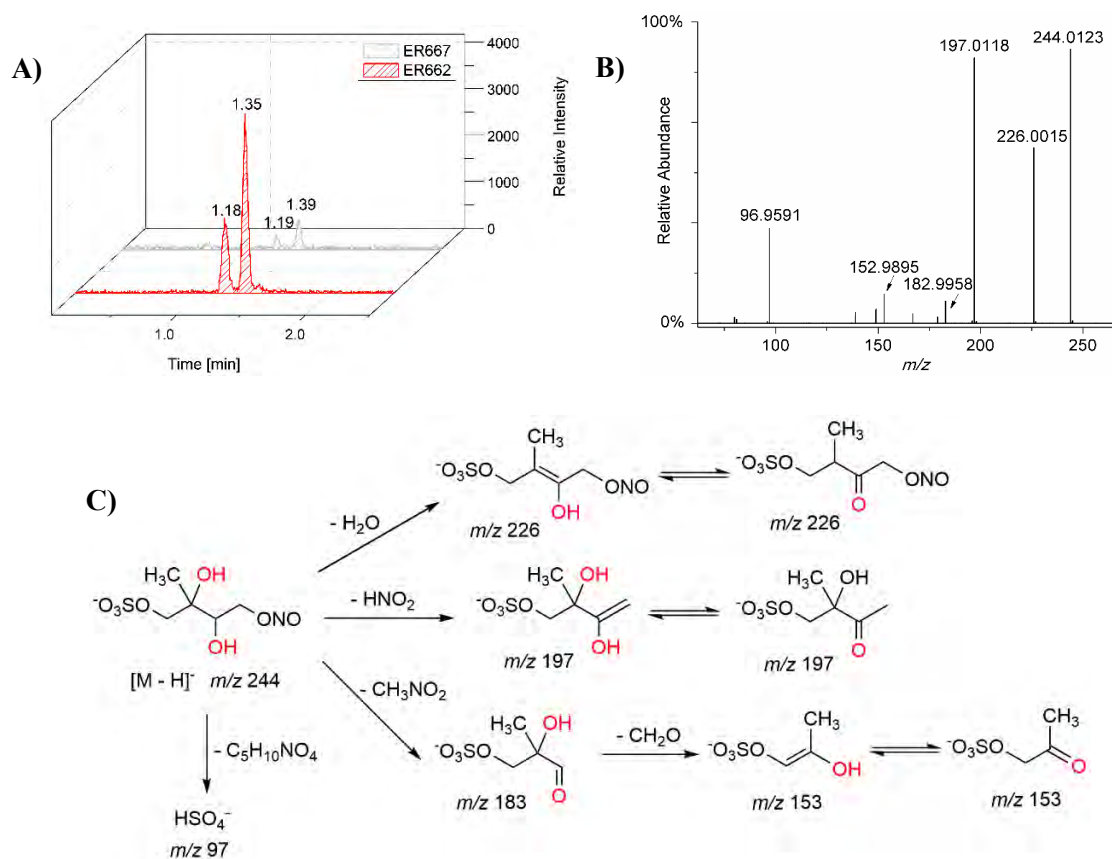
likely serve as an identifying tracer of highly oxidized isoprene SOA. However, further study is warranted to rationalize its formation mechanism in the atmosphere.



**Figure 28.** Extracted Ion Chromatograms (EIC) of 2-methyltartaric acid organosulfate with MW 244 from field studies and smog-chamber experiments (A); ESI(-)product ion mass spectrum recorded at RT = 0.58 min peak for SOA from Godów fine aerosol (B); and the proposed fragmentation pathway (C)

Another ISO-related compound detected in smog chamber and fine aerosol samples, was the organosulfate with the MW 244 (**Fig. 28**). That SOA component was not detected previously. The accurate mass of the deprotonated compound ( $C_5H_7O_9S$ : 242.9816 Da, error +0.2 mDa) was recorded at RT = 0.58 min in the Godów sample. Like for the OS with MW 230, a longer oxidation pathway can be suggested for that unknown organosulfate compared to the formation of sulfated-2-methyltetrols. Two resolved peaks of identical accurate masses can be noted, indicating the presence of two chiral centers in the molecule (**Fig. 28 B and C**). The first eluting diastereoisomer corresponds to a highly intensive chromatographic peak, while the second one has a trace intensity, suggesting hindered formation both in the smog-chamber experiments and fine aerosol. A detailed analysis of the product ion mass spectrum indicated the MW 244 compound was 2-methyltartaric acid organosulfate (**Fig. 28 B and C**, only the mass spectrum of the major diastereoisomer is shown). The recorded ESI(-) mass spectrum shows abundant fragment ions at  $m/z$  163, which may form by the  $SO_3$  loss from the precursor ion. Further fragmentation of  $m/z$  163 ion, i.e., a neutral water loss,

is followed by decarboxylation to  $m/z$  101. However, the absence of the bisulfate ion in the product ion mass spectrum indicates a lack of a proton adjacent to the sulfated residue, and thus suggests the sulfation of a secondary hydroxyl group (Spolnik et al., 2018).



**Figure 29.** Extracted Ion Chromatograms (EIC) of 2-methyltetrol nitrosooxy-organosulfate with MW 245 from smog-chamber experiments (A; not detected in field samples); ESI(-) product ion mass spectrum at RT = 1.35 min registered for SOA from the ER662 acidic seed aerosol experiment (B); and the proposed fragmentation pathway (C)

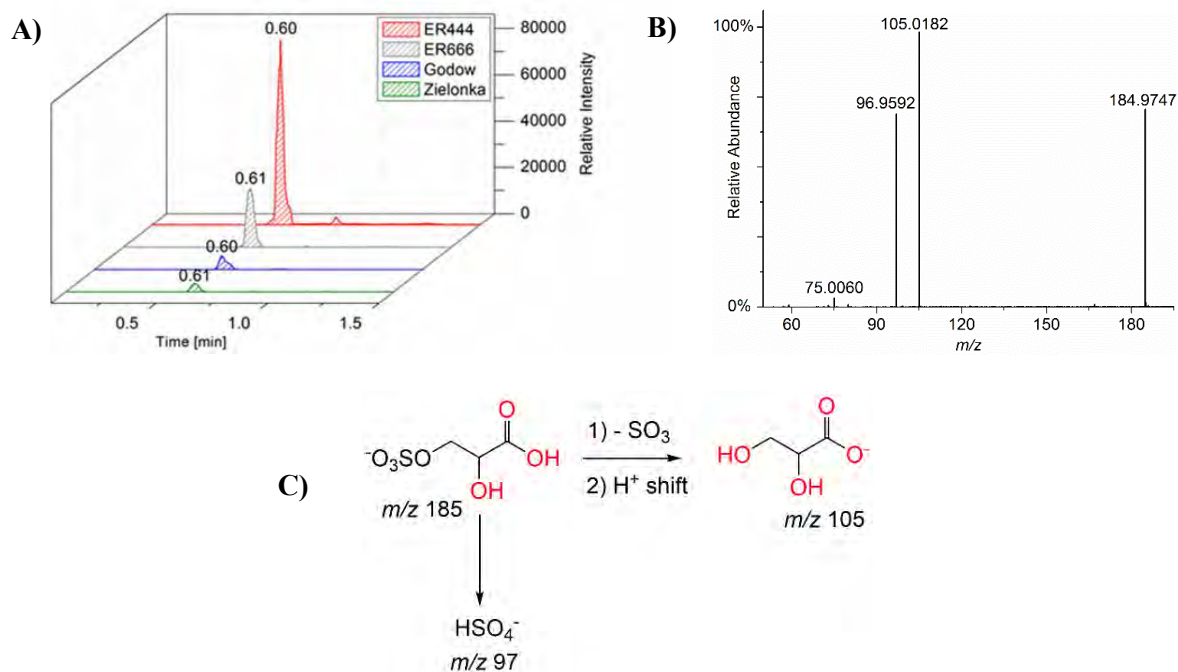
The last compound with MW 245 was detected in smog chamber samples but not in ambient aerosol (Fig. 29). Probably, that compound was a reactive reaction intermediate in formation of ISO SOA. Two baseline-resolved peaks with identical product ion mass spectra can be attributed to diastereoisomers with a retained isoprene backbone (Fig. 29 A). Surratt and co-workers (2007a) observed the formation of a similar compound in the isoprene photooxidation experiment under high-NO<sub>x</sub> conditions and proposed it was 2-methylglyceric acid nitrooxy-organosulfate. However, the high-resolution mass data indicate the MW 245 components have a C<sub>5</sub>-skeleton and are 2-methyltetrol nitrosooxy-organosulfates (NSOS). The  $m/z$  244 →  $m/z$  226 transition in the product ion mass spectrum (Fig. 29 B) points to the intact secondary hydroxyl moiety

of the 2-methyltetrol skeleton. Moreover, the lack of HNO<sub>3</sub> elimination from the deprotonated precursor ion [M-H]<sup>-</sup> (*m/z* 244) clearly excludes the presence of the nitrooxy group. The abundant *m/z* 197 ion, which forms through the HNO<sub>2</sub> loss, can be associated with the presence of the -O-NO residue in the molecule. The accurate mass of the deprotonated compound (C<sub>5</sub>H<sub>10</sub>NO<sub>8</sub>S: 244.0123 Da, error -0.4 mDa) was recorded at RT = 1.35 min for ER662 acidic seed sample. The structure assigned here to the abundant MW 245 component from ER662 acidic seed experiment along with proposed fragmentation pathway are presented in **Figure 29**.

### 3.3.2 Organosulfates formation from butadiene

The approach to 13BD aerosol was like that for ISO SOA. Samples from smog-chamber experiments were compared to samples of fine aerosol collected at various sites – Diabla Góra and Zielonka (influenced mainly by biogenic precursors) and Godów (influenced by biogenic and anthropogenic precursors). To keep the experimental and ambient conditions as similar as possible, the experiments carried under high relative humidity were selected: ER444 at RH 44% (acidic seeds) and ER666 at RH 49% (non-acidic seeds). In this Chapter, the Extracted Ion Chromatograms with recorded product ion mass spectra of novel 13BD SOA components detected in smog-chamber experiments and fine aerosol were presented (**Figs 30 – 35**). The fragmentation pathways were also described. The compounds detected and characterized both in smog chamber and ambient aerosol were: glyceric acid organosulfate (MW 184), 2(3H)-furanone, dihydro-3,4-dihydroxy- organosulfate (MW 198), malic acid organosulfate (MW 214), threonic acid organosulfate (MW 216), 1,2,3,4- butanetetrol nitrooxy-organosulfate (MW 247), threonic acid nitrooxy-organosulfate (MW 261; trace amounts in Godów fine aerosol, **Fig. 35**). Some compounds were detected solely in the smog chamber SOA (**Figs. 36 – 39**). The comparison shows that butadiene SOA from the smog chamber studies in the presence of acidic seed aerosol and NO<sub>x</sub> is a reasonable approximation of the ambient SOA at the sites considered, even though only Godów was significantly influenced by anthropogenic pollutants (NO<sub>x</sub>), and Zielonka and Diabla Góra slightly, mostly by biomass burning and vehicle exhausts. Probably, even small amounts of NO<sub>x</sub> in the ambient atmosphere are sufficient for the formation of those compounds, just as for isoprene SOA. The proposed tentative structures for detected compounds were based on high-resolution mass data and product ion mass spectra recorded for separated components. However, some peaks in the Extracted Ion Chromatograms may correspond

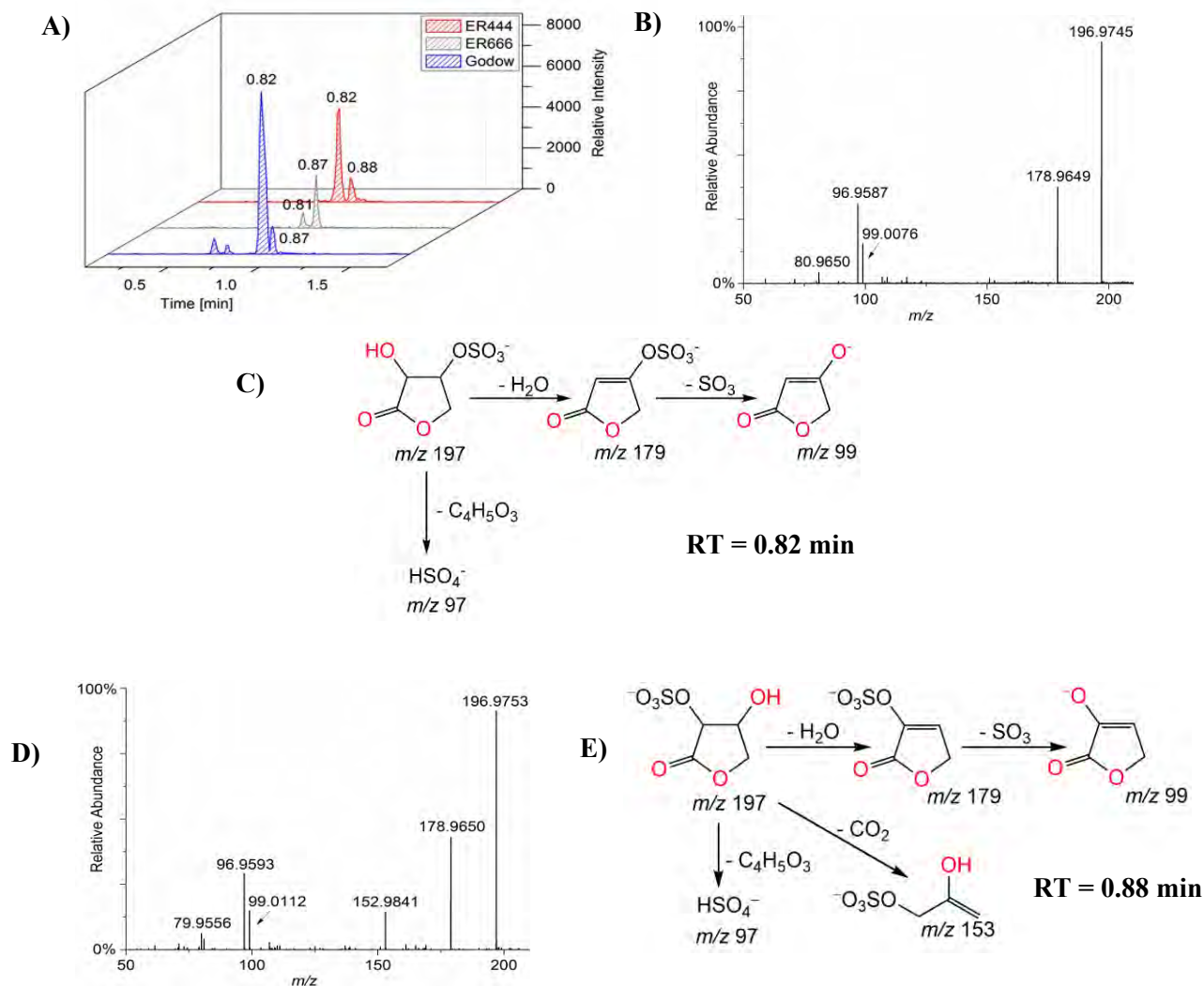
to more than one compound, especially in ambient aerosol samples where the co-elution of ions likely occurs. Proposed structures for newly identified compounds follow the assumptions described in Chapter 3.1.1 and Nestorowicz et al. (2018). All data presented in this Chapter have been included in Jaoui, Nestorowicz et al. (2023, submitted).



**Figure 30.** Extracted Ion Chromatograms (EIC) of glyceric acid organosulfate with MW 186 from smog-chamber experiments (A); ESI(-) product ion mass spectrum recorded at RT = 0.60 min for SOA from the ER444 acidic seed aerosol experiment (B); and the proposed fragmentation pathway (C)

One of the main and abundant 13BD SOA components was detected at  $m/z$  185 for the smog chamber and fine aerosol samples (**Fig. 30 A**). To my best knowledge, this OS with MW 186 has not been detected previously in ambient aerosol. The accurate mass of the deprotonated component ( $C_3H_5O_7S$ : 184.9747 Da; error +0.9 mDa) was recorded in the ER444 acidic seed experiment at RT = 0.60 min. The corresponding EIC chromatograms revealed one highly intensive peak. A detailed interpretation of product ion mass spectrum allowed to propose the MW 186 compound was glyceric acid organosulfate (**Fig. 30 B**). The main abundant fragment ion  $m/z$  105 in the mass spectrum may be explained through the  $SO_3$  elimination from the precursor  $[M-H]^-$  ion. The other abundant fragment ion detected was bisulfate ion with  $m/z$  97 ( $HSO_4^-$ ); however it does not unambiguously indicate the sulfation at a primary hydroxyl group in the molecule. The proposed fragmentation pathway for the MW 186 organosulfate is presented

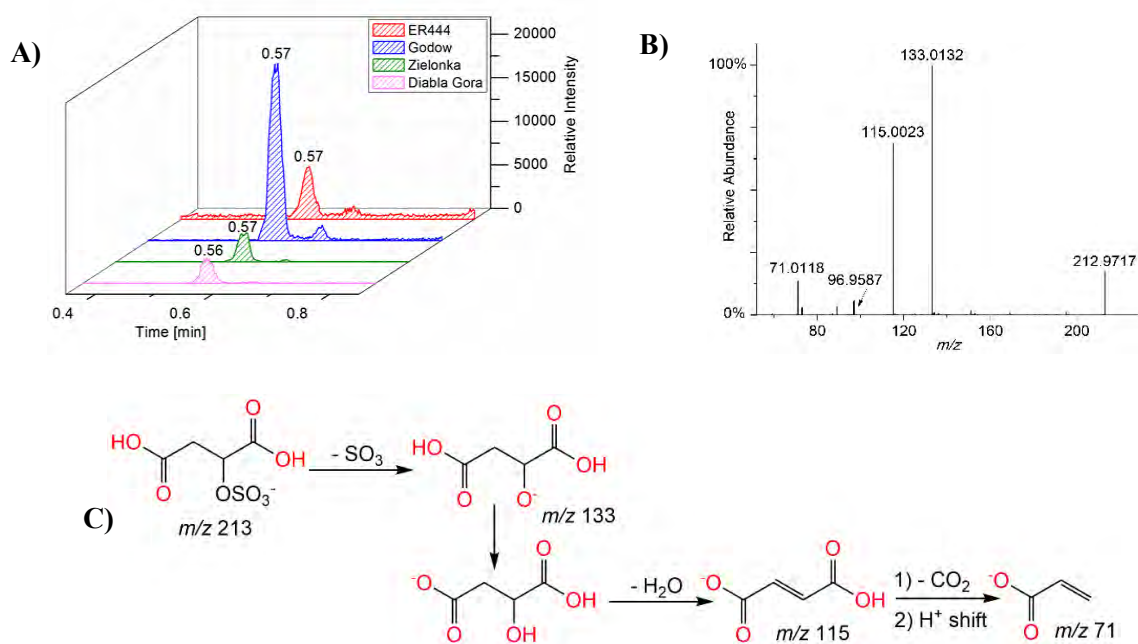
in **Fig. 30 C**. Moreover, the fragmentation pattern recorded for this 13BD components is similar to one obtained for methylglyceric acid OS from ISO SOA (compare **Fig. 21** in Chapter 3.3.1).



**Figure 31.** Extracted Ion Chromatograms (EIC) of 2(3H)-furanone, dihydro-3,4-dihydroxy-organosulfate with MW 198 from field studies and smog-chamber experiments (A); ESI(-) product ion mass spectra recorded at RT = 0.82 min (B) and at RT = 0.88 min (D) for SOA from ER444 acidic seed aerosol experiment; and the proposed fragmentation pathways (C, E)

Other newly identified component of 13BD SOA was 2(3H)-furanone, dihydro-3,4-dihydroxy-organosulfate with  $m/z$  197. Two baseline-resolved peaks with consistent MS profiles indicate two different isomeric forms of the MW 198 compound detected in considerable amounts in the smog chamber and Godów ambient fine aerosol samples (**Fig. 31 A**). The detailed interpretation of ESI(-) mass spectra for two peaks eluting at RT = 0.82 min and RT = 0.88 min indicated two 2(3H)-furanone, dihydro-3,4-dihydroxy-OSs: each bearing a sulfate moiety at the secondary hydroxyl group of

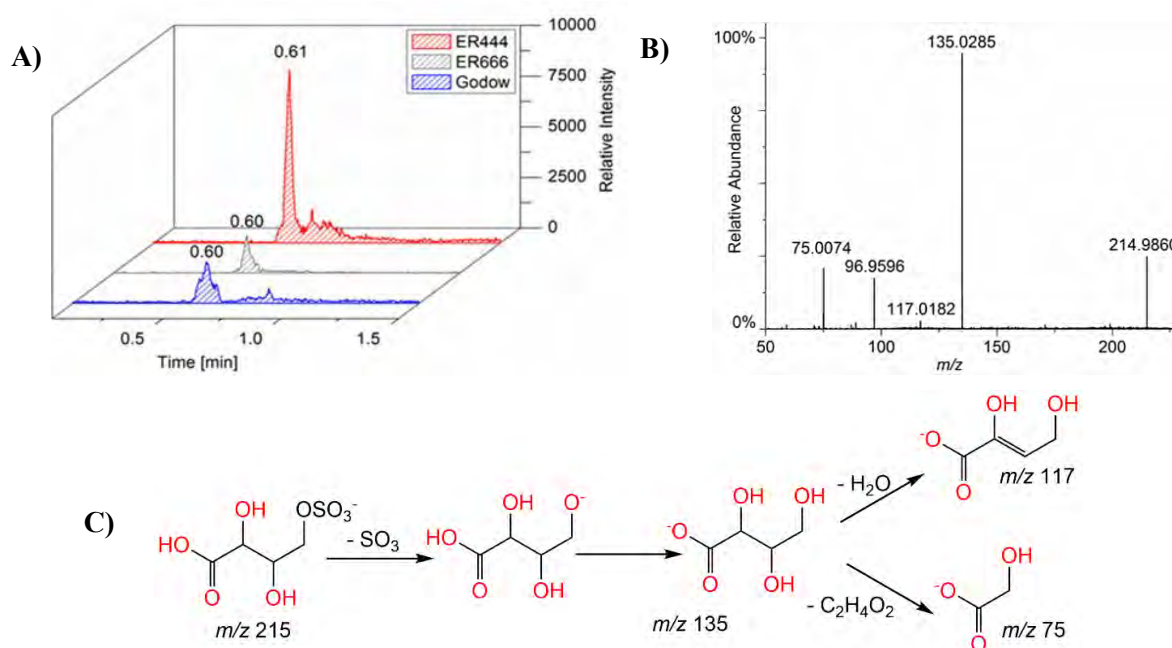
C<sub>4</sub>-cyclic lactone (**Fig. 31, C and E**). The product ion mass spectrum obtained for the first peak eluting at RT = 0.82 min (**Fig. 31 B**) shows the main transition of  $m/z$  197 →  $m/z$  179, which correspond to a neutral loss of H<sub>2</sub>O moiety from the precursor [M-H]<sup>-</sup> ion. Besides, a bisulfate ion (HSO<sub>4</sub><sup>-</sup>) at  $m/z$  97 was detected. The accurate mass of the deprotonated component (C<sub>4</sub>H<sub>5</sub>O<sub>7</sub>S: 196.9745 Da; error -1.1 mDa) was recorded in the ER444 acidic seed sample at RT = 0.82 min. The main fragmentation pathway of the second isomer eluting at RT = 0.87 min (**Fig. 32 D and E**) corresponds to a neutral loss of H<sub>2</sub>O molecule, resulting in  $m/z$  179, followed by SO<sub>3</sub> elimination. The product ion mass spectrum revealed the CO<sub>2</sub> loss, which corresponds to the transition  $m/z$  197 →  $m/z$  153. The accurate mass of the deprotonated component (C<sub>4</sub>H<sub>5</sub>O<sub>7</sub>S: 196.9753 Da; error -0.3 mDa) was recorded for the ER444 acidic seed aerosol at RT = 0.88 min. The revised structures for both isomers of 2(3H)-furanone, dihydro-3,4-dihydroxy- OS with the MW 198, along with the proposed fragmentation pathways, were shown in **Fig. 31**.



**Figure 32.** Extracted Ion Chromatograms (EIC) of malic acid organosulfate with MW 214 from field studies and smog-chamber experiments (A); ESI(-) product ion mass spectrum recorded at RT = 0.57 min for SOA from Godów fine aerosol (B); and the proposed fragmentation pathway (C)

One of the SOA component detected in significant amounts in fine aerosol and smog chamber samples was determined at  $m/z$  213 (**Figure 32 A**). One highly intensive peak at 0.57 min can be assigned to that 13BD component. The accurate mass of the deprotonated component (C<sub>4</sub>H<sub>5</sub>O<sub>8</sub>S: 212.9717 Da; error -1.2 mDa) was recorded

for Godów sample at RT = 0.57 min. That compound has not been reported previously in the literature. High-resolution data strongly suggested long oxidation pathway for this compound. A detailed interpretation of the product ion mass spectrum allowed to assign its structure to malic acid organosulfate (**Fig. 32 B**). The spectrum reveals abundant fragment  $m/z$  133 ion as the base peak, which may be explained through the  $\text{SO}_3$  elimination from the precursor  $[\text{M}-\text{H}]^-$  ion. Further fragmentation of  $m/z$  133 ion, i.e., a neutral loss of  $\text{H}_2\text{O}$  and  $\text{CO}_2$ , reveals the presence of  $-\text{CO}_2\text{H}$  residues in the structure. The proposed fragmentation pathway for the novel malic acid organosulfate is presented in **Fig. 32 C**.

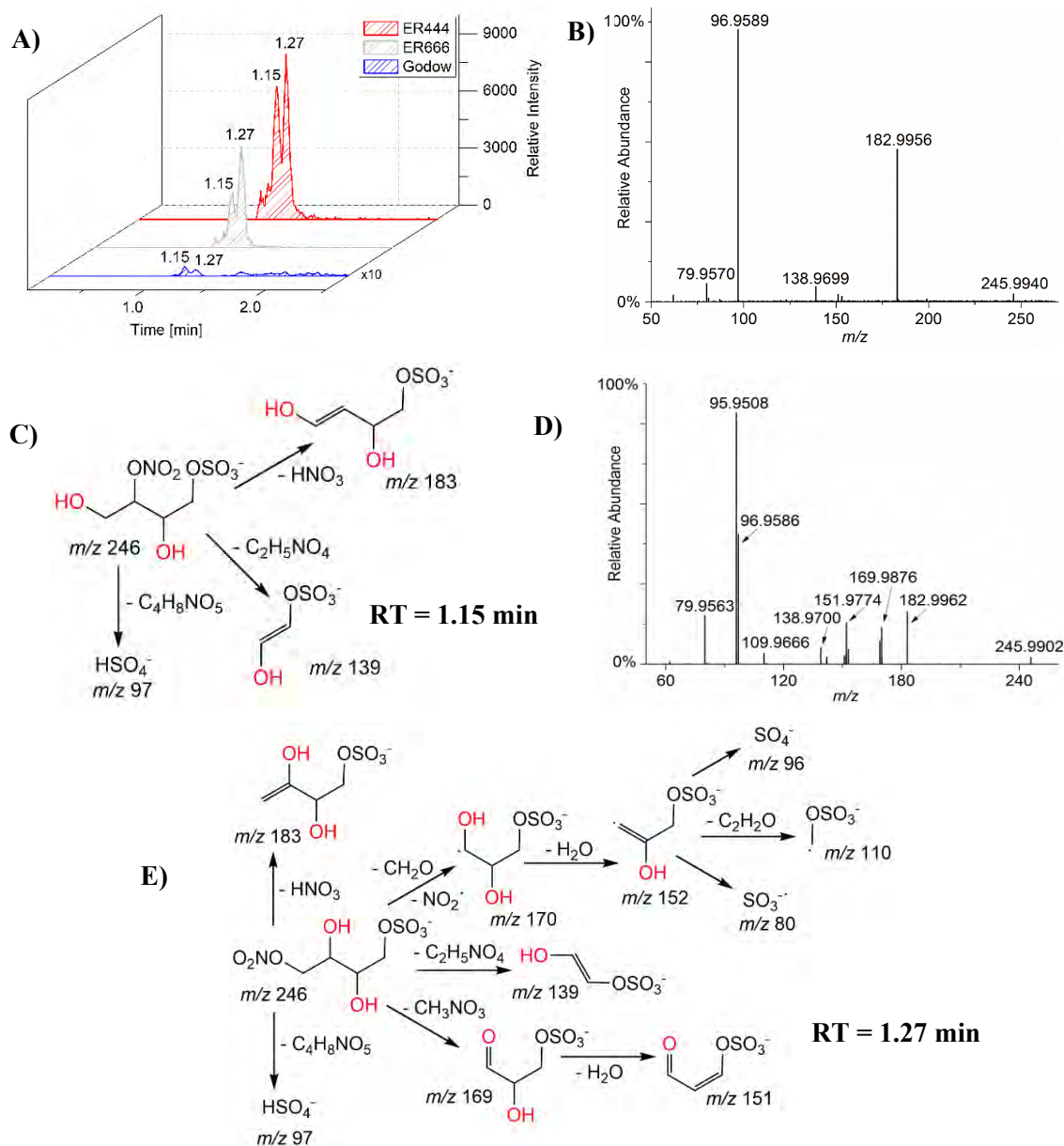


**Figure 33.** Extracted Ion Chromatograms (EIC) of threonic acid organosulfate with MW 216 from field studies and smog-chamber experiments (A); ESI(-) product ion mass spectrum recorded at RT = 0.61 min for SOA from ER444 acidic seed aerosol experiment (B); and the proposed fragmentation pathway (C)

Another considerable 13BD SOA component was detected at  $m/z$  215 in the smog chamber, and in smaller amounts in fine aerosol samples (**Fig. 33 A**). One highly intensive peak can be assigned to the unknown MW 216 compound. It has not been reported previously in the literature. The accurate mass of the deprotonated component ( $\text{C}_4\text{H}_7\text{O}_8\text{S}$ : 214.9860 Da; error -0.2 mDa), recorded at RT = 0.61 min for the ER444 acidic seed aerosol, indicates long formation pathway of that OS like for malic acid organosulfate. A detailed interpretation of the product ion mass spectrum allowed to identify the OS as threonic acid organosulfate (**Fig. 33 B**). The spectrum reveals an abundant fragment ion at  $m/z$  135, which may be explained with the  $\text{SO}_3$  elimination from the parent  $[\text{M}-\text{H}]^-$

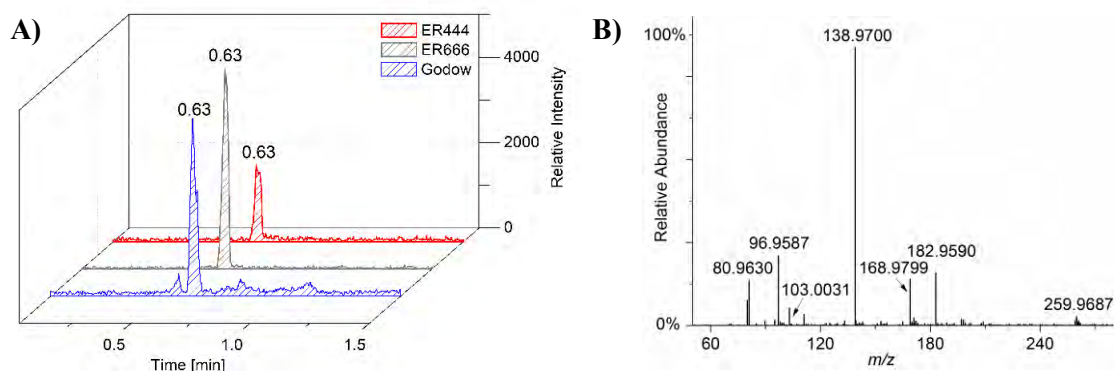


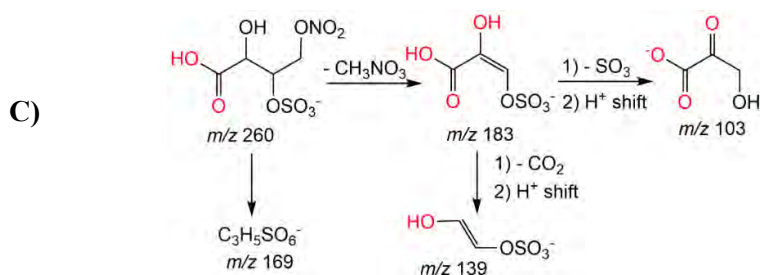
ion. Further fragmentation of  $m/z$  149 ion, i.e., a neutral loss of  $\text{H}_2\text{O}$ , reveals the presence of  $-\text{O}-\text{SO}_3\text{H}$  and  $-\text{CO}_2\text{H}$  residues in the MW 216 organosulfate. However, bisulfate ion ( $m/z$  97) in the product ion mass spectrum does not unambiguously reveal the sulfation at the primary hydroxyl group in the molecule. The proposed fragmentation pathway for threonic acid organosulfate is presented in **Fig. 33 C**. The fragmentation pattern proposed for that compound is similar to one for 3-methylthreonic acid OS from isoprene SOA (compare **Fig. 25** in Chapter 3.3.1).



**Figure 34.** Extracted Ion Chromatograms (EIC) of 1,2,3,4-butanetrol nitrooxy-organosulfate with MW 247 from field studies and smog-chamber experiments (A); ESI(-) product ion mass spectra recorded at RT = 1.15 min (B) and RT = 1.27 min for SOA from ER444 acidic seed aerosol experiment (D); and the proposed fragmentation pathways (C, E)

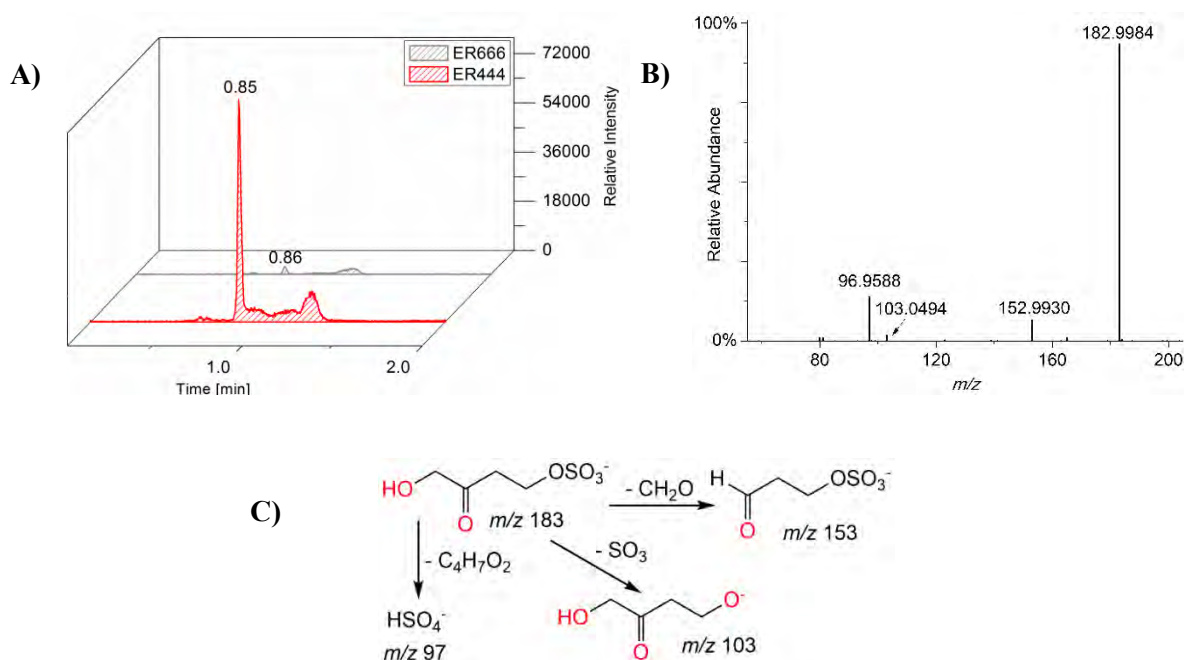
The most abundant novel component of 13BD SOA generated in smog chamber was 1,2,3,4-butanetetrol nitrooxy-organosulfate ( $m/z$  246). Two partially resolved peaks with identical MS profiles indicate two isomeric forms of the MW 247 compound detected also in ambient fine aerosol in trace amounts (**Fig. 34 A**). The detailed interpretation of ESI(-) mass spectra recorded for the isomers eluting at RT = 1.15 min and RT = 1.27 min led to two structures for 1,2,3,4-butanetetrol NOS: bearing a nitrooxy moiety substituted either at the primary or the secondary hydroxyl group of C<sub>4</sub>- skeleton (**Figs. 34 C and E**). The product ion mass spectrum (**Fig. 32 B**) obtained for the first peak eluting at RT = 1.15 min corresponds to a neutral loss of HNO<sub>3</sub> moiety from the precursor [M-H]<sup>-</sup> ion, resulting in  $m/z$  183 as a base peak, and to a bisulfate ion (HSO<sub>4</sub><sup>-</sup>) at  $m/z$  97. Another diagnostic ion at  $m/z$  139 can result from a combined loss of C<sub>2</sub>H<sub>5</sub>O<sub>2</sub> and NO<sub>2</sub> moieties. The accurate mass of the deprotonated component (C<sub>4</sub>H<sub>8</sub>O<sub>9</sub>SN: 245.9940 Da; error -2.0 mDa) was recorded at RT = 1.15 min for the ER444 acidic seed aerosol. The main fragmentation pathway of the second isomer eluting at RT = 1.27 min (**Fig. 34 D and E**) corresponds to a neutral loss of HNO<sub>3</sub> moiety, resulting in an  $m/z$  183 base peak, and to a bisulfate ion at  $m/z$  97 and sulfate radical anion at  $m/z$  96. Another diagnostic ion at  $m/z$  170 can be assigned to a combined loss of NO<sub>2</sub> and CH<sub>2</sub>O. The accurate mass of the deprotonated compound (C<sub>4</sub>H<sub>8</sub>O<sub>9</sub>SN: 245.9902 Da; error -1.8 mDa) was recorded at RT = 1.27 min for the ER444 acidic seed aerosol. **Figure 34** (panel C and E) shows the revised structures of two isomeric 1,2,3,4-butanetetrol NOS forms with the MW 247 along with the proposed fragmentation pathway.





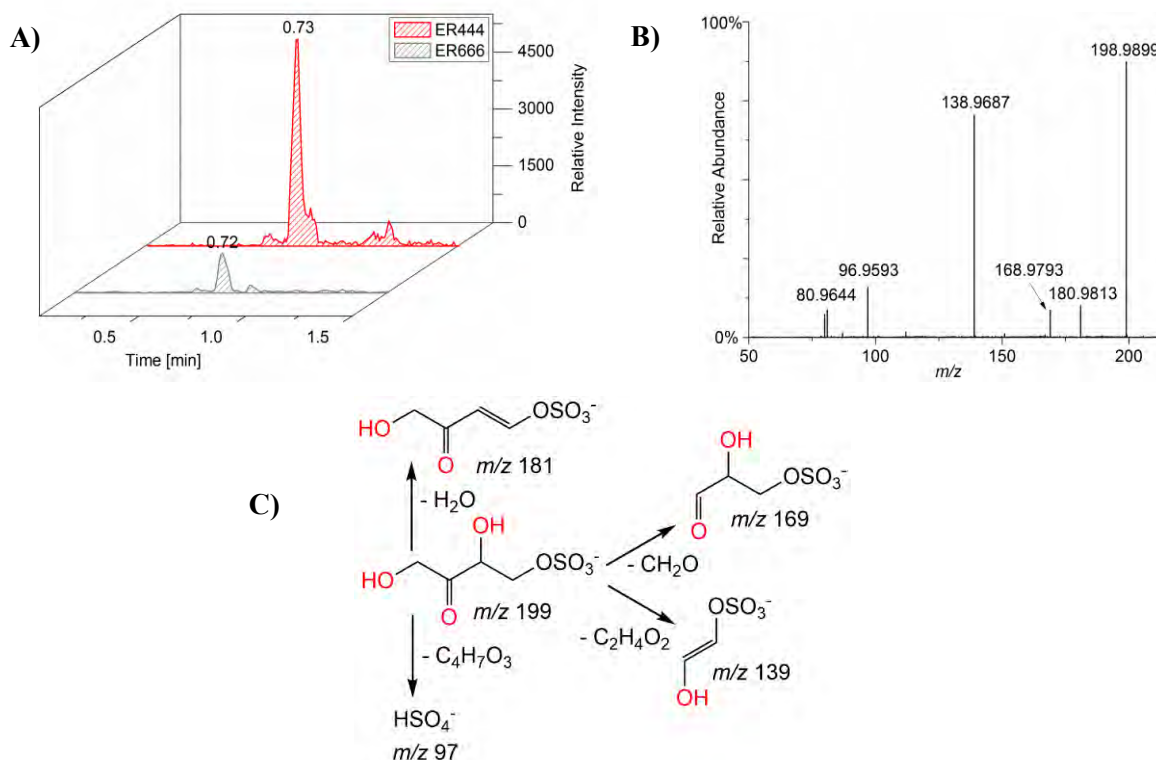
**Figure 35.** Extracted Ion Chromatograms (EIC) of threonic acid nitrooxy-organosulfate with MW 261 from field studies and smog-chamber experiments (A); ESI(-) product ion mass spectrum recorded at RT = 0.63 min for SOA from ER666 non-acidic seed aerosol experiment (B); and the proposed fragmentation pathway (C)

Based on the UPLC-MS analyses, the last 13BD-related compound with the MW 261 detected in noticeable amounts in fine ambient aerosol and smog chamber samples was identified as threonic acid nitrooxy-organosulfate (**Fig. 35 A**). That compound has not been reported previously. It has main fragmentation transitions of  $m/z\ 260 \rightarrow m/z\ 183$  (a combined loss of  $\text{CH}_3\text{NO}_3$  moiety) and  $m/z\ 183 \rightarrow m/z\ 139$  (a loss of  $\text{CO}_2$ ) as shown for ER666 non-acidic seed aerosol (**Fig. 35 C**). The high-resolution mass for this 13BD SOA component eluting at RT = 0.63 min ( $\text{C}_4\text{H}_7\text{NO}_{10}\text{S}$ : 259.9687 Da, error -2.5 mDa) indicates the structure of NOS. Due to its high oxidation state, threonic acid nitrooxy-organosulfate may serve as a tracer of highly oxidized butadiene SOA.



**Figure 36.** Extracted Ion Chromatograms (EIC) 2-butanone, 1,4-dihydroxy-organosulfate with MW 184 from smog-chamber experiments, not detected in field samples (A); ESI(-) product ion mass spectrum recorded at RT = 0.85 min for SOA from ER444 acidic seed aerosol experiment (B); and the proposed fragmentation pathway (C)

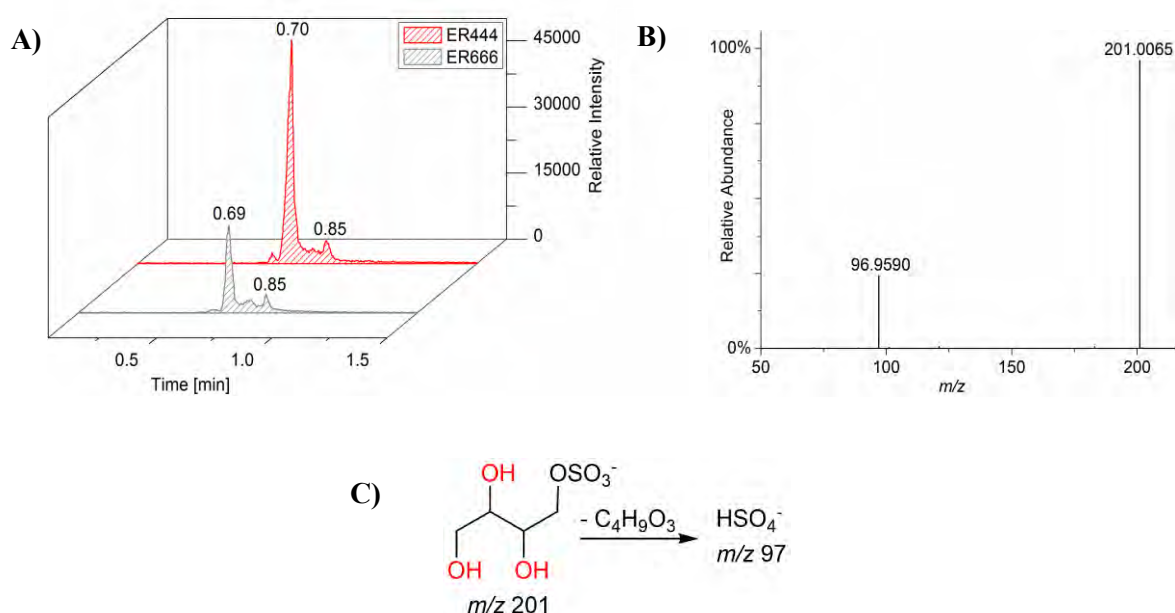
**Figure 36** shows that the newly identified 13BD SOA component with MW 184 was not detected in ambient aerosol. The deprotonated compound  $[M-H]^-$  ion associated with the main chromatographic peak and its accurate mass ( $C_4H_7O_6S$ : 182.9984 Da, error +2.1 mDa) recorded at RT = 0.85 min for ER444 acidic seed aerosol revealed the compound had a butane backbone. A detailed interpretation of the product ion mass spectrum allowed to identify the structure of MW 184 unknown compound as 2-butanone, 1,4-dihydroxy- organosulfate (**Fig. 36 B**). The main fragment ion at  $m/z$  153 can be explained through the  $CH_2O$  elimination from the precursor  $[M-H]^-$  ion. The other transition of  $m/z$  183  $\rightarrow$   $m/z$  139 can be explained by the loss of  $SO_3$  from the precursor ion. A bisulfate ion was detected, however, it does not unambiguously reveal the sulfation at a primary hydroxyl group. The proposed fragmentation pathway for the organosulfate with MW 184 is presented in **Fig. 36 C**.



**Figure 37.** Extracted Ion Chromatograms (EIC) of 2-butanone, 1,3,4-trihydroxy-organosulfate with MW 200 from smog-chamber experiments, not detected in field samples (A); ESI(-) product ion mass spectrum recorded at RT = 0.73 min for SOA from ER444 acidic seed aerosol experiment (B); and the proposed fragmentation pathway (C)

**Figure 37** presents the smog-chamber 13BD SOA component with MW 200 eluting at RT = 0.73 min, which was not detected in ambient aerosol. The accurate mass of the deprotonated compound ( $C_4H_7O_7S$ : 198.9899 Da, error -1.4 mDa) was recorded at RT = 0.73 min for ER444 acidic seed aerosol experiment. A detailed interpretation of

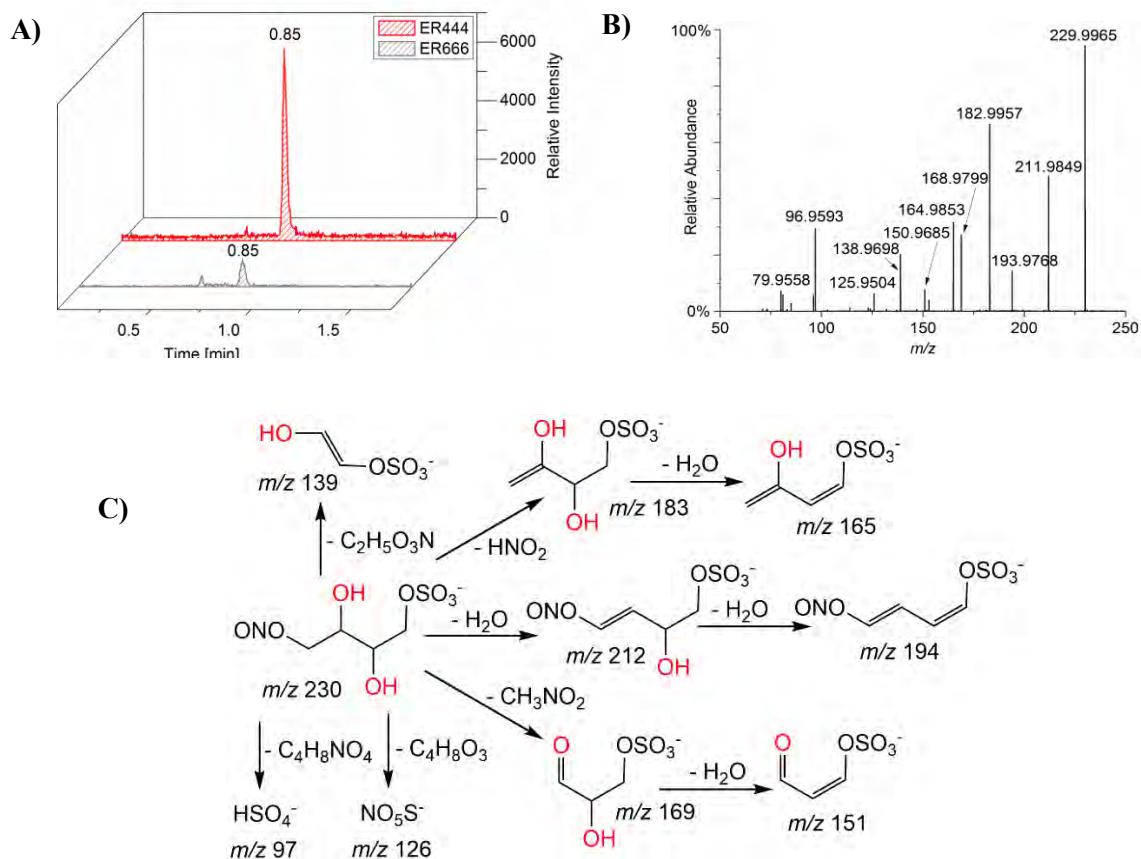
the product ion mass spectrum allowed to identify the MW 200 unknown compound as 2-butanone, 1,3,4-trihydroxy- organosulfate (**Fig. 37 B**). The proposed fragmentation pathway is presented in **Fig. 37 C**. Three main transitions from the precursor ion are:  $m/z$  199  $\rightarrow$   $m/z$  181 (neutral loss of  $\text{H}_2\text{O}$ ),  $m/z$  199  $\rightarrow$   $m/z$  169 (loss of  $\text{CH}_2\text{O}$ ),  $m/z$  199  $\rightarrow$   $m/z$  139 (loss of  $\text{C}_2\text{H}_4\text{O}_2$ ). The proposed structure of 2-butanone, 1,3,4-trihydroxy- OS formed in 13BD SOA was not reported previously. However, Gomez-Gonzalez et al. (2008) also found an unknown compound with MW 200 in ambient aerosol from K-Puszt (Hungary) but the main transition they observed was  $m/z$  199  $\rightarrow$   $m/z$  155 (loss of  $\text{C}_2\text{H}_4\text{O}$ ). Based on the low-resolution product ion mass spectrum, they proposed a tentative 2-hydroxy-1,4-butanedialdehyde structure.



**Figure 38.** Extracted Ion Chromatograms (EIC) of 1,2,3,4-butanetetrol organosulfate with MW 202 from smog-chamber experiments, not detected in field samples (A); ESI(-) product ion mass spectrum recorded at RT = 0.70 min for SOA from ER444 acidic seed aerosol experiment (B); and the proposed fragmentation pathway (C)

The second abundant compound detected in 13BD SOA from smog chamber but not in fine aerosol, was 1,2,3,4-butanetetrol organosulfate with MW 202 (**Fig. 38**). The deprotonated compound  $[\text{M}-\text{H}]^-$  ion associated with the main chromatographic peak and the accurate mass ( $\text{C}_4\text{H}_9\text{O}_7\text{S}$ : 201.0065 Da, error -0.4 mDa) recorded at RT = 0.70 min for ER444 acidic seed aerosol revealed the compound had a butane backbone. The only fragment ion detected found in the recorded product ion mass spectrum (**Fig. 38 B**) was the abundant bisulfate ion with  $m/z$  97 ( $\text{HSO}_4^-$ ). The exact position of the sulfate group in the  $\text{C}_4$ - skeleton could not be predicted. In this case,

bisulfate ion does not unambiguously reveal the sulfation at a primary hydroxyl group in the molecule. The fragmentation pattern obtained for 1,2,3,4-butanetretol OS is similar to that of 2-methyltetrol OS in isoprene SOA (compare **Fig. 24** in Chapter 3.3.1).



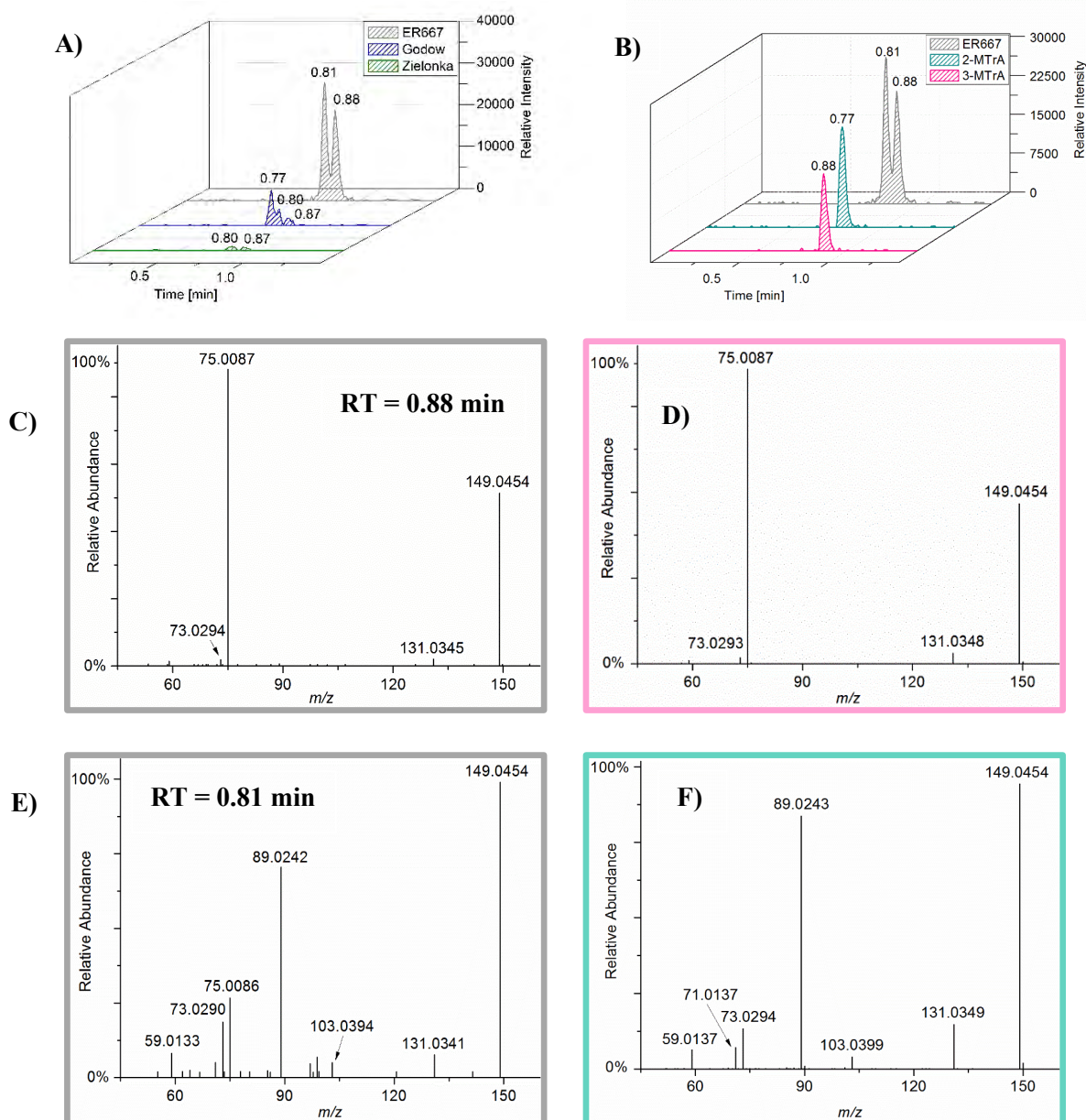
**Figure 39.** Extracted Ion Chromatograms (EIC) of 1,2,3,4- butanetretol nitrosooxy-organosulfate with MW 231 from smog-chamber experiments, not detected in field samples (A); ESI(-) product ion mass spectra recorded at RT = 0.85 min for SOA from ER444 acidic seed aerosol experiment (B); and the proposed fragmentation pathway (C)

**Figure 39** presents the smog chamber-generated 13BD SOA component with the MW 231, which was not detected in ambient aerosol. Probably, that compound is a reactive reaction intermediate in the formation of 13BD SOA. One sharp chromatographic peak and the high-resolution  $\text{OSO}_3^-$  mass data indicate the MW 231 unknown component had a  $\text{C}_4$ -skeleton of 1,2,3,4- butanetretol nitrosooxy-organosulfate (NSOS). The accurate mass ( $\text{C}_4\text{H}_8\text{NO}_8\text{S}$ : 229.9965 Da, error -0.5 mDa) was recorded at RT = 0.85 min for ER444 acidic seed experiment. The product ion mass spectrum for 1,2,3,4- butanetretol NSOS along with proposed fragmentation pathway is presented in **Fig. 39 B** and **C**. The  $m/z$  230  $\rightarrow$   $m/z$  212  $\rightarrow$   $m/z$  194 transitions indicate the detachment of two  $\text{H}_2\text{O}$  groups from the  $\text{C}_4$ -skeleton. Moreover, the lack of  $\text{HNO}_3$  elimination from the deprotonated precursor  $[\text{M}-\text{H}]^-$  ion ( $m/z$  230) excludes the presence of the nitrooxy

group in the molecule. The abundant  $m/z$  183 ion, which forms through the  $\text{HNO}_2$  loss, can be associated with the existence of the  $-\text{O}-\text{NO}$  residue. The proposed structure of 1,2,3,4- butanetetrol NSOS formed in 13BD SOA was not reported previously.

### 3.3.3 Organic acids formation from isoprene

Organic acids that originate from the oxidation of biogenic compounds like isoprene are SOA components with high oxygen to carbon (O/C) ratios serving as highly oxygenated molecular (HOM) tracers (Noziere et al., 2015). The formation of HOM tracers with  $\text{O/C} \geq 1$  in ISO SOA has been investigated in the smog-chamber experiments at high concentration of nitrogen oxides ( $\text{NO}_x$ ) run with acidic or non-acidic aerosol seeds. Organic acids from isoprene were also determined in  $\text{PM}_{2.5}$  aerosol samples collected in various regions of Poland, mainly Zielonka and Godów stations, and analyzed using Orbitrap UPLC-MS technique (**Figures 40** and **41**). 2-methyltartaric acid (2-MTA), 2-methylthreonic acid and 3-methylthreonic acids (2-MTrA and 3-MTrA) were detected both in the smog-chamber and field samples, so they can represent aged ISO SOA. The proposed structures of both HOM tracers were confirmed with Orbitrap UPLC-MS analyses by a comparison of the retention times, accurate mass spectral signatures and product ion mass spectra. Recorded product ion mass spectra of synthesized standards, including 2-MTrA, 3-MTrA and 2-MTA, have been used for that comparison. The synthesis procedure involved, i.a. the hydrolysis of appropriate lactone *cis*-diols under alkaline conditions to the final products. The complete synthesis procedures were described in Chapter 2.2.1. Mass spectra of synthesized standard compounds and filter extracts from smog chamber and ambient aerosol samples were compared in **Figures 40** and **41**. All data presented in this Chapter were published in Jaoui et al. (2019).

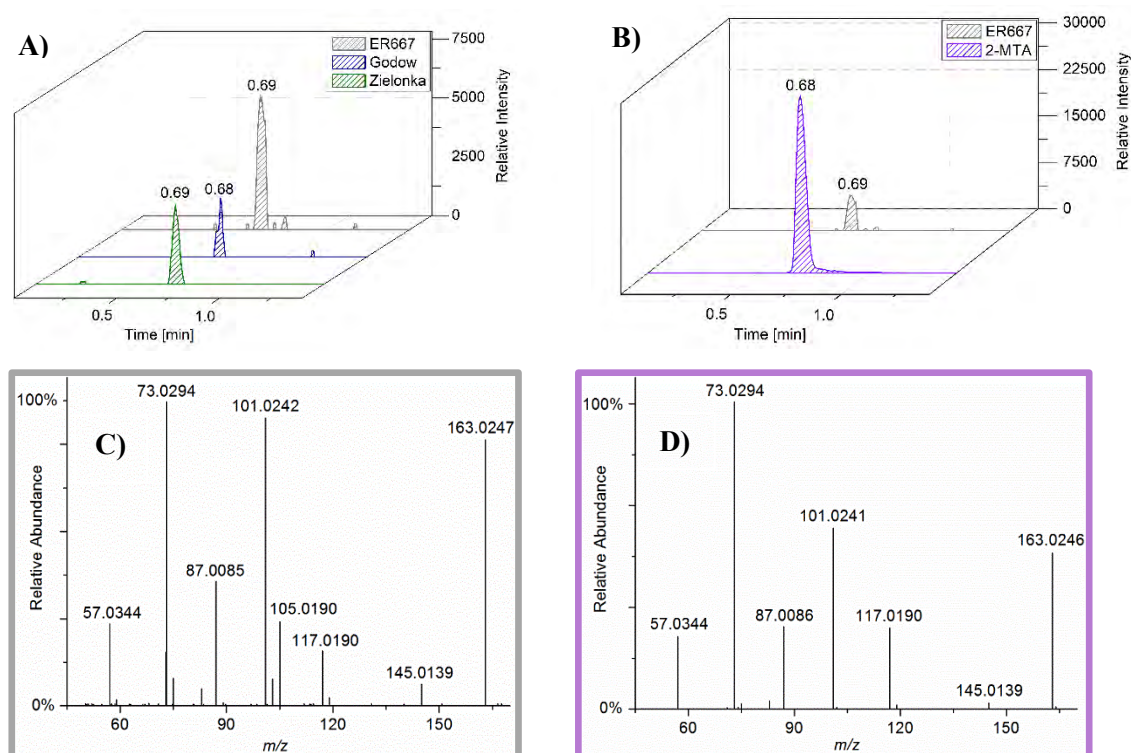


**Figure 40.** Extracted Ion Chromatograms (EIC) of methylthreonic acids (MTrA; MW 150) from smog-chamber experiments and field studies (A) and standard compounds (B); and ESI(-) product ion mass spectra for SOA from ER667 non-acidic seed aerosol experiment recorded at RT = 0.88 min (C) and 0.81 min (E) and for the corresponding standard compounds 3-MTrA and 2-MTrA (D, F, resp.)

**Figure 40** shows the Extracted Ion Chromatograms and high-resolution ESI(-) product ion mass spectra recorded for methylthreonic acids. Panels **A** and **B** in **Figure 40** compare fine aerosol samples and authentic standards of 2-MTrA and 3-MTrA with samples from the ER667 non-acidic seed smog-chamber experiment. Panels **C** and **E** show the product ion mass spectra of 3-MTrA and 2-MTrA (MW 150) from the ER667 sample eluting at RT = 0.88 min and RT = 0.81 min, respectively. The accurate mass of the deprotonated component was  $C_5H_9O_5$ : 149.0454 Da, error +0.4 mDa. Panels **D**



and **F** in **Fig. 40** show the product ion mass spectra of the synthesized 3-methylthreonic acid and 2-methylthreonic acid, respectively. The accurate mass of the deprotonated standard  $[M-H]^-$  ion was  $C_5H_9O_5$ : 149.0454 Da, error +0.4 mDa. Moreover, the compound with  $C_5H_{10}O_5$  structure has been observed in other oxidation studies and field samples, and was suggested the main HOM tracer (Krechmer et al., 2015). UPLC-MS technique provided highly-reliable mass measurements for the proposed HOMs. The recorded product ion mass spectra of 2-MTrA and 3-MTrA standard compounds and analytes detected in the smog chamber are similar. Nevertheless, using reversed-phase chromatography on HSS T3 C18 column generated a co-elution of signals of EIC chromatograms obtained for smog-chamber and ambient aerosol samples. The presence of two asymmetric carbon atoms, and thus two chiral centers in the structures of identified methylthreonic acids makes each of them a pair of diastereoisomers. Therefore one chromatographic peak of 2-methylthreonic acid (2-MTrA) with 2-methylerythronic acid (2-MErA) at  $RT = 0.77\text{--}0.81$  min, and one peak of 3-methylthreonic acid (3-MTrA) with 3-methylerythronic acid (3-MErA) at  $RT = 0.88$  min was observed.



**Figure 41.** Extracted Ion Chromatograms (EIC) of methyltartaric acid (MTA; MW 164) of smog-chamber samples and field samples (A), and standard compound (B); and ESI(-) product ion mass spectra at  $RT = 0.68$  min registered for SOA from the ER667 non-acidic seed aerosol experiment (C) and at  $RT = 0.69$  min for the standard compound (D)

**Figure 41** shows the Extracted Ion Chromatograms with high-resolution ESI(-) product ion mass spectra recorded for 2-methyltartaric acid. **Figures 41 A and B** compare smog-chamber experiments with fine aerosol samples and authentic 2-MTA standard. The product ion mass spectrum of the compound with MW 164 eluting at RT = 0.69 min in the ER667 non-acidic seed experiment is shown in **Fig. 41 C**. The accurate mass of the deprotonated component  $[M-H]^-$  ion was  $C_5H_7O_6$ : 163.0247 Da, error +0.4 mDa. The product ion mass spectrum of the synthesized 2-methyltartaric acid standard is shown in **Fig. 41 D**. The accurate mass of the deprotonated standard compound was ( $C_5H_7O_6$ : 163.0246 Da, error +0.3 mDa) is consistent with an elemental composition of the deprotonated  $C_5H_8O_6$  with a MW 164. The proposed structure has been confirmed by comparing the product ion mass spectra of smog-chamber sample with a standard compound. The slight discrepancies between fragment ions in the product ion mass spectra can be explained by the coelution of diastereoisomers of 2-methyltartaric acid during the reversed-phase chromatography on HSS T3 C18 column of the smog chamber sample, which provided a single peak for two isomers. In addition, 2-methyltartaric acid OS was also found in Godów and Zielonka fine aerosol (**Fig. 28**). Product ion mass spectra of those compounds (2-MTA and its organosulfate) clearly indicate, that both of them follow a similar fragmentation pattern. Based on that comparison, the recorded MS/MS spectrum of 2-MTA standard strongly supports the proposed structure of the organosulfate. The proposed fragmentation pathways for above-mentioned organic acids: 2-MTrA, 3-MTrA, and 2-MTA were presented in the Appendix (**Figs. A6 – A8**, respectively).

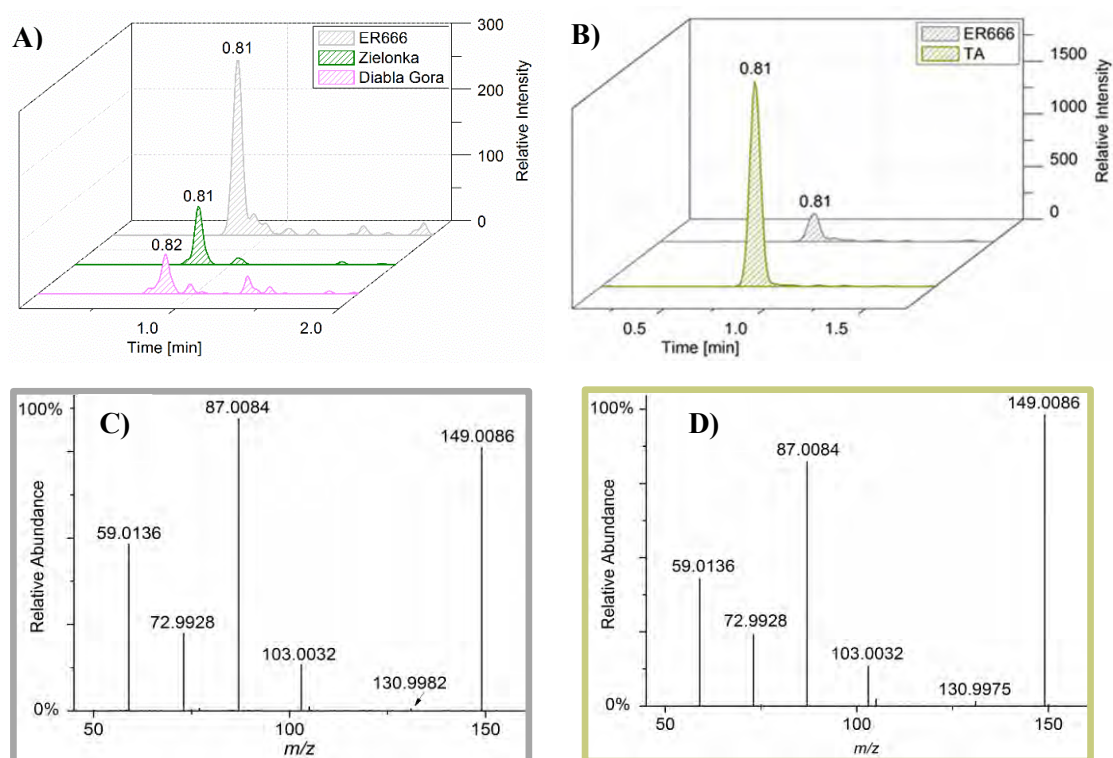
Ambient aerosol samples contained trace amounts of 2-MTrA and 3-MTrA (**Fig. 40**) and 2-MTA (**Fig. 41**), which indicates that those compounds form in the atmosphere inefficiently, convert rapidly to other compounds, or are removed from the atmosphere by some other mechanism. However, both ISO SOA components were detected in the field samples from Zielonka and Godów, and smog-chamber experiments. Notwithstanding, the detection of these oxygenated acids provided evidence for presence of isoprene HOMs in ambient aerosol and give molecular evidence for ISO aging. The obtained results are useful for modeling the formation and growth of aerosol particles influenced by isoprene emissions, including the prediction of the OA particles properties, and formation of cloud droplets. The chemical composition of ISO SOA has been reported in several studies, however methylthreonic acids and methyltartaric acid have not been previously reported as structurally-resolved particle-phase ISO oxidation

products. Jaoui et al. (2019) were the first to provide the molecular evidence for isoprene hydroxy carboxylic acids as SOA products formed due to aerosol aging.

### 3.3.4 Organic acids formation from butadiene

Chapter 3.3.3 showed that organic acids from isoprene can serve as highly oxygenated molecular (HOM) tracers in fine aerosol. In this Chapter, the formation of 13BD organic acids as HOM tracers in the smog-chamber SOA was investigated in the presence of high nitrogen oxides (NO<sub>x</sub>) and acidic and non-acidic aerosol seeds. To determine the contribution of aged butadiene products to ambient aerosol, PM<sub>2.5</sub> aerosol samples were collected at various regions of Poland, mainly Zielonka, Diabla Góra and Godów monitoring stations, and analyzed with UPLC-MS technique (**Figures 42 – 45**). The hydroxy acids from 1,3-butadiene, like tartaric acid (MW 150), threonic and erythronic acid (MW 136), and malic acid (MW 134), were previously reported by Jaoui et al. (2014). However, those compounds were identified tentatively. In this Chapter, I confirmed their formation using the authentic standards. Moreover, the structure of a novel HOM was revealed, mainly tartronic acid (MW 120), which can represent aged 13BD SOA, as it occurred in trace amounts both in the smog chamber and field samples. The proposed structures of HOM tracers were confirmed with UPLC-MS analyses by comparing the retention times, accurate mass spectral signatures and product ion mass spectra. The MS/MS spectra of standard compounds have been used to verify the 13BD HOMs identification. The threonic acid standard was synthesized based on the hydrolysis of appropriate lactone *cis*-diol under alkaline conditions. The detailed description of the synthesis procedure was presented in the Chapter 2.2.2.

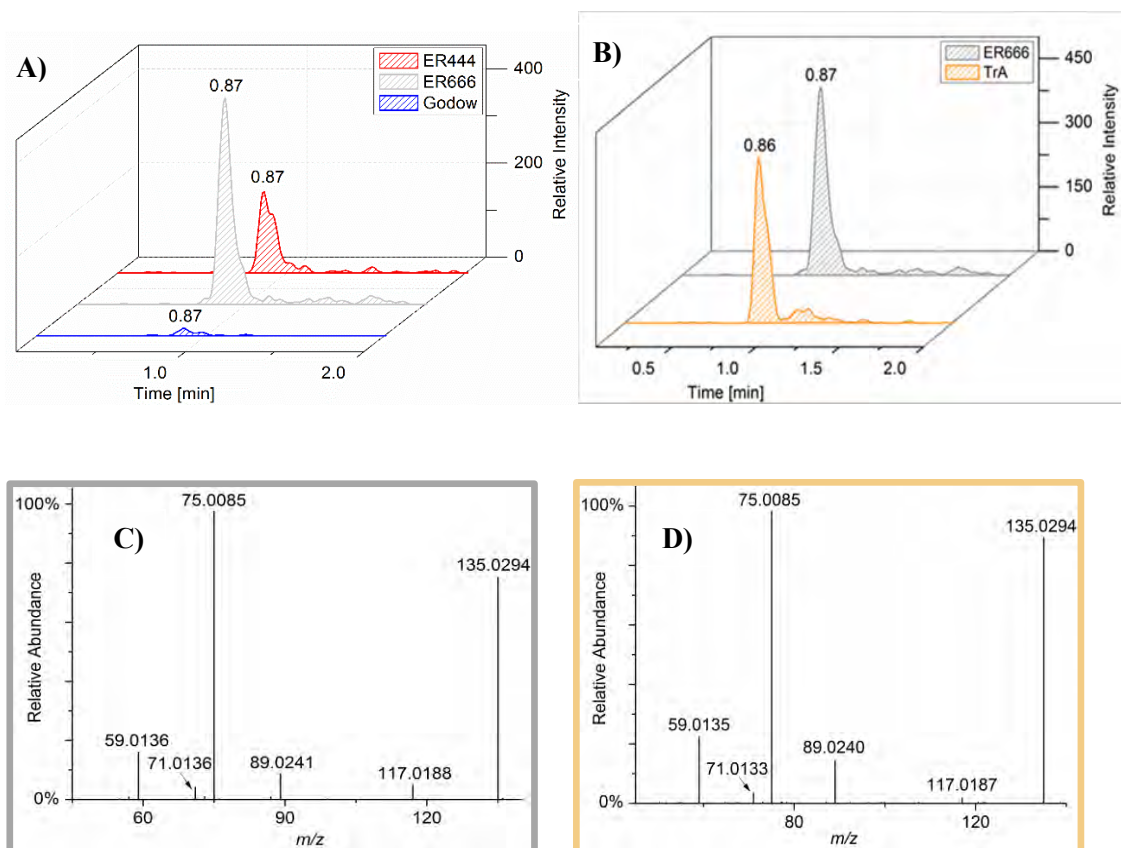
Anthropogenic precursors can significantly contribute to atmospheric SOA, even though they are less numerous and abundant than the biogenic precursors. The components of smog chamber and ambient samples are compared with standard compounds in **Figures 42 – 45**. The corresponding retention times (RT) and fragmentation pathways agreed very well. Moreover, proposed fragmentation pathways of selected organic acids are presented in the Appendix (**Figs. A9–A12**). All data presented in this Chapter have been included in Jaoui, Nestorowicz et al. (2023, submitted).



**Figure 42.** Extracted Ion Chromatograms (EIC) of tartaric acid (TA; MW 150) from smog-chamber and field samples (A), and standard compound (B); and ESI(-) product ion mass spectra at RT = 0.81 min registered for SOA from the ER666 non-acidic seed aerosol (C), and for the standard compound (D)

**Figure 42** shows the Extracted Ion Chromatograms and high-resolution ESI(-) product ion mass spectra of tartaric acid. It compares a smog chamber sample with fine aerosol (panel **A**) and the authentic TA standard (panel **B**). The product ion mass spectrum of the MW 150 SOA component from 13BD ER666 smog-chamber experiment (non-acidic seeds) eluting at RT = 0.81 min is shown in **Fig. 42 C**. The accurate mass of the deprotonated component ( $C_4H_5O_6^-$ : 149.0086 Da, error 0.0 mDa) was recorded at RT = 0.81 min. The product ion mass spectrum of TA standard is shown in **Fig. 42 D**. The accurate mass of the deprotonated standard compound  $[M-H]^-$  ion ( $C_4H_5O_6^-$ : 149.0086 Da, error 0.0 mDa) was recorded at the RT = 0.81 min. It is consistent with the elemental composition of deprotonated ion of  $C_4H_6O_6$  molecule with MW 150. Based on that mass-spectrometric consistency, the structure of TA was assigned to the sample component. Trace amounts of TA were found in fine aerosol collected in Zielonka and Diabla Góra. Tartaric acid is a well-known tracer in ambient aerosol and was detected in urban (Kawamura and Ikushima, 1993; Rohrl and Lammel, 2002;), rural

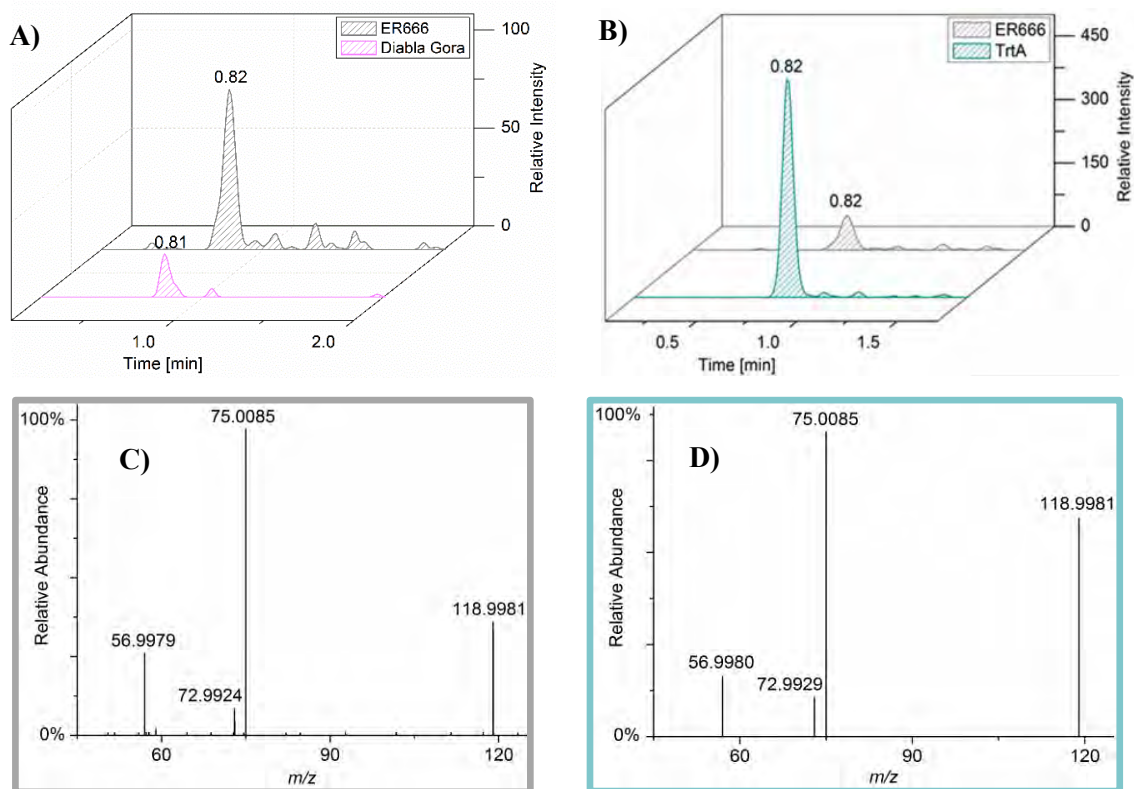
(Rohrl and Lammel, 2002) and forested areas (Clayes and Maenhaut, 2021). Lately, it was suggested to occur in SOA from toluene (Lau et al., 2021).



**Figure 43.** Extracted Ion Chromatograms (EIC) of threonic acid (TrA; MW 136) from smog-chamber experiments and filed samples (A), and the standard compound (B); and ESI(-) product ion mass spectra registered at RT = 0.87 min for SOA from the ER666 non-acidic seed aerosol experiment (C), and at RT = 0.86 min for the standard compound (D)

**Figure 43** shows the Extracted Ion Chromatograms and high-resolution ESI(-) product ion mass spectra of threonic acid (MW 136). It compares the smog-chamber sample with the fine aerosol (panel A) and authentic TrA standard (panel B). The product ion mass spectrum of the MW 136 SOA component from the 13BD ER666 smog-chamber experiment (non-acidic seeds) eluting at RT = 0.87 min is shown in **Fig. 43 C**. The accurate mass of the deprotonated compound  $[M-H]^-$  ion ( $C_4H_7O_5$ : 135.0294 Da, error +0.1 mDa) was recorded at RT = 0.87 min. The product ion mass spectrum of TrA standard is shown in **Fig. 43 D**. The accurate mass of the deprotonated standard  $[M-H]^-$  ion ( $C_4H_7O_5$ : 135.0294 Da, error + 0.1 mDa) was recorded at RT = 0.86 min. Based on the consistency of the product ion mass spectra, the structure of TrA was assigned to the sample component. Only trace amounts of TrA were found in fine aerosol collected in Godów, so I suggest that it forms in the atmosphere inefficiently, is a reactive reaction

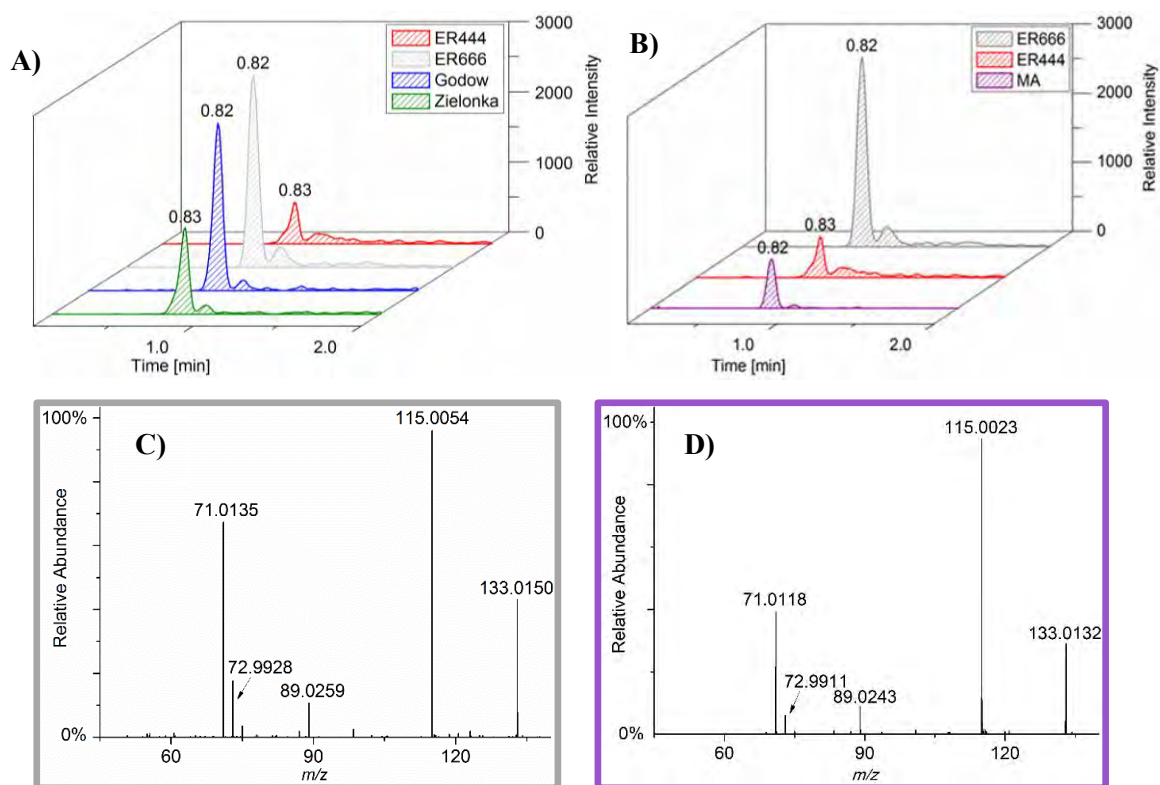
intermediate, or it is removed by other mechanisms. It is worth to point out that threonic acid OS was also found in Godów fine aerosol (see **Fig. 33**). The product ion mass spectra recorded for threonic acid and its organosulfate clearly show, that they follow a similar fragmentation pattern. Hence, the MS/MS spectrum of TrA standard verifies the proposed structure of TrA organosulfate (Chapter 3.3.2).



**Figure 44.** Extracted Ion Chromatograms (EIC) of tartronic acid (TrtA; MW 120) for smog-chamber experiments, and field samples (A), and for the standard compound (B); and ESI(-) product ion mass spectra registered at RT = 0.82 min for SOA from the ER666 non-acidic seed experiment (C) and the standard compound (D)

Another novel 13BD SOA component found in trace amounts in PM<sub>2.5</sub> aerosol and smog chamber samples was determined at  $m/z$  119 (**Figure 44**). A single peak was observed for that component (**Fig. 44 A and B**). The accurate mass of the deprotonated  $[M-H]^-$  ion ( $C_3H_3O_5$ : 118.9981 Da, error 0.0 mDa) was recorded at RT = 0.82 min in a sample from the ER666 non-acidic seed experiment. The product ion mass spectrum of TrtA standard is shown in **Fig. 44 D**. The accurate mass of the standard compound ( $C_3H_3O_5$ : 118.9981 Da, error 0.0 mDa) was recorded at RT = 0.82 min and is consistent with the elemental composition of the deprotonated  $C_3H_4O_5$  (MW 120). The proposed structure has been confirmed by comparing the product ion mass spectra of the smog chamber sample with that of the standard compound. High-resolution data strongly

suggested greater oxidation pathway for this compound, as it has high O/C ratio. Only trace amounts of TrtA were found in fine aerosol collected in Diabla Góra, so the acid most probably forms in the atmosphere inefficiently, converts rapidly to other compounds, or is removed by other mechanisms. Tartronic acid has never been reported in the 13BD SOA context.



**Figure 45.** Extracted Ion Chromatograms (EIC) of malic acid (MA; MW 134) for smog-chamber and , field samples (A), and for the standard compound (B); and the ESI(-) product ion mass spectra registered at RT = 0.82 min for SOA from the ER666 non-acidic seed aerosol experiment (C) and the standard compound (D)

The last organic acid found in reasonable amounts in smog chamber and ambient aerosol samples was malic acid (MW 134). **Figure 45** shows the Extracted Ion Chromatograms and the high-resolution ESI(-) product ion mass spectra and of MA. **Figure 45** compares smog-chamber samples with aerosol samples (panel A) and with the authentic MA standard (panel B). The product ion mass spectrum of 13BD SOA component from the smog-chamber experiment ER666 (non-acidic seed) is shown in **Fig. 45 C**. The accurate mass of that component ( $C_4H_5O_5$ : 133.0150 Da, error -1.3 mDa) was recorded at RT = 0.82 min. The product ion mass spectrum of MA standard compound is shown in **Fig. 45 D**. The accurate mass of the standard compound ( $C_4H_5O_5$ : 133.0132 Da, error - 0.5 mDa) was recorded at RT = 0.82 min. The proposed structure of the SOA component was confirmed against the authentic standard by comparison of

the product ion mass spectra. Malic acid was highly abundant in fine aerosol collected at Godów and Zielonka. This may be caused by other possible formation pathways in the atmosphere. Malic acid is a well-known tracer in AA. It forms by the photooxidation of semivolatile carboxylic acids emitted during biomass burning, e.g. succinic acid (Kawamura and Gagosian, 1990; Kawamura and Ikushima, 1993; Kundu et al., 2010). It was also found in SOA from toluene (Lau et al, 2021). Now, I can conclude that other considerable source of MA in the atmospheric aerosol is 1,3-butadiene emission. It is worth to point out that malic acid OS was also found in Godów and Zielonka fine aerosol (**Fig. 32**). The product ion mass spectra recorded for malic acid and its organosulfate clearly indicate, that both compounds follow a similar fragmentation pattern. Hence, the MS/MS spectrum of MA standard confirms the proposed structure of MA organosulfate. In addition, proposed fragmentation pathways for above-mentioned organic acids: TA, TrA, TrtA and MA were presented in the Appendix (**Figs. A9 – A12**, respectively).

The ambient aerosol samples analyzed contained only trace amounts of TrA, TA and TrtA (**Figs. 40 – 42**), indicating that those compounds either form in the atmosphere inefficiently, or convert rapidly to other compounds, or are otherwise removed from AA. On the contrary, malic acid was detected in significant amounts both in the smog chamber and ambient aerosol samples. Therefore, those highly oxidized acids may indicate the 13BD transformation in the atmosphere, including the aging of 13BD aerosol. That may be useful for better understanding and modelling of atmospheric processes, including aerosol formation and growth, changing properties OA particles and nucleation of clouds. The chemical composition of 13BD SOA, including the organic hydroxy acids formation, has been reported (Jaoui et al., 2014). However, the structures of 13BD SOA components were identified only tentatively and I confirmed them here using appropriate authentic standards. The UPLC-MS analyses allowed a more accurate identification of the organosulfates derived from the acids. Furthermore, one novel compound was detected – tartronic acid with MW 120, which has not been previously reported as a particle-phase 13BD oxidation product.

### 3.4 Ambient fine aerosol

This Chapter describes the semi-quantitative estimation of significant and novel isoprene and butadiene SOA products in ambient aerosol with reference to the smog-chamber data on the influence of RH on SOA formation and to the relevant



physicochemical and meteorological data available for sampling sites. Revealing the ISO and 13BD SOA composition in the laboratory enabled the identification of many components of ambient aerosol. The concentrations of identified components were correlated with organic carbon (OC), elemental carbon (EC), and PM<sub>2.5</sub> concentrations. Besides, the air mass back trajectories were calculated for selected sampling sites to analyze the possible inflow of PM components.

### 3.4.1 OC and EC concentrations

**Table 20** shows organic carbon (OC), elemental carbon (EC), and PM<sub>2.5</sub> concentrations in the air ( $\mu\text{g m}^{-3}$ ) determined for the collected ambient aerosol samples. In the Godów campaign, the average organic carbon (OC) constituted 29.6 % of the PM<sub>2.5</sub> mass within the 22.8 – 37.5% range. The average elemental carbon (EC) was less than 4.7% within the 3.8 – 5.5% range. In the Diabla Góra campaign, the average organic carbon (OC) constituted 41.1% of the PM<sub>2.5</sub> mass within 36.3 – 44.0% range. The average elemental carbon (EC) was less than 1.7% within the 1.6 – 1.8% range. In the Zielonka campaign, the average organic carbon (OC) constituted 51.1% of the PM<sub>2.5</sub> mass within 41.6 – 83.9% range. The average elemental carbon (EC) was 2.5% within the 1.7 – 3.1% range. In the Kaskada campaign, the average organic carbon (OC) constituted 40.8% of the PM<sub>2.5</sub> mass within the range of 36.8 – 47.8% The elemental carbon (EC) accounted for 8.9% within the range of 3.9 – 23.1%. Moreover, **Table 21** compares PM<sub>2.5</sub>, OC, EC concentrations in the air for ambient aerosol samples collected at several world sites. The values at Diabla Góra, Godów, Zielonka, and Kaskada were among the lowest.

**Table 20:** Organic carbon (OC), elemental carbon (EC) and PM<sub>2.5</sub> concentrations in the air ( $\mu\text{g m}^{-3}$ ) determined for the collected ambient aerosol samples

Sampling site	Sample name	OC ( $\mu\text{g m}^{-3}$ )	EC ( $\mu\text{g m}^{-3}$ )	OC / EC	PM <sub>2.5</sub> ( $\mu\text{g m}^{-3}$ )*	OC/PM <sub>2.5</sub> (%)	EC/PM <sub>2.5</sub> (%)
Godów	Godów_1	4.0 ± 0.2	0.6 ± 0.1	6.2	17.0	22.8	3.8
	Godów_2	5.3 ± 0.3	1.1 ± 0.1	4.7	21.0	25.2	5.3
	Godów_3	6.4 ± 0.4	0.8 ± 0.1	8.1	24.0	26.5	3.3
	Godów_4	6.4 ± 0.4	0.9 ± 0.1	6.8	17.0	37.5	5.5
	Godów_5	5.5 ± 0.3	0.8 ± 0.1	6.8	15.0	36.3	5.3
Diabla Góra	B017	5.1 ± 0.3	0.2 ± 0.1	26.8	11.6	44.0	1.6
	B018	5.0 ± 0.3	0.2 ± 0.1	26.2		42.9	1.6
	B019	5.0 ± 0.3	0.2 ± 0.1	26.3	11.1	43.0	1.7
	B020	4.0 ± 0.3	0.2 ± 0.1	20.2		36.3	1.8
	B021	4.3 ± 0.3	0.2 ± 0.1	23.8		10.9	39.3
Zielonka	L022	6.3 ± 0.4	0.2 ± 0.1	17.0	15.1	41.6	2.5
	L023	6.7 ± 0.4	0.4 ± 0.1	17.3		44.7	2.6
	L024	9.0 ± 0.6	0.2 ± 0.1	49.9	10.6	83.9	1.7
	L025	4.5 ± 0.3	0.3 ± 0.1	15.9		42.1	2.6
	L026	3.8 ± 0.3	0.3 ± 0.1	13.9		8.7	43.2
Kaskada	K8043	6.1 ± 0.4	0.7 ± 0.1	8.5	14.5	42.3	5.0
	K8044	5.2 ± 0.3	0.9 ± 0.1	5.8	10.9	47.8	8.3
	K8045	3.9 ± 0.3	0.4 ± 0.1	9.9	9.9	38.9	3.9
	K8046	8.5 ± 0.5	5.1 ± 0.3	1.7	22.3	38.3	23.1
	K8047	5.2 ± 0.3	0.6 ± 0.1	9.0	14.1	36.8	4.1

\* PM<sub>2.5</sub> concentrations for Kaskada and Godów sampling sites were available on <https://powietrze.gios.gov.pl/>

**Table 21:** Mean concentrations ( $\mu\text{g m}^{-3}$ ) of  $\text{PM}_{2.5}$ , OC and EC observed in this study and at selected worldwide sites (adapted from Rudzinski et al., 2022)

	Rural sites	Sub-urban sites	Urban sites	This study	Referances
<b>PM<sub>2.5</sub></b>			9 – 24 <sup>i)</sup>		<sup>a)</sup> Clements et al., 2016
			25 ± 10 <sup>j)</sup>		<sup>b)</sup> Kristensson et al. 2020
			23 – 45 <sup>c)</sup>		<sup>c)</sup> Błaszczuk et al., 2017
			31 ± 3 <sup>k)</sup>		<sup>d)</sup> ChooChuay et al., 2020a
	8 ± 5 <sup>a)</sup>	41 <sup>e)</sup>		18.8 ± 3.6 <sup>Godów</sup>	<sup>e)</sup> Hu et al., 2008
	19 ± 9 <sup>b)</sup>	28 – 58 <sup>f)</sup>		11.2 ± 0.4 <sup>Diabla Góra</sup>	<sup>f)</sup> Ho et al., 2002
	16 – 70 <sup>c)</sup>	68 ± 35 <sup>g)</sup>		11.5 ± 3.3 <sup>Zielonka</sup>	<sup>g)</sup> Islam et al., 2020
	42 ± 13 <sup>d)</sup>	66 – 132 <sup>h)</sup>		13.5 ± 2.3 <sup>Kaskada</sup>	<sup>h)</sup> Wang et al., 2017
			50 ± 20 <sup>m)</sup>		<sup>i)</sup> Mikuska et al., 2017
			36 – 64 <sup>f)</sup>		<sup>j)</sup> Salma et al., 2017
		102 ± 74 <sup>n)</sup>		<sup>k)</sup> Rudzinski et al., 2022	
		77 – 183 <sup>o)</sup>		<sup>l)</sup> Lewandowska et al., 2018	
				<sup>m)</sup> Bootdee et al., 2016	
				<sup>n)</sup> Feng et al., 2019	
				<sup>o)</sup> Wang et al., 2019	
<b>OC</b>			5 ± 2 <sup>j)</sup>		<sup>b)</sup> Kristensson et al. 2020
			9 ± 6 <sup>l)</sup>		<sup>e)</sup> Hu et al., 2008
			7 – 14 <sup>f)</sup>		<sup>f)</sup> Ho et al., 2002
			15 ± 8 <sup>i)</sup>		<sup>g)</sup> Islam et al., 2020
	2 ± 1 <sup>p)</sup>	5 – 7 <sup>f)</sup>		5.5 ± 1.0 <sup>Godów</sup>	<sup>j)</sup> Salma et al., 2017
	5 ± 3 <sup>b)</sup>	8 <sup>e)</sup>		4.7 ± 0.5 <sup>Diabla Góra</sup>	<sup>k)</sup> Rudzinski et al., 2022
	0.1 - 9.9 <sup>r)</sup>	18 ± 10 <sup>g)</sup>		6.0 ± 2.1 <sup>Zielonka</sup>	<sup>l)</sup> Lewandowska et al., 2018
	13 ± 2 <sup>s)</sup>			5.8 ± 1.7 <sup>Kaskada</sup>	<sup>p)</sup> Laongsri and Harrison, 2013
			6 – 18 <sup>u)</sup>		<sup>r)</sup> Puxbaum et al., 2007
			10 ± 1 <sup>k)</sup>		<sup>s)</sup> Gatari and Boman, 2003
				<sup>t)</sup> Gao et al., 2020	
				<sup>u)</sup> Liu et al., 2019	

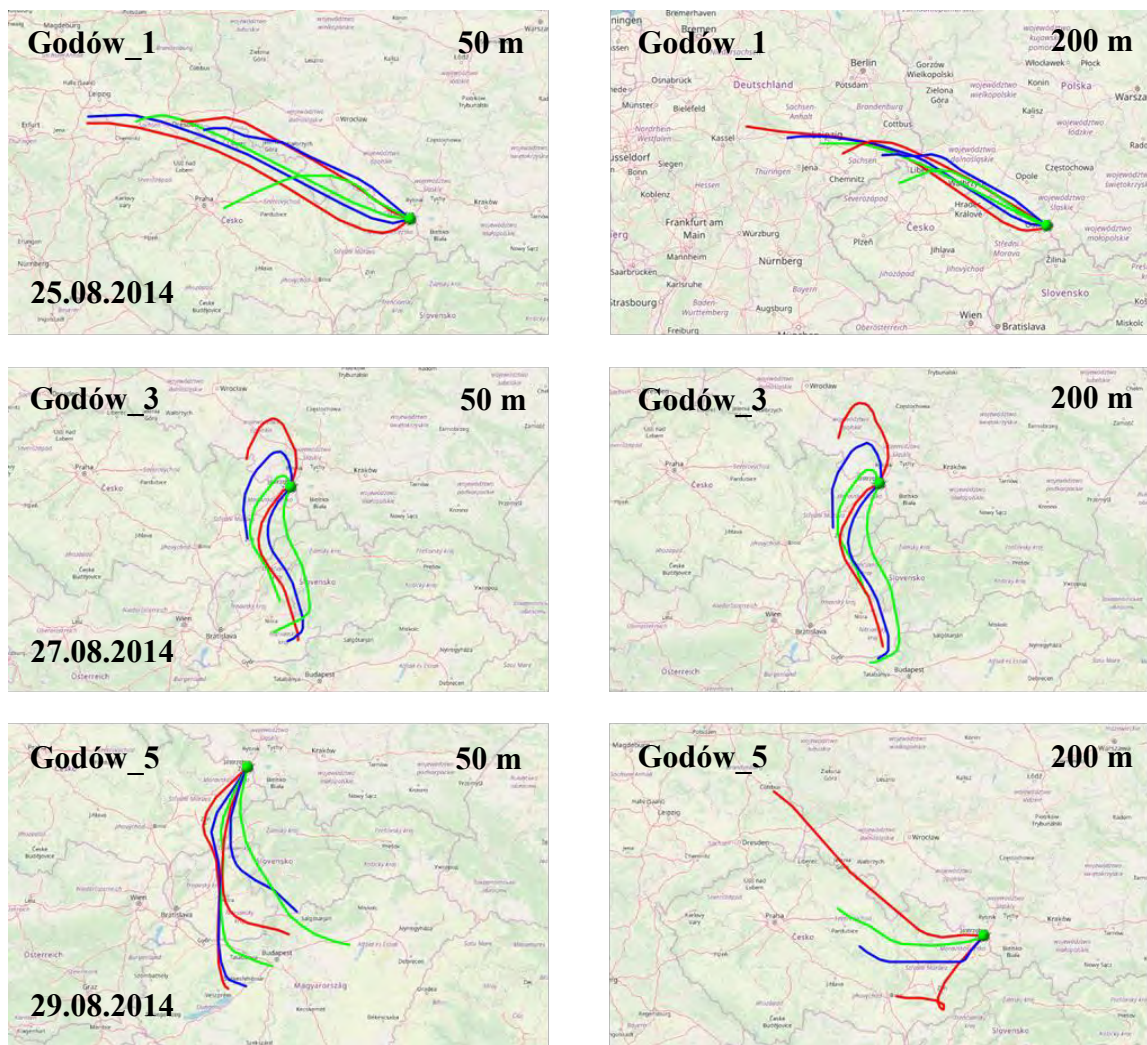
**Table 21 (continued):** Mean concentrations ( $\mu\text{g m}^{-3}$ ) of  $\text{PM}_{2.5}$ , OC and EC observed in this study and at selected worldwide sites (adapted from Rudzinski et al., 2022)

	Rural sites	Sub-urban sites	Urban sites	This study	Referances
<b>EC</b>	$0.6 \pm 0.3$ <sup>b)</sup>	1 <sup>e)</sup> 1 – 2 <sup>f)</sup> 9 $\pm$ 6 <sup>g)</sup>	1.1 $\pm$ 0.4 <sup>j)</sup> 1.1 $\pm$ 0.1 <sup>k)</sup> 2 $\pm$ 1 <sup>l)</sup> 3 $\pm$ 1 <sup>w)</sup> 4 $\pm$ 2 <sup>t)</sup> 3– 6 <sup>u)</sup> 4 – 8 <sup>f)</sup>	0.9 $\pm$ 0.2 <sup>Godów</sup> 0.2 $\pm$ 0.1 <sup>Diabla Góra</sup> 0.3 $\pm$ 0.1 <sup>Zielonka</sup> 1.5 $\pm$ 1.7 <sup>Kaskada</sup>	<sup>b)</sup> Kristensson et al. 2020 <sup>e)</sup> Hu et al., 2008 <sup>f)</sup> Ho et al., 2002 <sup>g)</sup> Islam et al., 2020 <sup>j)</sup> Salma et al., 2017 <sup>k)</sup> Rudzinski et al., 2022 <sup>l)</sup> Lewandowska et al., 2018 <sup>t)</sup> Gao et al., 2020 <sup>u)</sup> Liu et al., 2019 <sup>w)</sup> ChooChuay et al. (2020b)

### 3.4.2 Back trajectories of air masses

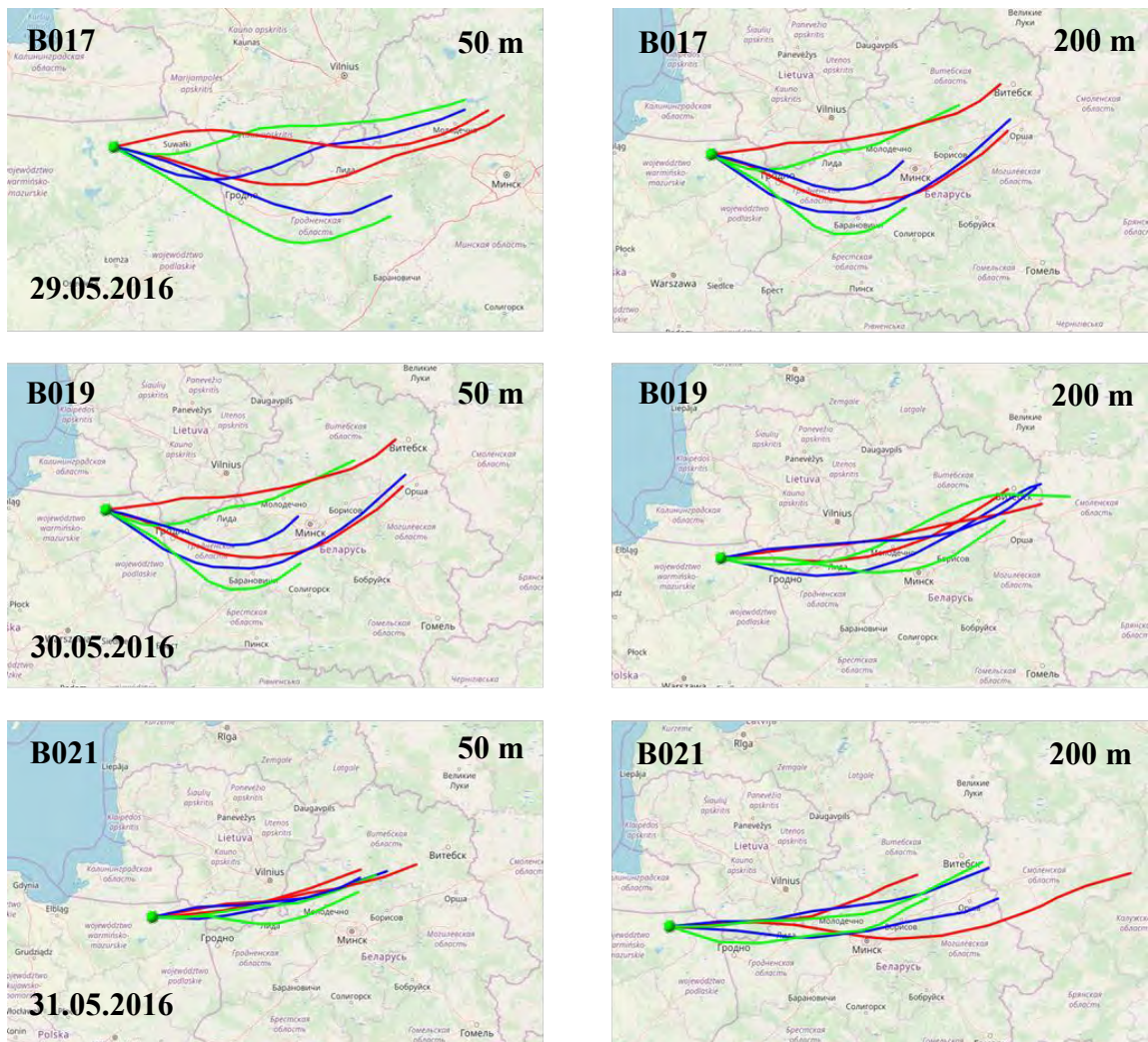
The chemical composition of fine aerosol particles strongly depends on the emission sources, lifetimes of compounds in the atmosphere, which range from minutes to months, geographical location, and meteorological conditions. Depending on those variables, the PM<sub>2.5</sub> fraction has a specific chemical composition in various world regions (Seinfeld and Pandis, 1998; Raes et al., 2000; Poschl, 2005; Juda-Rezler and Toczko, 2016). Isoprene and butadiene are aerosol precursors which react in the atmosphere – their lifetimes vary from hours to days. Besides, particulate matter originates from sources that are local or remote to the sampling sites. To find the origin and the path of aerosol particles inflowing to a sampling site, air mass back trajectories are calculated at given height and time intervals. In order to determine the origin of air masses inflowing to the selected sampling points, 24-hour back trajectories of inflowing air masses were calculated every 4 hours for the exposure period of each aerosol sampling filter. The back trajectories were calculated at the heights of 50 m and 200 m above ground level. Back trajectories were calculated with the freely available HYSPLIT model (Stein et al., 2015, Ralph et al., 2017), available *on-line* at the NOAA Air Resources Laboratory, USA website, which simulates the flow of air masses on local to global scales based on the stored meteorological data. Below are presented backward trajectories to:

- (1) Godów; between 25–29 August 2014 for 50 m and 200 m above ground level and 24 h flow period (**Fig. 46**);
- (2) Diabla Góra; between 29–31 May 2016 for 50 m and 200 m above ground level and 24 h flow period (**Fig. 47**);
- (3) Zielonka; between 25–27 July 2016 for 50 m and 200 m above ground level and 24 h flow period (**Fig. 48**);
- (4) Kaskada; between 20–22 July 2018 for 50 m and 200 m above ground level and 24 h flow period (**Fig. 49**).



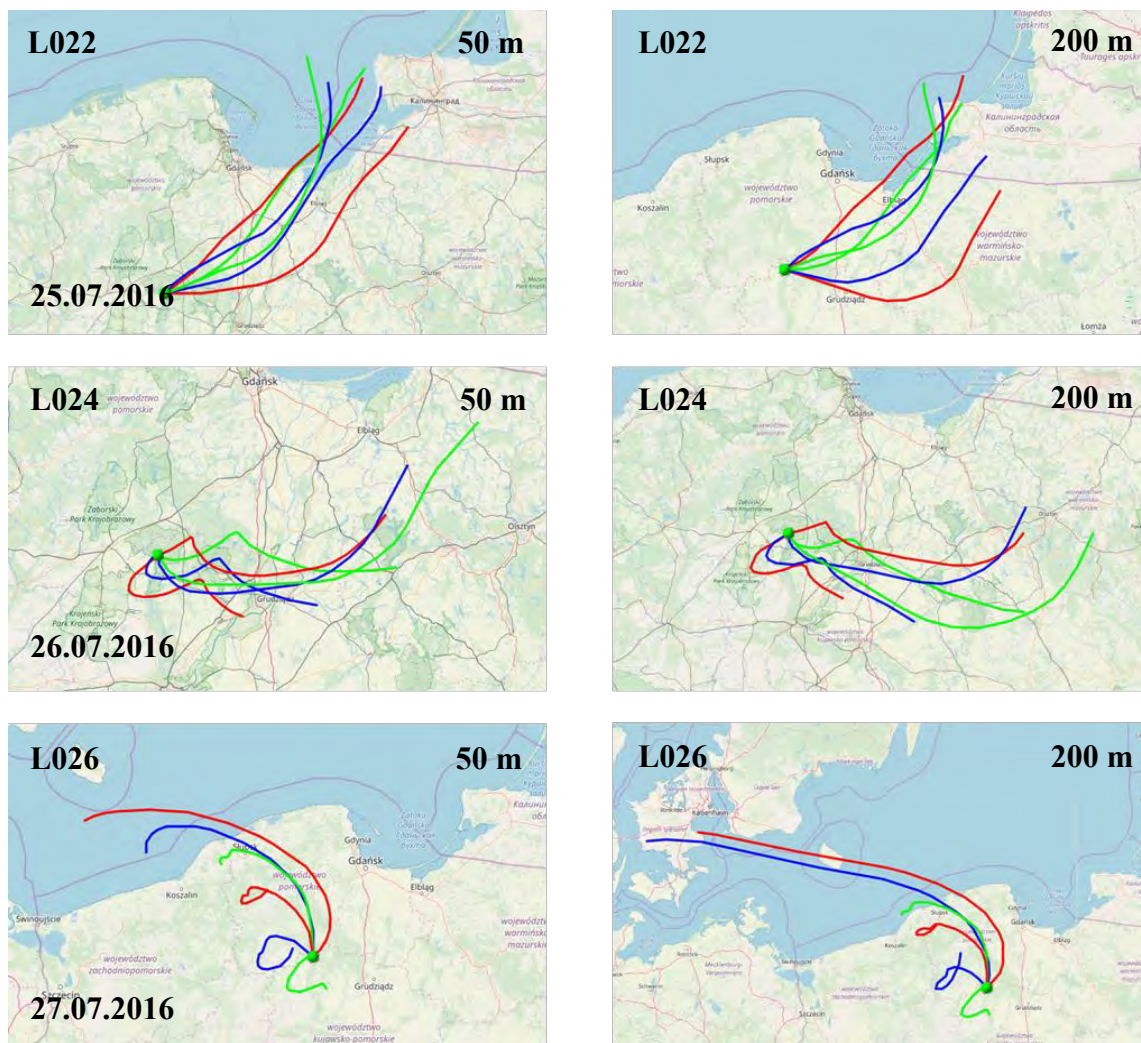
**Figure 46.** 24 h back trajectories of air masses to Godów between 25–29.08.2014 at 7:00 AM at 50 m and 200 m above ground level (every 4 h)

The analysis of air masses to Godów showed that, on a scale of 24 hours and 50 m above ground level, the major part of air masses drifted at the first day of sampling (Godów\_1) from the west directions (from Germany), and at third and fifth day of sampling (Godów\_3, Godów\_5, resp.) the direction of air masses changed to south. The air flow was mostly from Hungary and Czech Republic. The analysis of 24 h back trajectories at 200 m above ground level indicated similar air flow direction, however on 29.08.2014 Godów ambient aerosol was also influenced by west air masses.



**Figure 47.** 24 h back trajectories of air masses to Diabla Góra between 29-31.05.2016 at 7:00 AM at 50 m and 200 m above ground level (every 4 h)

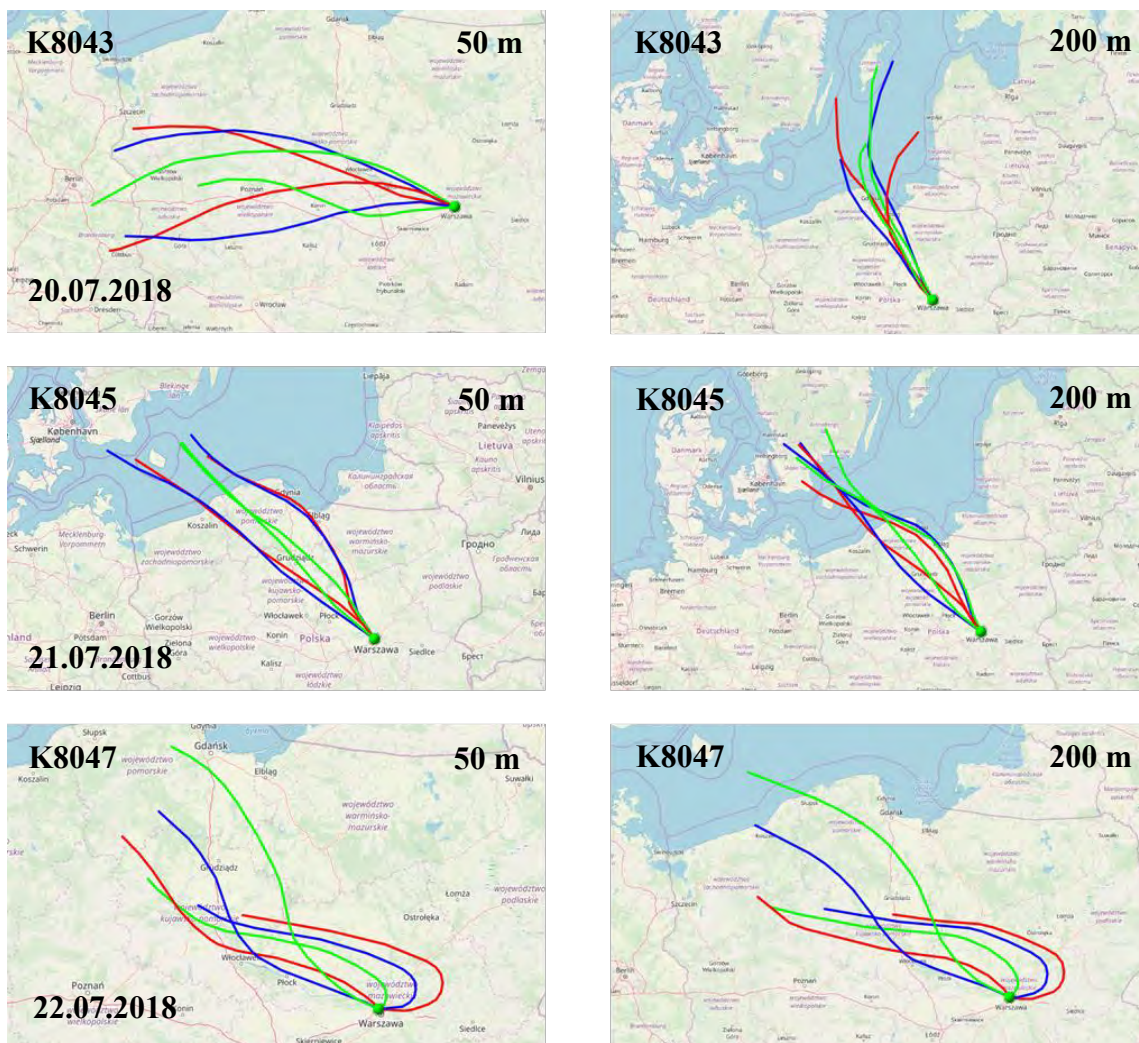
The analysis of air masses to Diabla Góra showed that, on a scale of 24 hours, 50 m and 200 m above ground level, the air masses drifted only from the east direction, mostly from Belarus and Russia.



**Figure 48.** 24 h backtrajectories of air masses to Zielonka between 25-27.07.2016 at 7:00 AM at 50 m and 200 m above ground level (every 4 h)

The calculated back trajectories to Zielonka showed that, on a scale of 24 hours, 50 m and 200 m above ground level, the airflow changed dynamically. The major air masses drifted from the north, northeast and northwest directions, mostly from the Baltic Sea and Lithuania.





**Figure 49.** 24 h back trajectories of air masses to Kaskada between 20-22.07.2018 at 7:00 AM at 50 m and 200 m above ground level (every 4 h)

The 24-hour back trajectories at 50 m above ground level showed that the major part of air masses drifted to Kaskada from the north and west directions. The back trajectories at 200 m above ground level are similar, however the first day of sampling (K8043) was also influenced by the north inflow.

### 3.4.3 Quantitative characterization of ambient aerosol

This Chapter focuses on the quantitative analysis of well-known and novel ISO and 13BD SOA components in the field aerosol samples, including several organosulfates. Organosulfates (OSs) have been widely identified in ambient PM<sub>2.5</sub>. These compounds contribute substantially to organic carbon in ambient fine aerosol (1–17%; Shakya and Peltier, 2013; Shakya and Peltier, 2015, Hettiyadura et al., 2019). They are associated with secondary organic aerosol (SOA) from both anthropogenic volatile organic compounds (AVOCs; Riva et al., 2015; Blair et al., 2016) and biogenic volatile organic compounds (BVOCs; Surratt et al., 2007a, 2008, Chan et al., 2011; Zhang et al., 2012; Barbosa et al., 2017; Riva et al., 2019). The formation of OSs in fine aerosol has been explained by several possible formation pathways summarized by Bruggemann et al. (2020):

- (a) acid-catalyzed reactive uptake of epoxides onto acidic aerosol (Iinuma et al., 2009; Surratt et al., 2010; Kristensen and Glasius, 2011; Lin et al., 2012; Riva et al., 2016 a,b; Barbosa et al., 2017; Duporte et al., 2020);
- (b) direct sulfate esterification (Iinuma et al., 2007 a,b; Surratt et al., 2008);
- (c) nucleophilic substitution and conversion of organonitrates into OSs in the aqueous phase (Darer et al., 2011; Hu et al., 2011);
- (d) sulfoxy-radicals-initiated oxidation of unsaturated compounds in the aqueous phase (Rudzinski et al., 2009; Noziere et al., 2010; Schindelka et al., 2013; Schone et al., 2014; Szmigielski, 2016; Wach et al., 2019; Huang et al., 2020);
- (e) direct reactions of SO<sub>2</sub> with unsaturated hydrocarbons (Passananti et al., 2016),
- (f) the heterogeneous reaction between SO<sub>2</sub> and aerosol-phase organic peroxides in the ozonolysis of unsaturated hydrocarbons at high and low RH levels (Ye et al., 2018; Wang et al., 2019).

Due to the ready formation in the atmosphere, organosulfates are very important in the chemistry and transformation of organic aerosols, since they enhance the cloud condensation nuclei activity (Hansen et al., 2015) and influence aerosol physicochemical properties, such as morphology, viscosity, acidity (Olson et al., 2019; Riva et al., 2019) as well as optical properties (Fleming et al., 2019). However, accurate quantification of OSs and other significant SOA components is still difficult, mostly due to the lack of authentic standards and uniform analytical procedures. Therefore, the results presented in this Chapter should rather be regarded as a semi-quantitative analysis or first estimation of the concentrations of individual SOA compounds in ambient aerosol samples –

organosulfates, nitrooxy- and nitrosooxy- organosulfates. However, the organic acids found in the field samples were quantified based on authentic standards.

### 3.4.3.1 Isoprene SOA

The concentrations of isoprene SOA components were measured in samples collected at the selected sites. Among compounds detected, the most abundant one was 2-methyltetrol nitrooxy-organosulfate (MW 261). Other major components were: 2-methylthreitol and 2-methylerythritol organosulfates (MW 216), together with 2,3,4-furantriol, tetrahydro-methyl organosulfate (MW 214) and 2(3H)-furanone, dihydro-3,4-dihydroxy-3-methyl- organosulfate (MW 212). The compounds detected in trace amounts were: methylthreonic acids (MW 150) and methyltartaric acid (MW 164), 3-methylthreonic acid nitrooxy-organosulfate (MW 275) and 2-methyltartaric acid organosulfate (MW 244). Trace amounts of 2-methylglyceric acid OS (MW 200) were found only in Kaskada and Zielonka fine aerosol. In addition, 3-methylthreonic acid organosulfate (MW 230) was detected in Zielonka and Godów samples, however the concentrations were below the determined Limit of Detection (LOD). Moreover, 2-methyltetrol NSOS with MW 245 was detected at LOD solely in Kaskada fine aerosol.

**Table 22** presents the ISO SOA components' mean concentrations ( $\text{ng m}^{-3}$ ) at the selected sampling sites. The highest concentration of isoprene-derived organosulfates occurred in Zielonka, where the sum of OSs+NOSs was  $474.9 \pm 149.3 \text{ ng m}^{-3}$ , whereas the lowest concentration occurred in Godów, where the sum of OSs+NOSs was  $87.6 \pm 46.1 \text{ ng m}^{-3}$ . Bryant et al. (2020) investigated the chemical composition of highly anthropogenically influenced ISO SOA in the capital city of China, Beijing, during the 2017 summer campaign. The authors showed that the mean concentrations ( $\text{ng m}^{-3}$ ) of the sum of ISO SOA components were  $82.5 \text{ ng m}^{-3}$ , ranging from  $1.9 \text{ ng m}^{-3}$  to  $718 \text{ ng m}^{-3}$ . The authors also analyzed the concentrations of particular ISO SOA components, including those with MW 200, 212, 214, 216, 230, 244, 245, and 275. In addition, Bryant et al. (2021) analyzed ISO SOA in Guangzhou, China. **Table 23** shows the concentrations ( $\text{ng m}^{-3}$ ) of selected ISO SOA compounds with reference to field campaigns from Beijing in 2017 (Bryant et al., 2020) and Guangzhou in 2019 (Bryant et al., 2021). Moreover, Jaoui et al. (2019) showed that concentrations of methyltartaric acid (MW 164) in Duke Forest, NC, U.S. ambient aerosol collected during 2003 summer campaign ranged from 1.5 to  $6.3 \text{ ng m}^{-3}$ , and the concentration of methylthreonic acids (MW 150) ranged from 0.2 to  $0.9 \text{ ng m}^{-3}$ .

**Table 22:** Mean concentrations ( $\text{ng m}^{-3}$ ) of ISO SOA components in this study and at other sites (Bryant et al., 2020, 2021)

Sampling site	MW 200	MW 212	MW 214	MW 216	MW 244	MW 261	MW 275	MW 150	MW 164	$\Sigma$ OSs+NOSs
Kaskada	$0.7 \pm 0.6$	$84.0 \pm 11.7$	$12.4 \pm 4.6$	$89.7 \pm 67.6$	$0.7 \pm 0.4$	$159.6 \pm 74.3$	$3.2 \pm 2.2$	$1.9 \pm 0.4$	$1.8 \pm 0.6$	$350.2 \pm 56.1$
Zielonka	$0.9 \pm 0.7$	$135.1 \pm 30.8$	$50.8 \pm 19.8$	$126.2 \pm 52.0$	$4.1 \pm 1.0$	$155.7 \pm 78.4$	$2.0 \pm 1.1$	$1.4 \pm 0.2$	$2.8 \pm 0.8$	$474.9 \pm 149.3$
Godów	< LOD	$22.3 \pm 13.7$	$2.2 \pm 2.2$	$6.5 \pm 6.6$	$1.5 \pm 0.3$	$55.0 \pm 23.7$	< LOD	$0.8 \pm 0.1$	< LOD	$87.6 \pm 46.1$
Diabla Góra	< LOD	$69.6 \pm 16.9$	$28.1 \pm 6.9$	$136.2 \pm 30.1$	$2.4 \pm 0.5$	$86.9 \pm 26.0$	$0.6 \pm 0.9$	$2.4 \pm 0.5$	$1.6 \pm 0.3$	$324.0 \pm 76.0$
Beijing China	21.5	14.0	10.6	11.8	0.11	12.6	9.17	-	-	261.7
Beijing China (min–max)	0.3 - 180.5	0.3 - 136.4	0.4 - 104.7	0.8 - 110.9	0.0 - 40.9	0.1 - 154.1	0.0 - 53.8	-	-	-
Guangzhou China	11.8	11.8	11.4	57.4	1.46	5.21	9.6	-	-	205.5

< LOD denotes that the compound was not detected in all analyzed samples and/or in trace amounts

ND – not detected

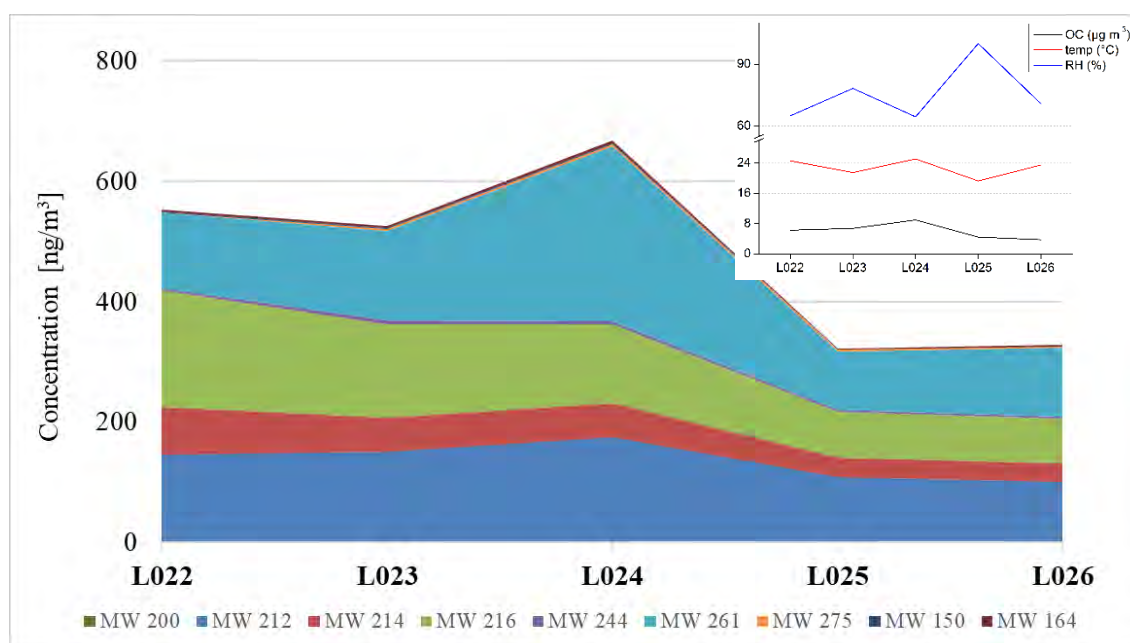
There are many reports on the quantitative detection of isoprene OSs and NOSs in ambient aerosol from various sites worldwide. However, most of the studies have been focused on the main and the most abundant 2-methyltetrol OSs. Chan et al. (2010) attempted to quantify 2-methyltetrol OSs in fine aerosol collected at two sampling sites in Atlanta and Yorkville in the southeastern U.S. The concentrations measured with UPLC-MS ranged between 6.7 – 64.0 ng m<sup>-3</sup> and 5.1 – 46.0 ng m<sup>-3</sup>, respectively. Kanellopoulos et al. (2022) measured the concentration of isoprene OSs at two urban sites in Greece during 2017-2018 campaign. The authors showed that isoprene-epoxydiol transformations may be a dominant pathway of ISO SOA formation, with the OSs with MW 212, MW 214 and MW 216 detected as the major ISO products at both sites. The OSs contribution to PM<sub>2.5</sub> aerosol at both sites ranged from 2.5 ± 1.2% and from 5.0 ± 2.5% for Athens and Patra in summer, respectively. Chen et al. (2021) quantitatively characterized OSs in PM<sub>2.5</sub> aerosol samples collected from 20 various sites during the 2016 summer campaign in the U.S. They found that in the eastern U.S., the mass of isoprene OSs accounted for 4 ± 2% of organic matter (OM) while the mean concentration was 130 ± 60 ng m<sup>-3</sup>. In the western part of U.S., the mean concentration of isoprene-derived OSs was 11 ng m<sup>-3</sup> and its total mass accounted for 0.5% ± 0.3 of OM. The most abundant ISO-derived organosulfate with MW 216 in summer was 24 ± 29 ng m<sup>-3</sup>. Glasius et al. (2018) measured organosulfates concentration in aerosol from an urban region in central Amazon during wet (February – March) and dry (August – October) seasons. OSs were dominantly formed from isoprene epoxydiols (IEPOX), averaging to 104 ± 73 ng m<sup>-3</sup> (15–328 ng m<sup>-3</sup>) during the wet season, and 610 ± 400 ng m<sup>-3</sup> (86–1962 ng m<sup>-3</sup>) during the dry season. The ISO-derived organosulfate with MW 216, constituted about 80% of the total organosulfate mass detected. Its concentration ranged from 83 ± 59 ng m<sup>-3</sup> (11–260 ng m<sup>-3</sup>) during the wet season, and 399 ± 308 ng m<sup>-3</sup> (39–1450 ng m<sup>-3</sup>) during the dry season. The OSs with the MW 214 occurred at the mean concentrations of 11.5 ± 9.3 (wet season) and 101 ± 61 ng m<sup>-3</sup> (dry season). Organosulfate with the MW 212 was detected only during the wet season at the level of 1.3 ± 1.5 ng m<sup>-3</sup>. The mean relative humidity was high through the sampling period: 74 ± 15% during the dry season and 81 ± 5% during the wet season. Although ISO OSs formation was enhanced during dry season, the correlation analysis did not confirm, that relative humidity directly affected their formation. Organosulfates contributed up to 3.5 ± 1.9% of aerosol OM during the wet season and 5.1 ± 2.5% during the dry season.

He et al. (2014) analyzed the chemical composition of the Pearl River Delta region in South China. The authors detected two main isoprene OSs – MW 216 and MW 200, however, both at the levels close to the LOD: 0.00 – 2.09 ng m<sup>-3</sup> and 0.00 – 1.06 ng m<sup>-3</sup>, respectively. Bryant and co-workers (2021) investigated the OSs and NOSs formation from biogenic precursors influenced by high anthropogenic emissions in Guangzhou, a southern Chinese megacity in the Pearl River Delta region. They showed that mean ISO-derived OSs and NOSs concentrations during summer were 181.8 ng m<sup>-3</sup> and 23.7 ng m<sup>-3</sup>, respectively. Moreover, those authors observed the enhanced formation of ISO OSs at temperatures above 30°C and in the presence of particulate sulfate (SO<sub>4</sub><sup>2-</sup>), suggesting the dominant formation pathway was heterogeneous reactions of oxidized ISO compounds. **Table 23** presents a comparison of two well-known and widely investigated ISO-derived OSs – methyltetrol OSs (MW 216) and methylglyceric acid OS (MW 200; adapted from Bryant et al., 2020).

**Table 23:** Mean concentrations (ng m<sup>-3</sup>) for two main ISO OSs with the MW 200 and the MW 216 determined in this study and reported in literature (adapted from Bryant et al., 2020)

Sampling site (year)	MW 200	MW 216	Reference
Amazon (2016)	-	390	Cui et al. (2018)
Amazon (2014)	0.7 (wet); 30.0 (dry)	83 (wet); 399 (dry)	Glasius et al. (2018)
Centreville, U.S. (2013)	10.7	217.0	Riva et al. (2019)
Look Rock, U.S. (2013)	10.0	169.5	Budlisulistiorini et al. (2015)
Atlanta, U.S. (2015)	53	1792	Hettiyadura et al. (2019)
Beijing, China (2016)	3.6	5.3	Wang et al. (2018)
Beijing, China (2017)	21.5	11.8	Bryant et al. (2020)
Guangzhou, China (2019)	11.8 (summer) 5.7 (winter)	57.4 (summer) 4.8 (winter)	Bryant et al. (2021)
U.S. (2016)	13	24	Chen et al. (2021)
Birmingham, U.S. (2013)	7.2	164.5	Rattanavaraha et al. (2016)
Zielonka, Poland (2016)	0.9	126.2	
Kaskada, Poland (2018)	0.7	89.7	
Diabla Góra, Poland (2016)	-	136.2	This study
Godów, Poland (2014)	-	6.5	

As **table 23** shows, the amount of methylglyceric acid OS (MW 200) was generally lower than that of methyltetrol OSs (MW 216), with the exception of Guangzhou and Beijing (Bryant et al. 2020, 2021). It was caused by diminished formation of MAE and higher concentrations of IEPOX in the atmosphere, especially in forested areas at higher temperatures (Lin et al., 2013; Worton et al., 2013). Therefore, isoprene SOA formation *via* IEPOX pathway is more significant than formation *via* MAE pathway. In addition, Hatch et al. (2011) conducted real-time ATOF-MS measurements in the ambient atmosphere, which revealed that the highest isoprene OSs concentrations occurred at night under a stable boundary layer. They suggested that gas-to-particle partitioning with subsequent aqueous-phase processing of the isoprene oxidation products played a key role in OSs formation. However, ISO OSs concentrations determined for Diabla Góra, Kaskada and Zielonka field samples with 12-hours day-and-night aerosol collection do not unequivocally confirm the findings of Hatch et al. (2011). The following figures and tables present the concentrations of selected isoprene SOA components found in ambient aerosol samples at those sites correlated with OC concentrations, temperature and relative humidity (**Figs. 50 – 53**). In addition, **tables 24 – 27** present the sum of OSs and NOSs contributions to the PM<sub>2.5</sub> aerosol and OC.



**Figure 50.** Concentrations of selected components of Zielonka ambient aerosol samples determined using UPLC-MS (the numerical values are listed in **table A11** in the Appendix)

Samples collected in Zielonka (Bory Tucholskie) were highly influenced by biogenic aerosol precursors. **Figure 50** shows the tendency observed for selected ISO

SOA components. The increase of NOS with MW 261 and a slight increase of other compounds detected in L024 day sample may be connected with the increase of NO<sub>x</sub> (3.2 µg m<sup>-3</sup>) and SO<sub>2</sub> (1.4 µg m<sup>-3</sup>) in the atmosphere the night before (see **table 10** in Chapter 2.1.2). Moreover, also OC concentration (9.0 µg m<sup>-3</sup>) for that sample was high. The notable decrease in concentrations may be related to the increasing RH level (up to 100% for L025 sample), which is consistent with the smog-chamber findings.

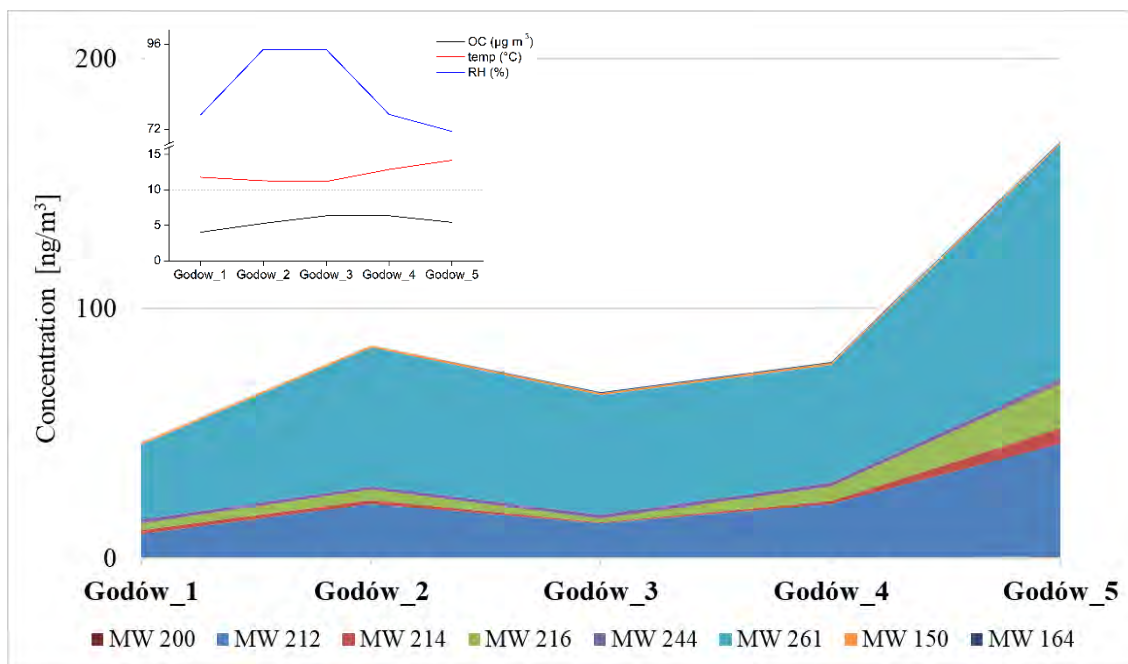
**Table 24** shows the contribution of detected ISO-derived compounds to OC and PM<sub>2.5</sub> masses of Zielonka ambient aerosol. For the analyzed sampling period, the mass share of ISO-related OSs and NOSs has not exceeded 8.7% of organic carbon, and 6.2% of PM<sub>2.5</sub> mass.

**Table 24:** Contribution of ISO-derived compounds to OC and PM<sub>2.5</sub> in Zielonka ambient aerosol samples

Sample	(Σ OSs+NOS) / OC (%)	(Σ OSs+NOS) / PM <sub>2.5</sub> (%)
L022	8.7	3.6
L023	7.7	3.5
L024	7.4	6.2
L025	7.2	3.0
L026	8.6	3.7
Average	7.9	4.0

Samples collected in Godów were highly influenced by biogenic and anthropogenic aerosol precursors. **Figure 51** shows the tendency of observed ISO SOA components. High concentration of ISO SOA components in Godów\_5 sample may be connected with relatively low RH level in the atmosphere (94.5% for Godów\_3 and 71.4% for Godów\_5 sample). In addition, that time a slight increase of SO<sub>2</sub> in the atmosphere occurred (up to 5 µg m<sup>-3</sup>; see **table 10** in Chapter 2.1.2) with the simultaneous change of airflow from west to south at 50 m above ground level. Those variables could influenced the growth of ISO SOA components in Godów samples.





**Figure 51.** Concentrations of selected components of Godów ambient aerosol samples determined using UPLC-MS (the numerical values are listed in **table A12** in the Appendix)

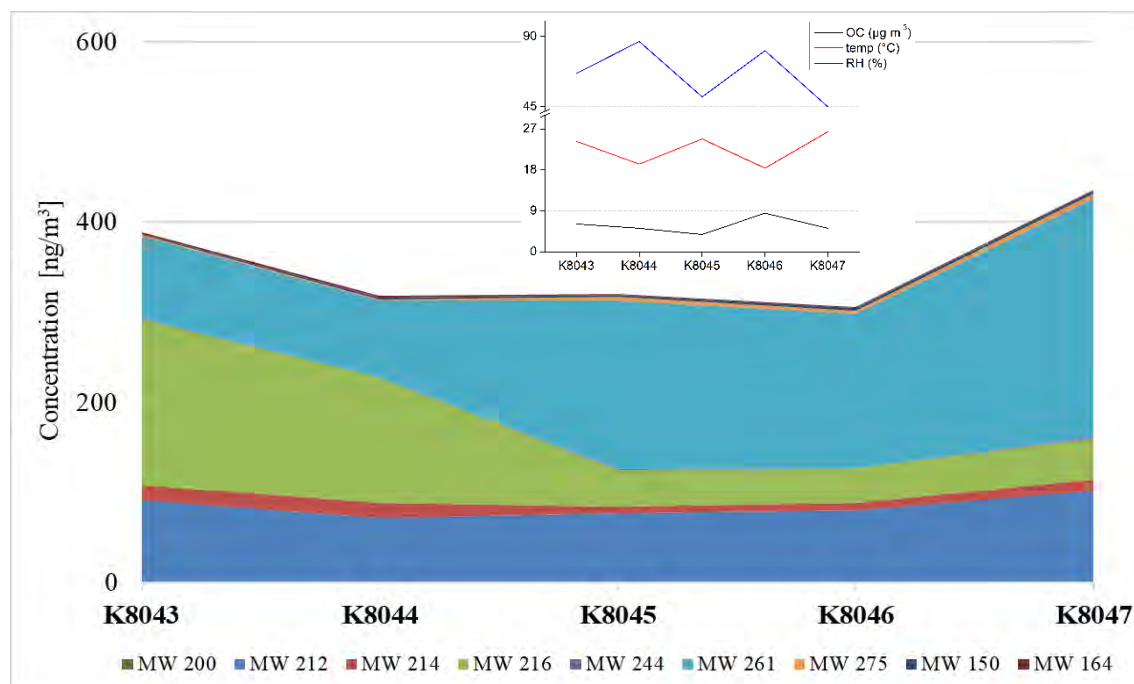
**Table 25** shows the contribution of detected ISO-derived organosulfates to OC and PM<sub>2.5</sub> masses in Godów ambient aerosol samples. For the analyzed sampling period, the average mass share of ISO-related OSs and NOSs has not exceeded 3.1% of OC and 1.1% of PM<sub>2.5</sub> mass.

**Table 25:** Contribution of ISO-derived compounds to OC and PM<sub>2.5</sub> in Godów ambient aerosol samples

Sample	( $\Sigma$ OSs+NOSs) / OC (%)	( $\Sigma$ OSs+NOSs) / PM <sub>2.5</sub> (%)
Godów_1	1.1	0.3
Godów_2	1.6	0.4
Godów_3	1.0	0.3
Godów_4	1.2	0.4
Godów_5	3.1	1.1
Average	1.6	0.5

Samples collected in Kaskada, a small park in northern Warsaw, were highly influenced by biogenic and anthropogenic aerosol precursors. **Figure 52** shows the tendency of observed ISO SOA components. The total concentration of ISO SOA components during selected period remained almost at the same level. However, the chemical composition of the samples changed. The considerable increase

in 2-methyltetrol NOS (MW 261) formation was observed, followed by the decay of 2-methyltetrols OS (MW 216). This particular observation was caused by a significant increase of the nitrogen oxides (NO<sub>x</sub>) concentration in the atmosphere, even up to 124.1 μg m<sup>-3</sup> (see **table 10** in Chapter 2.1.2), so that the most abundant compound detected was NOS 261. The second major ISO-derived compound detected was OS with the MW 212, which concentration remained almost constant during the sampling period.



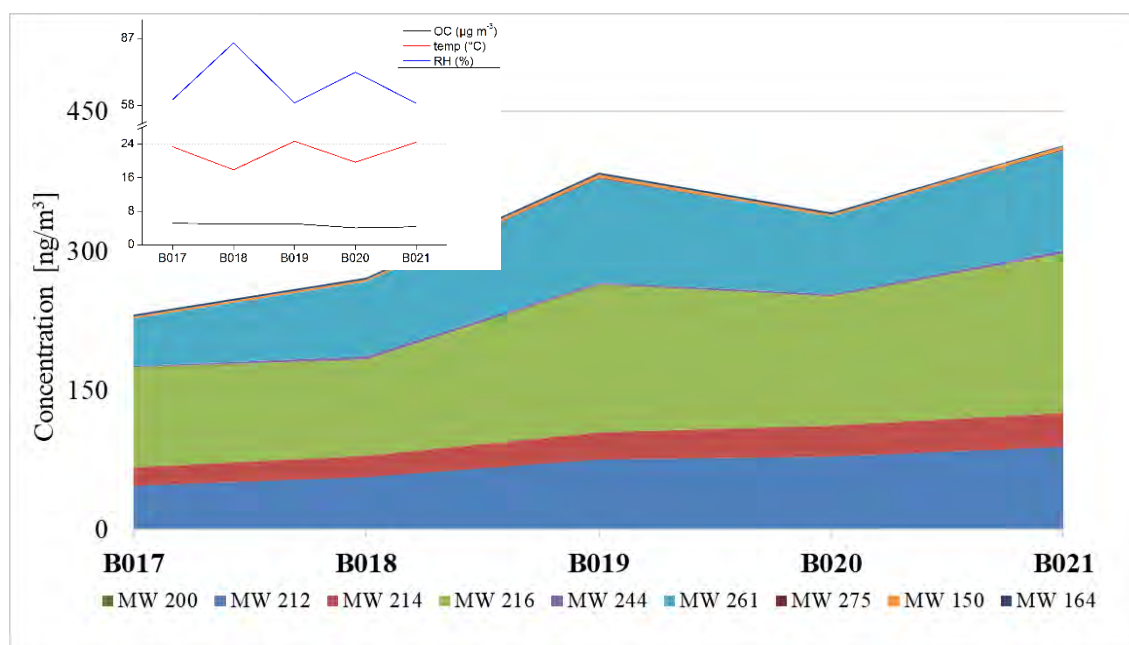
**Figure 52.** Concentrations of selected components of Kaskada ambient aerosol samples determined using UPLC-MS (the numerical values are listed in **table A13** in the Appendix)

**Table 26** shows the contribution of detected ISO-derived organosulfates in OC and PM<sub>2.5</sub> of Kaskada ambient aerosol. For the analyzed sampling period, the average share of ISO-related OSs and NOSs has not exceeded 8.3% of OC and 3.2% of PM<sub>2.5</sub> mass.

**Table 26:** Contribution of ISO-derived compounds to OC and PM<sub>2.5</sub> in Kaskada ambient aerosol samples

Sample	( $\Sigma$ OSs+NOSs) / OC (%)	( $\Sigma$ OSs+NOSs) / PM <sub>2.5</sub> (%)
K8043	6.3	2.7
K8044	6.0	2.9
K8045	8.2	3.2
K8046	3.5	1.4
K8047	8.3	3.1
Average	6.5	2.6

Samples collected in Diabla Góra, a rural forested area, were highly influenced by biogenic aerosol precursors. **Figure 53** shows the tendency of observed ISO SOA components.



**Figure 53.** Concentrations of selected components of Diabla Góra ambient aerosol samples determined using UPLC-MS (the numerical values are listed in **table A14** in the Appendix)

The total concentration of ISO SOA components mildly increased during the analyzed period, probably due to the gradually decreasing RH level. In addition, 24-hour air mass back trajectories indicated a constant airflow to Diabla Góra from the east direction. In contrast to other locations, the main isoprene-derived compound found was 2-methyltetrol organosulfate (MW 216).

**Table 27** shows the contribution of detected ISO-derived organosulfates in OC and PM<sub>2.5</sub> of Diabla Góra ambient aerosol. For the analyzed sampling period, the average share of ISO-related OSs and NOSs has not exceeded 9.6% of OC and 3.8% of PM<sub>2.5</sub> mass.

**Table 27:** Contribution of ISO-derived compounds to OC and PM<sub>2.5</sub> in Diabla Góra ambient aerosol samples

Sample	( $\Sigma$ OSs+NOSs) / OC (%)	( $\Sigma$ OSs+NOSs) / PM <sub>2.5</sub> (%)
B017	4.5	2.0
B018	5.4	2.3
B019	7.6	3.4
B020	8.4	3.0
B021	9.6	3.8
Average	7.1	2.9

The highest contribution of detected ISO SOA components in OC has been demonstrated in Zielonka and Diabla Góra sampling stations (7.9 % and 7.1%, respectively), where very likely the highest isoprene emission occurred. Moreover, both sites are forested rural areas, slightly influenced by nitrogen oxides (NO<sub>x</sub>). Therefore, the share of nitrooxy-organosulfate with MW 261 formed were lower, comparing to Godów and Kaskada more influenced by anthropogenic emissions. The highest amounts of ISO SOA were found in Zielonka ambient aerosol.

#### 3.4.3.2 Butadiene SOA

The concentrations of butadiene SOA components in samples from selected sampling sites were determined. Among compounds detected, the most abundant 13BD-derived product was malic acid (MW 134) and its organosulfate (MW 214). Other compounds detected were tartaric acid (MW 150) and threonic acid (MW 136). 1,2,3,4-butanetetrol nitroorganosulfates (MW 247), glyceric acid organosulfate (MW 186) and 2(3*H*)-furanone, dihydro-3,4-dihydroxy- organosulfate (MW 198) were found in trace amounts. Butanetetrol NOS was detected solely in urban and highly anthropogenically influenced areas – Kaskada and Godów. Although threonic acid was detected at Godów, Zielonka and Diaba Góra sampling sites, its OS occurred only in trace amounts in Zielonka and Godów samples. Moreover, traces of tartronic acid (MW 120)

were found solely in Diabla Góra samples. At other sampling sites, TrtA was not detected at all. 13BD components found in smog-chamber experiments, such as 2-butanone, 1,4-dihydroxy- organosulfate (MW 184), 2-butanone, 1,3,4-trihydroxy- organosulfate (MW 200), 1,2,3,4-butanetetrol organosulfate (MW 202), 1,2,3,4- butanetetrol nitrosooxy-organosulfate (MW 231) have not been found in ambient aerosol collected at the sampling sites.

**Table 28** presents the mean concentrations of 13BD SOA components in collected samples. The highest concentration of butadiene-derived organosulfates was detected in Zielonka ( $14.0 \pm 5.3 \text{ ng m}^{-3}$ ), whereas the lowest concentration – in Godów ( $5.8 \pm 1.0 \text{ ng m}^{-3}$ ). The same dependence was found for organic acids, with the highest values for Zielonka ( $105.9 \pm 38.7 \text{ ng m}^{-3}$ ), and the lowest for Godów ( $13.4 \pm 2.4 \text{ ng m}^{-3}$ ). In particular, 1,3-butadiene OSs and NOSs were not reported previously.

**Table 28:** Mean concentrations ( $\text{ng m}^{-3}$ ) determined in this study for 13BD SOA components

Sampling site	MW 186	MW 198	MW 214	MW 216	MW 247	MW 134	MW 136	MW 150	$\Sigma$ OSs+NOSs	$\Sigma$ acids
Kaskada	< LOD	ND	$6.5 \pm 0.7$	ND	$0.7 \pm 0.9$	$58.5 \pm 20.7$	ND	$4.4 \pm 0.2$	$7.4 \pm 1.5$	$62.9 \pm 20.8$
Zielonka	$0.6 \pm 0.6$	ND	$13.3 \pm 5.0$	< LOD	ND	$93.7 \pm 31.7$	$6.9 \pm 6.6$	$5.2 \pm 0.7$	$14.0 \pm 5.3$	$105.9 \pm 38.7$
Godów	< LOD	< LOD	$4.0 \pm 0.6$	< LOD	$1.5 \pm 0.3$	$11.9 \pm 2.3$	< LOD	$1.5 \pm 0.1$	$5.8 \pm 1.0$	$13.4 \pm 2.4$
Diabla Góra	< LOD	ND	$6.9 \pm 0.7$	ND	ND	$54.5 \pm 13.1$	$0.7 \pm 0.9$	$4.0 \pm 0.2$	$6.9 \pm 0.7$	$59.1 \pm 13.8$

< LOD denotes that the compound was not detected in all analyzed samples and/or in trace amounts

ND – not detected

MA, TrA and TA were characterized as a biomass burning aerosol components (Falkovich et al., 2005). Those compounds were observed previously in ambient samples. MA is considered not to have a primary source and originate from the photooxidation of dicarboxylic acids, such as succinic acid. Unsaturated hydrocarbons of biogenic and anthropogenic origin and various fatty acids are considered the MA possible precursors (Rozaini, 2012; Hu and Yu, 2013). As reported previously by Jaoui et al. (2014), concentrations of malic acid and threonic acid were determined in ambient samples from Bakersfield, CA, U.S. during May – June 2010 campaign using a GC-MS *off-line* analysis. The amounts of those compounds ranged from 0.0 to 14.1 ng m<sup>-3</sup> while the total PM<sub>2.5</sub> mass varied from 0.06 to 1.17 µg m<sup>-3</sup>. Rohrl and Lammel (2002) observed TA in ambient aerosol collected during the 1998 campaign in Germany, with the mean concentration of 5.1 ng m<sup>-3</sup> (0.2 – 40.0 ng m<sup>-3</sup>). They also detected MA at the average level of 42 ng m<sup>-3</sup> (0.5 – 194 ng m<sup>-3</sup>). Fu et al. (2008b) determined the mean concentrations of MA and TA collected at the Mt. Tai summit in North China Plain: 68.2 and 5.07 µg m<sup>-3</sup>, respectively. Hu and Yu (2013) reported MA concentrations in ambient aerosol samples collected in Hong Kong, China, and compared them with MA concentrations at other world sites. **Table 29** shows the reported concentrations of malic acid contained in PM<sub>2.5</sub> aerosol samples. The values measured in this study are consistent with the reported ranges.

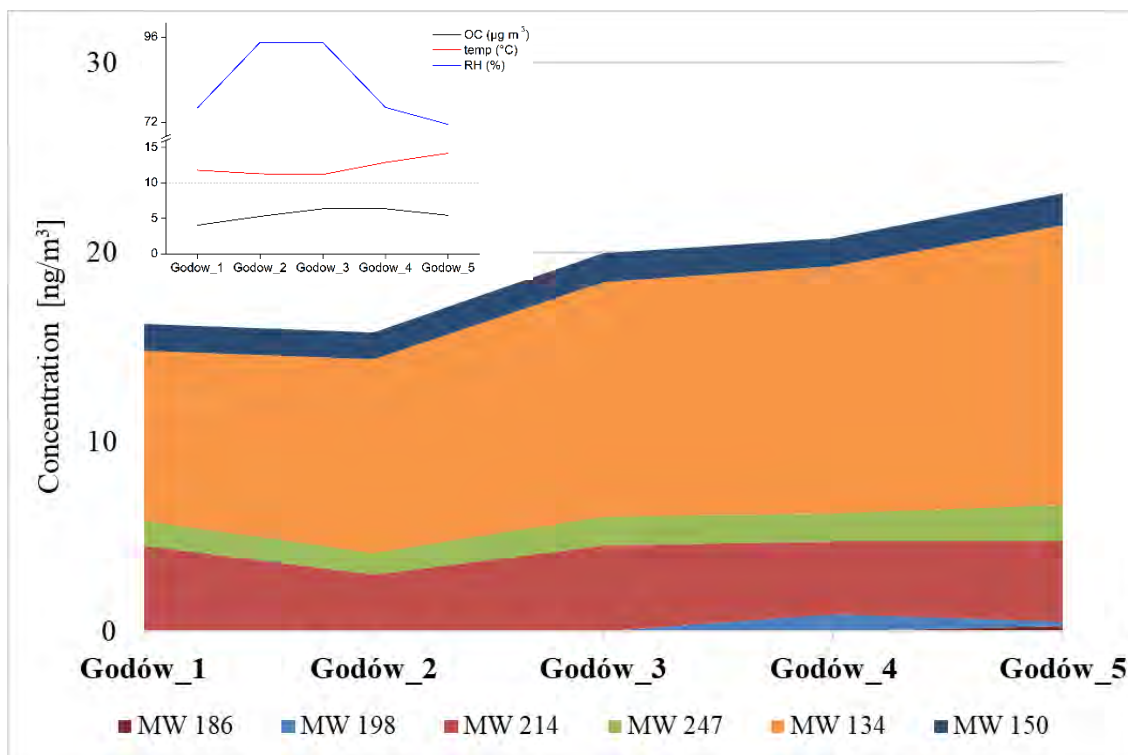
**Table 29:** Mean concentrations of malic acid ( $\text{ng m}^{-3}$ ) in  $\text{PM}_{2.5}$  samples (adapted from Hu and Yu, 2013 and determined in this work)

Sampling site (year)	MA	Reference
Rondonia, Brazil (1999)	67.3 (12–146)	Graham et al., 2002
Tokyo, Japan (1989)	27.3 (2.9–99.1)	Kawamura and Yasui, 2005
Julich, Germany (2002-2003)	39 (22–62)	Kourtchev et al., 2008
K-pusztá, Hungary (2003)	40 (16–78)	Kourtchev et al., 2009
Mt.Tai, China (2006)	68.2 (10–236)	Fu et al., 2008b
Changbai Mt., China (2007)	77 (65–88)	
Chongming Island, China (2006)	79 (16–173)	Wang et al., 2008
Jiangfenglin, China (2006)	46 (15–122)	
Hong Kong, China (2006)	209 (9–662)	Hu et al., 2008
Hong Kong, China (2006)	155 (20–179)	Hu and Yu, 2013
Zielonka, Poland (2016)	93.7 (53.5–118.5)	
Kaskada, Poland (2018)	58.5 (40.0–84.9)	This study
Diabla Góra, Poland (2016)	54.5 (38.9–74.7)	
Godów, Poland (2014)	11.9 (9.0–14.7)	

The concentrations of selected butadiene secondary organic aerosol components found in ambient aerosol samples were correlated with OC concentrations, temperature and relative humidity levels (**Figs. 54 – 55, 57 – 58**). **Tables 30 – 33** present the collective contribution of 13BD OSs and NOSs to  $\text{PM}_{2.5}$  and OC.

Ambient aerosol samples collected at Godów sampling site were influenced by anthropogenic precursors. Therefore, AA contained a variety of compounds originated from 1,3-butadiene (**Fig. 54**). The main components detected were: malic acid (MW 134), its organosulfate (MW 214), tartaric acid (MW 150), and butanetetrol NOS (MW 247). The highest concentration of 13BD SOA components was observed in Godów\_4 and Godów\_5 samples, which also contained glyceric acid OS (MW 186) and 2(3H)-furanone, dihydro-3,4-dihydroxy- OS (MW 198). Those two samples could be affected by the lowest RH level – from 94.5% for Godów\_3 sample to 71.4% for Godów\_5 sample. Besides, the airflow from west to south direction might influence the formation of 13BD SOA in Godów samples.





**Figure 54.** Concentrations of selected components in Godów ambient aerosol samples determined using UPLC-MS (the numerical values are listed in **table A15** in the Appendix)

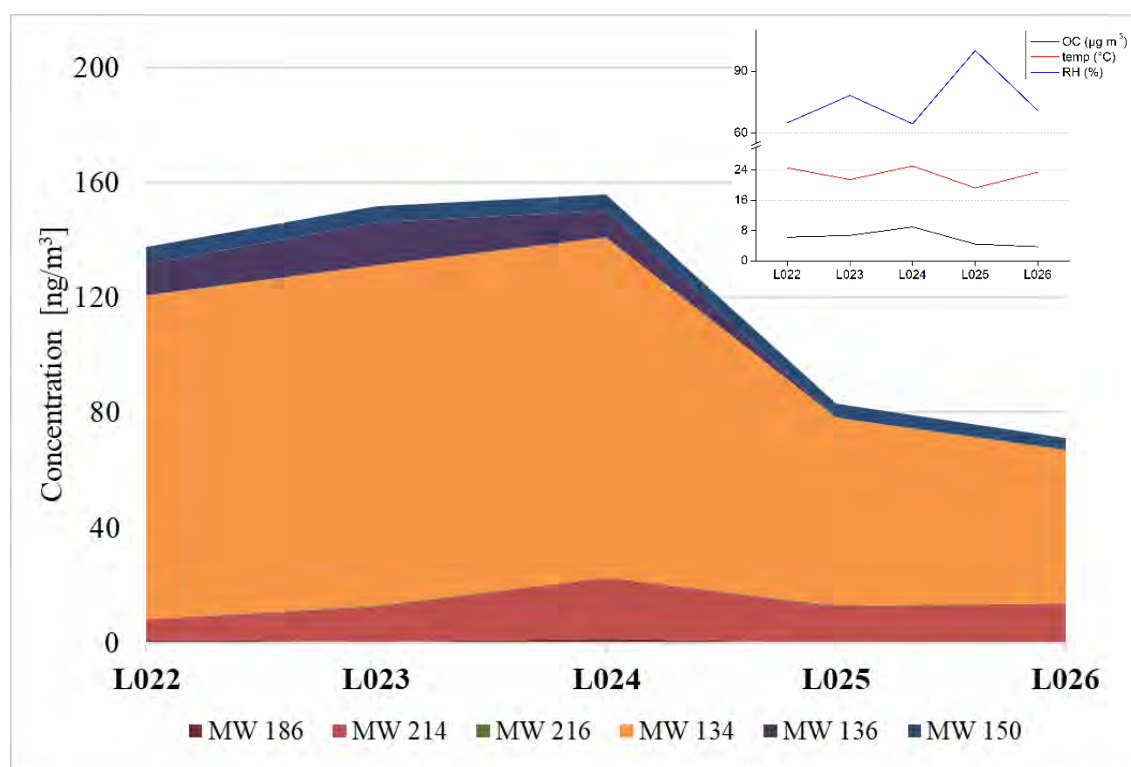
**Table 30** shows the contribution of 13BD-derived organosulfates to OC and PM<sub>2.5</sub> in Godów samples. The average sum of detected OSs and NOSs constituted 0.11% of OC (0.08 – 0.14%), and 0.03% of PM<sub>2.5</sub> mass (0.02 – 0.04%). 13BD SOA constituted around 10-fold less of organic matter and PM<sub>2.5</sub> mass, than isoprene-derived components.

**Table 30:** Contribution of detected 13BD-derived compounds in OC and PM<sub>2.5</sub> (%) of Godów ambient aerosol

Sample	( $\Sigma$ OSs+NOSs) / OC (%)	( $\Sigma$ OSs+NOSs) / PM <sub>2.5</sub> (%)
Godów_1	0.14	0.03
Godów_2	0.08	0.02
Godów_3	0.09	0.03
Godów_4	0.10	0.04
Godów_5	0.12	0.04
Average	0.11	0.03

The samples collected in Zielonka (Bory Tucholskie) were also highly influenced by anthropogenic aerosol precursors. The most abundant components of ambient aerosol collected were malic acid (MW 134;  $93.7 \pm 31.7 \text{ ng m}^{-3}$ ) and its organosulfate (MW 214;  $13.3 \pm 5.0 \text{ ng m}^{-3}$ ) (**Fig 55**). Those components may indicate the enhanced

biomass burning processes in the immediate vicinity of the sampling site. High amount of 13BD compounds detected in L024 day sample may be connected to the increase of  $\text{NO}_x$  ( $3.2 \mu\text{g m}^{-3}$ ) and  $\text{SO}_2$  ( $1.4 \mu\text{g m}^{-3}$ ) in the atmosphere the night before (see **table 10** in Chapter 2.1.2). Moreover, the OC concentration in that sample was high ( $9.0 \mu\text{g m}^{-3}$ ). The notable decrease of components concentration in L025 and L026 samples might result from the increased RH level (up to 100% for L025 sample).



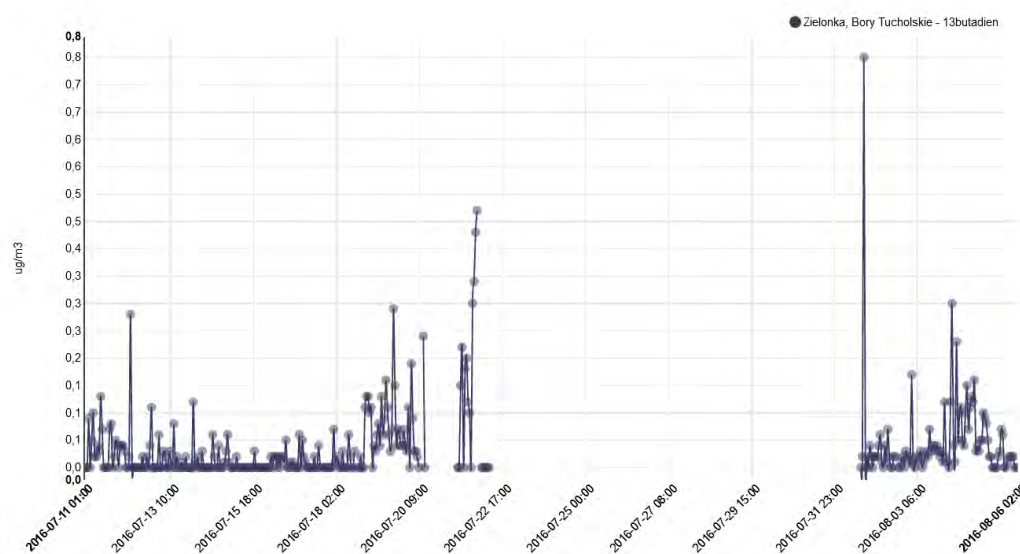
**Figure 55.** Concentrations of selected components of Zielonka ambient aerosol samples determined using UPLC-MS (the numerical values are listed in **table A16** in the Appendix)

**Table 31** shows the contribution of the 13BD-derived compounds to OC and  $\text{PM}_{2.5}$  of Zielonka ambient aerosol samples. The average sum of 13BD-related OSs constituted 0.24% of OC (0.11 – 0.36%), and 0.12% of  $\text{PM}_{2.5}$  mass (0.05 – 0.20%). In Zielonka, 13BD SOA contributed about 30 times less to OC and  $\text{PM}_{2.5}$  than the ISO-derived compounds.

**Table 31:** Contribution of 13BD-derived compounds to OC and PM<sub>2.5</sub> (%) in Zielonka ambient aerosol

Sample	( $\Sigma$ OSs) / OC (%)	( $\Sigma$ OSs) / PM <sub>2.5</sub> (%)
L022	0.11	0.05
L023	0.19	0.08
L024	0.24	0.20
L025	0.29	0.12
L026	0.36	0.16
Average	0.24	0.12

1,3-butadiene is present in the rural areas like Zielonka surrounded by the Bory Tucholskie forests. **Figure 56** shows 1,3-butadiene concentrations in the atmosphere determined in Zielonka on the dates preceding and following the sampling period during 2016 summer campaign (unfortunately, the measurements stopped between 22 – 31 July due to the autosampler failure). Nevertheless, 13BD was unquestionably present in the air during aerosol sampling.

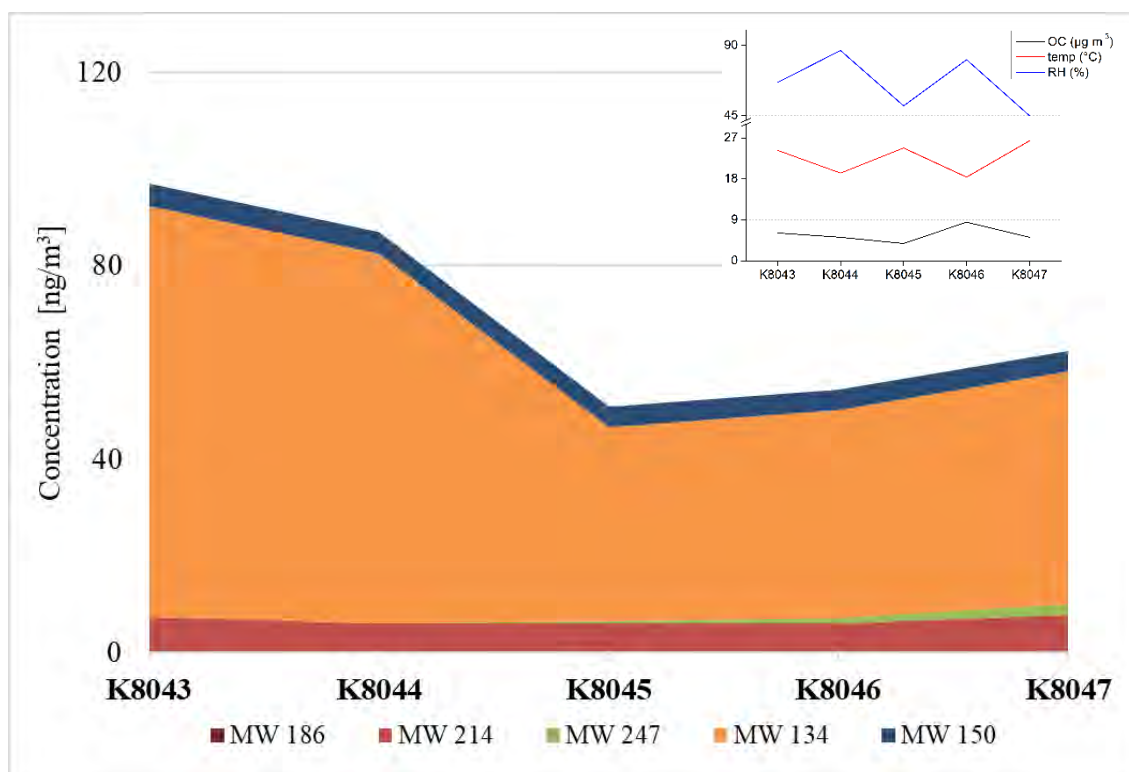


**Figure 56.** 1,3-butadiene concentrations in the air at the Zielonka sampling site during 2016 summer campaign

[https://powietrze.gios.gov.pl/pjp/current/station\\_details/archive/232#](https://powietrze.gios.gov.pl/pjp/current/station_details/archive/232#)

Samples collected in Kaskada were affected by urban anthropogenic precursors. **Figure 57** shows the concentrations of 13BD SOA components in collected aerosol samples. The total concentration of 13BD SOA components dropped in K8045 sample, mostly due to decrease in MA content. Moreover, in K8045 – K8047 samples, a noticeable increase of butanetetrol NOS (MW 247) was observed, which might result

from the increased concentration of nitrogen oxides (NO<sub>x</sub>) in the atmosphere (up to 124.1 μg m<sup>-3</sup>). The most abundant compound was malic acid (MW 134). Traces of glyceric acid organosulfate with MW 186 were found.



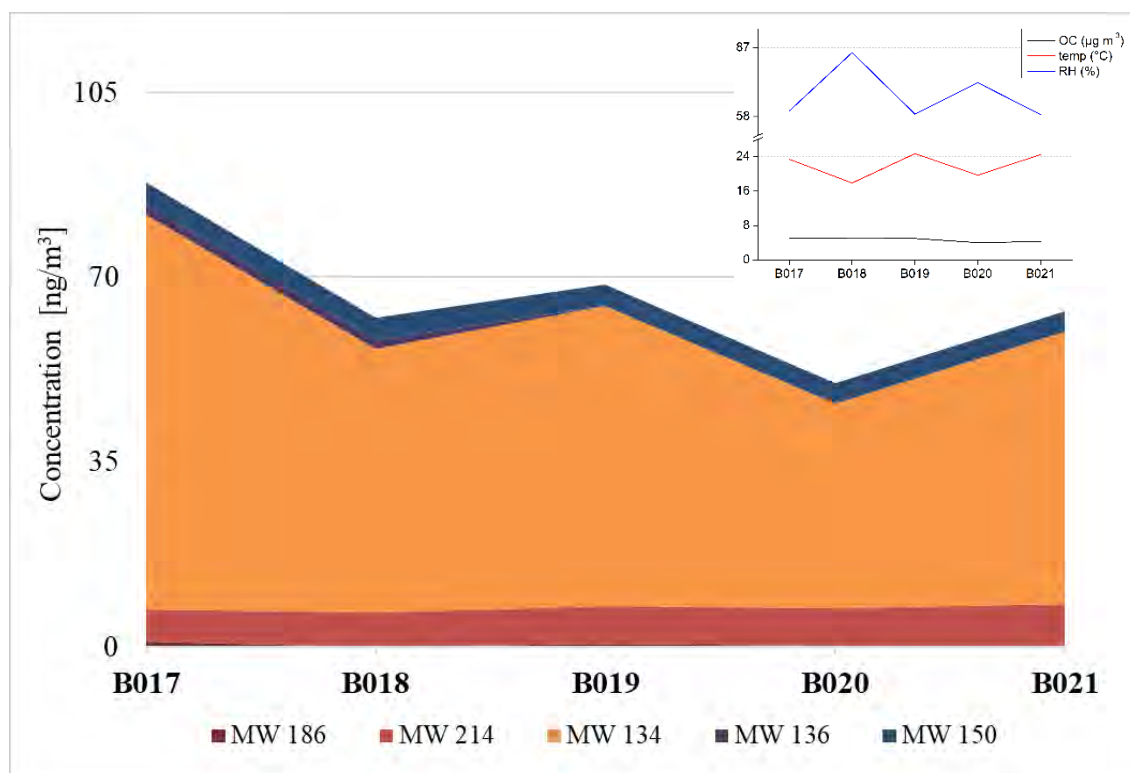
**Figure 57.** Concentrations of selected components in Kaskada ambient aerosol samples determined using UPLC-MS (the numerical values are listed in **table A17** in the Appendix)

**Table 32** shows the contribution of detected 13BD-derived components to OC and PM<sub>2.5</sub> in Kaskada ambient aerosol. The average sum of OSs and NOSs constituted 0.14% of OC (0.08 – 0.19%), and 0.06% of PM<sub>2.5</sub> mass (0.03 – 0.07%), which is about 40 times less than the contribution of isoprene-derived components.

**Table 32:** Contribution of 13BD-derived compounds to OC and PM<sub>2.5</sub> (%) in Kaskada ambient aerosol

Sample	( $\Sigma$ OSs+NOSs) / OC (%)	( $\Sigma$ OSs+NOSs) / PM <sub>2.5</sub> (%)
K8043	0.12	0.05
K8044	0.12	0.06
K8045	0.17	0.07
K8046	0.08	0.03
K8047	0.19	0.07
Average	0.14	0.06

**Figure 58** shows the concentrations of 13BD SOA components in ambient aerosol from Diabla Góra. The total concentration of compounds gently decreased during the analyzed period, in contrary to the increasing isoprene-derived SOA. The main 13BD-derived compounds found were malic acid (MW 134), its organosulfate (MW 214) and tartaric acid (MW 150). In the B017 and B018 samples, a small amounts of threonic acid (MW 136) and glyceric acid OS (MW 186) were detected. 24-hour air mass back trajectories indicated a constant airflow to Diabla Góra from the east direction.



**Figure 58.** Concentrations of selected components in Diabla Góra ambient aerosol samples determined using UPLC-MS (the numerical values are listed in **table A18** in the Appendix)

**Table 33** shows the contribution of 13BD-derived organosulfates to OC and PM<sub>2.5</sub> in Diabla Góra ambient aerosol. The average sum of ISO-related OSs constituted 0.15% of OC (0.12 – 0.19%), and 0.06% of PM<sub>2.5</sub> mass (0.05 – 0.07%). In Diabla Góra, 13BD SOA contributed about 30 times less to OC and PM<sub>2.5</sub> than the ISO-derived compounds.

**Table 33:** Contribution of 13BD-derived compounds to OC and PM<sub>2.5</sub> (%) in Diabla Góra ambient aerosol

Sample	( $\Sigma$ OSs) / OC (%)	( $\Sigma$ OSs) / PM <sub>2.5</sub> (%)
B017	0.12	0.05
B018	0.13	0.05
B019	0.14	0.06
B020	0.17	0.06
B021	0.19	0.07
Average	0.15	0.06

The highest contribution of 13BD SOA components in collected aerosol samples has been demonstrated at the Zielonka sampling site, with malic acid and its organosulfate as the most abundant compounds (93.7 and 13.3  $\mu\text{g m}^{-3}$ , respectively). The source of those compounds in the atmosphere are direct emission of 1,3-butadiene and biomass burning in nearby households. The butadiene SOA was less chemically diverse than the isoprene SOA. Moreover, the results obtained from the field studies differ from the smog-chamber experiments. In case of ISO SOA, most of the compounds formed in the smog-chamber SOA occurred in ambient aerosol samples in high or at least trace amounts. On the contrary, some compounds derived from butadiene in the smog-chamber experiments were not detected in ambient aerosol, so they may not form easily in the atmosphere. The most important difference was the lack of 1,2,3,4-butanetetrol OS (MW 202) in aerosol samples, while its isoprene-derived analogue, 2-methyltetrol OS (MW 216) occurred abundantly and was a key tracer of ISO SOA. That comparison suggests that the dominant formation pathway of 13BD SOA in the atmosphere is rather through acrylic acid epoxide (AAE; see **Scheme 4** in Chapter 1.1.2.2), than 2,3-epoxy-1,4-butanediol (BEPOX), as additionally confirmed by the detection of glyceric acid OS (MW 186). The conclusion is also supported by the formation of threonic acid (MW 136) *via* AAE (Jaoui et al., 2014), and by the presence of TrA OS (MW 216) and its lactone form 2(3H)-furanone, dihydro-3,4-dihydroxy- organosulfate (MW 198) in aerosol samples (Wach et al. 2020).

## 4. Summary and conclusions

The research reported in this Ph.D. thesis aimed to thoroughly investigate the chemical composition of secondary organic aerosol (SOA) formed from two structurally similar precursors – isoprene and 1,3-butadiene. Although the two compounds are homologs, they are emitted into the atmosphere from totally different sources. Isoprene is the most abundant and widely studied biogenic VOC, while 1,3-butadiene is a VOC of the anthropogenic origin. The formation of SOA from ISO and 13BD was examined in collaboration with the U.S. Environmental Protection Agency (U.S. EPA) in a series of experiments conducted in an in-door smog chamber. The effect of relative humidity and acidity of seed aerosol on the formation of ISO and 13BD components was investigated. Contrary to other studies, the concentrations of the majority of ISO and 13BD compounds detected and the total yields of secondary organic carbon (SOC) decreased with increasing RH level, more sharply in experiments with acidic seed than non-acidic. Thus, the increase of the liquid water content of an aerosol system did not promote the formation of ISO and 13BD organosulfates, nitrooxy- and nitrosooxy- organosulfates. Under acidic conditions and low RH levels, the formation of isoprene and butadiene products containing sulfate moieties was enhanced, comparing to non-acidic conditions at the same RH level. For instance, the observed concentrations of NOS with MW 261, OSs with MW 216 and MW 214 (ISO SOA), and NOS with MW 247, OS with MW 202 (13BD SOA) were even 10 times higher. On the other hand, the formation of ISO and 13BD highly oxygenated acids was greater in non-acidic seed experiments, without any substantial effect of RH variation.

The observed ISO- and 13BD-derived products were characterized using UPLC-ESI-HRMS technique followed by a thorough interpretation of obtained analytical data, including product ion mass spectra with accurate mass measurements. All mass spectrometric analyses were performed in the negative ion mode, as the investigated compounds had reasonable ionization efficiencies to deprotonated ions ( $[M-H]^-$ ). The molecular structures of newly identified compounds were elucidated. For OS, NOS, and NSOS, the proposed structures were tentative, with the diagnostic ions such as bisulfate anions ( $HSO_4^-$ ,  $m/z$  97), bisulfite anions ( $HSO_3^-$ ,  $m/z$  81), and sulfate radical anions ( $SO_3^{\cdot-}$ ,  $m/z$  80 and  $SO_4^{\cdot-}$ ,  $m/z$  96) observed in each case. The chemical structures proposed for highly oxygenated acids formed from isoprene and 1,3-butadiene were based on the product ion mass spectra and confirmed against appropriate synthesized

or purchased standard compound. The syntheses of novel ISO organic hydroxy acids – 2-methyltartaric acid and 2- and 3-methylthreonic acids were performed. The compounds were obtained with high purity (>98%) and good yields (55-75%), and their chemical structures were confirmed by spectroscopic (NMR) and spectrometric methods (MS). The ISO-derived organic hydroxy acids were proposed as highly oxygenated molecular (HOM) tracers of aged isoprene aerosol as they were also found in ambient aerosol samples in amounts ranging from 0.8 to 2.8 ng m<sup>-3</sup> on average. Moreover, several novel SOA components were discovered, i.a. 3-methylthreonic acid organosulfate (MW 230), 2-methylthreonic acid nitrooxy-organosulfate (MW 275) and 2-methyltartaric acid organosulfate (MW 244) for ISO SOA, and glyceric acid organosulfate (MW 186), malic acid organosulfate (MW 214), threonic acid organosulfate (MW 216) and 1,2,3,4-butanetetrol nitrooxy-organosulfate (MW 247) for 13BD SOA, which were also found in ambient aerosol from trace to substantial amounts.

In order to prove the link between smog-chamber experiments and ambient atmospheric processes, the UPLC-MS analyses of fine ambient aerosol (PM<sub>2.5</sub>) samples collected at four various sites in Poland were conducted. High concentrations and diversity of isoprene SOA components detected in Zielonka (Bory Tucholskie) and Diabla Góra (Puszcza Borecka) sampling sites revealed a large share of terrestrial vegetation in local emissions. The total amount of detected ISO OSs and NOS at those sampling sites were 474.9 ± 149.3 ng m<sup>-3</sup> and 324.0 ± 76.0 ng m<sup>-3</sup>, which accounted for approximately 7.9 % and 7.1 % of the total OC mass, respectively. The most abundant compounds were NOS (MW 261), OS (MW 216) and OS (MW 212), which contributed significantly to the chemical composition of ISO SOA. Moreover, Zielonka ambient aerosol was the richest one in 13BD SOA components, although not as chemically diverse as in ISO SOA. The total amount of detected OSs and NOS was 14.0 ± 5.3 ng m<sup>-3</sup>, which accounted for 0.24 % of the OC mass. In addition, malic acid, a known secondary organic aerosol tracer, and its organosulfate (MW 214) were highly abundant 13BD-derived components at all investigated sites. The greatest amounts of those compounds were detected in Zielonka: 93.7 ± 31.7 ng m<sup>-3</sup> and 13.3 ± 5.0 ng m<sup>-3</sup>, respectively. Their sources in the atmosphere could be direct 1,3-butadiene emission and biomass burning in nearby households. 1,2,3,4-butanetetrol OS (MW 202) was not detected in ambient aerosol, while its analogue 2-methyltetrol OS (MW 216) formed from isoprene was a highly abundant key tracer of ISO SOA. That finding proved inconsistent with the initial hypothesis that both precursors react in the same way in the atmosphere and suggests that



the dominant formation pathway of 13BD SOA in the atmosphere is rather through acrylic acid epoxide (AAE), than 2,3-epoxy-1,4-butanediol (BEPOX). Due to the multiplicity of variables that ultimately affect the chemical composition of SOA in the atmosphere, it is difficult to unambiguously correlate the meteorological data, air mass back trajectories and other physicochemical parameters with specific ISO and 13BD SOA compounds and their yields. Such efforts require a full scale modeling of atmospheric chemistry that was beyond the scope of this thesis. However, some events were easy to explain, e.g., a considerable increase in 2-methyltetrol NOS (MW 261) formation followed by the decay of 2-methyltetrols OS (MW 216) in Kaskada ambient aerosol caused by the increase of nitrogen oxides (NO<sub>x</sub>) in the atmosphere.

Organosulfates are expected to enhance the capacity of ambient aerosol as cloud condensation nuclei (CCN) impacting the air quality as proposed by e.g., Hansen et al. (2015) and recently by Peng et al. (2021). The data obtained in this study will pave the way for better description of the complex and time-varying chemical composition of secondary organic aerosol and may improve the performance of air quality models. However, true effects of organosulfates, nitrooxy- and nitrosooxy- organosulfates – including the components identified in this thesis – on the properties of SOA, and the possible influence on human health and life remain unknown and warrant further atmospheric chemical studies.

To sum up, this Ph.D. thesis presents results of the comprehensive studies on the chemical composition of isoprene and 1,3-butadiene SOA, which forms in the troposphere, the lower part of the Earth's atmosphere. Advanced research tools, including smog chambers and hyphenated mass spectrometry techniques were used for that purpose. The influence of relative humidity and acidity on the formation of individual 13BD and ISO SOA components was examined. Moreover, several significant and novel 13BD- and ISO-derived components were identified and their concentrations were measured in both, smog-chamber experiments and ambient fine aerosol.

## 5. References

1. Acquavella, J. F. (1996). "Butadiene epidemiology: A summary of results and outstanding issues." *Toxicology* **113**(1-3): 148-156.
2. Aksoyoglu, S., et al. (2017). "Secondary inorganic aerosols in Europe: sources and the significant influence of biogenic VOC emissions, especially on ammonium nitrate." *Atmospheric Chemistry and Physics* **17**(12): 7757-7773.
3. Alloway, B. J., and Ayres, D. C., (1999). "Chemiczne podstawy zanieczyszczenia środowiska." *Wydawnictwo Naukowe PWN*, Warszawa
4. Amodio, M., et al. (2013). "Assessment of Impacts Produced by Anthropogenic Sources in a Little City near an Important Industrial Area (Modugno, Southern Italy)." *Scientific World Journal*.
5. Andersson-Skold, Y. and D. Simpson (2001). "Secondary organic aerosol formation in northern Europe: A model study." *Journal of Geophysical Research-Atmospheres* **106**(D7): 7357-7374.
6. Andreae, M. O. (2019). "Emission of trace gases and aerosols from biomass burning - an updated assessment." *Atmospheric Chemistry and Physics* **19**(13): 8523-8546.
7. Andreae, M. O. and P. J. Crutzen (1997). "Atmospheric aerosols: Biogeochemical sources and role in atmospheric chemistry." *Science* **276**(5315): 1052-1058.
8. Andreae, M. O. and P. Merlet (2001). "Emission of trace gases and aerosols from biomass burning." *Global Biogeochemical Cycles* **15**(4): 955-966.
9. Andreae, M. O. and D. Rosenfeld (2008). "Aerosol-cloud-precipitation interactions. Part 1. The nature and sources of cloud-active aerosols." *Earth-Science Reviews* **89**(1-2): 13-41.
10. Angove, D. E., et al. (2006). "The characterisation of secondary organic aerosol formed during the photodecomposition of 1,3-butadiene in air containing nitric oxide." *Atmospheric Environment* **40**(24): 4597-4607.
11. Anttinen-Klemetti, T., et al. (2006). "Inhalation exposure to 1,3-butadiene and styrene in styrene-butadiene copolymer production." *International Journal of Hygiene and Environmental Health* **209**(2): 151-158.
12. Atkinson, R. and J. Arey (2003). "Gas-phase tropospheric chemistry of biogenic volatile organic compounds: a review." *Atmospheric Environment* **37**: S197-S219.
13. Attygalle, A. B., et al. (2001). "Collisionally-induced dissociation mass spectra of organic sulfate anions." *Journal of the Chemical Society-Perkin Transactions 2*(4): 498-506.
14. Baek, B. H. and V. P. Aneja (2004). "Measurement and analysis of the relationship between ammonia, acid gases, and fine particles in eastern North Carolina." *Journal of the Air & Waste Management Association* **54**(5): 623-633.
15. Baek, B. H., et al. (2004). "Chemical coupling between ammonia, acid gases, and fine particles." *Environmental Pollution* **129**(1): 89-98.
16. Baek, S. O. and R. A. Jenkins (2004). "Characterization of trace organic compounds associated with aged and diluted sidestream tobacco smoke in a controlled atmosphere - volatile organic compounds and polycyclic aromatic hydrocarbons." *Atmospheric Environment* **38**(38): 6583-6599.
17. Baker, A. R., et al. (2000). "Distribution and sea-air fluxes of biogenic trace gases in the eastern Atlantic Ocean." *Global Biogeochemical Cycles* **14**(3): 871-886.
18. Baker, J., et al. (2005). "Formation and reaction of hydroxycarbonyls from the reaction of OH radicals with 1,3-butadiene and isoprene." *Environmental Science & Technology* **39**(11): 4091-4099.
19. Barbosa, T. S., et al. (2017). "Chemical characterization of organosulfates from the hydroxyl radical-initiated oxidation and ozonolysis of cis-3-hexen-1-ol." *Atmospheric Environment* **162**: 141-151.
20. Bateman, A. P., et al. (2008). "The effect of solvent on the analysis of secondary organic aerosol using electrospray ionization mass spectrometry." *Environmental Science & Technology* **42**(19): 7341-7346.

21. Bates, K. H. and D. J. Jacob (2019). "A new model mechanism for atmospheric oxidation of isoprene: global effects on oxidants, nitrogen oxides, organic products, and secondary organic aerosol." *Atmospheric Chemistry and Physics* **19**(14): 9613-9640.
22. Bayer-Oglesby, L., et al. (2005). "Decline of ambient air pollution levels and improved respiratory health in Swiss children." *Environmental Health Perspectives* **113**(11): 1632-1637.
23. Beckett, K. P. et al. (2000). "Effective tree species for local air quality management." *Journal of Arboriculture* **26**(1): 12-19.
24. Bedini, E., et al. (2016). "Chemical Derivatization of Sulfated Glycosaminoglycans." *European Journal of Organic Chemistry* **2016**(18): 3018-3042.
25. Beelen, R., et al. (2008). "Long-term effects of traffic-related air pollution on mortality in a Dutch cohort (NLCS-AIR study)." *Environmental Health Perspectives* **116**(2): 196-202.
26. Bell, R. W., et al. (1991). THE 1990 TORONTO PERSONAL EXPOSURE PILOT (PEP) STUDY. 1991 Technology Transfer Conf : Environmental Research, Toronto, Canada.
27. Bell, J. N. B., and Treshow, M., (2004). "Zanieczyszczenie powietrza a zdrowie roślin." *Wydawnictwa Naukowo-Techniczne*, Warszawa.
28. Berndt, T. and O. Boge (2007). "Atmospheric reaction of OH radicals with 1,3-butadiene and 4-hydroxy-2-butenal." *Journal of Physical Chemistry A* **111**(48): 12099-12105.
29. Birch, M. E. and R. A. Cary (1996). "Elemental carbon-based method for monitoring occupational exposures to particulate diesel exhaust." *Aerosol Science and Technology* **25**(3): 221-241.
30. Black, F., et al. (1998). "Preparation of automobile organic emission surrogates for photochemical model validation." *Atmospheric Environment* **32**(14-15): 2443-2451.
31. Blair, S. L., et al. (2017). "Molecular Characterization of Organosulfur Compounds in Biodiesel and Diesel Fuel Secondary Organic Aerosol." *Environmental Science & Technology* **51**(1): 119-127.
32. Blaszczyk, E., et al. (2017). "Polycyclic aromatic hydrocarbons bound to outdoor and indoor airborne particles (PM<sub>2.5</sub>) and their mutagenicity and carcinogenicity in Silesian kindergartens, Poland." *Air Quality Atmosphere and Health* **10**(3): 389-400.
33. Bond, T. C., et al. (2013). "Bounding the role of black carbon in the climate system: A scientific assessment." *Journal of Geophysical Research-Atmospheres* **118**(11): 5380-5552.
34. Bond, T. C., et al. (2004). "A technology-based global inventory of black and organic carbon emissions from combustion." *Journal of Geophysical Research-Atmospheres* **109**(D14).
35. Bootdee, S., et al. (2016). "Determination of PM<sub>2.5</sub> and polycyclic aromatic hydrocarbons from incense burning emission at shrine for health risk assessment." *Atmospheric Pollution Research* **7**(4): 680-689.
36. Borbon, A., et al. (2003). "Developing receptor-oriented methods for non-methane hydrocarbon characterisation in urban air –part I: source identification." *Atmospheric Environment* **37**(29): 4051-4064.
37. Borrego, C. and Miranda, A. I. (2007). "Air Pollution Modeling and Its Application". *XIX NATO Science for Peace and Security*, Series C: Environmental Security
38. Briggs, G. A. D. (1990). "ULTRASOUND - ITS CHEMICAL, PHYSICAL AND BIOLOGICAL EFFECTS - SUSLIK,KS." *Interdisciplinary Science Reviews* **15**(2): 190-191.
39. Bruggemann, M., et al. (2017). "Real-time detection of highly oxidized organosulfates and BSOA marker compounds during the F-BEACH 2014 field study." *Atmospheric Chemistry and Physics* **17**(2): 1453-1469.
40. Bruggemann, M., et al. (2019). "Quantification of known and unknown terpenoid organosulfates in PM<sub>10</sub> using untargeted LC-HRMS/MS: contrasting summertime rural Germany and the North China Plain." *Environmental Chemistry* **16**(5): 333-346.
41. Bruggemann, M., et al. (2020). "Organosulfates in Ambient Aerosol: State of Knowledge and Future Research Directions on Formation, Abundance, Fate, and Importance." *Environmental Science & Technology* **54**(7): 3767-3782.
42. Bryant, D. J., et al. (2020). "Strong anthropogenic control of secondary organic aerosol formation from isoprene in Beijing". *Atmospheric Chemistry and Physics* **20**: 7531-7552.

43. Bryant, D. J., et al. (2021). "Importance of Oxidants and Temperature in the Formation of Biogenic Organosulfates and Nitrooxy Organosulfates." *Acs Earth and Space Chemistry* **5**(9): 2291-2306.
44. Budisulistiorini, S. H., et al. (2015). "Examining the effects of anthropogenic emissions on isoprene-derived secondary organic aerosol formation during the 2013 Southern Oxidant and Aerosol Study (SOAS) at the Look Rock, Tennessee ground site." *Atmospheric Chemistry and Physics* **15**(15): 8871-8888.
45. Burkhardt, J. (2010). "Hygroscopic particles on leaves: nutrients or desiccants?" *Ecological Monographs* **80**(3): 369-399.
46. Calogirou, A., et al. (1999). "Gas-phase terpene oxidation products: a review." *Atmospheric Environment* **33**(9): 1423-1439.
47. Canonaco, F., et al. (2013). "SoFi, an IGOR-based interface for the efficient use of the generalized multilinear engine (ME-2) for the source apportionment: ME-2 application to aerosol mass spectrometer data." *Atmospheric Measurement Techniques* **6**(12): 3649-3661.
48. Carlton, A. G., et al. (2006). "Link between isoprene and secondary organic aerosol (SOA): Pyruvic acid oxidation yields low volatility organic acids in clouds." *Geophysical Research Letters* **33**(6).
49. Carlton, A. G., et al. (2009). "A review of Secondary Organic Aerosol (SOA) formation from isoprene." *Atmospheric Chemistry and Physics* **9**(14): 4987-5005.
50. Chan, M. N., et al. (2011). "Influence of aerosol acidity on the chemical composition of secondary organic aerosol from beta-caryophyllene." *Atmospheric Chemistry and Physics* **11**(4): 1735-1751.
51. Chan, M. N., et al. (2010). "Characterization and Quantification of Isoprene-Derived Epoxydiols in Ambient Aerosol in the Southeastern United States." *Environmental Science & Technology* **44**(12): 4590-4596.
52. Chen, Q., et al. (2015). "Submicron particle mass concentrations and sources in the Amazonian wet season (AMAZE-08)." *Atmospheric Chemistry and Physics* **15**(7): 3687-3701.
53. Chen, Y. L., et al. (2020b). "Chemical characterization of secondary organic aerosol at a rural site in the southeastern US: insights from simultaneous high-resolution time-of-flight aerosol mass spectrometer (HR-ToF-AMS) and FIGAERO chemical ionization mass spectrometer (CIMS) measurements." *Atmospheric Chemistry and Physics* **20**(14): 8421-8440.
54. Chen, Y. Z., et al. (2021). "Seasonal Contribution of Isoprene-Derived Organosulfates to Total Water-Soluble Fine Particulate Organic Sulfur in the United States." *Acs Earth and Space Chemistry* **5**(9): 2419-2432.
55. Chen, Y. Z., et al. (2020a). "Heterogeneous Hydroxyl Radical Oxidation of Isoprene-Epoxydiol-Derived Methyltetrol Sulfates: Plausible Formation Mechanisms of Previously Unexplained Organosulfates in Ambient Fine Aerosols." *Environmental Science & Technology Letters* **7**(7): 460-468.
56. ChooChuay, C., et al. (2020a). "Long-range Transboundary Atmospheric Transport of Polycyclic Aromatic Hydrocarbons, Carbonaceous Compositions, and Water-soluble Ionic Species in Southern Thailand." *Aerosol and Air Quality Research* **20**(7): 1591-1606.
57. ChooChuay, C., et al. (2020b). "Impacts of PM<sub>2.5</sub> sources on variations in particulate chemical compounds in ambient air of Bangkok, Thailand." *Atmospheric Pollution Research* **11**(9): 1657-1667.
58. Claeys, M., et al. (2004a). "Formation of secondary organic aerosols through photooxidation of isoprene." *Science* **303**(5661): 1173-1176.
59. Claeys, M. and W. Maenhaut (2021). "Secondary Organic Aerosol Formation from Isoprene: Selected Research, Historic Account and State of the Art." *Atmosphere* **12**(6).
60. Claeys, M., et al. (2004b). "Formation of secondary organic aerosols from isoprene and its gas-phase oxidation products through reaction with hydrogen peroxide." *Atmospheric Environment* **38**(25): 4093-4098.
61. Clements, N., et al. (2016). "Comparisons of urban and rural PM<sub>10-2.5</sub> and PM<sub>2.5</sub> mass concentrations and semi-volatile fractions in northeastern Colorado." *Atmospheric Chemistry and Physics* **16**(11): 7469-7484.

62. Cohen, A. J., et al. (2005). "The global burden of disease due to outdoor air pollution." Journal of Toxicology and Environmental Health-Part a-Current Issues **68**(13-14): 1301-1307.
63. Cohen, A. J., et al. (2017). "Estimates and 25-year trends of the global burden of disease attributable to ambient air pollution: an analysis of data from the Global Burden of Diseases Study 2015." Lancet **389**(10082):1907-1918.
64. Colbeck, I. and M. Lazaridis (2010). "Aerosols and environmental pollution." Naturwissenschaften **97**(2): 117-131.
65. Cubison, M. J., et al. (2011). "Effects of aging on organic aerosol from open biomass burning smoke in aircraft and laboratory studies." Atmospheric Chemistry and Physics **11**(23): 12049-12064.
66. Cui, T. Q., et al. (2018). "Development of a hydrophilic interaction liquid chromatography (HILIC) method for the chemical characterization of water-soluble isoprene epoxydiol (IEPOX)-derived secondary organic aerosol." Environmental Science-Processes & Impacts **20**(11): 1524-1536.
67. Curren, K. C., et al. (2006). "Ambient air 1,3-butadiene concentrations in Canada (1995-2003): seasonal, day of week variations, trends, and source influences." Atmospheric Environment **40**(1): 170-181.
68. Czoschke, N. M., et al. (2003). "Effect of acidic seed on biogenic secondary organic aerosol growth." Atmospheric Environment **37**(30): 4287-4299.
69. D'Ambro, E. L., et al. (2017). "Isomerization of Second-Generation Isoprene Peroxy Radicals: Epoxide Formation and Implications for Secondary Organic Aerosol Yields." Environmental Science & Technology **51**(9): 4978-4987.
70. D'Ambro, E. L., et al. (2019). "Chamber-based insights into the factors controlling epoxydiol (IEPOX) secondary organic aerosol (SOA) yield, composition, and volatility." Atmospheric Chemistry and Physics **19**(17): 11253-11265.
71. Dangler, M., et al. (1987). "A DIRECT FTIR METHOD FOR IDENTIFYING FUNCTIONAL-GROUPS, IN SIZE SEGREGATED ATMOSPHERIC AEROSOLS." Atmospheric Environment **21**(4): 1001-1004.
72. Darer, A. I., et al. (2011). "Formation and Stability of Atmospherically Relevant Isoprene-Derived Organosulfates and Organonitrates." Environmental Science & Technology **45**(5): 1895-1902.
73. David, E. and V. C. Niculescu (2021). "Volatile Organic Compounds (VOCs) as Environmental Pollutants: Occurrence and Mitigation Using Nanomaterials." International Journal of Environmental Research and Public Health **18**(24).
74. De Gouw, J. and J. L. Jimenez (2009). "Organic Aerosols in the Earth's Atmosphere." Environmental Science & Technology **43**(20): 7614-7618.
75. De Gouw, J. A., et al. (2005). "Budget of organic carbon in a polluted atmosphere: Results from the New England Air Quality Study in 2002." Journal of Geophysical Research-Atmospheres **110**(D16).
76. De Hoffmann, E., and Stroobant, V., (2007). "Mass spectrometry: Principles and Applications." John Wiley & Sons, New York.
77. DeCarlo, P. F., et al. (2010). "Investigation of the sources and processing of organic aerosol over the Central Mexican Plateau from aircraft measurements during MILAGRO." Atmospheric Chemistry and Physics **10**(12): 5257-5280.
78. Dechapanya, W., et al. (2004). "Estimates of anthropogenic secondary organic aerosol formation in Houston, Texas." Aerosol Science and Technology **38**: 156-166.
79. Derwent, R. G., et al. (1995). "Analysis and interpretation of air quality data from an urban roadside location in central London over the period from July 1991 to July 1992." Atmospheric Environment **29**(8): 923-946.
80. Diskin, A. M., et al. (2003). "Time variation of ammonia, acetone, isoprene and ethanol in breath: a quantitative SIFT-MS study over 30 days." Physiological Measurement **24**: 107-119.
81. Docherty, K. S., et al. (2008). "Apportionment of Primary and Secondary Organic Aerosols in Southern California during the 2005 Study of Organic Aerosols in Riverside (SOAR-1)." Environmental Science & Technology **42**(20): 7655-7662.

82. Dollard, G. J., et al. (2001). "Ambient concentrations of 1,3-butadiene in the UK." Chemico-Biological Interactions **135**: 177-206.
83. Dollard, G. J., et al. (2007). "Observed trends in ambient concentrations of C-2-C-8 hydrocarbons in the United Kingdom over the period from 1993 to 2004." Atmospheric Environment **41**(12): 2559-2569.
84. Dommen, J., et al. (2006). "Laboratory observation of oligomers in the aerosol from isoprene/NO<sub>x</sub> photooxidation." Geophysical Research Letters **33**(13).
85. Downs, S. H., et al. (2007). "Reduced exposure to PM<sub>10</sub> and attenuated age-related decline in lung function." New England Journal of Medicine **357**(23): 2338-2347.
86. Doyle, M., et al. (2004). "Effects of 1,3-butadiene, isoprene, and their photochemical degradation products on human lung cells." Environmental Health Perspectives **112**(15): 1488-1495.
87. Duporte, G., et al. (2020). "Experimental Study of the Formation of Organosulfates from alpha-Pinene Oxidation. 2. Time Evolution and Effect of Particle Acidity." Journal of Physical Chemistry A **124**(2): 409-421.
88. Eatough, D. J., et al. (1990). "THE CHEMICAL CHARACTERIZATION OF ENVIRONMENTAL TOBACCO-SMOKE." Environmental Technology **11**(11): 1071-1085.
89. Edney, E. O., et al. (2005). "Formation of 2-methyl tetrols and 2-methylglyceric acid in secondary organic aerosol from laboratory irradiated isoprene/NO<sub>x</sub>/SO<sub>2</sub>/air mixtures and their detection in ambient PM<sub>2.5</sub> samples collected in the eastern United States." Atmospheric Environment **39**(29): 5281-5289.
90. EEA report (2014). "Air quality in Europe". European Environmental Agency
91. EEA website (2023). "How air pollution affects our health", <https://www.eea.europa.eu/en/topics/in-depth/air-pollution/eow-it-affects-our-health>, June 2023
92. Ekberg, A., et al. (2009). "Isoprene emission from wetland sedges." Biogeosciences **6**: 601-613.
93. Ekstrom, S., et al. (2009). "The Cloud Condensation Nuclei (CCN) properties of 2-methyltetrols and C<sub>3</sub>-C<sub>6</sub> polyols from osmolality and surface tension measurements." Atmospheric Chemistry and Physics **9**(3): 973-980.
94. Falkovich, A. H., et al. (2005). "Low molecular weight organic acids in aerosol particles from Rondonia, Brazil, during the biomass-burning, transition and wet periods." Atmospheric Chemistry and Physics **5**: 781-797.
95. Fall, R., and Copley, D. (2000). "Bacterial sources and sinks of isoprene, a reactive atmospheric hydrocarbon." Environmental Microbiology **2**(2): 123-130.
96. Fang, Z., et al. (2021). "Secondary organic aerosols produced from photochemical oxidation of secondarily evaporated biomass burning organic gases: Chemical composition, toxicity, optical properties, and climate effect." Environment International **157**.
97. Fattorusso, C. et al. (2011). "Antimalarials based on the dioxane scaffold of plakortin. A concise synthesis and SAR studies." Bioorganic & Medicinal Chemistry **19**: 312-320.
98. Feltham, E. J., et al. (2000). "Reactions of alkenes with ozone in the gas phase: a matrix-isolation study of secondary ozonides and carbonyl-containing reaction products." Spectrochimica Acta Part A: Molecular and Biomolecular Spectroscopy **56** (13), 15: 2605-2616.
99. Feng, B. H., et al. (2019). "High level of source-specific particulate matter air pollution associated with cardiac arrhythmias." Science of the Total Environment **657**: 1285-1293.
100. Fenske, J. D., and Paulson, S. E. (1999). "Human breath emissions of VOCs." Journal of the Air & Waste Management Association **49**(5): 594-598.
101. Finessi, E., et al. (2012). "Determination of the biogenic secondary organic aerosol fraction in the boreal forest by NMR spectroscopy." Atmospheric Chemistry and Physics **12**(2): 941-959.
102. Finlayson-Pitts B. J. and Pitts J. N. Jr. (2000). "Chemistry of the Upper and Lower Atmosphere, Theory, Experiments, and Applications", Elsevier
103. Flanner, M. G., et al. (2007). "Present-day climate forcing and response from black carbon in snow." Journal of Geophysical Research-Atmospheres **112**(D11).

104. Fleming, L. T., et al. (2019). "Formation of Light-Absorbing Organosulfates during Evaporation of Secondary Organic Material Extracts in the Presence of Sulfuric Acid." *ACS Earth and Space Chemistry* **3**(6): 947-957.
105. Froyd, K. D., et al. (2010). "Contribution of isoprene-derived organosulfates to free tropospheric aerosol mass." *Proceedings of the National Academy of Sciences of the United States of America* **107**(50): 21360-21365.
106. Fu, P. Q., et al. (2008b). "Organic molecular compositions and temporal variations of summertime mountain aerosols over Mt. Tai, North China Plain." *Journal of Geophysical Research-Atmospheres* **113**(D19).
107. Fu, T. M., et al. (2008a). "Global budgets of atmospheric glyoxal and methylglyoxal, and implications for formation of secondary organic aerosols." *Journal of Geophysical Research-Atmospheres* **113**(D15).
108. Gaffney, J. S., et al. (2015). "Characterization of Fine Mode Atmospheric Aerosols by Raman Microscopy and Diffuse Reflectance FTIR." *Journal of Physical Chemistry A* **119**(19): 4524-4532.
109. Gallimore, P. J., et al. (2017). "Online molecular characterisation of organic aerosols in an atmospheric chamber using extractive electrospray ionisation mass spectrometry." *Atmospheric Chemistry and Physics* **17**(23): 14485-14500.
110. Gao, S., et al. (2006). "Characterization of polar organic components in fine aerosols in the southeastern United States: Identity, origin, and evolution." *Journal of Geophysical Research-Atmospheres* **111**(D14).
111. Gao, X. M., et al. (2020). "Measurements of Indoor and Outdoor Fine Particulate Matter during the Heating Period in Jinan, in North China: Chemical Composition, Health Risk, and Source Apportionment." *Atmosphere* **11**(9).
112. Gaeggeler, K., et al. (2008). "Residential wood burning in an Alpine valley as a source for oxygenated volatile organic compounds, hydrocarbons and organic acids." *Atmospheric Environment* **42**(35): 8278-8287.
113. Gaston, C. J., et al. (2014a). "Reactive Uptake of an Isoprene-Derived Epoxydiol to Submicron Aerosol Particles." *Environmental Science & Technology* **48**(19): 11178-11186.
114. Gaston, C. J., et al. (2014b). "Reactive uptake of N<sub>2</sub>O<sub>5</sub> to internally mixed inorganic and organic particles: the role of organic carbon oxidation state and inferred organic phase separations." *Atmospheric Chemistry and Physics* **14**(11): 5693-5707.
115. Gatari, M. J. and J. Boman (2003). "Black carbon and total carbon measurements at urban and rural sites in Kenya, East Africa." *Atmospheric Environment* **37**(8): 1149-1154.
116. Gentner, D. R., et al. (2012). "Elucidating secondary organic aerosol from diesel and gasoline vehicles through detailed characterization of organic carbon emissions." *Proceedings of the National Academy of Sciences of the United States of America* **109**(45): 18318-18323.
117. Giere, R. and X. Querol (2010). "Solid Particulate Matter in the Atmosphere." *Elements* **6**(4): 215-222.
118. Giglio, L., et al. (2013). "Analysis of daily, monthly, and annual burned area using the fourth-generation global fire emissions database (GFED4)." *Journal of Geophysical Research-Biogeosciences* **118**(1): 317-328.
119. Glasius, M., et al. (2018). "Organosulfates in aerosols downwind of an urban region in central Amazon." *Environmental Science-Processes & Impacts* **20**(11): 1546-1558.
120. Glasius, M. and A. H. Goldstein (2016). "Recent Discoveries and Future Challenges in Atmospheric Organic Chemistry." *Environmental Science & Technology* **50**(6): 2754-2764.
121. Golden, R. and S. Holm (2017). "Indoor Air Quality and Asthma: Has Unrecognized Exposure to Acrolein Confounded Results of Previous Studies?" *Dose-Response* **15**(1).
122. Goldstein, A. H. and I. E. Galbally (2009). "Known and unexplored organic constituents in the Earth's atmosphere." *Geochimica Et Cosmochimica Acta* **73**(13): A449-A449.
123. Gomez-Gonzalez, Y., et al. (2008). "Characterization of organosulfates from the photooxidation of isoprene and unsaturated fatty acids in ambient aerosol using liquid chromatography/(-) electrospray ionization mass spectrometry." *Journal of Mass Spectrometry* **43**(3): 371-382.

124. Graham, B., et al. (2002). "Water-soluble organic compounds in biomass burning aerosols over Amazonia - 1. Characterization by NMR and GC-MS." Journal of Geophysical Research-Atmospheres **107**(D20).
125. Grieshop, A. P., et al. (2009a). "Laboratory investigation of photochemical oxidation of organic aerosol from wood fires 2: analysis of aerosol mass spectrometer data." Atmospheric Chemistry and Physics **9**(6): 2227-2240.
126. Grieshop, A. P., et al. (2009b). "Laboratory investigation of photochemical oxidation of organic aerosol from wood fires 1: measurement and simulation of organic aerosol evolution." Atmospheric Chemistry and Physics **9**(4): 1263-1277.
127. Griffin, R. J., et al. (2005). "Development and initial evaluation of a dynamic species-resolved model for gas phase chemistry and size-resolved gas/particle partitioning associated with secondary organic aerosol formation." Journal of Geophysical Research-Atmospheres **110**(D5).
128. Grosjean, D., et al. (1994). "ATMOSPHERIC CHEMISTRY OF OLEFINS - A PRODUCT STUDY OF THE OZONE ALKENE REACTION WITH CYCLOHEXANE ADDED TO SCAVENGE OH." Environmental Science & Technology **28**(1): 186-196.
129. Guenther, A., et al. (1995). "A GLOBAL-MODEL OF NATURAL VOLATILE ORGANIC-COMPOUND EMISSIONS." Journal of Geophysical Research-Atmospheres **100**(D5): 8873-8892.
130. Guenther, A. B., et al. (2012). "The Model of Emissions of Gases and Aerosols from Nature version 2.1 (MEGAN2.1): an extended and updated framework for modeling biogenic emissions." Geoscientific Model Development **5**(6): 1471-1492.
131. Haapanala, S., et al. (2006). "Measurements of hydrocarbon emissions from a boreal fen using the REA technique." Biogeosciences **3**: 103-112.
132. Hallquist, M., et al. (2009). "The formation, properties and impact of secondary organic aerosol: current and emerging issues." Atmospheric Chemistry and Physics **9**(14): 5155-5236.
133. Hansel, A., et al. (1999). "Proton-transfer-reaction mass spectrometry (PTR-MS): on-line monitoring of volatile organic compounds at volume mixing ratios of a few pptv." Plasma Sources Science & Technology **8**(2): 332-336.
134. Hansen, A. M. K., et al. (2015). "Hygroscopic properties and cloud condensation nuclei activation of limonene-derived organosulfates and their mixtures with ammonium sulfate." Atmospheric Chemistry and Physics **15**(24): 14071-14089.
135. Hatch, L. E., et al. (2011). "Measurements of Isoprene-Derived Organosulfates in Ambient Aerosols by Aerosol Time-of-Flight Mass Spectrometry - Part 1: Single Particle Atmospheric Observations in Atlanta." Environmental Science & Technology **45**(12): 5105-5111.
136. Hatch, L. E., et al. (2011). "Measurements of Isoprene-Derived Organosulfates in Ambient Aerosols by Aerosol Time-of-Flight Mass Spectrometry-Part 2: Temporal Variability and Formation Mechanisms." Environmental Science & Technology **45**(20): 8648-8655.
137. Heal, M. R., et al. (2012). "Particles, air quality, policy and health." Chemical Society Reviews **41**(19): 6606-6630.
138. Heal, M. R., et al. (2012). "Particles, air quality, policy and health." Chemical Society Reviews **41**(19): 6606-6630.
139. Hearn, J. D. and G. D. Smith (2004). "A chemical ionization mass spectrometry method for the online analysis of organic aerosols." Analytical Chemistry **76**(10): 2820-2826.
140. HEI report (2007). "Mobile-Source Air Toxics: A Critical Review of the Literature on Exposure and Health Effects." Special Report 16, Health Effects Institute, Boston, MA.
141. Hellen, H., et al. (2006). "C2-C10 hydrocarbon emissions from a boreal wetland and forest floor." Biogeosciences **3**: 167-174.
142. Hennigan, C. J., et al. (2011). "Chemical and physical transformations of organic aerosol from the photo-oxidation of open biomass burning emissions in an environmental chamber." Atmospheric Chemistry and Physics **11**(15): 7669-7686.
143. Hettiyadura, A. P. S., et al. (2019). "Organosulfates in Atlanta, Georgia: anthropogenic influences on biogenic secondary organic aerosol formation." Atmospheric Chemistry and Physics **19**(5): 3191-3206.
144. Hettiyadura, A. P. S., et al. (2017). "Qualitative and quantitative analysis of atmospheric organosulfates in Centreville, Alabama." Atmospheric Chemistry and Physics **17**(2): 1343-1359.



145. Hettiyadura, A. P. S., et al. (2015). "Determination of atmospheric organosulfates using HILIC chromatography with MS detection." Atmospheric Measurement Techniques **8**(6): 2347-2358.
146. Hinds, W. C. (1998). "Aerosol technology. Properties, behaviour, and measurement of airborne particles." Second Edition. John Wiley & Sons, Inc., New York.
147. Ho, K. F., et al. (2002). "Carbonaceous characteristics of atmospheric particulate matter in Hong Kong." Science of the Total Environment **300**(1-3): 59-67.
148. Holloway, A. M., and Wayne, R. P. (2015). "Atmospheric Chemistry." Royal Society of Chemistry
149. Hu, D., et al. (2008). "Contributions of isoprene, monoterpenes, beta-caryophyllene, and toluene to secondary organic aerosols in Hong Kong during the summer of 2006." Journal of Geophysical Research-Atmospheres **113**.
150. Hu, D. and J. Z. Yu (2013). "Secondary organic aerosol tracers and malic acid in Hong Kong: seasonal trends and origins." Environmental Chemistry **10**(5): 381-394.
151. Hu, K. S., et al. (2011). "Thermodynamics and kinetics of the hydrolysis of atmospherically relevant organonitrates and organosulfates." Atmospheric Chemistry and Physics **11**(16): 8307-8320.
152. Huang, L. B., et al. (2020). "Radical-Initiated Formation of Aromatic Organosulfates and Sulfonates in the Aqueous Phase." Environmental Science & Technology **54**(19): 11857-11864.
153. Hughes, K. & International Programme on Chemical Safety (IPCS) (2001). "1,3-Butadiene : human health aspects." World Health Organization.
154. Huneus, N., et al. (2011). "Global dust model intercomparison in AeroCom phase I." Atmospheric Chemistry and Physics **11**(15): 7781-7816.
155. Hurst, H. E. (2007). Toxicology of 1,3-butadiene, chloroprene, and isoprene. Reviews of Environmental Contamination and Toxicology, Vol 189. G. W. Ware. New York, Springer. **189**: 131-179.
156. Hussein, T., et al. (2018). "Accumulation and coarse mode aerosol concentrations and carbonaceous contents in the urban background atmosphere in Amman, Jordan." Arabian Journal of Geosciences **11**(20).
157. IARC monographs (2012). "Chemical Agents and Related Occupations". Volume 100F, page 333, International Agency for Research on Cancer.
158. Iinuma, Y., et al. (2009). "Laboratory chamber studies on the formation of organosulfates from reactive uptake of monoterpene oxides." Physical Chemistry Chemical Physics **11**(36): 7985-7997.
159. Iinuma, Y., et al. (2007a). "Evidence for the existence of organosulfates from beta-pinene ozonolysis in ambient secondary organic aerosol." Environmental Science & Technology **41**(19): 6678-6683.
160. Iinuma, Y., et al. (2007b). "The formation of organic sulfate esters in the limonene ozonolysis secondary organic aerosol (SOA) under acidic conditions." Atmospheric Environment **41**(27): 5571-5583.
161. Ion, A. C., et al. (2005). "Polar organic compounds in rural PM<sub>2.5</sub> aerosols from K-puszt, Hungary, during a 2003 summer field campaign: Sources and diel variations." Atmospheric Chemistry and Physics **5**: 1805-1814.
162. IPCC (2001). "Climate Change 2001. The Scientific Basis" (eds J.T. Houghton, Y. Ding, D.J. Griggs, M. Noguer, P.J. van der Linden, X. Dai, K. Maskell, and C.A. Johnson). Intergovernmental Panel on Climate Change, Cambridge University Press, Cambridge and New York, p. 881.
163. Islam, M. R., et al. (2020). "Ambient air quality in the Kathmandu Valley, Nepal, during the pre-monsoon: concentrations and sources of particulate matter and trace gases." Atmospheric Chemistry and Physics **20**(5): 2927-2951.
164. Jacobson, M. C., et al. (2000). "Organic atmospheric aerosols: Review and state of the science." Reviews of Geophysics **38**(2): 267-294.
165. Jacobson, M. Z., (2002). "Atmospheric pollution: History, science, and regulation." Cambridge University Press, Cambridge.

166. Jaenicke, R. (1988). "Aerosol physics and chemistry, in Landolt-Börnstein Numerical Data and Functional Relationship in Science and Technology." New Series Group V, Geophysics and Space Research, Meteorology, vol. 4 (ed. G. Fischer), Springer-Verlag, Heidelberg, pp. 391-457.
167. Jaenicke, R. (2005). "Abundance of cellular material and proteins in the atmosphere." Science **308**(5718): 73-73.
168. Jang, M. S., et al. (2002). "Heterogeneous atmospheric aerosol production by acid-catalyzed particle-phase reactions." Science **298**(5594): 814-817.
169. Jaoui, M., et al. (2010). "Formation of organic tracers for isoprene SOA under acidic conditions." Atmospheric Environment **44**(14): 1798-1805.
170. Jaoui, M., et al. (2004). "Identification and quantification of aerosol polar oxygenated
171. Jaoui, M., et al. (2014). "Atmospheric oxidation of 1,3-butadiene: characterization of gas and aerosol reaction products and implications for PM2.5." Atmospheric Chemistry and Physics **14**(24): 13681-13704.
172. Jaoui, M., et al. (2018). "Characterization of aerosol nitroaromatic compounds: Validation of an experimental method." Journal of Mass Spectrometry **53**(8): 680-692.
173. Jaoui, M., et al. (2019). "Organic Hydroxy Acids as Highly Oxygenated Molecular (HOM) Tracers for Aged Isoprene Aerosol." Environmental Science & Technology **53**(24): 14516-14527.
174. Jenkin, M. E., et al. (1998). "Peroxy radical kinetics resulting from the OH-Initiated oxidation of 1,3-butadiene, 2,3-dimethyl-1,3-butadiene and isoprene." Journal of Atmospheric Chemistry **29**(3): 267-298.
175. Jimenez, J. L., et al. (2009). "Evolution of Organic Aerosols in the Atmosphere." Science **326**(5959): 1525-1529.
176. Johnson, D., et al. (2004). "Simulating the Formation of Secondary Organic Aerosol from the Photooxidation of Toluene." Environmental Chemistry **1**(3): 150-165.
177. Johnson, D., et al. (2005). "Simulating the formation of secondary organic aerosol from the photooxidation of aromatic hydrocarbons." Environmental Chemistry **2**(1): 35-48.
178. Johnston, M. V. and D. E. Kerecman (2019). Molecular Characterization of Atmospheric Organic Aerosol by Mass Spectrometry. Annual Review of Analytical Chemistry, Vol 12. P. W. Bohn and J. E. Pemberton. **12**: 247-274.
179. Johnstone R. A. W., and Rose, M. E. (2001). "Spektrometria mas. Podręcznik dla chemików i biochemików." Wydawnictwo Naukowe PWN, Warszawa.
180. JRC report (2009). "Measurement of Elemental and Organic Carbon in Europe. Report of the preparatory workshop for a future standard measurement method." JRC Scientific and Technical Reports, European Commission Joint Research Centre
181. Juda-Rezler, K. and Toczko, B. (2016). "Pyły drobne w atmosferze. Kompendium wiedzy o zanieczyszczeniu powietrza pyłem zawieszonym w Polsce." Główny Inspektorat Ochrony Środowiska
182. Kanakidou, M., et al. (2005). "Organic aerosol and global climate modelling: a review." Atmospheric Chemistry and Physics **5**: 1053-1123.
183. Kanellopoulos, P. G., et al. (2022). "PM2.5-bound organosulfates in two Eastern Mediterranean cities: The dominance of isoprene organosulfates." Chemosphere **297**.
184. Kawamura, K. and R. B. Gagosian (1990). "MIDCHAIN KETOCARBOXYLIC ACIDS IN THE REMOTE MARINE ATMOSPHERE - DISTRIBUTION PATTERNS AND POSSIBLE FORMATION MECHANISMS." Journal of Atmospheric Chemistry **11**(1-2): 107-122.
185. Kawamura, K. and K. Ikushima (1993). "SEASONAL-CHANGES IN THE DISTRIBUTION OF DICARBOXYLIC-ACIDS IN THE URBAN ATMOSPHERE." Environmental Science & Technology **27**(10): 2227-2235.
186. Kawamura, K., and Yasui, O. (2005). "Diurnal changes in the distribution of dicarboxylic acids, ketocarboxylic acids and dicarbonyl in the urban Tokyo atmosphere." Atmos. Environ. **39**: 1945.
187. Kesselmeier, J., and Staudt, M. (1999). "Biogenic Volatile Organic Compounds (VOC): An Overview on Emission, Physiology and Ecology." Journal of Atmospheric Chemistry **33**: 23-88.

188. Khan, F. (2021). "Chemical profiling and toxicological assessment of atmospheric aerosol using human lung cells." Ph.D. thesis, Institute of Physical Chemistry PAS, Warszawa.
189. Khare, P. and D. R. Gentner (2018). "Considering the future of anthropogenic gas-phase organic compound emissions and the increasing influence of non-combustion sources on urban air quality." Atmospheric Chemistry and Physics **18**(8): 5391-5413.
190. Kilanowicz, A. et al. (2018). "Buta-1,3-diene: Documentation of proposed values of occupational exposure limits (OELs)." Podstawy i Metody Oceny Środowiska Pracy **4**(98): 43–85.
191. Kim, K. H., et al. (2015). "A review on the human health impact of airborne particulate matter." Environment International **74**: 136-143.
192. Kleindienst, T. E., et al. (2006). "Secondary organic carbon and aerosol yields from the irradiations of isoprene and alpha-pinene in the presence of NO<sub>x</sub> and SO<sub>2</sub>." Environmental Science & Technology **40**(12): 3807-3812.
193. Kleindienst, T. E., et al. (2007). "Estimates of the contributions of biogenic and anthropogenic hydrocarbons to secondary organic aerosol at a southeastern US location." Atmospheric Environment **41**(37): 8288-8300.
194. Klejnowski, K., et al. (2017). "Characterization and Seasonal Variations of Organic and Elemental Carbon and Levoglucosan in PM<sub>10</sub> in Krynica Zdroj, Poland." Atmosphere **8**(10).
195. Kolodziejczyk, A. (2020). "Badania fizykochemiczne produktów utleniania  $\alpha$ -pinenu w aspekcie powstawania wtórnego aerozolu atmosferycznego." Ph.D. thesis, Institute of Physical Chemistry PAS, Warszawa.
196. Kourtchev, I., et al. (2005). "Observation of 2-methyltetrols and related photo-oxidation products of isoprene in boreal forest aerosols from Hyytiälä, Finland." Atmospheric Chemistry and Physics **5**: 2761-2770.
197. Kourtchev, I., et al. (2009). "Characterization of Atmospheric Aerosols at a Forested Site in Central Europe." Environmental Science & Technology **43**(13): 4665-4671.
198. Kourtchev, I., et al. (2008). "Polar organic marker compounds in PM<sub>2.5</sub> aerosol from a mixed forest site in western Germany." Chemosphere **73**(8): 1308-1314.
199. Kozakiewicz, J. (2021). "Monitoring prekursorów ozonu w stacji tła krajowego „Bory Tucholskie” – raport za rok 2020." GLÓWNY INSPEKTORAT OCHRONY ŚRODOWISKA
200. Kramp, F. and S. E. Paulson (2000). "The gas phase reaction of ozone with 1,3-butadiene: formation yields of some toxic products." Atmospheric Environment **34**(1): 35-43.
201. Krechmer, J. E., et al. (2015). "Formation of Low Volatility Organic Compounds and Secondary Organic Aerosol from Isoprene Hydroxyhydroperoxide Low-NO Oxidation." Environmental Science & Technology **49**(17): 10330-10339.
202. Krewski, D., et al. (2009). "Extended follow-up and spatial analysis of the American Cancer Society linking particulate air pollution and mortality." Boston, MA, Health Effects Institute (HEI Research Report 140).
203. Kristensen, K., et al. (2016). "Denuder/filter sampling of organic acids and organosulfates at urban and boreal forest sites: Gas/particle distribution and possible sampling artifacts." Atmospheric Environment **130**: 36-53.
204. Kristensen, K. and M. Glasius (2011). "Organosulfates and oxidation products from biogenic hydrocarbons in fine aerosols from a forest in North West Europe during spring." Atmospheric Environment **45**(27): 4546-4556.
205. Kristensen, K., et al. (2020). "The Aarhus Chamber Campaign on Highly Oxygenated Organic Molecules and Aerosols (ACCHA): particle formation, organic acids, and dimer esters from alpha-pinene ozonolysis at different temperatures." Atmospheric Chemistry and Physics **20**(21): 12549-12567.
206. Kristensson, A., et al. (2020). "Source Contributions to Rural Carbonaceous Winter Aerosol in North-Eastern Poland." Atmosphere **11**(3).
207. Kroll, J. H., et al. (2006). "Secondary organic aerosol formation from isoprene photooxidation." Environmental Science & Technology **40**(6): 1869-1877.
208. Kroll, J. H. and J. H. Seinfeld (2008). "Chemistry of secondary organic aerosol: Formation and evolution of low-volatility organics in the atmosphere." Atmospheric Environment **42**(16): 3593-3624.

209. Kulmala, M., et al. (2004). "A new feedback mechanism linking forests, aerosols, and climate." Atmospheric Chemistry and Physics **4**: 557-562.
210. Kundu, S., et al. (2010). "Molecular distributions of dicarboxylic acids, ketocarboxylic acids and alpha-dicarbonyls in biomass burning aerosols: implications for photochemical production and degradation in smoke layers." Atmospheric Chemistry and Physics **10**(5): 2209-2225.
211. Kuzma, J. et al. (1995). "Bacteria produce the volatile hydrocarbon isoprene." Current Microbiology **30**: 97-103.
212. Lanz, V. A., et al. (2007). "Source apportionment of submicron organic aerosols at an urban site by factor analytical modelling of aerosol mass spectra." Atmospheric Chemistry and Physics **7**(6): 1503-1522.
213. Lanz, V. A., et al. (2008). "Source attribution of submicron organic aerosols during wintertime inversions by advanced factor analysis of aerosol mass spectra." Environmental Science & Technology **42**(1): 214-220.
214. Laongsri, B. and R. M. Harrison (2013). "Atmospheric behaviour of particulate oxalate at UK urban background and rural sites." Atmospheric Environment **71**: 319-326.
215. Lau, Y. S., et al. (2021). "Chemical Composition of Gas and Particle Phase Products of Toluene Photooxidation Reaction under High OH Exposure Condition." Atmosphere **12**(7).
216. Leber, A. P. (2001). "Overview of isoprene monomer and polyisoprene production processes." Chemico-biological Interactions **135-136**: 169-173.
217. Letcher, T. M., (2015). "Climate Change - Observed Impacts on Planet Earth". ATMOSPHERIC AEROSOLS AND THEIR ROLE IN CLIMATE CHANGE, Chapter 27: 449-463.
218. Lewandowska, A. U., et al. (2018). "Benzo(a)pyrene parallel measurements in PM1 and PM2.5 in the coastal zone of the Gulf of Gdansk (Baltic Sea) in the heating and non-heating seasons." Environmental Science and Pollution Research **25**(20): 19458-19469.
219. Lewandowski, M., et al. (2008). "Primary and secondary contributions to ambient PM in the midwestern United States." Environmental Science & Technology **42**(9): 3303-3309.
220. Lewandowski, M., et al. (2015). "Atmospheric oxidation of isoprene and 1,3-butadiene: influence of aerosol acidity and relative humidity on secondary organic aerosol." Atmospheric Chemistry and Physics **15**(7): 3773-3783.
221. Li, A.J. et al. (2021). "A review of environmental occurrence, toxicity, biotransformation and biomonitoring of volatile organic compounds." Environmental Chemistry and Ecotoxicology **3**: 91-116.
222. Liao, H., et al. (2003). "Interactions between tropospheric chemistry and aerosols in a unified general circulation model." Journal of Geophysical Research-Atmospheres **108**(D1).
223. Liao, H., et al. (2004). "Global radiative forcing of coupled tropospheric ozone and aerosols in a unified general circulation model." Journal of Geophysical Research-Atmospheres **109**(D16).
224. Lim, C. Y., et al. (2019). "Secondary organic aerosol formation from the laboratory oxidation of biomass burning emissions." Atmospheric Chemistry and Physics **19**(19): 12797-12809.
225. Lin, Y. H., et al. (2014). "Light-Absorbing Oligomer Formation in Secondary Organic Aerosol from Reactive Uptake of Isoprene Epoxydiols." Environmental Science & Technology **48**(20): 12012-12021.
226. Lin, Y. H., et al. (2013). "Investigating the influences of SO<sub>2</sub> and NH<sub>3</sub> levels on isoprene-derived secondary organic aerosol formation using conditional sampling approaches." Atmospheric Chemistry and Physics **13**(16): 8457-8470.
227. Lin, Y. H., et al. (2012). "Isoprene Epoxydiols as Precursors to Secondary Organic Aerosol Formation: Acid-Catalyzed Reactive Uptake Studies with Authentic Compounds." Environmental Science & Technology **46**(1): 250-258.
228. Lindberg, S. E., et al. (1982). "ATMOSPHERIC DEPOSITION OF METALS TO FOREST VEGETATION." Science **215**(4540): 1609-1611.
229. Liousse, C., et al. (1996). "A global three-dimensional model study of carbonaceous aerosols." Journal of Geophysical Research-Atmospheres **101**(D14): 19411-19432.

230. Liu, H. J., et al. (2019). "Seasonal variation, formation mechanisms and potential sources of PM<sub>2.5</sub> in two typical cities in the Central Plains Urban Agglomeration, China." Science of the Total Environment **657**: 657-670.
231. Liu, J. M., et al. (2016). "Efficient Isoprene Secondary Organic Aerosol Formation from a Non-IEPDX Pathway." Environmental Science & Technology **50**(18): 9872-9880.
232. Liu, X. Y., et al. (1999). "Hydroxyl radical and ozone initiated photochemical reactions of 1,3-butadiene." Atmospheric Environment **33**(18): 3005-3022.
233. Loeffler, K. W., et al. (2006). "Oligomer formation in evaporating aqueous glyoxal and methyl glyoxal solutions." Environmental Science & Technology **40**(20): 6318-6323.
234. Logan, B. A., et al. (2000). "Biochemistry and physiology of foliar isoprene production." Trends in Plant Science **5**: 477-481
235. Loomis, D., et al. (2013). "The carcinogenicity of outdoor air pollution." Lancet Oncology **14**(13): 1262-1263.
236. Lukacs, H., et al. (2009). "Quantitative assessment of organosulfates in size-segregated rural fine aerosol." Atmospheric Chemistry and Physics **9**(1): 231-238.
237. Markert, B. (1995). "Sample preparation (cleaning, drying, homogenization) for trace element analysis in plant matrices." Science of the Total Environment **176**(1-3): 45-61.
238. Matsunaga, S., et al. (2002). "In situ measurement of isoprene in the marine air and surface seawater from the western North Pacific." Atmospheric Environment **36**: 6051-6057.
239. McDonald, A. G., et al. (2007). "Quantifying the effect of urban tree planting on concentrations and depositions of PM<sub>10</sub> in two UK conurbations." Atmospheric Environment **41**(38): 8455-8467.
240. McLaren, R., et al. (1996). "Analysis of motor vehicle sources and their contribution to ambient hydrocarbon distributions at urban sites in Toronto during the Southern Ontario oxidants study." Atmospheric Environment **30**(12): 2219-2232.
241. McNeill, V. F. (2017). Atmospheric Aerosols: Clouds, Chemistry, and Climate. Annual Review of Chemical and Biomolecular Engineering, Vol 8. J. M. Prausnitz. **8**: 427-444.
242. Mikuska, P., et al. (2017). "Seasonal variability of monosaccharide anhydrides, resin acids, methoxyphenols and saccharides in PM<sub>2.5</sub> in Brno, the Czech Republic." Atmospheric Pollution Research **8**(3): 576-586.
243. Miljevic, B., et al. (2014). "To Sonicate or Not to Sonicate PM Filters: Reactive Oxygen Species Generation Upon Ultrasonic Irradiation." Aerosol Science and Technology **48**(12): 1276-1284.
244. Mitchell, R., et al. (2010). "Rates of particulate pollution deposition onto leaf surfaces: Temporal and inter-species magnetic analyses." Environmental Pollution **158**(5): 1472-1478.
245. Montero-Montoya, R., et al. (2018). "Volatile Organic Compounds in Air: Sources, Distribution, Exposure and Associated Illnesses in Children." Annals of Global Health **84**(2): 225-238.
246. Mutzel, A., et al. (2015). "Highly Oxidized Multifunctional Organic Compounds Observed in Tropospheric Particles: A Field and Laboratory Study." Environmental Science & Technology **49**(13): 7754-7761.
247. Mutzel, A., et al. (2013). "An improved method for the quantification of SOA bound peroxides." Atmospheric Environment **67**: 365-369.
248. Namieśnik, J., Jamrogiewicz, Z., (1998). "Fizykochemiczne metody kontroli zanieczyszczeń środowiska." Wydawnictwo Naukowo-Techniczne, Warszawa
249. Nash, D. G., et al. (2006). "Aerosol mass spectrometry: An introductory review." International Journal of Mass Spectrometry **258**(1-3): 2-12.
250. Nazaroff, W. W. and C. J. Weschler (2004). "Cleaning products and air fresheners: exposure to primary and secondary air pollutants." Atmospheric Environment **38**(18): 2841-2865.
251. Nestorowicz, K., et al. (2018). "Chemical composition of isoprene SOA under acidic and non-acidic conditions: effect of relative humidity." Atmospheric Chemistry and Physics **18**(24): 18101-18121.
252. Nguyen, Q. T., et al. (2014). "Understanding the anthropogenic influence on formation of biogenic secondary organic aerosols in Denmark via analysis of organosulfates and related oxidation products." Atmospheric Chemistry and Physics **14**(17): 8961-8981.

253. Nguyen, T. B., et al. (2015). "Mechanism of the hydroxyl radical oxidation of methacryloyl peroxyxynitrate (MPAN) and its pathway toward secondary organic aerosol formation in the atmosphere." Physical Chemistry Chemical Physics **17**(27): 17914-17926.
254. Nguyen, T. B., et al. (2011). "Effect of humidity on the composition of isoprene photooxidation secondary organic aerosol." Atmospheric Chemistry and Physics **11**(14): 6931-6944.
255. Niessen, W. M. A., (2007). "Liquid Chromatography – Mass spectrometry." 3rd edition. Chromatographic science series, vol. 97
256. Notario, A., et al. (1997). "Kinetics of Cl atom reactions with butadienes including isoprene." Chemical Physics Letters **281**(4-6): 421-425.
257. Noziere, B., et al. (2009). "Products and Kinetics of the Liquid-Phase Reaction of Glyoxal Catalyzed by Ammonium Ions (NH<sub>4</sub><sup>+</sup>)." Journal of Physical Chemistry A **113**(1): 231-237.
258. Noziere, B., et al. (2010). "Radical-initiated formation of organosulfates and surfactants in atmospheric aerosols." Geophysical Research Letters **37**.
259. Noziere, B., et al. (2011). "Atmospheric chemistry in stereo: A new look at secondary organic aerosols from isoprene." Geophysical Research Letters **38**.
260. Noziere, B., et al. (2015). "The Molecular Identification of Organic Compounds in the Atmosphere: State of the Art and Challenges." Chemical Reviews **115**(10): 3919-3983.
261. Oliva, S. R. and H. Raitio (2003). "Review of cleaning techniques and their effects on the chemical composition of foliar samples." Boreal Environment Research **8**(3): 263-272.
262. Olson, C. N., et al. (2011). "Hydroxycarboxylic Acid-Derived Organosulfates: Synthesis, Stability, and Quantification in Ambient Aerosol." Environmental Science & Technology **45**(15): 6468-6474.
263. Pacifico, F., et al. (2009). "Isoprene emissions and climate." Atmospheric Environment **43**(39): 6121-6135.
264. Pankow, J. F. (1994). "AN ABSORPTION-MODEL OF GAS-PARTICLE PARTITIONING OF ORGANIC-COMPOUNDS IN THE ATMOSPHERE." Atmospheric Environment **28**(2): 185-188.
265. Pankow, J. F., et al. (2004). "Delivery levels and behavior of 1,3-butadiene, acrylonitrile, benzene, and other toxic volatile organic compounds in mainstream tobacco smoke from two brands of commercial cigarettes." Chemical Research in Toxicology **17**(6): 805-813.
266. Passananti, M., et al. (2016). "Organosulfate Formation through the Heterogeneous Reaction of Sulfur Dioxide with Unsaturated Fatty Acids and Long-Chain Alkenes." Angewandte Chemie-International Edition **55**(35): 10336-10339.
267. Pathak, R. K., et al. (2009). "Summertime PM<sub>2.5</sub> ionic species in four major cities of China: nitrate formation in an ammonia-deficient atmosphere." Atmospheric Chemistry and Physics **9**(5): 1711-1722.
268. Paulot, F., et al. (2009). "Unexpected Epoxide Formation in the Gas-Phase Photooxidation of Isoprene." Science **325**(5941): 730-733.
269. Pedersen, T. and K. Sehested (2001). "Rate constants and activation energies for ozonolysis of isoprene methacrolein and methyl-vinyl-ketone in aqueous solution: Significance to the in-cloud ozonation of isoprene." International Journal of Chemical Kinetics **33**(3): 182-190.
270. Pedersen, D. S., et al. (2009). "A Concise Route to Branched Erythrono-gamma-lactones. Synthesis of the Leaf-Closing Substance Potassium (+/-)-(2R,3R)-2,3,4-Trihydroxy-2-methylbutanoate." Journal of Organic Chemistry **74**(11): 4400-4403.
271. Peng, C., et al. (2021). "Interactions of organosulfates with water vapor under sub- and supersaturated conditions." Atmospheric Chemistry and Physics **21**(9): 7135-7148.
272. Penn, A. and C. A. Snyder (1996). "1,3 butadiene, a vapor phase component of environmental tobacco smoke, accelerates arteriosclerotic plaque development." Circulation **93**(3): 552-557.
273. Penuelas, J., and Staudt, M. (2010). "BVOCs and global change." Trends in Plant Science **15**(3): 133-144.
274. Perri, M. J., et al. (2010). "Organosulfates from glycolaldehyde in aqueous aerosols and clouds: Laboratory studies." Atmospheric Environment **44**(21-22): 2658-2664.

275. Płaziak, A. S. (1997). "Spektrometria masowa związków organicznych." Wydawnictwo Naukowe UAM, Poznań
276. Poschl, U. (2005). "Atmospheric Aerosols: Composition, Transformation, Climate and Health Effects." Angewandte Chemie **44**, issue 46: 7520-7540.
277. Poletini, A. (2006). "Applications of LC-MS in Toxicology." Pharmaceutical Press, Wielka Brytania
278. Pope, C. A., et al. (2002). "Lung cancer, cardiopulmonary mortality, and long-term exposure to fine particulate air pollution." Jama-Journal of the American Medical Association **287**(9): 1132-1141.
279. Pope, C. A., and Dockery, D.W. (2006) "Health Effects of Fine Particulate Air Pollution: Lines that Connect." Journal of the Air & Waste Management Association, **56**:6, 709-742
280. Poulain, L., et al. (2010). "Towards closing the gap between hygroscopic growth and CCN activation for secondary organic aerosols - Part 3: Influence of the chemical composition on the hygroscopic properties and volatile fractions of aerosols." Atmospheric Chemistry and Physics **10**(8): 3775-3785.
281. Pouli A.E., et al. (2003). "The cytotoxic effect of volatile organic compounds of the gas phase of cigarette smoke on lung epithelial cells." Free Radical Biology and Medicine **34**(3): 345-355.
282. Prather, K. A., et al. (2008). "Analysis of Atmospheric Aerosols." Annual Review of Analytical Chemistry **1**: 485-514.
283. Pratt, K. A. and K. A. Prather (2012a). "Mass spectrometry of atmospheric aerosols: Recent developments and applications. Part I: Off-line mass spectrometry techniques." Mass Spectrometry Reviews **31**(1): 1-16.
284. Pratt, K. A. and K. A. Prather (2012b). "Mass spectrometry of atmospheric aerosols: Recent developments and applications. Part II: On-line mass spectrometry techniques." Mass Spectrometry Reviews **31**(1): 17-48.
285. Prządka, Z. et al. (2012). "Uniformity of distribution of particulate matter on filters used in high volume samplers." Ochrona Środowiska i Zasobów Naturalnych, **54**, pp. 236–247.
286. Putaud, J. P., et al. (2004). "European aerosol phenomenology-2: chemical characteristics of particulate matter at kerbside, urban, rural and background sites in Europe." Atmospheric Environment **38**(16): 2579-2595.
287. Putaud, J. P., et al. (2010). "A European aerosol phenomenology-3: Physical and chemical characteristics of particulate matter from 60 rural, urban, and kerbside sites across Europe." Atmospheric Environment **44**(10): 1308-1320.
288. Puxbaum, H., et al. (2007). "Levoglucosan levels at background sites in Europe for assessing the impact of biomass combustion on the European aerosol background." Journal of Geophysical Research-Atmospheres **112**(D23).
289. Raes, F. et al. (2000). "Formation and cycling of aerosols in the global troposphere." Atmospheric Environment **34**(25): 4215-4240.
290. Raizenne, M. E., et al. (1989). "ACUTE LUNG-FUNCTION RESPONSES TO AMBIENT ACID AEROSOL EXPOSURES IN CHILDREN." Environmental Health Perspectives **79**: 179-185.
291. Rattanavaraha, W., et al. (2016). "Assessing the impact of anthropogenic pollution on isoprene-derived secondary organic aerosol formation in PM<sub>2.5</sub> collected from the Birmingham, Alabama, ground site during the 2013 Southern Oxidant and Aerosol Study." Atmospheric Chemistry and Physics **16**(8): 4897-4914.
292. Reggente, M., et al. (2019). "Analysis of functional groups in atmospheric aerosols by infrared spectroscopy: systematic intercomparison of calibration methods for US measurement network samples." Atmospheric Measurement Techniques **12**(4): 2287-2312.
293. Reid, J. S., et al. (1998). Physical, chemical, and radiative characteristics of the smoke dominated regional hazes over Brazil. Journal of Geophysical Research-Atmospheres **103**(D24): 32059-32080.

294. Ren, A. L., et al. (2016). Effects of Ozone concentration and relative humidity on secondary organic aerosol formation from reactions of 1,3-butadiene with ozone. Proceedings of the 2016 5th International Conference on Environment, Materials, Chemistry and Power Electronics. X. Xiao and P. Han. Paris, Atlantis Press. **84**: 201-205.
295. Riedel, T. P., et al. (2015). "Heterogeneous Reactions of Isoprene-Derived Epoxides: Reaction Probabilities and Molar Secondary Organic Aerosol Yield Estimates." Environmental Science & Technology Letters **2**(2): 38-42.
296. Riesz, P., et al. (1985). "FREE-RADICAL GENERATION BY ULTRASOUND IN AQUEOUS AND NONAQUEOUS SOLUTIONS." Environmental Health Perspectives **64**: 233-252.
297. Riva, M., et al. (2016a). "Effect of Organic Coatings, Humidity and Aerosol Acidity on Multiphase Chemistry of Isoprene Epoxydiols." Environmental Science & Technology **50**(11): 5580-5588.
298. Riva, M., et al. (2016b). "Chemical characterization of secondary organic aerosol constituents from isoprene ozonolysis in the presence of acidic aerosol." Atmospheric Environment **130**: 5-13.
299. Riva, M., et al. (2017). "Multiphase reactivity of gaseous hydroperoxide oligomers produced from isoprene ozonolysis in the presence of acidified aerosols." Atmospheric Environment **152**: 314-322.
300. Riva, M., et al. (2019). "Increasing Isoprene Epoxydiol-to-Inorganic Sulfate Aerosol Ratio Results in Extensive Conversion of Inorganic Sulfate to Organosulfur Forms: Implications for Aerosol Physicochemical Properties." Environmental Science & Technology **53**(15): 8682-8694.
301. Riva, M., et al. (2015). "Evidence for an Unrecognized Secondary Anthropogenic Source of Organosulfates and Sulfonates: Gas-Phase Oxidation of Polycyclic Aromatic Hydrocarbons in the Presence of Sulfate Aerosol." Environmental Science & Technology **49**(11): 6654-6664.
302. Robinson, A. L., et al. (2007). "Rethinking Organic Aerosols: Semivolatile Emissions and Photochemical Aging." Science, **315**, 1259–1262.
303. Rohner, N. L., et al (2004). "Electrochemical and theoretical aspects of electrospray ionisation". Phys. Chem. Chem. Phys., **6**, 3056-3068
304. Rohrl, A. and G. Lammel (2002). "Determination of malic acid and other C-4 dicarboxylic acids in atmospheric aerosol samples." Chemosphere **46**(8): 1195-1199.
305. Rozzaini M. Z. H. (2012). "The Chemistry of Dicarboxylic Acids in the Atmospheric Aerosols." Atmospheric Aerosols - Regional Characteristics - Chemistry and Physics, InterchOpen.
306. Rudzinski, K. J. (2004). "Degradation of isoprene in the presence of sulphony radical anions." Journal of Atmospheric Chemistry **48**(2): 191-216.
307. Rudzinski, K. J. (2006). "Heterogeneous and Aqueous-Phase Transformations of Isoprene." in: Barnes, I., and Rudzinski, K. J. (eds) Environmental Simulation Chambers: Application to Atmospheric Chemical Processes. Nato Science Series: IV: Earth and Environmental Science **62**, Springer, Dordrecht
308. Rudzinski, K. J., et al. (2009). "Reactions of isoprene and sulphony radical-anions - a possible source of atmospheric organosulphites and organosulphates." Atmospheric Chemistry and Physics **9**(6): 2129-2140.
309. Rudzinski, K. J., et al. (2022). "Winter sources of PM2.5 pollution in Podkowa Lesna, a Central-European garden town (Mazovia, Poland)." Environmental Science and Pollution Research **29**(56): 84504-84520.
310. Rudzinski, K. J., et al. (2016). "Aqueous-phase story of isoprene - A mini-review and reaction with HONO." Atmospheric Environment **130**: 163-171.
311. Safieddine, S. A., et al. (2017). "The global nonmethane reactive organic carbon budget: A modeling perspective." Geophysical Research Letters **44**(8): 3897-3906.
312. Sakurai, K., et al. (2013). "Reliable passive-sampling method for determining outdoor 1,3-butadiene concentrations in air." Atmospheric Environment **80**: 198-203.



313. Salma, I., et al. (2017). "Source apportionment of carbonaceous chemical species to fossil fuel combustion, biomass burning and biogenic emissions by a coupled radiocarbon-levoglucosan marker method." Atmospheric Chemistry and Physics **17**(22): 13767-13781.
314. Santos, L. S., et al. (2006). "Mimicking the atmospheric OH-radical-mediated photooxidation of isoprene: formation of cloud-condensation nuclei polyols monitored by electrospray ionization mass spectrometry." Rapid Communications in Mass Spectrometry **20**(14): 2104-2108.
315. Sato, K. (2008). "Detection of nitrooxypolyols in secondary organic aerosol formed from the photooxidation of conjugated dienes under high-NO<sub>x</sub> conditions." Atmospheric Environment **42**(28): 6851-6861.
316. Sato, K., et al. (2011). "Secondary organic aerosol formation from the photooxidation of isoprene, 1,3-butadiene, and 2,3-dimethyl-1,3-butadiene under high NO<sub>x</sub> conditions." Atmospheric Chemistry and Physics **11**(14): 7301-7317.
317. Saxena, P. and L. M. Hildemann (1996). "Water-soluble organics in atmospheric particles: A critical review of the literature and application of thermodynamics to identify candidate compounds." Journal of Atmospheric Chemistry **24**(1): 57-109.
318. Schell, B., et al. (2001). "Modeling the formation of secondary organic aerosol within a comprehensive air quality model system." Journal of Geophysical Research-Atmospheres **106**(D22): 28275-28293.
319. Schindelka, J., et al. (2013). "Sulfate radical-initiated formation of isoprene-derived organosulfates in atmospheric aerosols." Faraday Discussions **165**: 237-259.
320. Schindler, C., et al. (2009). "Improvements in PM<sub>10</sub> Exposure and Reduced Rates of Respiratory Symptoms in a Cohort of Swiss Adults (SAPALDIA)." American Journal of Respiratory and Critical Care Medicine **179**(7): 579-587.
321. Schone, L., et al. (2014). "Atmospheric aqueous phase radical chemistry of the isoprene oxidation products methacrolein, methyl vinyl ketone, methacrylic acid and acrylic acid - kinetics and product studies." Physical Chemistry Chemical Physics **16**(13): 6257-6272.
322. Seinfeld, J. H., and Pandis, S. N. (1998, 2006, 2016). "Atmospheric Chemistry and Physics: from Air Pollution to Climate Change". 1st-3rd Edition, John Wiley & Sons, New York.
323. Seinfeld, J. H. and J. F. Pankow (2003). "Organic atmospheric particulate material." Annual Review of Physical Chemistry **54**: 121-140.
324. Shakya, K. M. and R. E. Peltier (2013). "Investigating Missing Sources of Sulfur at Fairbanks, Alaska." Environmental Science & Technology **47**(16): 9332-9338.
325. Shakya, K. M. and R. E. Peltier (2015). "Non-sulfate sulfur in fine aerosols across the United States: Insight for organosulfate prevalence." Atmospheric Environment **100**: 159-166.
326. Shalamzari, M. S., et al. (2013). "Mass spectrometric characterization of organosulfates related to secondary organic aerosol from isoprene." Rapid Communications in Mass Spectrometry **27**(7): 784-794.
327. Shao, Y. Q., et al. (2022). "Chemical composition of secondary organic aerosol particles formed from mixtures of anthropogenic and biogenic precursors." Atmospheric Chemistry and Physics **22**(15): 9799-9826.
328. Sharkey, T. D., et al. (2008). "Isoprene emission from plants: Why and how." Annals of Botany **101**(1): 5-18.
329. Shaw, S. L., et al. (2003). "Isoprene production by Prochlorococcus, a marine cyanobacterium, and other phytoplankton." Marine Chemistry **80**: 227-245.
330. Shilling, J. E., et al. (2013). "Enhanced SOA formation from mixed anthropogenic and biogenic emissions during the CARES campaign." Atmospheric Chemistry and Physics **13**(4): 2091-2113.
331. Shrivastava, M., et al. (2017). "Recent advances in understanding secondary organic aerosol: Implications for global climate forcing." Reviews of Geophysics **55**(2): 509-559.
332. Silverstein, R. M., et al. (2008). "Spektroskopowe metody identyfikacji związków organicznych." Wydawnictwo Naukowe PWN, Warszawa
333. Sindelarova, K., et al. (2014). "Global data set of biogenic VOC emissions calculated by the MEGAN model over the last 30 years." Atmospheric Chemistry and Physics **14**(17): 9317-9341.

334. Sorsa, M., et al. (1996). "Assessment of environmental and occupational exposures to butadiene as a model for risk estimation of petrochemical emissions." *Mutagenesis* **11**(1): 9-17.
335. Spolnik, G., et al. (2018). "Improved UHPLC-MS/MS Methods for Analysis of Isoprene-Derived Organosulfates." *Analytical Chemistry* **90**(5): 3416-3423.
336. Spolnik, G., et al. (2020). "Tracing the biogenic secondary organic aerosol markers in rain, snow and hail." *Chemosphere* **251**
337. Squizzato, S., et al. (2013). "Factors determining the formation of secondary inorganic aerosol: a case study in the Po Valley (Italy)." *Atmospheric Chemistry and Physics* **13**(4): 1927-1939.
338. Srivastava, D., et al. (2022). "Formation of secondary organic aerosols from anthropogenic precursors in laboratory studies." *Npj Climate and Atmospheric Science* **5**(1).
339. Stockwell, W. R., et al. (2003). "The Treasure Valley secondary aerosol study II: modeling of the formation of inorganic secondary aerosols and precursors for southwestern Idaho." *Atmospheric Environment* **37**(4): 525-534.
340. Stone, E. A., et al. (2012). "Characterization of organosulfates in atmospheric aerosols at Four Asian locations." *Atmospheric Environment* **47**: 323-329.
341. Stutz, J., et al. (2010). "Nocturnal NO<sub>3</sub> radical chemistry in Houston, TX." *Atmospheric Environment* **44**(33): 4099-4106.
342. Sun, J. M. and P. A. Ariya (2006). "Atmospheric organic and bio-aerosols as cloud condensation nuclei (CCN): A review." *Atmospheric Environment* **40**(5): 795-820.
343. Surratt, J. D., et al. (2010). "Reactive intermediates revealed in secondary organic aerosol formation from isoprene." *Proceedings of the National Academy of Sciences of the United States of America* **107**(15): 6640-6645.
344. Surratt, J. D., et al. (2008). "Organosulfate formation in biogenic secondary organic aerosol." *Journal of Physical Chemistry A* **112**(36): 8345-8378.
345. Surratt, J. D., et al. (2007a). "Evidence for organosulfates in secondary organic aerosol." *Environmental Science & Technology* **41**(2): 517-527.
346. Surratt, J. D., et al. (2007b). "Effect of acidity on secondary organic aerosol formation from isoprene." *Environmental Science & Technology* **41**(15): 5363-5369.
347. Surratt, J. D., et al. (2006). "Chemical composition of secondary organic aerosol formed from the photooxidation of isoprene." *Journal of Physical Chemistry A* **110**(31): 9665-9690.
348. Szmigielski, R. (2016). "Evidence for C-5 organosulfur secondary organic aerosol components from in-cloud processing of isoprene: Role of reactive SO<sub>4</sub> and SO<sub>3</sub> radicals." *Atmospheric Environment* **130**: 14-22.
349. Szmigielski, R. (2013). "The chemistry of organosulfates and organonitrates" in: *Disposal of dangerous chemicals in urban areas and mega cities: role of oxides and acids of nitrogen in atmospheric chemistry*, edited by: Barnes, I. and Rudzinski, K. J., Springer, ISBN 978-94-007-5036-4, 211-226
350. Szmigielski, R., et al. (2007). "3-methyl-1,2,3-butanetricarboxylic acid: An atmospheric tracer for terpene secondary organic aerosol." *Geophysical Research Letters* **34**(24).
351. Szmigielski, R., et al. (2010). "The acid effect in the formation of 2-methyltetrols from the photooxidation of isoprene in the presence of NO<sub>x</sub>." *Atmospheric Research* **98**(2-4): 183-189.
352. Tallis, M., et al. (2011). "Estimating the removal of atmospheric particulate pollution by the urban tree canopy of London, under current and future environments." *Landscape and Urban Planning* **103**(2): 129-138.
353. Thompson, J. E. (2018). "Airborne Particulate Matter Human Exposure and Health Effects." *Journal of Occupational and Environmental Medicine* **60**(5): 392-423.
354. Thornton-Manning, J. R., et al. (1997). "Comparison of the disposition of butadiene epoxides in Sprague-Dawley rats and B6C3F(1) mice following a single and repeated exposures to 1,3-butadiene via inhalation." *Toxicology* **123**(1-2): 125-134.
355. Tkacik, D. S., et al. (2017). "A dual-chamber method for quantifying the effects of atmospheric perturbations on secondary organic aerosol formation from biomass burning emissions." *Journal of Geophysical Research-Atmospheres* **122**(11): 6043-6058.
356. Tolocka, M. P., et al. (2004). "Formation of oligomers in secondary organic aerosol." *Environmental Science & Technology* **38**(5): 1428-1434.

357. Tolocka, M. P. and B. Turpin (2012). "Contribution of Organosulfur Compounds to Organic Aerosol Mass." Environmental Science & Technology **46**(15): 7978-7983.
358. Tomasi C. et al. (2017). "Atmospheric Aerosols: Life Cycles and Effects on Air Quality and Climate." First Edition, John Wiley & Sons, New York
359. Tovstiga, T. E., et al. (2014). "Characterization of multiple fragmentation pathways initiated by collision-induced dissociation of multifunctional anions formed by deprotonation of 2-nitrobenzenesulfonylglycine." Journal of Mass Spectrometry **49**(2): 168-177.
360. Tsigaridis, K., et al. (2014). "The AeroCom evaluation and intercomparison of organic aerosol in global models." Atmospheric Chemistry and Physics **14**(19): 10845-10895.
361. Tsigaridis, K. and M. Kanakidou (2003). "Global modelling of secondary organic aerosol in the troposphere: a sensitivity analysis." Atmospheric Chemistry and Physics **3**: 1849-1869.
362. Tsigaridis, K., et al. (2006). "Change in global aerosol composition since preindustrial times." Atmospheric Chemistry and Physics **6**: 5143-5162.
363. U.S. EPA report (1989). "Nonmethane Organic Compound Monitoring Program (Final Report 1988)." Urban Air Toxics Monitoring Program, vol. **2**, United States Environmental Protection Agency Washington, DC.
364. U.S. EPA report (1996). "Locating and estimating air emissions from sources of 1,3-butadiene." EPA-454/R-96-008, United States Environmental Protection Agency, Office of Air Quality Planning and Standards, Research Triangle Park, NC.
365. U.S. EPA report (2002). "Health Assessment of 1,3-butadiene." EPA/600/P-98/001F, Office of Research and Development, United States Environmental Protection Agency, Washington, DC.
366. U.S. EPA report (2004). "Air quality criteria for particulate matter." Environmental Protection Agency, Washington, DC.
367. Vallecillos, L., et al. (2019). "Determination of 1,3-butadiene degradation products in air samples by thermal desorption-gas chromatography-mass spectrometry." Atmospheric Environment **196**: 95-102.
368. Volkamer, R., et al. (2006). "Secondary organic aerosol formation from anthropogenic air pollution: Rapid and higher than expected." Geophysical Research Letters **33**(17).
369. Volkamer, R., et al. (2009). "Secondary Organic Aerosol Formation from Acetylene (C<sub>2</sub>H<sub>2</sub>): seed effect on SOA yields due to organic photochemistry in the aerosol aqueous phase." Atmospheric Chemistry and Physics **9**(6): 1907-1928.
370. Wach, P., et al. (2019). "Radical oxidation of methyl vinyl ketone and methacrolein in aqueous droplets: Characterization of organosulfates and atmospheric implications." Chemosphere **214**: 1-9.
371. Wach, P., et al. (2020). "Structural Characterization of Lactone-Containing MW 212 Organosulfates Originating from Isoprene Oxidation in Ambient Fine Aerosol." Environmental Science & Technology **54**(3): 1415-1424
372. Wang, J., et al. (2017). "Contamination and health risk assessment of PAHs in soils and crops in industrial areas of the Yangtze River Delta region, China." Chemosphere **168**: 976-987.
373. Wang, S. Y., et al. (2019). "Organic Peroxides and Sulfur Dioxide in Aerosol: Source of Particulate Sulfate." Environmental Science & Technology **53**(18): 10695-10704.
374. Wang, W., et al. (2005). "Characterization of oxygenated derivatives of isoprene related to 2-methyltetrols in Amazonian aerosols using trimethylsilylation and gas chromatography/ion trap mass spectrometry." Rapid Communications in Mass Spectrometry **19**(10): 1343-1351.
375. Wang, W., et al. (2008). "Polar organic tracers in PM<sub>2.5</sub> aerosols from forests in eastern China." Atmospheric Chemistry and Physics **8**(24): 7507-7518.
376. Watson, J. G., et al (2005). "Summary of Organic and Elemental Carbon/Black Carbon Analysis Methods and Intercomparisons". Aerosol and Air Quality Research, Vol. **5**, No.1, pp. 65-102.
377. Wennberg, P. O., et al. (2018). "Gas-Phase Reactions of Isoprene and Its Major Oxidation Products." Chemical Reviews **118**(7): 3337-3390.
378. Went, F. W. (1960). "BLUE HAZES IN THE ATMOSPHERE." Nature **187**(4738): 641-643.

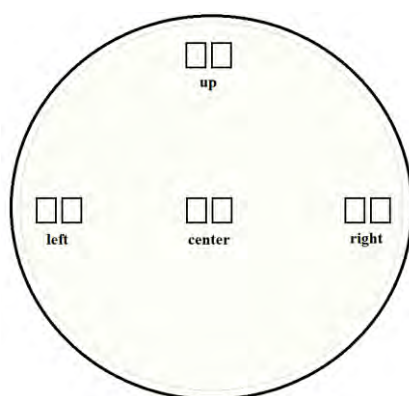
379. Weschler, C. J. and W. W. Nazaroff (2008). "Semivolatile organic compounds in indoor environments." Atmospheric Environment **42**(40): 9018-9040.
380. WHO guideline (2005). "1,3-butadiene." Air Quality Guidelines, 2nd Edition, chapter 5.3, World Health Organization.
381. WHO guideline (2006). "Health risks of particulate matter from long-range transboundary air pollution." Regional Office for Europe & Joint WHO/Convention Task Force on the Health Aspects of Air Pollution, World Health Organization
382. WHO report (2013). "Health effects of particulate matter - Policy implications for countries in eastern Europe. Caucasus and central Asia." World Health Organization
383. WHO guideline (2021). "Particulate matter (PM<sub>2.5</sub> and PM<sub>10</sub>), ozone, nitrogen dioxide, sulfur dioxide and carbon monoxide." World Health Organization global air quality guidelines, Geneva
384. Widziewicz, K., et al. (2015). "Metals distribution on the surface of quartz fiber filters used for particulate matter collection." Archives of Environmental Protection **41**(4): 3-10.
385. Wilkins, K., and Larsen, K. (1996). "Volatile organic compounds from garden waste." Chemosphere **32**(10): 2049-2055.
386. Woodruff, T. J., et al. (2007). "Estimating risk from ambient concentrations of acrolein across the United States." Environmental Health Perspectives **115**(3): 410-415.
387. Ye, J. H., et al. (2018). "Novel pathway of SO<sub>2</sub> oxidation in the atmosphere: reactions with monoterpene ozonolysis intermediates and secondary organic aerosol." Atmospheric Chemistry and Physics **18**(8): 5549-5565.
388. Ye, Y., et al. (1998). "Evaporative emissions of 1,3-butadiene from petrol-fuelled motor vehicles." Atmospheric Environment **32**(14-15): 2685-2692.
389. Yokelson, R. J., et al. (2009). "Emissions from biomass burning in the Yucatan." Atmospheric Chemistry and Physics **9**(15): 5785-5812.
390. Yuan, B., et al. (2013). "VOC emissions, evolutions and contributions to SOA formation at a receptor site in eastern China." Atmospheric Chemistry and Physics **13**(17): 8815-8832.
391. Yuan, B., et al. (2012). "Volatile organic compounds (VOCs) in urban air: How chemistry affects the interpretation of positive matrix factorization (PMF) analysis." Journal of Geophysical Research-Atmospheres **117**.
392. Zanca, N., et al. (2017). "Characterizing source fingerprints and ageing processes in laboratory-generated secondary organic aerosols using proton-nuclear magnetic resonance (H-1-NMR) analysis and HPLC HULIS determination." Atmospheric Chemistry and Physics **17**(17): 10405-10421.
393. Zappoli, S., et al. (1999). "Inorganic, organic and macromolecular components of fine aerosol in different areas of Europe in relation to their water solubility." Atmospheric Environment **33**(17): 2733-2743.
394. Zhang, H., et al. (2011). "Effect of relative humidity on SOA formation from isoprene/NO photooxidation: enhancement of 2-methylglyceric acid and its corresponding oligoesters under dry conditions." Atmospheric Chemistry and Physics **11**(13): 6411-6424.
395. Zhang, H. F., et al. (2012). "Organosulfates as Tracers for Secondary Organic Aerosol (SOA) Formation from 2-Methyl-3-Buten-2-ol (MBO) in the Atmosphere." Environmental Science & Technology **46**(17): 9437-9446.
396. Zhang, Q., et al. (2007). "Ubiquity and dominance of oxygenated species in organic aerosols in anthropogenically-influenced Northern Hemisphere midlatitudes." Geophysical Research Letters **34**(13).
397. Zhou, S. M., et al. (2018). "Identification of organic hydroperoxides and peroxy acids using atmospheric pressure chemical ionization-tandem mass spectrometry (APCI-MS/MS): application to secondary organic aerosol." Atmospheric Measurement Techniques **11**(5): 3081-3089.
398. Zuth, C., et al. (2018). "Ultrahigh-Resolution Mass Spectrometry in Real Time: Atmospheric Pressure Chemical Ionization Orbitrap Mass Spectrometry of Atmospheric Organic Aerosol." Analytical Chemistry **90**(15): 8816-8823.

## 6. Appendix

Below are presented data to which I refer in the main text of the Ph.D. thesis.

**Table A1:** Qualitative comparison of ambient aerosol filter extraction techniques for selected main isoprene SOA components

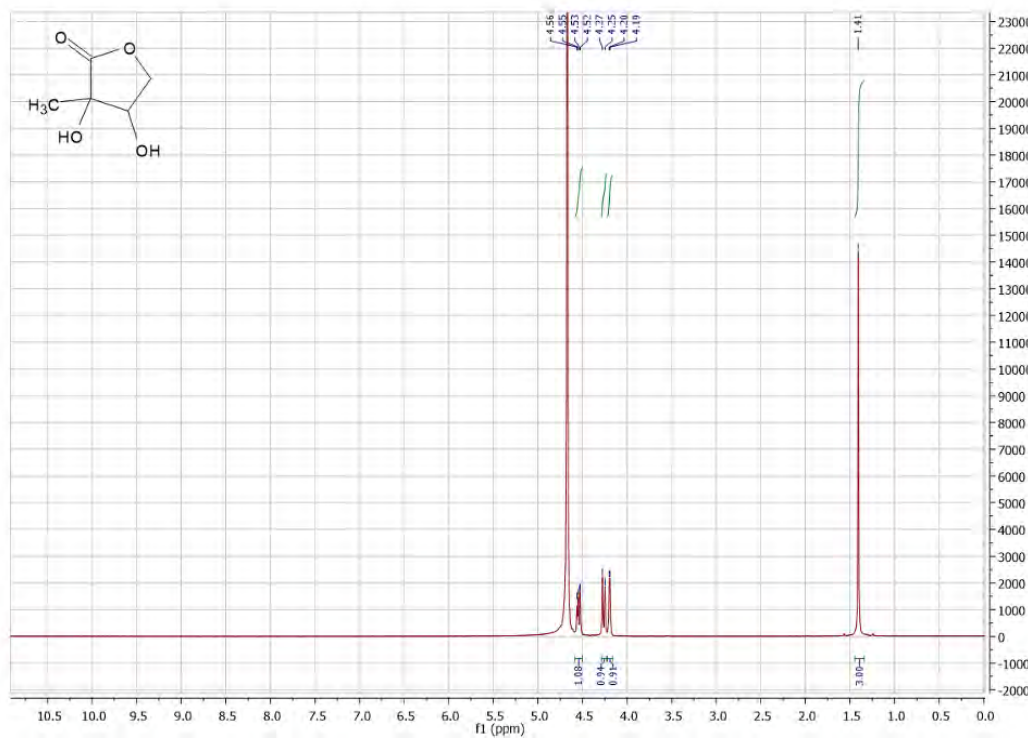
Organosulfate (MW)	Average Peak Area	
	60 min x 15 mL MeOH	30 min x 15 mL MeOH (x2)
200	50 ± 5	30 ± 7
212	113 ± 15	66 ± 10
214	57 ± 9	44 ± 6
216	291 ± 16	293 ± 14



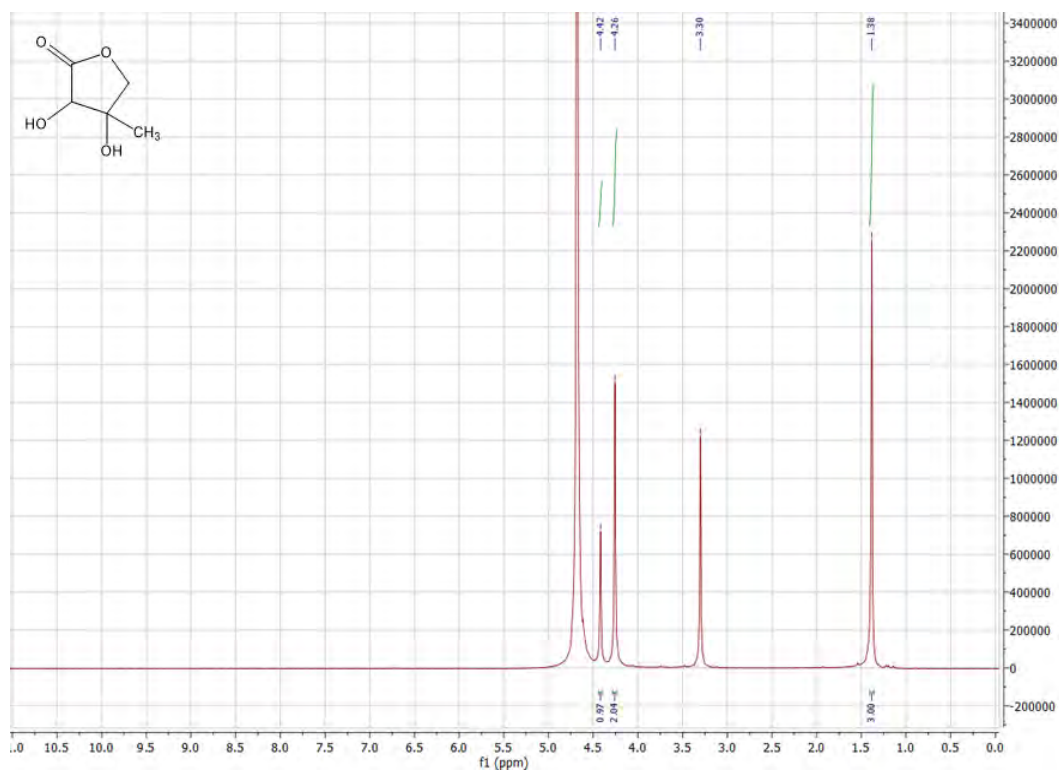
**Scheme A1.** Homogeneity test – scheme of punches taken for UPLC-MS analyses from Zielonka ambient aerosol filter

**Table A2:** Qualitative results of sample injection repeatability obtained for authentic and surrogate standard compounds

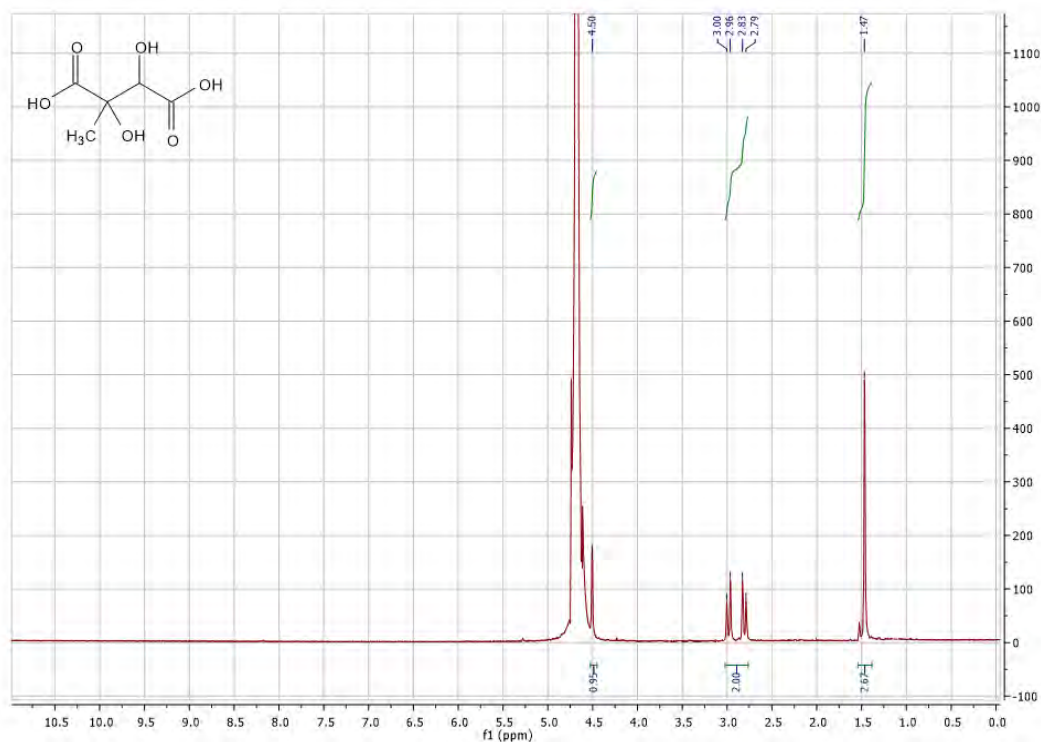
Standard compound	Peak Area						Average Peak Area
	inj. 1	inj. 2	inj. 3	inj. 4	inj. 5	inj. 6	
pentyl sulfate	4249	4222	4260	4067	3944	4267	4168 ± 121
3-methyl threonic acid	9025	11808	8304	10116	11585	9854	10115 ± 1262
DL-tartaric acid	6122	6205	6342	4882	4488	4759	5466 ± 768
D-threonic acid	1705	1655	1526	1790	1540	1448	1610 ± 117
tartronic acid	1943	2258	2260	1728	1744	1685	1936 ± 242
malic acid	2761	2845	2617	2912	2578	2970	2781 ± 145



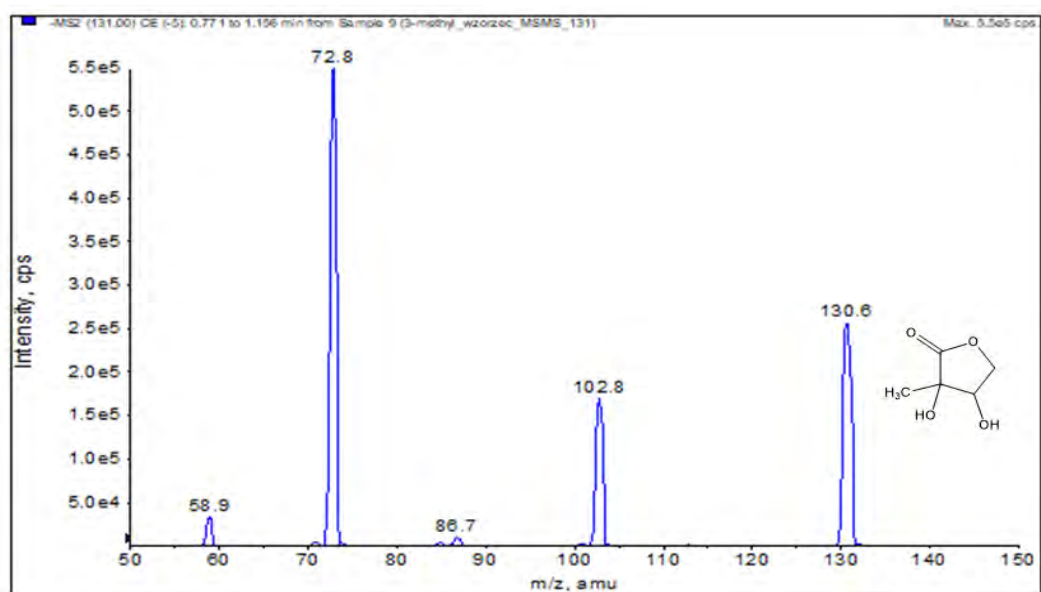
**Figure A1.**  $^1\text{H}$  NMR spectrum of dihydro-3,4-dihydroxy-3-methyl-2(3H)-furanone



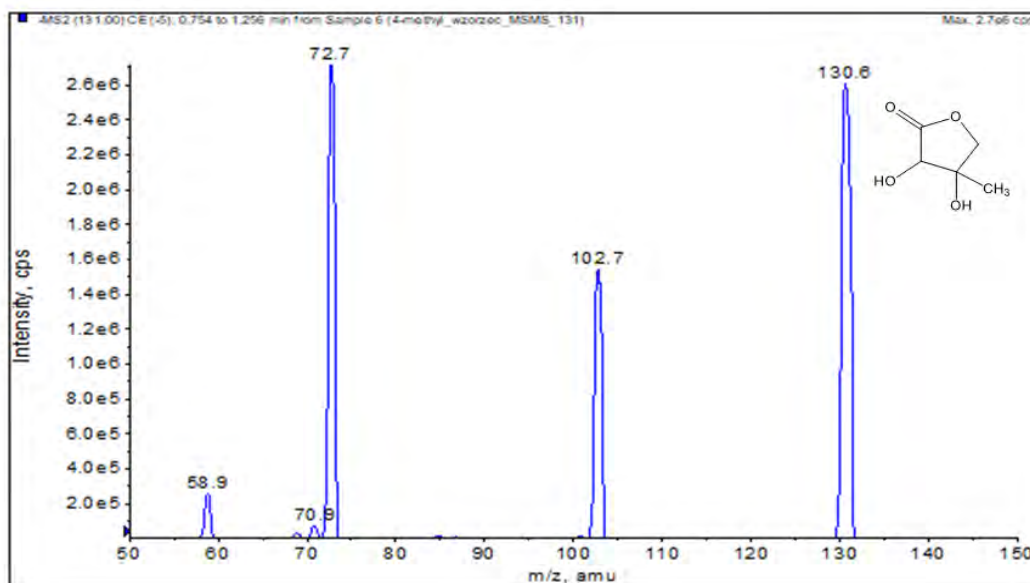
**Figure A2.**  $^1\text{H}$  NMR spectrum of dihydro-3,4-dihydroxy-4-methyl-2(3H)-furanone



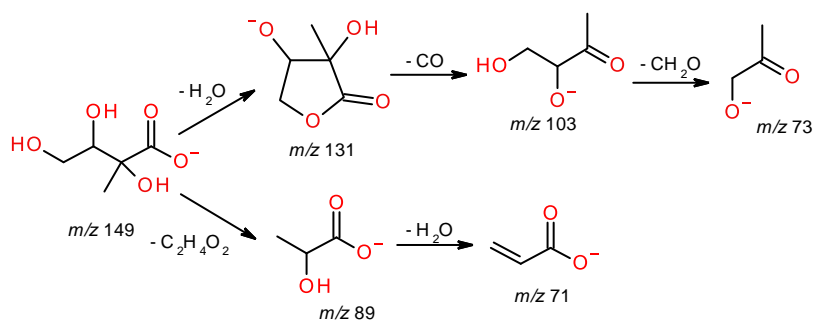
**Figure A3.**  $^1\text{H}$  NMR spectrum of 2-methyltartaric acid (2-MTA)



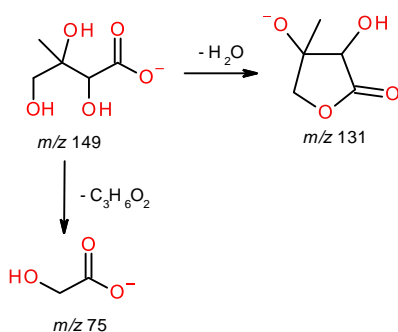
**Figure A4.** Direct low-resolution ESI(-) product ion mass spectrum registered for dihydro-3,4-dihydroxy-3-methyl-2-(3H)-furanone (MW 132) on API 3000 spectrometer (CE = 5 eV)



**Figure A5.** Direct low-resolution ESI(-) product ion mass spectrum registered for dihydro-3,4-dihydroxy-4-methyl-2-(3H)-furanone (MW 132) on API 3000 spectrometer (CE = 5 eV)

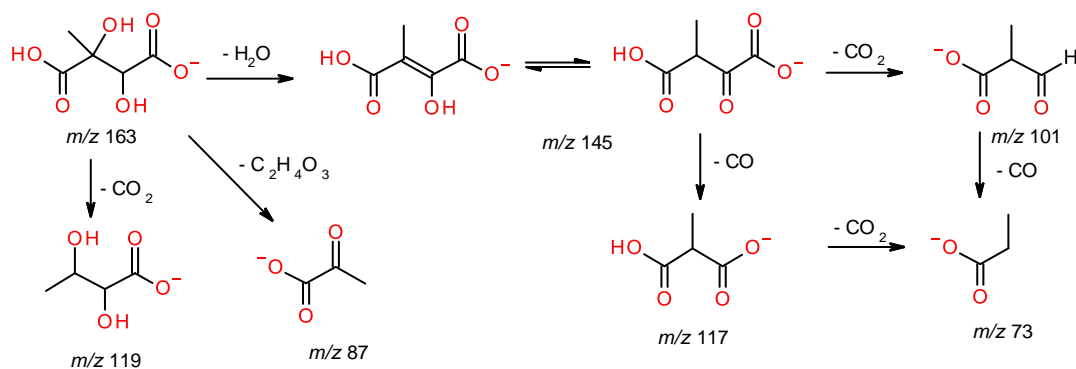


**Figure A6.** Proposed fragmentation pathway of 2-methylthreonic acid (MW 150) eluting at RT = 0.77 min based on (-)electrospray product ion mass spectrum registered for the standard compound after alkaline hydrolysis of dihydro-3,4-dihydroxy-3-methyl-2-(3H)-furanone

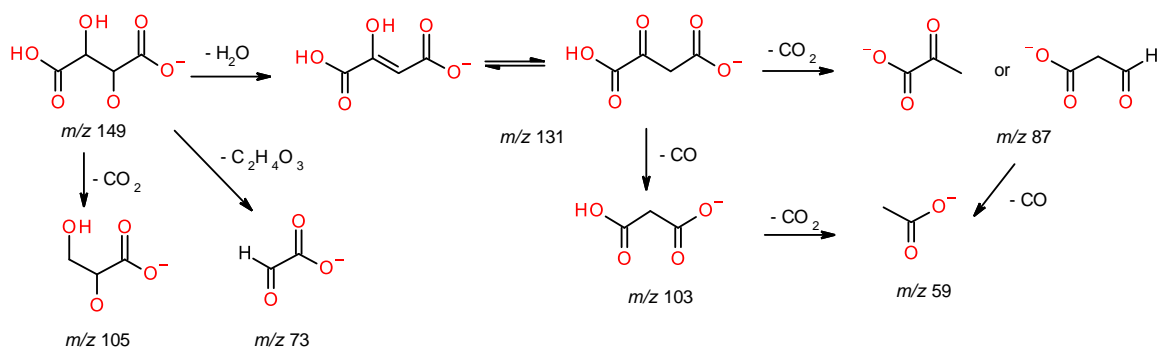


**Figure A7.** Proposed fragmentation pathway of 3-methylthreonic acid (MW 150) eluting at RT = 0.88 min based on (-)electrospray product ion mass spectrum registered for the standard compound after alkaline hydrolysis of dihydro-3,4-dihydroxy-4-methyl-2-(3H)-furanone

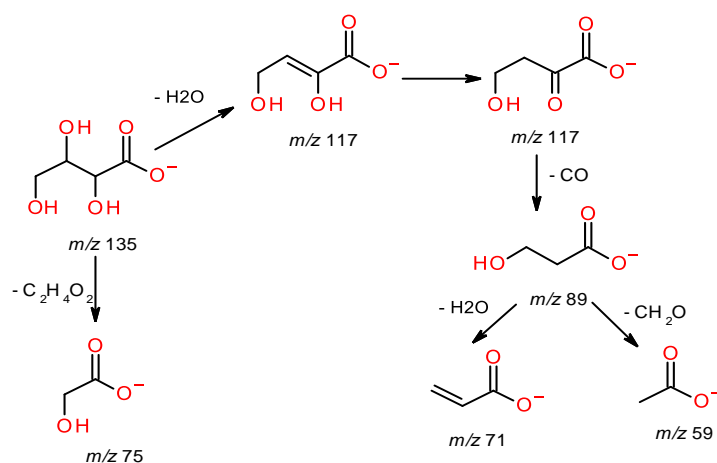




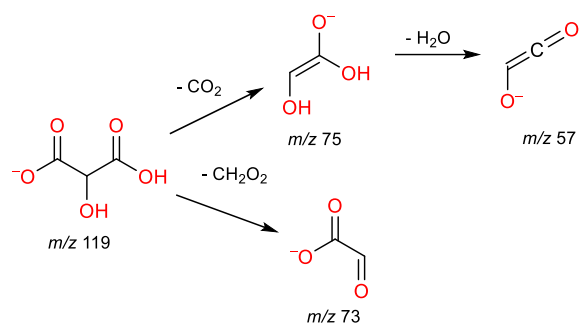
**Figure A8.** Proposed fragmentation pathway of 2-methyltartaric acid (MW 164) eluting at RT = 0.68 min based on (-)electrospray product ion mass spectrum registered for the standard compound



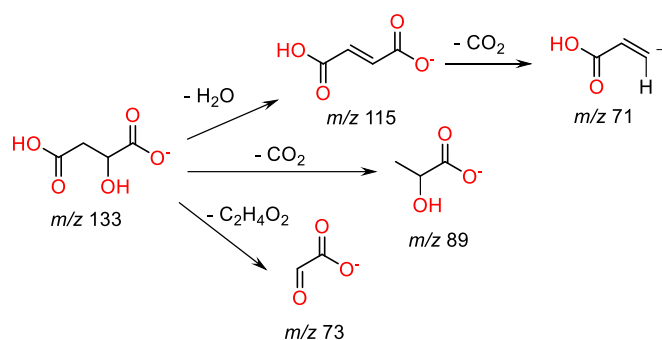
**Figure A9.** Proposed fragmentation pathway of tartaric acid (MW 150) eluting at RT = 0.81 min based on (-)electrospray product ion mass spectrum registered for the standard compound



**Figure A10.** Proposed fragmentation pathway of threonic acid (MW 136) eluting at RT = 0.87 min based on (-)electrospray product ion mass spectrum registered for the standard compound after alkaline hydrolysis of D-threono-lactone



**Figure A11.** Proposed fragmentation pathway of tartronic acid (MW 120) eluting at  $RT = 0.82$  min based on (-)electrospray product ion mass spectrum registered for the standard compound



**Figure A12.** Proposed fragmentation pathway of malic acid (MW 134) eluting at  $RT = 0.82$  min based on (-)electrospray product ion mass spectrum registered for the standard compound

**Table A3:** Concentrations ( $\text{ng m}^{-3}$ ) of OS, NOS and NSOS products from the ISO acidic-seed experiments determined using UPLC-MS

ER662	MW 198	MW 200	MW 212	MW 214	MW 216	MW 230	MW 244	MW 261	MW 275
RH (8%)	225.4 ± 5.9	18.7 ± 0.6	838.5 ± 4.8	456.2 ± 10.1	1850.4 ± 43.1	17.7 ± 3.1	528.3 ± 5.6	5163.8 ± 21.0	19.9 ± 1.1
RH (18%)	81.3 ± 2.7	11.5 ± 0.4	201.7 ± 8.0	122.5 ± 1.7	657.8 ± 5.8	11.8 ± 0.4	130.1 ± 2.4	2574.0 ± 24.9	19.1 ± 1.1
RH (28%)	47.9 ± 4.0	10.6 ± 1.3	147.4 ± 9.4	135.3 ± 7.1	306.5 ± 9.0	42.5 ± 1.9	46.7 ± 1.4	1014.6 ± 14.0	8.0 ± 0.5
RH (44%)	13.8 ± 2.7	7.9 ± 0.7	155.2 ± 3.0	86.4 ± 6.2	109.9 ± 3.5	32.8 ± 2.1	28.9 ± 2.1	592.2 ± 24.4	4.6 ± 0.8

**Table A4:** Concentrations ( $\text{ng m}^{-3}$ ) of OS, NOS and NSOS products from the ISO non-acidic-seed experiments determined using UPLC-MS

ER667	MW 198	MW 200	MW 212	MW 214	MW 216	MW 230	MW 244	MW 261	MW 275
RH (9%)	7.7 ± 0.7	3.3 ± 0.6	40.9 ± 3.5	54.2 ± 3.5	191.8 ± 7.7	ND	7.4 ± 0.1	394.7 ± 4.9	ND
RH (19%)	28.8 ± 3.6	6.2 ± 0.2	ND	38.0 ± 2.8	145.5 ± 5.6	1.9 ± 0.8	ND	302.0 ± 7.8	ND
RH (29%)	19.1 ± 0.5	5.4 ± 0.3	ND	23.1 ± 1.6	82.5 ± 6.1	ND	ND	147.3 ± 4.7	ND
RH (39%)	18.1 ± 0.6	9.1 ± 0.7	ND	22.9 ± 1.9	76.0 ± 6.7	1.2 ± 0.4	ND	134.1 ± 4.8	ND
RH (49%)	13.5 ± 2.5	6.5 ± 0.4	ND	24.8 ± 1.3	65.3 ± 4.0	ND	ND	108.8 ± 1.7	ND

ND – not detected

**Table A5:** Concentrations ( $\text{ng m}^{-3}$ ) of organic acids from the ISO acidic-seed experiments (ER662) determined using UPLC-MS

ER662	MW 150	MW 164
RH (8%)	$7.9 \pm 0.3$	ND
RH (18%)	$3.6 \pm 0.2$	ND
RH (28%)	$3.4 \pm 0.3$	ND
RH (44%)	ND	ND

ND – not detected

**Table A6:** Concentrations ( $\text{ng m}^{-3}$ ) of organic acids from the ISO non-acidic-seed experiments (ER667) determined using UPLC-MS

ER667	MW 150	MW 164
RH (9%)	$14.8 \pm 0.6$	$7.1 \pm 0.2$
RH (19%)	$34.6 \pm 1.7$	$7.3 \pm 0.6$
RH (29%)	$28.2 \pm 0.7$	$6.6 \pm 0.4$
RH (39%)	$16.3 \pm 0.5$	$6.5 \pm 0.2$
RH (49%)	$16.6 \pm 0.2$	$6.3 \pm 0.1$

**Table A7:** Concentrations ( $\text{ng m}^{-3}$ ) of OS, NOS and NSOS products from the 13BD acidic-seed experiments determined using UPLC-MS

ER444	MW 184	MW 186	MW 198	MW 200	MW 202	MW 214	MW 216	MW 231	MW 247
RH (10%)	$133.7 \pm 3.2$	$106.3 \pm 3.8$	$27.2 \pm 0.5$	$27.7 \pm 0.5$	$230.7 \pm 6.1$	$7.2 \pm 1.0$	$11.3 \pm 2.0$	$75.6 \pm 4.3$	$3251.5 \pm 29.5$
RH (31%)	$80.3 \pm 5.4$	$90.3 \pm 3.8$	$20.8 \pm 0.9$	$12.8 \pm 0.9$	$112.6 \pm 5.6$	$6.8 \pm 1.2$	$5.7 \pm 1.9$	$37.7 \pm 2.8$	$1969.1 \pm 113.5$
RH (50%)	$48.7 \pm 2.2$	$52.9 \pm 2.9$	$4.8 \pm 0.1$	$7.2 \pm 0.6$	$57.0 \pm 2.3$	$5.2 \pm 1.7$	$2.7 \pm 0.7$	$25.9 \pm 3.5$	$1293.7 \pm 24.4$
RH (62%)	$35.5 \pm 1.4$	$34.8 \pm 1.9$	$9.4 \pm 1.6$	$8.0 \pm 0.8$	$51.2 \pm 3.1$	ND	ND	$25.2 \pm 1.6$	$957.3 \pm 26.7$

ND – not detected

**Table A8:** Concentrations ( $\text{ng m}^{-3}$ ) of OS, NOS and NSOS products from the 13BD non-acidic-seed experiments determined using UPLC-MS

ER666	MW 184	MW 186	MW 198	MW 200	MW 202	MW 214	MW 216	MW 231	MW 247
RH (11%)	$3.0 \pm 0.5$	$64.9 \pm 2.9$	ND	ND	$12.0 \pm 1.5$	$1.8 \pm 0.3$	$2.2 \pm 0.4$	ND	$455.1 \pm 6.0$
RH (20%)	ND	$70.9 \pm 0.5$	ND	ND	$7.8 \pm 0.8$	$2.8 \pm 0.5$	$1.1 \pm 0.4$	ND	$444.5 \pm 2.8$
RH (29%)	ND	$74.8 \pm 4.9$	ND	ND	$2.9 \pm 0.4$	$2.1 \pm 0.3$	$0.1 \pm 0.4$	ND	$349.4 \pm 2.0$
RH (39%)	ND	$85.9 \pm 3.2$	ND	ND	$2.0 \pm 0.6$	$4.5 \pm 0.8$	$1.0 \pm 0.5$	ND	$291.9 \pm 1.7$
RH (49%)	ND	$82.8 \pm 2.0$	ND	ND	$2.7 \pm 0.3$	$4.3 \pm 0.6$	$2.2 \pm 0.6$	ND	$361.2 \pm 2.4$
RH (60%)	ND	$59.4 \pm 2.5$	ND	ND	$1.1 \pm 0.3$	$1.7 \pm 0.3$	$0.7 \pm 0.3$	ND	$186.0 \pm 4.9$

ND – not detected

**Table A9:** Concentrations ( $\text{ng m}^{-3}$ ) of organic acids from the 13BD acidic-seed experiments (ER444) determined using UPLC-MS

ER444	MW 120	MW 134	MW 136	MW 150
RH (10%)	16.1 ± 2.7	85.6 ± 1.6	91.1 ± 10.5	ND
RH (31%)	17.1 ± 1.7	89.4 ± 2.5	56.6 ± 3.1	ND
RH (50%)	17.8 ± 2.2	103.5 ± 4.3	91.4 ± 3.5	ND
RH (62%)	ND	87.7 ± 4.4	74.8 ± 5.2	ND

ND – not detected

**Table A10:** Concentrations ( $\text{ng m}^{-3}$ ) of organic acids from the 13BD non-acidic-seed experiments (ER666) determined using UPLC-MS

ER666	MW 120	MW 134	MW 136	MW 150
RH (11%)	17.5 ± 2.7	282.6 ± 5.2	172.7 ± 4.1	13.6 ± 0.6
RH (20%)	19.8 ± 3.6	298.5 ± 4.5	167.1 ± 3.1	13.0 ± 0.8
RH (29%)	19.4 ± 1.2	299.9 ± 10.1	139.6 ± 4.6	12.2 ± 0.2
RH (39%)	11.7 ± 1.2	271.6 ± 8.0	108.0 ± 7.1	9.8 ± 1.1
RH (49%)	12.8 ± 0.8	348.9 ± 8.8	134.5 ± 4.0	10.7 ± 0.6
RH (60%)	23.2 ± 0.7	288.3 ± 10.6	102.5 ± 10.3	8.9 ± 0.4

**Table A11:** Concentrations ( $\text{ng m}^{-3}$ ) of ISO products from Zielonka ambient aerosol determined using UPLC-MS

Zielonka	MW 200	MW 212	MW 214	MW 216	MW 244	MW 261	MW 275	MW 150	MW 164
L022	0.7 ± 0.5	145.2 ± 6.9	79.1 ± 1.8	194.2 ± 5.4	3.2 ± 0.6	125.8 ± 3.9	0.3 ± 0.2	1.3 ± 0.1	3.3 ± 0.5
L023	1.4 ± 0.2	149.5 ± 4.0	56.2 ± 1.1	155.8 ± 4.7	5.2 ± 1.5	149.5 ± 3.9	2.8 ± 0.7	1.3 ± 0.2	3.2 ± 0.1
L024	1.9 ± 0.5	173.6 ± 1.9	55.2 ± 3.1	131.0 ± 3.4	5.2 ± 0.9	291.7 ± 4.2	3.0 ± 0.6	1.8 ± 0.3	3.4 ± 0.3
L025	0.6 ± 0.2	107.6 ± 5.5	32.2 ± 2.7	76.0 ± 2.2	3.3 ± 0.5	97.3 ± 4.1	2.5 ± 0.9	1.2 ± 0.3	1.9 ± 0.1
L026	ND	99.9 ± 2.5	31.4 ± 1.0	73.7 ± 2.2	3.6 ± 1.3	114.2 ± 3.1	1.5 ± 0.2	1.4 ± 0.1	1.8 ± 0.1

ND – not detected

**Table A12:** Concentrations ( $\text{ng m}^{-3}$ ) of ISO products from Godów ambient aerosol determined using UPLC-MS

Godów	MW 200	MW 212	MW 214	MW 216	MW 244	MW 261	MW 275	MW 150	MW 164
Godów_1	ND	$9.7 \pm 0.9$	$1.3 \pm 0.1$	$3.1 \pm 0.4$	$1.3 \pm 0.1$	$30.2 \pm 0.1$	ND	$0.7 \pm 0.1$	ND
Godów_2	ND	$21.6 \pm 1.2$	$1.8 \pm 0.5$	$4.1 \pm 0.6$	$1.1 \pm 0.5$	$55.9 \pm 2.0$	ND	$0.7 \pm 0.1$	ND
Godów_3	ND	$13.7 \pm 1.2$	$0.6 \pm 0.1$	$1.6 \pm 0.2$	$1.5 \pm 0.1$	$48.0 \pm 0.9$	ND	$0.7 \pm 0.2$	$0.4 \pm 0.1$
Godów_4	ND	$21.6 \pm 0.2$	$1.3 \pm 0.2$	$5.7 \pm 0.7$	$1.5 \pm 0.2$	$46.9 \pm 3.3$	ND	$0.9 \pm 0.1$	$0.5 \pm 0.1$
Godów_5	$0.6 \pm 0.2$	$45.1 \pm 1.4$	$6.1 \pm 0.4$	$17.9 \pm 0.3$	$1.9 \pm 0.4$	$94.0 \pm 1.9$	$0.8 \pm 0.2$	$0.7 \pm 0.2$	$0.5 \pm 0.1$

ND – not detected

**Table A13:** Concentrations ( $\text{ng m}^{-3}$ ) of ISO products from Kaskada ambient aerosol determined using UPLC-MS

Kaskada	MW 200	MW 212	MW 214	MW 216	MW 244	MW 261	MW 275	MW 150	MW 164
K8043	$0.5 \pm 0.1$	$91.0 \pm 5.4$	$16.8 \pm 1.4$	$184.4 \pm 2.8$	$0.8 \pm 0.3$	$91.4 \pm 0.9$	$0.4 \pm 0.3$	$1.4 \pm 0.1$	$2.6 \pm 0.1$
K8044	$0.4 \pm 0.2$	$71.4 \pm 2.3$	$17.2 \pm 0.6$	$138.6 \pm 7.1$	$0.5 \pm 0.2$	$84.7 \pm 3.3$	$1.3 \pm 0.3$	$1.7 \pm 0.2$	$2.1 \pm 0.3$
K8045	ND	$77.3 \pm 1.9$	$7.6 \pm 0.6$	$40.5 \pm 2.8$	$0.5 \pm 0.2$	$186.5 \pm 2.8$	$5.0 \pm 1.0$	$2.0 \pm 0.1$	$1.1 \pm 0.2$
K8046	$0.9 \pm 0.4$	$79.6 \pm 3.0$	$8.1 \pm 1.2$	$38.8 \pm 1.3$	$0.2 \pm 0.2$	$170.8 \pm 1.1$	$3.6 \pm 0.8$	$2.2 \pm 0.2$	$1.3 \pm 0.3$
K8047	$1.6 \pm 0.7$	$100.6 \pm 2.3$	$12.2 \pm 2.2$	$46.2 \pm 3.1$	$1.3 \pm 0.4$	$264.4 \pm 5.6$	$3.2 \pm 0.3$	$2.4 \pm 0.2$	$1.7 \pm 0.1$

ND – not detected

**Table A14:** Concentrations ( $\text{ng m}^{-3}$ ) of ISO products from Diabla Góra ambient aerosol determined using UPLC-MS

Diabla Góra	MW 200	MW 212	MW 214	MW 216	MW 244	MW 261	MW 275	MW 150	MW 164
B017	ND	47.3 ± 4.1	20.3 ± 2.0	107.2 ± 5.1	1.5 ± 0.2	51.2 ± 3.7	ND	1.5 ± 0.2	2.1 ± 0.1
B018	ND	57.4 ± 1.7	22.0 ± 0.4	104.4 ± 7.6	2.9 ± 0.5	80.1 ± 4.9	ND	2.9 ± 0.2	1.3 ± 0.1
B019	0.3 ± 0.2	75.1 ± 4.2	30.0 ± 2.4	158.2 ± 7.0	2.7 ± 0.1	111.5 ± 1.5	1.7 ± 0.1	2.7 ± 0.2	1.5 ± 0.1
B020	ND	79.1 ± 4.5	33.1 ± 3.0	139.3 ± 6.3	2.2 ± 0.5	83.7 ± 1.9	ND	2.2 ± 0.1	1.4 ± 0.3
B021	0.4 ± 0.3	89.1 ± 1.1	36.2 ± 3.2	171.8 ± 4.8	2.6 ± 1.0	108.2 ± 0.8	1.4 ± 0.8	2.6 ± 0.2	1.6 ± 0.1

ND – not detected

**Table A15:** Concentrations ( $\text{ng m}^{-3}$ ) of 13BD products from Zielonka ambient aerosol determined using UPLC-MS

Zielonka	MW 186	MW 214	MW 216	MW 134	MW 136	MW 150
L022	0.9 ± 0.6	7.1 ± 0.6	ND	112.9 ± 2.0	10.7 ± 4.3	5.9 ± 1.1
L023	0.4 ± 0.1	12.2 ± 1.7	0.4 ± 0.3	118.4 ± 2.7	14.7 ± 5.7	5.6 ± 0.7
L024	1.4 ± 0.5	21.2 ± 1.4	ND	118.5 ± 8.9	9.3 ± 5.3	5.8 ± 0.2
L025	ND	12.6 ± 1.4	0.3 ± 0.2	65.4 ± 2.2	ND	4.7 ± 0.8
L026	ND	13.4 ± 2.4	ND	53.5 ± 1.1	ND	4.3 ± 0.2

ND – not detected



**Table A16:** Concentrations ( $\text{ng m}^{-3}$ ) of 13BD products from Godów ambient aerosol determined using UPLC-MS

Godów	MW 186	MW 198	MW 214	MW 247	MW 134	MW 150
Godów_1	ND	ND	$4.6 \pm 0.2$	$1.3 \pm 0.2$	$9.0 \pm 0.1$	$1.4 \pm 0.1$
Godów_2	ND	ND	$3.0 \pm 0.4$	$1.1 \pm 0.2$	$10.3 \pm 0.3$	$1.4 \pm 0.1$
Godów_3	ND	ND	$4.5 \pm 0.6$	$1.5 \pm 0.4$	$12.4 \pm 0.8$	$1.5 \pm 0.1$
Godów_4	ND	$0.9 \pm 0.2$	$3.8 \pm 0.5$	$1.5 \pm 0.2$	$13.0 \pm 0.7$	$1.5 \pm 0.1$
Godów_5	$0.3 \pm 0.2$	$0.3 \pm 0.2$	$4.2 \pm 0.7$	$1.9 \pm 0.3$	$14.7 \pm 0.8$	$1.7 \pm 0.1$

ND – not detected

**Table A17:** Concentrations ( $\text{ng m}^{-3}$ ) of 13BD products from Kaskada ambient aerosol determined using UPLC-MS

Kaskada	MW 186	MW 214	MW 247	MW 134	MW 150
K8043	$0.2 \pm 0.2$	$7.1 \pm 1.1$	ND	$84.8 \pm 1.4$	$4.7 \pm 0.3$
K8044	ND	$6.0 \pm 1.3$	ND	$76.5 \pm 2.2$	$4.5 \pm 0.3$
K8045	$0.1 \pm 0.2$	$6.0 \pm 1.3$	$0.5 \pm 0.6$	$40.0 \pm 2.1$	$4.3 \pm 0.6$
K8046	ND	$6.1 \pm 1.4$	$1.0 \pm 1.2$	$43.1 \pm 2.4$	$4.3 \pm 0.4$
K8047	$0.3 \pm 0.2$	$7.4 \pm 1.6$	$2.2 \pm 2.2$	$48.1 \pm 0.9$	$4.4 \pm 0.6$

ND – not detected

**Table A18:** Concentrations ( $\text{ng m}^{-3}$ ) of 13BD products from Diabla Góra ambient aerosol determined using UPLC-MS

Diabla Góra	MW 186	MW 214	MW 134	MW 136	MW 150
B017	$0.9 \pm 0.3$	$6.2 \pm 0.1$	$74.7 \pm 2.2$	$1.8 \pm 1.2$	$4.3 \pm 0.3$
B018	ND	$6.3 \pm 0.3$	$50.0 \pm 2.7$	$1.6 \pm 1.4$	$4.2 \pm 0.1$
B019	$0.5 \pm 0.3$	$7.0 \pm 0.4$	$57.0 \pm 1.2$	ND	$4.0 \pm 0.2$
B020	$0.2 \pm 0.3$	$7.0 \pm 0.7$	$38.9 \pm 0.8$	ND	$3.8 \pm 0.2$
B021	ND	$8.0 \pm 0.1$	$51.7 \pm 1.5$	ND	$3.8 \pm 0.4$

*ND – not detected*



## List of publications and patent applications

Jaoui, M.; **Nestorowicz, K.**; Rudzinski, K. J.; Lewandowski, M.; Kleindienst, T. E.; Torres, J.; Bulska, E.; Danikiewicz, W.; Szmigielski, R., Atmospheric oxidation of 1,3-butadiene: influence of relative humidity on chemical composition of secondary organic aerosol. *Atmos. Chem. Phys.* **2023**, submitted.

Rudzinski, K. J.; Sarang, K.; **Nestorowicz, K.**; Asztemborska, M.; Zyfka-Zagrodzinska, E.; Skotak, K.; Szmigielski, R., Winter sources of PM<sub>2.5</sub> pollution in Podkowa Lesna, a Central-European garden town (Mazovia, Poland). *Environmental Science and Pollution Research* **2022**, 29 (56), 84504-84520.

Patent application P.440646, „Kompozycja wabiąca chrząszcze z rodzaju Monochamus, zwłaszcza chrząszcze gatunku żerdzianka sosnowka (*Monochamus galloprovincialis* (Oliv.)), zestaw dyspenserów do wabienia chrząszczy z rodzaju Monochamus, zastosowanie kompozycji oraz zastosowanie zestawu dyspenserów”, March **2022**

Sarang, K.; Otto, T.; Rudzinski, K.; Schaefer, T.; Grgic, I.; **Nestorowicz, K.**; Herrmann, H.; Szmigielski, R., Reaction Kinetics of Green Leaf Volatiles with Sulfate, Hydroxyl, and Nitrate Radicals in Tropospheric Aqueous Phase. *Environ. Sci. Technol.* **2021**, 55 (20), 13666-13676

Jaoui, M.; Szmigielski, R.; **Nestorowicz, K.**; Kolodziejczyk, A.; Sarang, K.; Rudzinski, K. J.; Konopka, A.; Bulska, E.; Lewandowski, M.; Kleindienst, T. E., Organic Hydroxy Acids as Highly Oxygenated Molecular (HOM) Tracers for Aged Isoprene Aerosol. *Environ. Sci. Technol.* **2019**, 53 (24), 14516-14527

**Nestorowicz, K.**; Jaoui, M.; Rudzinski, K. J.; Lewandowski, M.; Kleindienst, T. E.; Spolnik, G.; Danikiewicz, W.; Szmigielski, R., Chemical composition of isoprene SOA under acidic and non-acidic conditions: effect of relative humidity. *Atmos. Chem. Phys.* **2018**, 18 (24), 18101-18121

Derewiaka D.; **Nestorowicz K.**; Wołosiak R.; Comparison of Fatty Acid Composition in Selected Dietary Supplements Containing Conjugated Linoleic Acid. *J Diet Suppl.* **2017** Jul 4;14(4):411-421.

## Oral presentations at national and international conferences

16–19<sup>th</sup> September 2019: XXVIII Sympozjum Zintegrowanego Monitoringu Środowiska Przyrodniczego pod patronatem Głównego Inspektora Ochrony Środowiska, Jeziorowskie, Polska

*Identyfikacja nowych markerów starzenia aerozolu izoprenowego w atmosferze*

28–29<sup>th</sup> June 2018: 12<sup>th</sup> Copernican International Young Scientists Conference, Toruń, Polska

*Atmospheric oxidation of isoprene: influence of aerosol acidity and relative humidity on chemical composition of secondary organic aerosol*

23–26<sup>th</sup> April 2018: 6<sup>th</sup> Conference of Polish Mass Spectrometry Society, Warszawa - Miedzeszyn, Polska

*Analysis of isoprene secondary organic aerosol by hyphenated mass spectrometry techniques*

17–21<sup>st</sup> September 2017: 60 Zjazd Polskiego Towarzystwa Chemicznego, PTChem' 17, Wrocław, Polska

*Analiza i identyfikacja składu wtórnego aerozolu atmosferycznego z wykorzystaniem techniki HPLC-MS*

## Poster presentations at national and international conferences

24–31<sup>st</sup> August 2019: European Aerosol Conference - EAC 2019, Gothenburg, Sweden  
*Formation of Highly Oxygenated Acids from Isoprene and Butadiene in Atmospheric Aerosol*

28–29<sup>th</sup> June 2018: 12<sup>th</sup> Copernican International Young Scientists Conference, Toruń, Poland

*Aqueous phase reaction of 2-methyl-3-buten-2-ol (MBO): implications for secondary organic aerosol (SOA) formation*

9<sup>th</sup> June 2017: XIV Warszawskie Seminarium Doktorantów Chemików, ChemSession'17, Warszawa, Polska

*Smog chamber experiments with secondary organic aerosols (SOA) from isoprene and 1,3-butadiene*



